THE JOURNAL
OF
CHEMICAL PHYSICS

VOLUME 18, NUMBER 2 FEBRUARY, 1950

Nuclear Magnetic Resonance Line Shape for a Triangular Configuration of Nuclei

E. R. ANDREW* AND R. BERSOHN
Department of Physics, Harvard University, Cambridge, Massachusetts
(Received August 15, 1949)

The nuclear resonance line shape observed in solids can often be accounted for quantitatively and (in the absence of quadrupole effects) may provide information concerning the orientation and internuclear distances of dipolar nuclei. As an example of this method, the line shapes for a rigid and rotating triangular configuration of such nuclei are calculated and compared with recent experiments.

THE line shapes observed in the nuclear resonance experiment in solids give structural information about groups of nuclei which are relatively isolated in the lattice. Moreover it should be possible to account quantitatively for the experimentally measured line shapes of such groups of nuclei. The first example of this method was that of Pake[1] who measured the separation and orientation of the proton pair in each water molecule of the crystal $CaSO_4 \cdot 2H_2O$. Gutowsky and Pake[2] have since measured the powder line shape at low temperatures of a number of compounds containing nuclei in a triangular configuration.

The purpose of this paper is to calculate the line shape for solids containing nuclei arranged in relatively isolated triangular groups both for the single crystal and the powder, and both for rigid groups and for groups rotating about any fixed axis. The calculated line shapes, modified by intermolecular broadening, are compared with those obtained experimentally by Gutowsky and Pake.

I. CALCULATION OF THE FINE STRUCTURE OF A TRIANGLE

The Hamiltonian for the interaction of three identical nuclei is[3]

$$H=g\beta H\sum_{i=1}^{3} I_{zi}+\sum_{i<j}(\mathbf{I}_i\cdot\mathbf{I}_j-3I_{zi}I_{zj})A_{ij} \qquad (1)$$

where

$$A_{ij}=g^2\beta^2/2r_{ij}^3(3\cos^2\theta_{ij}-1).$$

θ_{ij} is the angle between the external field $\mathbf{H}$, and $\mathbf{r}_{ij}$, the vector connecting nuclei i and j.

The states of the three spin system are conveniently labelled by the eigenvalues of I_1^2, I_2^2, I_3^2, $\mathfrak{I}^2$, I^2 and I_z where $\mathfrak{I}=\mathbf{I}_1+\mathbf{I}_2$, $\mathbf{I}=\mathfrak{I}+\mathbf{I}_3$, and $I_z=I_{1z}+I_{2z}+I_{3z}$. For nuclei of spin $\frac{1}{2}$ the matrix of the Hamiltonian becomes

$$\begin{array}{cccc} M_I=\frac{3}{2} & I=\frac{3}{2} & \begin{pmatrix} -2x & 0 & 0 & 0 \\ 0 & 2x & a & b \\ 0 & a & 0 & 0 \\ 0 & b & 0 & 0 \end{pmatrix} & \\ M_I=\frac{1}{2}\begin{cases} I=\frac{3}{2} \\ I=\frac{1}{2} \\ I=\frac{1}{2} \end{cases} & \begin{matrix} \\ \mathfrak{I}=0 \\ \mathfrak{I}=1 \end{matrix} & & \end{array}$$

where

$$x=\tfrac{1}{4}(A_{12}+A_{23}+A_{13}) \qquad b=\sqrt{2}/4(2A_{12}-A_{13}-A_{23})$$
$$a=(6)^{\frac{1}{2}}/4(A_{13}-A_{23}) \qquad y^2=x^2+a^2+b^2.$$

The matrix for $M_I=-\frac{3}{2}, -\frac{1}{2}$ is identical.

The characteristic values of the dipole-dipole energy are $-2x$, 0, $x+y$, and $x-y$. The general result shown in Fig. 1 is that the line whose energy was at $\hbar\omega=g\beta H$ is now split into a central undeviated component flanked by three pairs with energy values $\pm(3x+y)$, $\pm 2y$, and $\pm(3x-y)$ relative to the unperturbed energy. The matrix elements x, a, b are complicated functions of the angle ψ between the external magnetic field and the normal to the plane of the triangle, and an azimuthal angle in the plane of the triangle; therefore both the position and intensities of the various components of the line will change markedly with angle. The experimental consequence is that the line shape of a single crystal should be highly anisotropic and this anisotropy should permit determination of molecular orientations.

* Commonwealth Fund Fellow from Cambridge University, England.

[1] G. E. Pake, J. Chem. Phys. **16**, 327 (1948).

[2] H. S. Gutowsky and G. E. Pake, J. Chem. Phys. **18**, 162 (1950).

[3] J. H. Van Vleck, Phys. Rev. **74**, 1168 (1948).

The transition probabilities are proportional to $|(n|I_x|n')|^2$ where n and n' are states between which magnetic dipole transitions are allowed. Because I_x commutes with $\mathfrak{I}^2$ and I^2 the selection rules are simply $\Delta\mathfrak{I}=0$, $\Delta I=0$ and $\Delta M_I=\pm 1$. The transition probabilities (normalized to one) for the various transitions are given in Table I.

If the triangle is equilateral, the values of x and y become:

$$x=\mu\alpha(\tfrac{1}{2}-\tfrac{3}{2}\cos^2\psi), \tag{2}$$

$$y=\mu\alpha[27/4\sin^4\psi-3\sin^2\psi+1]^{\frac{1}{2}} \tag{3}$$

where $\alpha=\frac{3}{2}\mu R^{-3}$, μ is the nuclear magnetic moment and R is the side of the equilateral triangle. In this case x and y are independent of the azimuth of the triangle; experiment can therefore only determine the angle of orientation of the plane of the triangle.

We define the field h as the difference $(H-H^*)$, where H is the applied field, and H^* is the resonant field for the nuclei at the radiofrequency in use. The fine structure of the resonance line in a single crystal consists then of a central line $h=0$, and three pairs of lines $h=\pm y/\mu$; $\pm(2x+y)/2\mu$; $\pm(3x-y)/2\mu$.

II. LINE-SHAPE FOR RIGID EQUILATERAL TRIANGULAR GROUPS IN POLYCRYSTALLINE MATERIAL

The orientation of the crystal grains of which the material is composed may be considered to be distributed uniformly over all directions. Hence the fraction of triangular groups for which the angle ψ lies in the interval $d\psi$ is $d(\cos\psi)$. For a single crystal line component $h(\psi)$, having probability $p(\psi)$, the powder lineshape $F(h)$ is therefore $p(\psi)d(\cos\psi)/dh$. It is now necessary to express $p(\psi)$ and $\cos\psi$ in terms of h using (2) and (3). The following results are obtained:

(i) The single crystal line component $h=0$ remains unchanged.

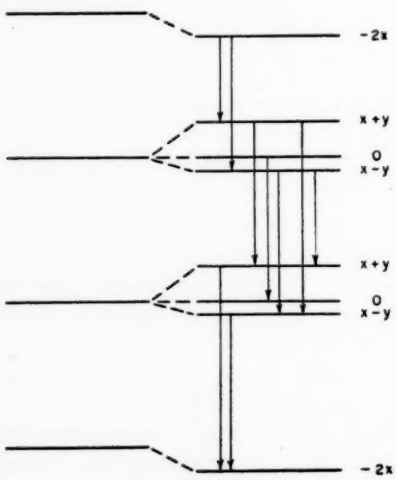

FIG. 1. Energy diagram for three nuclei of spin ½ arrows denote allowed transitions.

(ii) For the line-component $h=y/\mu$:

$$F(h)=\frac{h}{72\alpha^2\gamma_1}\left[1-\frac{\alpha^2}{4h^2}\left(\frac{4}{3}\pm 3\gamma_1\right)\right]\left(\frac{7}{9}\pm\gamma_1\right)^{-\frac{1}{2}} \tag{4}$$

where

$$\gamma_1=\frac{2}{9}\left(\frac{3h^2}{\alpha^2}-2\right)^{\frac{1}{2}}.$$

The + sign is to be taken for $(\frac{2}{3})^{\frac{1}{2}}\alpha<h<\alpha$.
The − sign is to be taken for $(\frac{2}{3})^{\frac{1}{2}}\alpha<h<(19)^{\frac{1}{2}}/2\alpha$.

(iii) For the line-components $h=(3x\pm y)/2\mu$:

$$F(h)=\frac{1}{24\alpha}\left[\frac{1}{9}\left(1-\frac{6h}{\alpha}\right)\pm\gamma_2\right]^{-\frac{1}{2}} \times\left[\frac{2}{9\gamma_2}\left(1\pm\frac{h}{\alpha}\right)\mp 1\right]\left[\frac{1-2\rho}{1-3\rho}\right] \tag{5}$$

TABLE I. Line strengths for a triangular group of nuclei.

Change in energy of transition from unperturbed value	Probability	Probability averaged over all orientations for equilateral case
0	$\frac{1}{8}\left(1+\frac{3x^2}{y^2}\right)$	0.19
$\pm 2y$	$\frac{3}{16}\left(1-\frac{x^2}{y^2}\right)$	0.31
$\pm(3x+y)$	$\frac{1}{8}\left(1+\frac{x}{y}\right)$	0.22
$\pm(3x-y)$	$\frac{1}{8}\left(1-\frac{x}{y}\right)$	0.28

where

$$\gamma_2=\frac{2}{9}\left[\frac{3h^2}{\alpha^2}+\frac{6h}{\alpha}+4\right]^{\frac{1}{2}}$$

and

$$\rho=\frac{\alpha}{4h}\left[\tfrac{2}{3}+2\frac{h}{\alpha}\mp 3\gamma_2\right].$$

The upper signs are to be taken for $-\alpha<h<\alpha/4((19)^{\frac{1}{2}}+3)$.

The lower signs are to be taken for $-2\alpha<h<-\alpha/4((19)^{\frac{1}{2}}-3)$.

(iv) For the line components $h=-y/\mu$, $-(3x\pm y)/2\mu$, it is only necessary to replace h by $-h$ in (4) and (5). Combining these results, the line shape shown in Fig. 2(a) is obtained.

III. LINE SHAPE FOR A ROTATING TRIANGULAR GROUP

The interaction Hamiltonian (1) must be modified when the nuclear pairs rotate with a frequency greater

than the frequency with which their position is measured in the nuclear resonance experiment. As discussed by Gutowsky and Pake, the coefficients A_{ij} which contain the position coordinates must be replaced by averages over the state of the motion.

For an equilateral triangle this replacement leads to new values of x and y which we will call x' and y':

$$x'=\mu\alpha(\tfrac{1}{2}-\tfrac{3}{2}\cos^2\eta)(\tfrac{1}{2}-\tfrac{3}{2}\cos^2\epsilon),$$

$$y'=\mu\alpha(\tfrac{1}{2}-\tfrac{3}{2}\cos^2\eta)\left(\frac{27}{4}\sin^4\epsilon-3\sin^2\epsilon+1\right)^{\frac{1}{2}} \quad (6)$$

where ϵ and η are respectively the angles which the normal to the triangle plane and the field H make with respect to the axis of rotation. The only assumption used concerning the state of motion is that it is periodic modulo $2\pi/3$ in an azimuth measuring rotation around the axis of rotation.

In the general case, there are still three pairs of lines and a central line. For the particular case of a triangle rotating about its normal, $\epsilon=0$ and $x'=-y'$. Consequently, only one pair of lines remains, each with probability $\frac{1}{4}$, flanking a central line, which has probability $\frac{1}{2}$. The pair of lines has the same angular dependence as that for a rigid pair of identical nuclei.[1] For polycrystalline material the line shape therefore consists of a central line together with:

$$F(h)=(1/8\sqrt{3}\alpha)(1\pm h/\alpha)^{-\frac{1}{2}} \quad (7)$$

for

$$-\alpha<\pm h<2\alpha.$$

This line shape is shown in Fig. 2(c).

IV. COMPARISON WITH EXPERIMENT

a. Rigid triangular group

Gutowsky and Pake[2] have measured the line shape for polycrystalline 1,1,1-trichloroethane at 90°K, shown in Fig. 2(b). Actually the derivative of the line-shape is measured, and the figure shows the integrated derivative curve. The unit of field along the abscissa is α, which was evaluated taking R, the side of the proton triangle, to be 1.79A; this is the accepted value for tetrahedrally distributed bonds.

The line shape calculated in II refers to isolated triangular groups. Neighboring groups broaden the line and smooth out the discontinuities. The broadened calculated line in Fig. 2(b) was obtained from Fig. 2(a) using a Gaussian broadening function in the manner described by Pake.[1] The use of a single Gaussian function is not rigorously justified but is a simple approximation which indicates the broadening effect of neighboring groups. The second moment of the Gaussian function which gave the best fit to the experimental curve was 2.1 gauss.[2] Since, as Gutowsky and Pake[2] point out, the second moment of the experimental curve is somewhat less than the theoretical value for a rigid structure, the discrepancy at the sides of the curve is not surprising. There is a large reduction in second moment at 140°K due to molecular rotation, and some residual molecular motion at 90°K probably accounts for the small discrepancy in second moment and line shape.

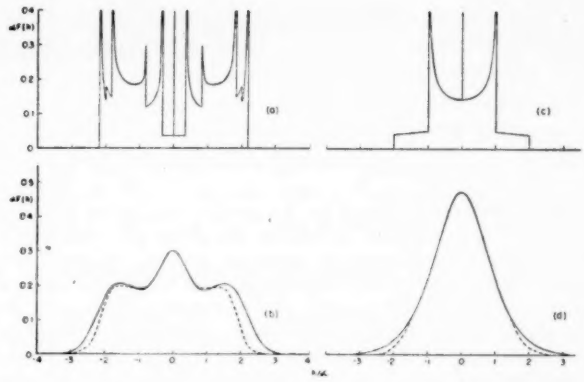

FIG. 2. Line shapes for three nuclei of spin $\frac{1}{2}$ at the corners of an equilateral triangle. a. Isolated rigid triangle. b. Rigid triangle broadened by neighbors. c. Isolated triangle rotating about the normal to its plane. d. Rotating triangle broadened by its neighbors. Dotted lines are the integrated experimental line shapes. Solid lines are calculated.

b. Rotating triangular group

Gutowsky and Pake[2] have also measured the line shape for polycrystalline acetonitrile at 93°K, shown in Fig. 2(d). The second moment of this line indicates either rotation or tunneling of the methyl group. The triangular groups are closer together in the lattice than in the case of methyl chloroform, with the result that there is scarcely any indication of fine structure in the broadened curve. (The derivative curve gives a rather more sensitive indication of structure than the line shape itself.) The broadened calculated curve shown in Fig. 2(d) was obtained from Fig. 2(c) using a Gaussian broadening function having a second moment of 5.5 gauss.[2] The agreement between the theoretical and experimental curves shows that the theory is at least consistent with experiment.

The authors would like to thank Professors J. H. Van Vleck and E. M. Purcell for their continued advice and help.

Structural Investigations by Means of Nuclear Magnetism. II. Hindered Rotation in Solids

H. S. GUTOWSKY* AND G. E. PAKE†‡
Gibbs Chemical Laboratory and the Lyman Laboratory of Physics, Harvard University, Cambridge Massachusetts
(Received August 15, 1949)

The experimental absorption line widths, for nuclei with spin 1/2, at nuclear magnetic resonance are given as a function of temperature for a number of molecular crystals. Temperatures ranged from 90°K to the melting points of the compounds. In some cases it has been possible to relate observed line structure and transitions in the line width to the existence and frequency of certain types of hindered rotational motion in the solid state. These deductions are based on mathematical considerations of the quantitative effect of such motions on the structure and second moment of an absorption line. It is emphasized that relatively low frequency motion of the order 10^5 cycles/second suffices to narrow the width of an absorption line from its value in the absence of that motion.

1,2-dichloroethane, 1,1,1-trichloroethane, and perfluoroethane were found to have line-width transitions coinciding with changes in crystal form and anomalies in the heat capacity. In 1,2-dichloroethane and perfluoroethane these transitions correspond to rotational motion about the long axis of the molecule. 1,1,1-trichloroethane has a line-width transition corresponding to this type of motion, but the heat capacity anomaly and change in crystal form coincides with a further small decrease in the line width to that characteristic of the liquid. A number of molecules including acetonitrile, methyl iodide, nitromethane, dimethyl mercury, and ammonia have absorption lines at 90°K corresponding to molecular rotation about the C_3 figure axis. Various other data and interpretations are presented for 2,2-dimethyl propane, methanol, ethanol, acetone, methylamine, and the ethyl halides. The possibility of estimating the potential barriers hindering rotation in solids from the line-width transitions is discussed.

1. INTRODUCTION

ROTATIONAL motion of molecules or atomic complexes in solids reveals itself through anomalies or transitions in a number of physical properties,[1,2] chief among which are perhaps the heat capacity, the dielectric constant, and the structure of the crystal lattice. Further evidence is presented by infra-red and Raman spectra, x-ray and electron diffraction, and, recently,[3] by the width of the lines which characterize radio-frequency resonance absorption by the Zeeman levels of nuclei within a given sample. In studying these rotational processes, one seeks data adequate to determine their nature, in addition to indicating their existence. This paper treats methods for extracting information from the structure and second moment of the nuclear magnetic resonance absorption line, which can be combined with other varieties of data to provide further insight into the actual rotational processes.

It is well known[4] that the characteristics of the absorption line depend not only upon the local nuclear configuration, but also upon the motion of a nucleus and that of its neighbors. The determination of the local nuclear configuration in rigid lattices from experimental line shapes is facilitated[4] by Van Vleck's calculation[5] of the second moment of the absorption line in terms of internuclear distances, nuclear spins, and nuclear gyromagnetic ratios. As stated earlier,[6] Van Vleck's calculation can be adapted to possible rotational motions, yielding a second moment dependent upon frequency and type of motion as well as upon the nuclear properties and internuclear distances. Thus, in favorable cases, a comparison between calculated and experimental second moments provides information concerning the rotational process.

2. LINE WIDTH AND THE RATE OF MOLECULAR REORIENTATION

Bloembergen, Purcell, and Pound[7] find the width of the absorption line in terms of the Debye correlation time, τ_c. To facilitate our discussion, we shall employ a *correlation frequency* or reorientation rate, defined as $\nu_c=(2\pi\tau_c)^{-1}$, which one may think of as an average rate at which significant changes occur in the atomic arrangement about a given nucleus. Then BPP Eq. (52) is re-expressed as

$$(\delta\nu)^2=A^2(2/\pi)\tan^{-1}[\alpha(\delta\nu/\nu_c)]. \quad (1)$$

The line width, on a frequency scale, is denoted $\delta\nu$. The factor α is the order of unity and encompasses the uncertainties arising from the integration limits in BPP Eq. (35) and from our inaccurate definition of $\delta\nu$ with respect to line shape. In practice, we shall take $\delta\nu$, or its counterpart δH which is measured on a magnetic field scale, as the separation between outermost points of maximum and minimum slope on the absorption curve. For the Lorentz line shape,[8] $2\pi\delta\nu$ is identical with the quantity $1/T_2$ appearing in the BPP equations.

---

* Now at Department of Chemistry, University of Illinois, Urbana, Illinois.
† Now at Department of Physics, Washington University, St. Louis, Missouri.
‡ Predoctoral Fellow of the National Research Council.
[1] A. Eucken, Zeits. f. Elektrochemie **45**, 126 (1939).
[2] C. P. Smyth, Chem. Rev. **19**, 329 (1936).
[3] N. L. Alpert, Phys. Rev. **75**, 398 (1949).
[4] Gutowsky, Kistiakowsky, Pake, and Purcell, J. Chem. Phys. **17**, 972 (1949), hereafter referred to as I.
[5] J. H. Van Vleck, Phys. Rev. **74**, 1168 (1948).
[6] H. S. Gutowsky and G. E. Pake, J. Chem. Phys. **16**, 1164 (1948).
[7] Bloembergen, Purcell, and Pound, Phys. Rev. **73**, 679 (1948), hereafter referred to as BPP.
[8] G. E. Pake and E. M. Purcell, Phys. Rev. **74**, 1184 (1948).

The constant A in Eq. (1) is evidently the width of the absorption line for a rigid lattice ($\nu_c \to 0$). As the reorientation rate increases and approaches the rigid-lattice width, A, $\delta\nu$ decreases. Since A is typically the order of 100 kilocycles/sec., the line will be narrowed usually by molecular reorientation at frequencies which are extremely low on a thermodynamic scale.

3. EFFECT OF ROTATION ON DIPOLAR SPLITTING

If the nuclei which are at resonance reside in a molecule, or atomic complex, which rotates in the crystal lattice, the energy of this system consists of its kinetic energy of rotation together with the potential energy of its position in the lattice and the Zeeman energy of its nuclear magnetic moments in the external magnetic field.

$$\mathcal{H} = \mathcal{H}_{\text{orb}} + \mathcal{H}_{\text{spin}}$$

$$\mathcal{H}_{\text{orb}} = p^2/2\mathfrak{I} + V(\theta, \phi) \tag{2}$$

$$\mathcal{H}_{\text{spin}} = -\sum_{j=1}^{n} g_j \beta \mathbf{H}_0 \mathbf{I}_{zj}$$

The potential function governing the rotation is $V(\theta, \phi)$, and the effective moment of inertia of the system is $\mathfrak{I}$, not to be confused with the nuclear spin operator $\mathbf{I}$. The external field $\mathbf{H}_0$ is taken along the z axis.

We suppose that the only significant perturbation arises from the dipole-dipole interaction between spins. This implies that the amplitude of the radiofrequency field, in practice about 10^{-2} gauss, is significantly less than the line width, that electric quadrupole broadening and effects of the electronic spins of paramagnetic atoms are absent or negligible and that magnetic field inhomogeneities (usually about 0.5 gauss) are sufficiently small to permit observation of the true line width. The dipolar perturbation is then

$$\mathcal{H}^{(1)} = \sum_{j>k} g_j g_k \beta^2 [\mathbf{I}_j \cdot \mathbf{I}_k r_{jk}^{-3} - 3\mathbf{I}_j \cdot \mathbf{r}_{jk} \mathbf{I}_k \cdot \mathbf{r}_{jk} r_{jk}^{-5}] \tag{3}$$

which is shown by the Van Vleck[5] to reduce to

$$\mathcal{H}_{\text{eff}}^{(1)} = \sum_{j>k} A_{jk} [\mathbf{I}_j \cdot \mathbf{I}_k - 3I_{zj} I_k]$$

$$A_{jk} = \tfrac{1}{2} g_j g_k \beta^2 r_{jk}^{-3} (3\cos^2\theta_{jk} - 1). \tag{4}$$

The matrix elements of $\mathcal{H}_{\text{eff}}^{(1)}$ are computed for the rigid lattice using spin eigenfunctions only and treating the factors A_{jk} as constants. The eigenfunctions of Eq. (2), however, are products of the eigenfunctions of the $\mathcal{H}_{\text{orb}}$ and those of $\mathcal{H}_{\text{spin}}$, inasmuch as spin and orbital coordinates are independent. The expectation value of the spin operator in brackets in Eq. (4) is, therefore, evaluated just as for the rigid lattice, but one now requires the expectation value of A_{jk} over the rotational motion of the system.

Inasmuch as the orbital eigenfunctions will not be known in general, we shall limit ourselves here to the rigid restricted plane rotor moving in a potential well periodic modulo $2\pi/n$ and to situations that permit the use of a classical average over the rotation. Moreover, according to Section 2 the reorientation frequency of a given rotational process should exceed the frequency-width of the absorption line if a unique line width is to exist for that process. In discussing the characteristics of the resonance in moving systems, it is assumed henceforth that this criterion is satisfied.

4. ROTATING PAIRS OF NUCLEAR MAGNETS

The considerations of the preceding section may be applied readily to an isoiated pair of like nuclei with spin 1/2 and internuclear separation r. The detailed line shape for the rigid lattice has been computed elsewhere;[9] the absorption line at fixed frequency consists of two components at magnetic fields given by

$$\mathbf{H}_0 = (h\nu/g\beta) \pm (3/2)\mu r^{-3}(3\cos^2\theta - 1). \tag{5}$$

If the two interacting nuclei move about an axis perpendicular to the line joining them as in Fig. 1, then in the expression for A_{jk} in Eq. (4)

$$3\cos^2\theta - 1 = 3\cos^2\phi \sin^2\theta' - 1,$$

where ϕ is the azimuthal or rotational angle of the internuclear vector OP about the rotation axis OA, which makes an angle θ' with the external field. For classical rotation, where $\phi = \omega t$, the average value of $\cos^2\phi$ over the rotation is 1/2, so that

$$\langle 3\cos^2\theta - 1 \rangle_{\text{rot}} = (3/2)\sin^2\theta' - 1 = (1/2)(1 - 3\cos^2\theta').$$

Thus, if the frequency of rotation $\omega/2\pi$ is larger than the frequency-width of the rigid-lattice resonance, then the corresponding absorption line has two components at

$$\mathbf{H}_0 = (h\nu/g\beta) \pm (3/4)\mu r^{-3}(1 - 3\cos^2\theta'). \tag{6}$$

If the two nuclei are in an n-fold potential

$$V(\theta, \phi) = (V_0/2)(1 + \cos n\phi),$$

tunneling may occur as an increasing temperature populates the higher levels within the minima or as the

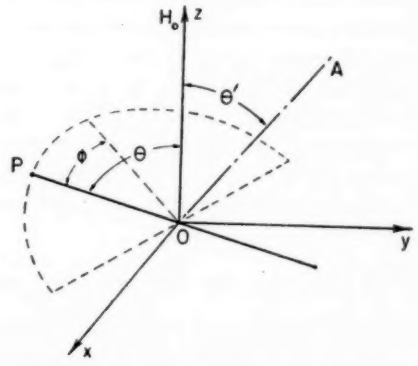

FIG. 1. Model for a nuclear pair in motion about an axis perpendicular to the internuclear axis.

[9] G. E. Pake, J. Chem. Phys. **16**, 327 (1948).

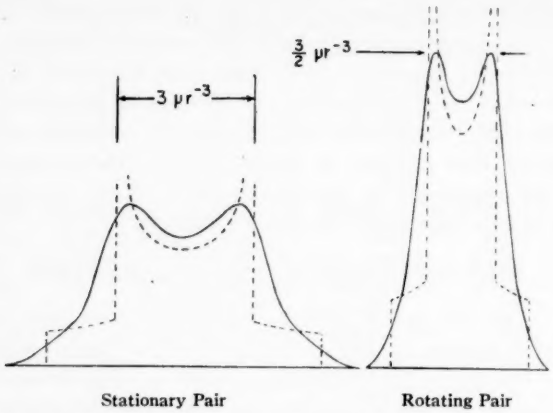

FIG. 2. Theoretical line shapes for a nuclear pair with spin 1/2 when stationary and when in motion about an axis perpendicular to the internuclear axis.

potential is altered by lattice changes. In this event, one considers that the system may be found in each of the n minimal positions with equal probability. For $n \geqslant 3$, the expectation value of $\cos^2\phi$ is also 1/2 over the eigenfunctions

$$\psi = \sum_{r=-\infty}^{\infty} a_r e^{ir n\phi}$$

corresponding to a rigid restricted plane rotor in such a potential.[10] In this respect, tunneling is indistinguishable from classical rotation; Eq. (6) gives the doublet positions for both cases and shows the doublet separation is half as great as for the stationary pair.

The dependence of the splitting in Eq. (6) on the orientation of the system with respect to $\mathbf{H}_0$ is similar in form to that in Eq. (5), the axis of rotation replacing the internuclear vector in specifying the orientation. The similarity is more complete for a powder sample, since random orientation of microcrystals provides all values of either θ or θ', whatever the state of motion. For a powdered solid in which the internuclear vector of the isolated pair is stationary at low temperatures but rotates or tunnels at higher temperatures, the absorption line should undergo a transition, becoming half as wide and correspondingly more intense at higher temperatures. The two curves of Fig. 2 represent calculated[9] line shapes corresponding to such a transition. In 1,2-dichloroethane, discussed in Section 7, the proton resonance undergoes just such a transition in which the line retains essentially the same shape but reduces to one-half the rigid-lattice width and becomes noticeably more intense.

5. EFFECT OF MOTION ON THE SECOND MOMENT

A spin system consisting of three protons situated at the vertices of an equilateral triangle occurs in organic molecules containing methyl (CH_3-) groups. The detailed line structure for an isolated triangular system in rotation about an axis normal to its plane may be determined using the foregoing methods. This problem, as well as its much more difficult counterpart for the rigid lattice, is treated in detail in the accompanying paper by Andrew and Bersohn.[11]

Further additions to the elementary spin system so complicate the detailed analysis that one is led to include the effects of nuclear motion in Van Vleck's calculation of the second moment of the absorption line. The considerations of Section 3 permit us to write Eq. (7) of I as

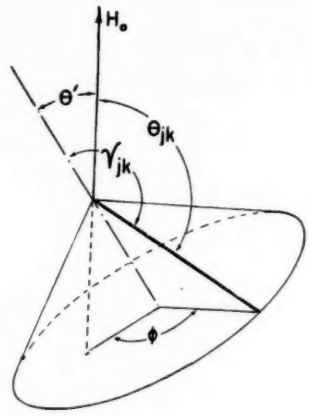

FIG. 3. Model for a nuclear pair in motion about any axis.

$$\Delta H_2^2 = (3/2)I(I+1)N^{-1}g^2\beta^2 \sum_{j>k} \langle 3\cos^2\theta_{jk} - 1\rangle^2 r_{jk}^{-6}$$

$$+ (1/3)N^{-1}\beta^2 \sum_{j>f} I_f(I_f+1)g_f^2\langle 3\cos^2\theta_{jf} - 1\rangle^2 r_{jf}^{-6}. \quad (8)$$

Here N is the number of nuclei at resonance in the elementary system of spins, and the subscripts f refer to all other nuclear species in the elementary system. The pointed brackets denote the average value of the orbital factor over the motion.

We treat first a classical rotation involving the azimuthal angle ϕ as in Fig. 3. The addition theorem for spherical harmonics[12] yields

$$\langle P_l(\cos\theta_{jk})\rangle_\phi = P_l(\cos\theta')P_l(\cos\gamma_{jk}), \quad (9)$$

the subscript ϕ denoting an average over the azimuthal angle. The angle γ_{jk} is the angle between the axis of rotation of r_{jk} and r_{jk} itself. For $l=2$, Eq. (9) becomes

$$\langle 3\cos^2\theta_{jk} - 1\rangle_\phi = (1/2)(3\cos^2\theta' - 1)(3\cos^2\gamma_{jk} - 1) \quad (10)$$

and the second moment for a system rotating about an

[10] R. Bersohn (private communication); a similar argument holds for the general potential $V(\theta,\phi) = \sum_{r=-\infty}^{\infty} V_r e^{ir n\phi}$.

[11] E. R. Andrew and R. Bersohn, J. Chem. Phys. **18**, 159 (1950).

[12] See e.g. H. Margenau and G. M. Murphy, *The Mathematics of Physics and Chemistry* (D. Van Nostrand Company, Inc., New York, 1943), p. 108, Eq. 3-61.

axis making an angle θ' with $\mathbf{H}_0$ is

$$\Delta H_2^2=(\tfrac{1}{4})(3\cos^2\theta'-1)^2[(\tfrac{3}{2})I(I+1)N^{-1}g^2\beta^2 \times\sum_{j>k} r_{jk}^{-6}(3\cos^2\gamma_{jk}-1)^2+(\tfrac{1}{3})N^{-1}\beta^2 \times\sum_{j>f} I_f(I_f+1)g_f^2 r_{jf}^{-6}(3\cos^2\gamma_{jf}-1)^2]. \quad (11)$$

In crystal powders, the axes of rotation are randomly distributed over the sphere of directions; the total effect of all microcrystals is found by averaging over the various values of θ'.

Since $(1/4)(3\cos^2\theta'-1)^2$ averaged over a sphere gives

$$\int_{\theta'=0}^{\theta'=\pi} \tfrac{1}{4}(3\cos^2\theta'-1)^2(\tfrac{1}{2}\sin\theta' d\theta')=\tfrac{1}{5},$$

the second moment for a powder is

$$(\Delta H_2^2)_{\text{powder}}=\frac{1}{4}\left[\frac{6}{5}I(I+1)N^{-1}g^2\beta^2 \times\sum_{j>k} r_{jk}^{-6}(3\cos^2\gamma_{jk}-1)^2+\frac{4}{15}N^{-1}\beta^2 \times\sum_{j>f} I_f(I_f+1)g_f^2 r_{jf}^{-6}(3\cos^2\gamma_{jf}-1)^2\right]. \quad (12)$$

For the special case in which all γ_{jk} and γ_{jf} are $\pi/2$, that is, if the rotational axis is perpendicular to all internuclear vectors which figure significantly in the broadening, Eq. (12) reduces to the statement that the second moment for a powder in which such rotation occurs is one-fourth as great as if the lattice were rigid. In the more general case, one applies the factor

$$F(\gamma)=\tfrac{1}{4}(3\cos^2\gamma_{jk}-1)^2,$$

plotted in Fig. 4, to the individual terms in the summation for the rigid lattice.

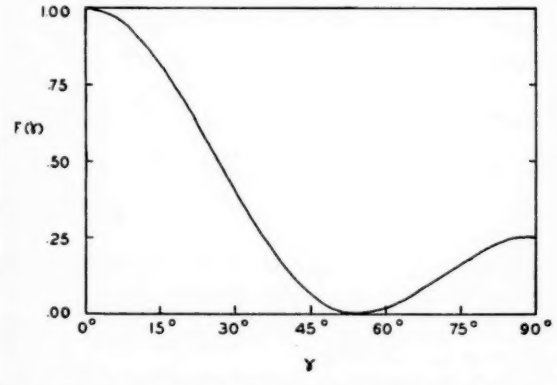

FIG. 4. The dependence of the second moment on the angle γ between the internuclear axis and the axis of motion.

The similarity noted in Section 4 between classical rotation and n-fold tunneling for $n\geqslant 3$ applies also to the effect of motion on the second moment. Other cases may be treated in the same fashion by obtaining the expectation values over the proper orbital eigenfunctions for the terms $\langle 3\cos^2\theta-1\rangle^2$ in Eq. (8).

6. EXPERIMENTAL DETAILS

The experimental apparatus and procedure are described in I. Determinations of the second moment give perhaps more insight into a rotational process than do measurements of the line width. However, the calculation of the second moment requires a detailed plot of the absorption line or its derivative,[8] and our cooling apparatus limited such data to fixed temperatures, in this instance room temperature and temperatures corresponding to liquid nitrogen and acetone-dry ice cooling. At intermediate temperatures only the line width was recorded; a single measurement usually required less than 15 seconds. The apparent line width is increased if the field modulation is not sufficiently smaller than the true line width. In graphs of δH *versus* temperature, the modulation is indicated by a vertical arrow which applies to all measurements in the temperature interval between it and the following arrow.

The intermediate temperatures were reached by permitting the cooling apparatus and sample, previously cooled with liquid nitrogen, to warm. The initial (maximum) rate of warming was about 4° per minute. Above 205°K, where acetone-dry ice was used, the warming rate was greatly reduced by the added heat capacity of the acetone and the smaller temperature differential. The temperature was measured by means of a copper-constantan thermocouple junction placed directly in the sample.

The probable error in a line width measurement is estimated at ± 0.3 gauss, and that in temperature is about 1°. Although most determinations were made during warming, occasional checks during cooling showed no hysteresis effects, within the limits of accuracy of the measurements. Of the samples used and not previously referred to in I, most were from commercial sources and of C.P. grade. The dimethyl mercury was infra-red spectroscopically pure and had a boiling point of 92.3–92.5°C. The 2,2-dimethyl pentane (neopentane) was prepared by and available through

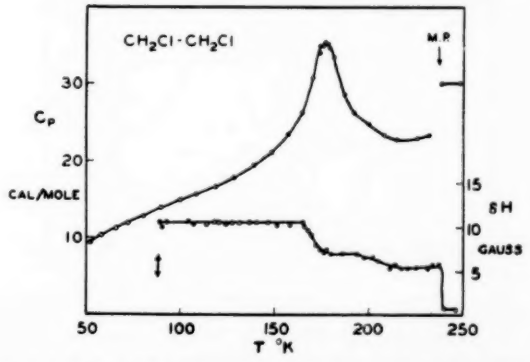

FIG. 5. Line width *versus* temperature and heat capacity curves for 1,2-dichloroethane.

the courtesy of K. Nozacki; its boiling point was 9.0–9.5°C. The ethanol was absolute, U.S.P.; and the methylamine was anhydrous from Bender and Hobein, München, Germany.

7. 1,2-DICHLOROETHANE: TWO ROTATING PAIRS OF NUCLEAR MAGNETS

The interactions between proton magnetic moments in the 1,2-dichloroethane molecule are found in I to be confined largely to the proton pair in each $-CH_2Cl$ group. Figure 5 shows the experimental line width, δH, of the proton resonance as a function of temperature and includes the heat capacity curve.[13] Detailed line shapes, measured at temperatures of 90° and 205°K are reproduced in Fig. 6. Ordinates of the two curves are not in the same units. The specific heat anomaly at 177°K is approximately coincident with the transition in line width from 10.5 gauss to 6.5 gauss between 165°K and 180°K. A further small decrease of about a gauss occurs near 210°K, above which the line width remains at 5.5 gauss up to the expected sharp transition at the melting point, 238°K.

In I, the 90°K curve of Fig. 6 is integrated and fitted to a computed curve, like that of Fig. 2, which corresponds to a proton-proton separation of 1.71 ±0.02A in a stationary $-CH_2Cl$ group. The constancy of the line width between 90°K and 165°K indicates that the molecule remains effectively stationary in the lattice over that temperature interval. The transition near 177°K to a line approximately half as wide suggests motion about an axis perpendicular to the vector between protons. Further evidence is presented by the curves of Fig. 6, which agree in form with those of Fig. 2 and which correspond closely to the respective

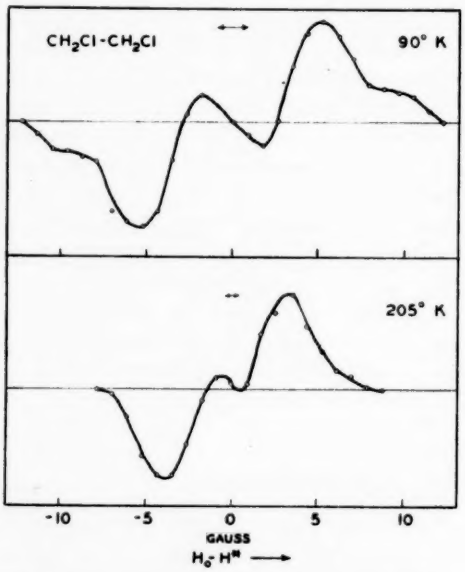

FIG. 6. Derivative curves of the proton magnetic resonance absorption line in 1,2-dichloroethane at 90°K and 205°K.

[13] K. S. Pitzer, J. Am. Chem. Soc. **62**, 331 (1940).

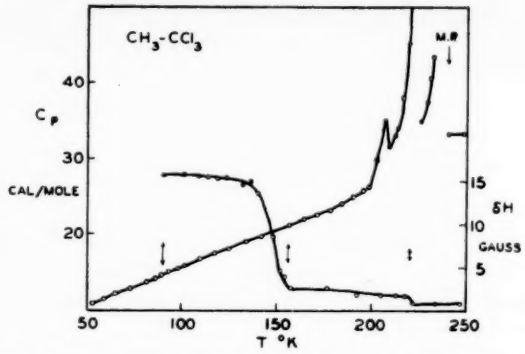

FIG. 7. Line width *versus* temperature and heat capacity curves for 1,1,1-trichloroethane.

doublet separations, $3\mu r^{-3}$ and $(3/2)\mu r^{-3}$, of Eqs. (5) and (6). One concludes that in solid 1,2-dichloroethane, at temperatures between 165°K and its melting point of 238°K, there is rotation or threefold or sixfold tunneling about an axis perpendicular to the lines connecting proton pairs at each end of the molecule. This axis is presumably not quite along the C−C bond, for the heavier Cl atoms tip the principal axis; in any event the axis remains perpendicular to the internuclear vector as required by this interpretation of the data.

The information gained from the line shape in 1,2-dichloroethane affords an opportunity for comparison with the more generally useful second moment considerations. The rigid lattice second moment of 18.2 gauss² (see I) may be divided into three major parts: the pair interaction, 14.2 gauss²; the interaction with other nuclear magnets in the same molecule, 2.5 gauss²; interactions with neighboring molecules, 1.5 gauss². Applying Eq. (12), the postulated motion should reduce the 14.2 gauss² contribution by 1/4, and the remaining 4 gauss² by approximately 2/3, giving $\Delta H_2^2 = 6.3$ gauss². Three detailed line plots (including that of Fig. 6) yield 7.2, 6.9, and 5.8 gauss² at 205°, 210°, and 218°K, respectively, reasonably consistent with the proposed rotation or tunneling.

The implication of the above data that there is no rotation about an axis perpendicular to the C−C bond below the melting point is consistent with dielectric constant measurements.[14]

The heat capacity anomaly is not fully explained by the motion that narrows the resonance. According to Section 2, the reorientation frequency at the center of the line-width transition is approximately the frequency-width of the rigid lattice resonance:

$$\nu_c(177°\text{K}) \cong \delta\nu = (\nu/H_0)\delta H = 40 \text{ kc/sec}.$$

Such a frequency is too low to account in itself for the heat capacity anomaly. However, it might initiate a change in crystal structure which could account for the anomaly.

These experiments do not indicate whether the observed motion involves rotation of one end of the

[14] A. H. White and S. O. Morgan, J. Chem. Phys. **5**, 655 (1937).

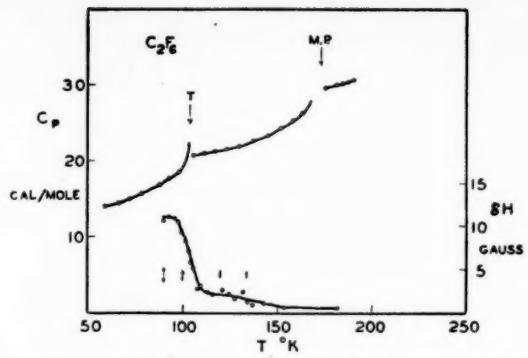

FIG. 8. Line width *versus* temperature and heat capacity curves for perfluoroethane.

molecule with respect to the other as well as motion of the molecule as a whole. The barrier to internal rotation[15] in the gas is about 3000 cal. mole^{-1}; since the heat of fusion is only 2100 cal. mole^{-1}, it is suggested that the predominant motion involves the molecule as a whole.

8. 1,1,1-TRICHLOROETHANE

The absorption line derivative of the proton resonance for this substance at 90°K has been given in I and is discussed in the accompanying paper.[11] Line width is plotted against temperature in Fig. 7, along with heat capacity data.[16] Both the shape[11] and the observed second moment,[4] 18.7 gauss^2, of the absorption line at 90°K correspond to a rigid lattice, with slight narrowing possibly attributable to tunneling of the CH_3-group with respect to a fixed —CCl_3 group. The rigid lattice second moment computed from theory is about 23 gauss^2, of which 21.2 gauss^2 arise from the three protons in the methyl group.

The line width above the transition which occurs near 145°K is much too small to correspond to the expectation for a simple motion of the methyl group about the axis of least moment of inertia. The low value of 0.7 gauss^2 for the second moment of an absorption line plotted at 208°K supports this view. Line shape studies at intermediately low temperatures would be helpful in attempting to settle on the combination of motions responsible for the narrowing.

At 220°K, the line narrows further to a width of about a gauss which persists through the melting point at 240.2°K. Both the specific heat[16] and the dielectric constant[17] confirm the excitation of new degrees of freedom: the former exhibits a 1786 cal. mole^{-1} anomaly at 224.2°K and the latter rises sharply with increasing temperature at 224°K, where the crystal also becomes isotropic. Gradual decrease of the dielectric constant below 220°K as temperature is decreased to 150°K supports the presence of residual low frequency motion below the transition.

[15] W. D. Gwinn and K. S. Pitzer, J. Chem. Phys. **16**, 303 (1948).
[16] Rubin, Levedahl, and Yost, J. Am. Chem. Soc. **66**, 279 (1944).
[17] A. Turkevich and C. P. Smyth, J. Am. Chem. Soc. **62**, 2648 (1940).

9. PERFLUOROETHANE

The derivative of the fluorine absorption line at 27.22 Mc/sec. is given in I for this substance at 90°K. Line width and the heat capacity[18] are plotted against temperature in Fig. 8. The second moment of 15.1 gauss^2 observed at 90°K corresponds to a rigid lattice.[4] Between 95°K and 110°K the line narrows from 11 gauss to 2.5 gauss, remaining fairly constant up to about 130°K where it further decreases to 0.5 gauss and then remains unchanged through the melting point, 173°K.

The first line-width transition parallels the heat capacity anomaly[18] at 104°K. The width between 130° and 160°K seems too low to correspond to motion about the C—C axis alone, but second moment values are necessary to settle this point. The further drop at 135°K evidently marks the onset of low frequency reorientation qualitatively similar to that in the liquid, since the line width is unchanged on melting.

10. THE TRIANGULAR ROTOR

Several absorption lines observed at 90°K probably correspond to rotation or tunneling of a triangular configuration of equidistant protons about an axis normal to their plane. Methyl groups contributed such lines in acetonitrile, methyl iodide, nitromethane, and dimethyl mercury; ammonia also gave such a line.

Figure 9 reproduces the derivative curve of the proton resonance in acetonitrile; the second moment is 6 gauss^2. The other compounds showed similar shape, though the fine structure was less well defined. Second moments observed at 90°K appear in Table I, along with computed values corresponding to motion about the C_3 axis of the molecules. Intermolecular broadening is not included in these computations, which are based on C—H distances of 1.10A and tetrahedral angles in the methyl groups. The N—H bond in NH_3 is taken[19] to be 1.014A and the pyramid height 0.381A. Allowing for

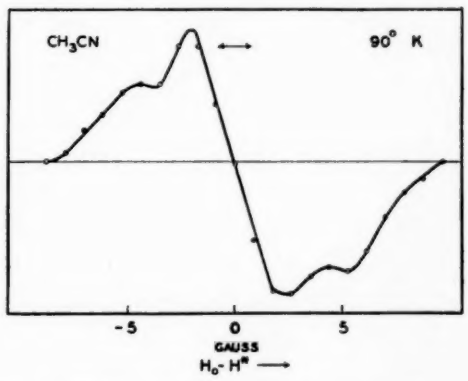

FIG. 9. Derivative curve of the proton magnetic resonance absorption line in acetonitrile at 90°K.

[18] E. L. Pace and J. G. Aston, J. Am. Chem. Soc. **70**, 566 (1948).
[19] G. Herzberg, *Infrared and Raman Spectra of Polyatomic Molecules* (D. Van Nostrand Company, Inc., New York, 1945), p. 439.

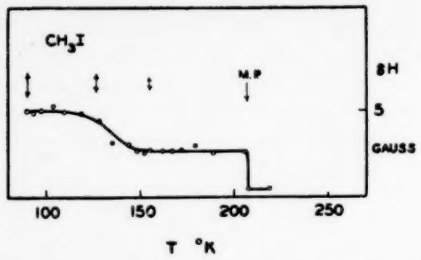

FIG. 10. Line width *versus* temperature curve for methyl iodide.

intermolecular broadening, the proposed motion is reasonably well supported by the table; computed second moments would be four times as great for the stationary molecule. The detailed analysis[11] of the line shape for acetonitrile indicates also the existence of the proposed motion.

Methyl iodide is the only compound of the group for which the line width was measured as a function of temperature. As indicated by Fig. 10, rotation, possibly of the C−I vector, sets in at 125°K. No dielectric constant data known to the authors extends below 175°K to bear on the question. However, the dielectric constants of nitromethane[20] and ammonia[2, 21] do not indicate rotations about an axis perpendicular to the figure axis, nor do their heat capacity curves[22, 23] show any anomalies.

TABLE I. Observed and theoretical values of ΔH_2^2 for triangular rotors.

Sample	Theoretical intramolecular	Observed
CH_3CN	5.3 gauss^2	6.0 gauss^2
CH_3I	5.4	8.4
CH_3NO_2	5.4	7.0
$Hg(CH_3)_2$	5.3	8.7
NH_3	9.7	9.7

11. OTHER COMPOUNDS STUDIED

The change of line width with temperature was examined for the proton resonance in a number of other compounds. Various data are reproduced in Figs. 11, 12, and 13.

Ammonium salts.—Line-width transitions were first observed in detail for the proton resonance in several ammonium compounds. A summary of these data has been presented earlier.[6]

2,2-Dimethyl propane.—The heat capacity[24] is compared with the line-width curve in Fig. 11. Our lowest attainable temperature was incapable of freezing out whatever motions lead to the 2.5 gauss line between 93°K and 193°K. The decrease to 1.5 gauss at 200°K implies further rotation of the molecule. One suspects that the nearly spherical symmetry of the molecule permits a high degree of rotational freedom to which the narrow lines in this solid may be attributed. The heat capacity anomaly at 140°K has no counterpart in the line width. Some evidence exists for a change in crystal form near this temperature.[25]

Methanol.—The molecule is interesting in that the line width (Fig. 12) is insensitive to temperature between 85°K and the melting point at 175.2°K, yet a specific heat anomaly[26, 27] and a dielectric constant transition[28] have been reported between 155°K and 160°K. It is possible[29] that these effects are associated with rotation of the hydroxyl group within the solid, as suggested by the small entropy of transition. If so, the line width, predominately contributed by the methyl group which might continue in motion, would be little affected.

Ethanol.—Whereas the line width in methanol does not become small until melting occurs, that in ethanol (Fig. 12) drops from a value of 10 gauss at 90°K to a width fixed by magnet inhomogeneities at a temperature 35°K below the melting point. No anomalous behavior of the heat capacity[26] has been observed above 90°K and detailed dielectric data below the melting point are lacking.

Acetone.—The methyl groups in this molecule apparently undergo low-frequency reorientation even at 90°K. The gradual decrease in line width (Fig. 12) to the melting point suggests a slow onset of rotation, in agreement with the frequency dependence[30] of the dielectric constant down to about 145°K.

Methylamine.—This molecule is of interest in con-

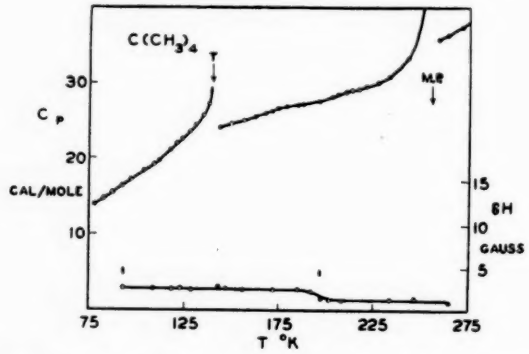

FIG. 11. Line width *versus* temperature and heat capacity curves for 2,2-dimethyl propane.

[20] C. P. Smyth and W. S. Walls, J. Chem. Phys. **3**, 557 (1935).
[21] C. S. Hitchcock and C. P. Smyth, J. Am. Chem. Soc. **55**, 1296 (1933).
[22] W. M. Jones and W. F. Giauque, J. Am. Chem. Soc. **69**, 983 (1947).
[23] Clusius, Hiller, and Vaughen, Zeits. f. physik. Chemie **B8**, 427 (1930).
[24] J. G. Aston and G. H. Messerly, J. Am. Chem. Soc. **58**, 2354 (1936).
[25] W. Wahl, Zeits. f. physik. Chemie **88**, 129 (1914).
[26] G. S. Parks, J. Am. Chem. Soc. **47**, 338 (1925).
[27] K. K. Kelley, J. Am. Chem. Soc. **51**, 180, 1145 (1929).
[28] C. P. Smyth and S. A. McNeight, J. Am. Chem. Soc. **58**, 1597 (1936).
[29] C. S. Hitchcock and C. P. Smyth, J. Am. Chem. Soc. **56**, 1084 (1934).
[30] S. A. McNeight and C. P. Smyth, J. Am. Chem. Soc. **58**, 1718 (1936).

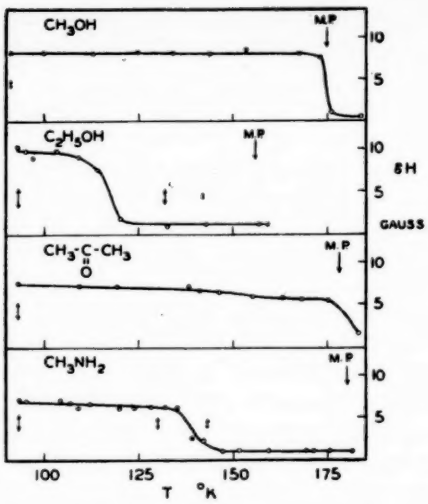

FIG. 12. Line width *versus* temperature curves for methanol, ethanol, acetone and methylamine.

nection with the high rotational mobility reported in I for ethane and disilane in the solid state.

The second moment of the proton resonance observed at 90°K is 20 gauss,[2] intermediate between the 40 gauss[2] expected for a rigid lattice and the 13 gauss[2] expected for motion about the C−N axis. There is a small decrease in the line width (Fig. 12) from 7 gauss at 90°K to 6 gauss at 125°K; a second moment measurement at the latter temperature is desirable. The line becomes narrow between 135°K and 150°K, remaining so up through the melting point at 180°K. The dielectric data[30] have been interpreted as opposing the proposed existence of molecular rotation in the solid, although the dielectric constant is frequency dependent. Hysteresis effects in the heat capacity[31] further obscure the state of affairs in this substance.

Ethyl halides; Impurity effects.—Figure 13 reproduces line-width curves for ethyl chloride, ethyl bromide, and ethyl iodide; these curves presumably indicate impurity effects. For all three, the dotted curves represent data obtained from old samples which had been opened and standing in the laboratory for several months; the bromide and iodide were deeply colored by free halogen. Freshly opened samples yielded the solid curves.

Both the observed line shape and second moment of ethyl chloride at 90°K indicate a rigid lattice. Although additional second moment data are needed to verify the conclusion, each curve has a transition from a probable rigid-lattice line to one about half as wide, which may correspond to rotation or tunneling about the C−C axis. The effect of impurity on the rate at which reorientation frequencies become great is pronounced.

The transitions in the purer samples occur within 10° of each other, near 115°K, and over like intervals of about 30°. No anomaly is observed in the low temperature heat capacity[32] of ethyl chloride.

12. DISCUSSION

Some general correlations and queries arise from the data reported above. It appears that light symmetrical groups, even when attached to a heavier framework, can exhibit rotation or tunneling about their figure axes for temperature ranges as great as 100° to 150° below the melting point of the solid. The fact that dimethyl mercury shows motion about the linear C−Hg−C axis at least 150° below its melting point while 1,1,1-trichloroethane does not at only 100° below its melting point suggests that internal hindrance is also important. The results concerning the dependence of motion, over two or three degrees of rotational freedom, on the symmetry of a system are in general accord with conclusions drawn from other data.[2] In addition, molecules such as ethane, disilane, perfluoroethane, and methylamine appear to have unexpected rotational mobility in the solid. Such data as these indicate experimentally the various degrees of hindrance to motion offered by the potential barriers within solids.

More detailed information regarding the hindering potentials should follow from refinements of the experimental methods and qualitative notions developed thus far. In a given system, the structure of an absorption line depends on the frequency and type of motion, which, in turn, are functions of temperature and the potentials in the solid. Therefore, in principle one should be able to relate the temperature dependence of

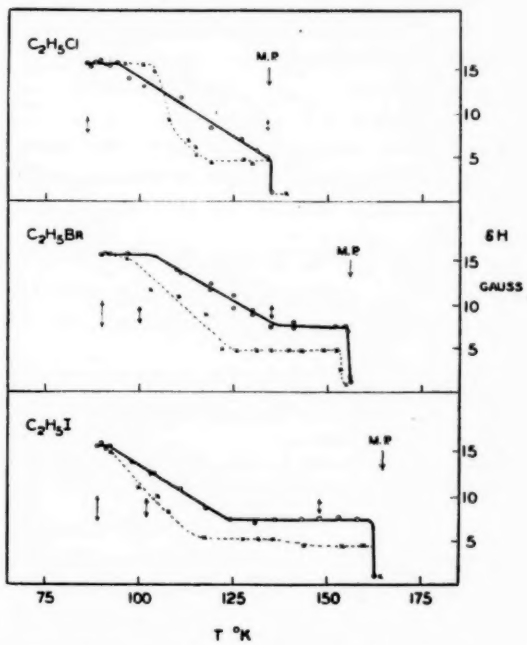

FIG. 13. Line width *versus* temperature curves for ethyl chloride, bromide and iodide.

[31] Aston, Siller, and Messerly, J. Am. Chem. Soc. **59**, 1743 (1937).

[32] J. Gordon and W. F. Giauque, J. Am. Chem. Soc. **70**, 1506 (1948).

the line structure to the potentials. Semi-quantitative information is obtainable from the present data and the earlier results of Bloembergen, Purcell, and Pound.[7] Equation (1) of Section 2 was obtained via BPP as a description of the line width in terms of the spectrum of random motions comprising thermal agitation and expresses the result that $\delta\nu$, for a perfectly homogeneous field, approaches zero asymptotically as ν_c increases above the rigid-lattice width A. To treat a transition from one definite line width to a narrower line characteristic of a specialized motion, an *ad hoc* adjustment of Eq. (1) is obtained by writing[33]

$$(\delta\nu)^2 = B^2 + C^2(2/\pi)\tan^{-1}(\alpha(\delta\nu/\nu_c)). \qquad (15)$$

The rigid lattice width is then

$$A = (B^2 + C^2)^{1/2}.$$

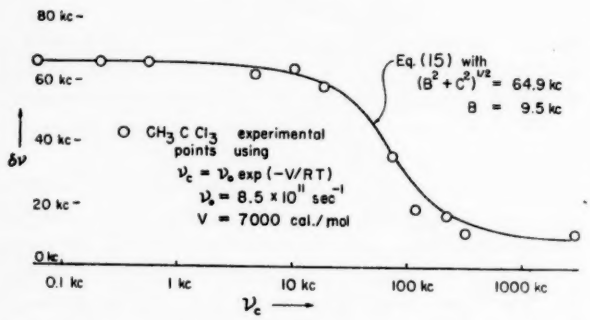

FIG. 14. The correlation frequency ν_c as a function of the line width $\delta\nu$, in frequency, for 1,1,1-trichloroethane.

In Fig. 14, the experimental line width *versus* temperature curve is fitted to Eq. (15) by assuming that ν_c varies with temperature as

$$\nu_c = \nu_0 e^{-V/RT}, \qquad (16)$$

a form met in the theory of rate processes.[34] The quantity V is analogous to the activation energy and should be closely related to the barrier hindering rotation.

The curve in Fig. 14 is fitted by $\nu_0 = 8.5\times10^{11}$ sec.$^{-1}$ and $V = 7000$ cal. mole^{-1}. These numbers probably have no significance beyond order of magnitude, but they are surprisingly near the values one can obtain from an approximate treatment[35] of the hindered rotor. The success of so rudimentary an effort as that associated with Fig. 14 suggests that rigorous theory might be developed along these lines. One should note that Eq. (16) ought not in general to be a rigorously valid expression for the reorientation or correlation frequency if tunneling is the mechanism involved; in this event ν_c would be expressed as a sum of properly weighted tunneling rates over the various populated levels within the n-fold potential well.

Another aspect of interest concerning the line-width transitions in the solid is whether or not they are cooperative phenomena. Although the potentials restricting motion are probably a function of that motion, low frequency motions such as we observe do not appear to be cooperatively coupled to as great an extent as melting phenomena. Solids such as methanol and the ethyl halides which have pre-melting broad lines, exhibit line-width transitions at the melting point that are practically discontinuous. In contrast the lower temperature line-width transitions are very gradual indeed. Moreover, the approximate non-cooperative treatment outlined above appears capable, on further refinement, of affording a reasonable interpretation of the observations. The coincidence of heat capacity and line-width transitions suggests that if the rotational frequency is the non-cooperative, slowly increasing inverse function of line width portrayed in Fig. 14, then the excess heat at the transitions must be due to structural changes. In this connection, it is to be noted that most such coincidences occur when the motion involves a fairly large moment of inertia and spatial extent, and then there is usually a concurrent, perhaps cooperative change in crystal structure.

13. ACKNOWLEDGMENT

We wish to express our appreciation to Professors G. B. Kistiakowsky and E. M. Purcell for their continued interest and support of this research as well as for their many helpful suggestions. It is also a pleasure to acknowledge the assistance of Mr. Richard Bersohn in developing some of the mathematical aspects.

Facilities for the experimental work were provided in part through a Frederick Gardner Cottrell Special Grant-in-Aid from the Research Corporation.

[33] R. Bersohn has pointed out that by introducing a separate correlation time associated with the specialized motion into the considerations of BPP, Eq. (15) can be derived explicitly and the factors B and C evaluated.

[34] Glasstone, Laidler, and Eyring, *The Theory of Rate Processes* (McGraw-Hill Book Company, Inc., New York, 1941), p. 548.

[35] Eyring, Walter, and Kimball, *Quantum Chemistry* (John Wiley and Sons, Inc., New York, 1944), p. 358.

The Thermodynamics of Flow Systems*

CHARLES F. CURTISS AND JOSEPH O. HIRSCHFELDER
Department of Chemistry and Naval Research Laboratory, University of Wisconsin, Madison, Wisconsin
(Received May 16, 1949)

The rate of change of entropy in a flow system is evaluated explicitly taking into account heat conductivity, viscosity, diffusion, and chemical reactions. The equations are developed rigorously from the kinetic theory of gases.

ALTHOUGH the usual discussion of entropy and the second law of thermodynamics is restricted to the consideration of systems in mechanical equilibrium, the concepts are useful in the treatment of nonequilibrium systems. In this paper we will consider the entropy and a statement of the second law applying to general hydrodynamic systems in which chemical reactions are taking place. Several recent papers[1] have considered this problem from the point of view of classical thermodynamics. Here we will use the methods of statistical mechanics making use of the results of kinetic theory. Since, at the present time, kinetic theory is restricted to the consideration of nearly perfect gases, our present treatment is restricted to this case. However, many of the conclusions are independent of this limitation. The results in general confirm those of the previous investigators, but the explicit appearance of the various diffusion terms is novel.

From the kinetic theory of gases we can obtain the hydrodynamic equations of change, along with expressions for the various transport coefficients in terms of intermolecular forces. Let n_i be the number of moles of species i per cm^3 of gas; ρ the density of the gas; ϵ the internal energy per gram of gas; and $\mathbf{v}$ be the mass average velocity. Then the equations of change can be written in terms of $\mathbf{q}$, the total heat flux vector; P, the pressure tensor; K_i, the rate of formation of molecules of i by chemical reaction in moles per cm^3; and $\mathbf{V}_i$, the diffusion velocity of species i. These latter quantities, which describe the irreversibility of the hydrodynamic flow, are discussed in more detail later. We shall use the operator D/Dt to indicate the time rate of change of a property following the fluid element. In terms of $\partial/\partial t$ the rate of change at a particular point:

$$D/Dt=\partial/\partial t+\mathbf{v}\cdot\nabla. \tag{1}$$

The equations of change are

(1) the equation of continuity for each component i

$$\rho\frac{D(n_i/\rho)}{Dt}=K_i-\nabla\cdot n_i\mathbf{V}_i, \tag{2}$$

(2) the over-all equation of continuity

$$\rho\frac{D(1/\rho)}{Dt}=\nabla\cdot\mathbf{v}, \tag{3}$$

(3) the equation of motion

$$\rho\frac{D\mathbf{v}}{Dt}=-\nabla\cdot\mathrm{P}, \tag{4}$$

(4) the energy balance equation**

$$\rho\frac{D\epsilon}{Dt}=-\nabla\cdot\mathbf{q}-\mathrm{P}:\nabla\mathbf{v}. \tag{5}$$

In a treatment of matter in (gross) mechanical equilibrium one can define "entropy" and then through a statistical mechanical analysis prove the second law. In a similar way one can use nonequilibrium statistical mechanics, i.e., kinetic theory, to describe flow processes and actually evaluate the irreversible changes in entropy. Under the nonequilibrium conditions it is possible to redefine the term "entropy." The definition should satisfy two requirements: (1) it must reduce to the usual definition under equilibrium conditions, and (2) it should lead to an easily interpreted statement of the second law. Actually the static definition of entropy is quite satisfactory. Letting σ be the entropy per gram, we have

$$\sigma=\textstyle\sum_i(n_i/\rho)\bar{S}_i, \tag{6}$$

where $\bar{S}_i$ is the partial molar entropy

$$\bar{S}_i=S_i^{(0)}-R\ln p_i, \tag{7}$$

$S_i^{(0)}$ being the entropy per mole at the prevailing local temperature, T, and at unit pressure, and p_i being the partial pressure of i,

$$p_i=n_iRT. \tag{8}$$

Here R is the usual gas constant.

We further introduce the chemical potential or partial molar free energy,

$$\mu_i=F_i^{(0)}+RT\ln p_i. \tag{9}$$

* This work was carried out under Contract NOrd 9938 with the United States Navy Bureau of Ordnance.

[1] C. Eckart, Phys. Rev. **58**, 267, 269, 919 (1940). R. C. Tolman and P. C. Fine, Rev. Mod. Phys. **20**, 51 (1948).

** The tensor operation $\mathrm{A}:\mathrm{B}$ is defined in the following manner $\mathrm{A}:\mathrm{B}=\sum_{ij}\mathrm{A}_{ij}\mathrm{B}_{ji}$.

Here $F_i^{(0)}$ is the Gibbs free energy at temperature, T, and unit pressure. In terms of these definitions and the usual thermodynamic relations it follows that

$$\frac{D\epsilon}{Dt}=T\frac{D\sigma}{Dt}-p\frac{D(1/\rho)}{Dt}+\sum_i \mu_i\frac{D(n_i/\rho)}{Dt}, \tag{10}$$

where p is the static pressure (as distinct from the pressure tensor P).

The rate of increase of entropy of a particular small element of volume moving with the fluid is

$$\rho(D\sigma/Dt). \tag{11}$$

This increase is made up of the following terms: (1) the reversible increase of entropy due to conduction of thermal energy,

$$\nabla\cdot[(\lambda/T)\nabla T], \tag{12}$$

where λ is the coefficient of thermal conductivity; (2) the reversible increase of entropy due to mass transport

$$-\nabla\cdot\sum_i n_i\bar{S}_i\mathbf{V}_i \tag{13}$$

(3) the increase in entropy due to irreversible processes, G. In terms of these quantities we have

$$\rho(D\sigma/Dt)-\nabla\cdot[(\lambda/T)\nabla T]+\nabla\cdot\sum_i n_i\bar{S}_i\mathbf{V}_i=G. \tag{14}$$

It will be shown that

$$G\geqslant 0. \tag{15}$$

This implies that the entropy of every element of the fluid changes at a rate that is algebraically greater than (or equal to) the changes caused by the reversible processes. This is stronger than the second law of thermodynamics which only requires that this be true of the entire system. If we had considered some other mechanisms for the transfer of energy, such as radiation, the stronger statement would no longer apply.

One obtains an expression for G from Eq. (10), then using the equations of change, Eqs. (2), (3), and (5), we find

$$G=-\frac{1}{T}\nabla\cdot\mathbf{q}-\nabla\cdot\left(\frac{\lambda}{T}\nabla T\right)+\frac{1}{T}(p\mathrm{I}-\mathrm{P}):\nabla\mathbf{v}$$

$$-\frac{1}{T}\sum_i \mu_i K_i+\sum_i\left[\frac{\mu_i}{T}\nabla\cdot n_i\mathbf{V}_i+\nabla\cdot n_i\bar{S}_i\mathbf{V}_i\right]. \tag{16}$$

The total heat flux vector[2] is made up of two terms, one due to heat conductivity, the other due to mass transport of energy:

$$\mathbf{q}=-\lambda\nabla T+\nabla\cdot\sum_i n_i H_i\mathbf{V}_i. \tag{17}$$

[2] This expression is a generalization of a result given by S. Chapman and T. G. Cowling, *The Mathematical Theory of Non-Uniform Gases* (Cambridge University Press, London, 1939), p. 145. The generalization is given by C. F. Curtiss and J. O. Hirschfelder, University of Wisconsin, CF-727. A small term depending on the coefficient of thermal diffusion appearing in the original expression is difficult to generalize. It is small and has been ignored. A compensating error is made in the expression for the diffusion velocity, Eq. (27).

Here H_i is the enthalpy per mole of substance i. Making use of Eq. (17), G can be written as the sum of four terms, each representing the irreversible entropy increase due to a particular physical process: heat conductivity, h; viscosity, v; diffusion, d; chemical reaction, c.

$$G=G_h+G_v+G_d+G_c, \tag{18}$$

where

$$G_h=\lambda(\nabla\ln T)^2, \tag{19}$$

$$G_v=(1/T)(p\mathrm{I}-\mathrm{P}):\nabla\mathbf{v}, \tag{20}$$

$$G_d=-(1/T)\sum_i\mathbf{V}_i\cdot\nabla p_i, \tag{21}$$

$$G_c=-(1/T)\sum_i\mu_i K_i. \tag{22}$$

We will discuss each of the four terms separately. Since each term is necessarily positive, it follows that G itself must be positive.

(a) Heat conductivity, G_h

It can be shown from the kinetic theory expressions that λ is positive. This is simply the requirement that thermal energy "flow downhill" and is one of the basic ideas of the second law. It is clear that G_h is essentially positive and represents the increase of entropy due to thermal conductivity.

(b) Viscosity, G_v

The usual expression for the pressure tensor is

$$\mathrm{P}=p\mathrm{I}-2\eta[(\nabla\mathbf{v})^{(S)}-\tfrac{1}{3}(\nabla\cdot\mathbf{v})\mathrm{I}] \tag{23}$$

where $(\nabla\mathbf{v})^{(S)}$ is the symmetric tensor obtained by averaging $\nabla\mathbf{v}$ with its transpose, and η is the coefficient of viscosity. The coefficient of viscosity is always positive. Using Eq. (23) and Eq. (20) we have

$$G_v=\frac{2\eta}{T}[(\nabla\mathbf{v})^{(S)}-\tfrac{1}{3}(\nabla\cdot\mathbf{v})\mathrm{I}]:\nabla\mathbf{v}. \tag{24}$$

The second tensor, $\nabla\mathbf{v}$, can be replaced by $(\nabla\mathbf{v})^{(S)}-\frac{1}{3}(\nabla\cdot\mathbf{v})\mathrm{I}$ since the first tensor is symmetric and traceless. Thus

$$G_v=\frac{2\eta}{T}[(\nabla\mathbf{v})^{(S)}-\tfrac{1}{3}(\nabla\cdot\mathbf{v})\mathrm{I}]:[(\nabla\mathbf{v})^{(S)}-\tfrac{1}{3}(\nabla\cdot\mathbf{v})\mathrm{I}]. \tag{25}$$

In this form we see that G_v is a sum of squares and hence

$$G_v\geqslant 0 \tag{26}$$

is a measure of the irreversible entropy increase due to the effect of viscous forces.

(c) Diffusion, G_d

An expression for the diffusion velocity, $\mathbf{V}_i$, of component i in a multicomponent mixture in terms of the binary diffusion constants, D_{ij}, is complicated. How-

ever, it is possible to show in general that[3]

$$\nabla\left(\frac{n_i}{n}\right)+\left(\frac{n_i}{n}-\frac{n_i m_i}{\rho}\right)\nabla \ln p=\sum_i \frac{n_i n_j}{n^2 D_{ij}}(\mathbf{V}_j-\mathbf{V}_i), \quad (27)$$

where $n=\sum_i n_i$ is the total number of moles per cm^3 and m_i is the molecular weight of i. Then, since the diffusion velocities are expressed relative to the mass average flow velocity,

$$\sum_i n_i m_i \mathbf{V}_i=0. \quad (28)$$

Thus we have

$$\frac{1}{p}\sum_i \mathbf{V}_i\cdot\nabla p_i=-\sum_{ij}\frac{n_i n_j}{2n^2 D_{ij}}(\mathbf{V}_j-\mathbf{V}_i)^2. \quad (29)$$

Thus from Eq. (21) we see that

$$G_d=\tfrac{1}{2}R\sum_{ij}\frac{n_i n_j}{nD_{ij}}(\mathbf{V}_i-\mathbf{V}_j)^2. \quad (30)$$

Since all the binary diffusion constants, D_{ij}, are positive, G_d is a sum of essentially positive terms and

$$G_d\geqslant 0. \quad (31)$$

This term represents the entropy increase due to diffusion.

(d) Chemical reactions, G_c

To understand the term G_c and show that it is essentially positive it is necessary to consider the various chemical reactions which might take place. Each one can be written in the stoichiometrical form

$$\beta_{1j}[1]+\beta_{2j}[2]+\cdots\rightarrow\eta_{1j}[1]+\eta_{2j}[2]+\cdots, \quad (32)$$

the β_{ij} and η_{ij} being integers and the $[i]$ indicating the ith species. Let the rate constant for the forward reaction be k_j and for the backward reaction k_j', so that the rate of the forward reaction is

$$k_j p_1^{\beta_{1j}} p_2^{\beta_{2j}}\cdots, \quad (33)$$

and similarly for the backward reaction. Then the total rate of formation of molecules of i by chemical reaction in moles per cm^3 is

$$K_i=\sum_j(\eta_{ij}-\beta_{ij})[k_j p_1^{\beta_{1j}} p_2^{\beta_{2j}}\cdots-k_j' p_1^{\eta_{1j}} p_2^{\eta_{2j}}\cdots] \quad (34)$$

the sum being over all "forward" reactions, the "backward" reactions being included by the presence of the second term. The equilibrium constant for a reaction is k_j/k_j' and can be written in terms of the free energy. Thus

$$\ln(k_j/k_j')=\sum_i(\eta_{ij}-\beta_{ij})[\mu_i-RT\ln p_i]. \quad (35)$$

[3] C. F. Curtiss and J. O. Hirschfelder, J. Chem. Phys. **17**, 550 (1949). Here we ignore the small contribution due to thermal diffusion. See footnote 2.

By combining Eqs. (22), (34), and (35), we find

$$G_c=R\sum_j[k_j p_1^{\beta_{1j}} p_2^{\beta_{2j}}\cdots-k_j' p_1^{\eta_{1j}} p_2^{\eta_{2j}}\cdots]\times\ln\frac{k_j p_1^{\beta_{1j}} p_2^{\beta_{2j}}\cdots}{k_j' p_1^{\eta_{1j}} p_2^{\eta_{2j}}\cdots}. \quad (36)$$

This term is essentially positive and measures the entropy increase due to the chemical reactions.

A convenient form for the function, G, which measures the rate of irreversible entropy production is obtained by combining the results of the previous paragraphs.

$$G=\lambda[\nabla\ln T]^2+\frac{2\eta}{T}[(\nabla\mathbf{v})^{(S)}-\tfrac{1}{3}(\nabla\cdot\mathbf{v})\mathbf{I}]:[(\nabla\mathbf{v})^{(S)}-\tfrac{1}{3}(\nabla\cdot\mathbf{v})\mathbf{I}]+\tfrac{1}{2}R\sum_{ij}\frac{n_i n_j}{nD_{ij}}(\mathbf{V}_i-\mathbf{V}_j)^2+R\sum_j[k_j p_1^{\beta_{1j}} p_2^{\beta_{2j}}\cdots-k_j' p_1^{\eta_{1j}} p_2^{\eta_{2j}}\cdots]\times\ln\frac{k_j p_1^{\beta_{1j}} p_2^{\beta_{2j}}\cdots}{k_j' p_1^{\eta_{1j}} p_2^{\eta_{2j}}\cdots}. \quad (37)$$

Throughout this development we have used the results of the kinetic theory of gases. This applies rigorously to nearly perfect gases. However, the results, to a good approximation, also apply to a general fluid system as may be seen from the following considerations. First of all, the transport equations, Eqs. (2), (3), (4), and (5), would still apply. Consequently the rate of irreversible entropy production is still given by Eq. (16). The definitions of entropy and chemical potential should now involve fugacities rather than pressures. The use of Eq. (17) for heat flux should still apply as long as the flow is laminar. Thus G can be broken up into the same components as given in Eqs. (19), (20), (21), and (22). It is clear that G_h is still positive. The discussion of G_v is limited to laminar flow and it would not apply to plastic flow in fluids which support transverse waves (since the form of Eq. (23) would no longer apply). The Eq. (29) for diffusion velocities has been proposed by Onsager as an empirical relation for liquids. On the basis of this relation, our expression for G_d is valid. The contribution due to chemical reactions, G_c, is only changed by the partial pressures being replaced by fugacities.

The authors wish to thank Dr. Carl Eckart for discussions concerning this work, and to thank the Navy Bureau of Ordnance for their financial support under Contract NOrd 9938.

Short-Lived Fission Products. II. Cs^{139} and Cs^{140}

NATHAN SUGARMAN
Argonne National Laboratory and Institute for Nuclear Studies, University of Chicago, Chicago, Illinois

AND

HAROLD RICHTER*
Argonne National Laboratory, Chicago, Illinois

(Received May 31, 1949)

Half-life values have been obtained for Cs^{139} and Cs^{140} by extraction of the Ba descendent activities from cesium silicotungstate precipitates. The half-life of Cs^{139} was found to be 9.5 ± 0.2 min. by this technique and that of Cs^{140}, 66 ± 2 sec. The value for the Cs^{139} half-life was confirmed by observation of a Cs sample isolated directly from irradiated uranyl nitrate.

HALF-LIFE OF Cs^{139}

THE technique of determining the half-life of an ancestor activity by timed precipitations and subsequent extraction of descendent activities[1] from the precipitates was used in this work to measure the half-life of Cs^{139}, parent of 85-min. Ba^{139}. In earlier studies Hahn and Strassmann[2,3] found a half-life of 7 min. by direct isolation of Cs, while Heyn, Aten, and Bakker[3,4] assigned a 10-min. half-life to the activity. In the present investigation the half-life of Cs^{139} was determined in two ways, first by extraction of Ba^{139} from cesium silicotungstate precipitates, and second, by radiochemical separation of Cs samples from irradiated uranyl nitrate and observation of the radioactivity.

The first technique involves precipitation of a Cs compound from an aliquot of irradiated solution and subsequent determination of the descendent activity in the Cs precipitate as a function of time of precipitation of the Cs. In principle the Cs compound used for the precipitation should precipitate Cs quickly and free of its antecedents or descendents if valid results are to be obtained. Since sufficient time was allowed for the decay of the I and Xe antecedents of Cs^{139} before the earliest precipitation was made there was no need to fulfill the criterion that the Cs compound should not carry down antecedent elements. On the other hand, it was necessary to establish that the Cs precipitates were not contaminated by *coseparated* radiobarium.

The first precipitate tested was cesium cobaltinitrite. It was found that under the conditions employed, where 50 mg Cs was precipitated in the presence of ~20 mg Ba carrier, and subsequent washings with 10 percent HAc, about 20 percent of the Ba coseparated with the Cs precipitate. This value was markedly enhanced when less Ba carrier was present. Cesium silicotungstate proved to be a more desirable precipitate. When 50 mg Cs was precipitated in the presence of ~20 mg Ba carrier and washed three times with $3M$ HCl containing silicotungstic acid, a separation factor from Ba of 1×10^4 was observed.

The details for precipitation of cesium silicotungstate and the subsequent radiochemical analysis for Ba follow. A solution of uranyl nitrate is irradiated in the pneumatic tube of the Argonne Heavy Water Pile for 10 sec. at an approximate flux of 10^{11} neutrons/cm^2 sec. Aliquots of the irradiated solution are transferred to centrifuge tubes containing 5 ml Cs carrier (~10 mg Cs/ml) and 2 ml of Ba carrier (~10 mg Ba/ml). The volumes are adjusted to 23 ml with unirradiated uranyl nitrate and the solutions are cooled. The precipitations of cesium silicotungstate are effected at the desired times after the end of the irradiation by pouring in a cooled mixture of 15 ml conc. HCl and 10 ml $0.13M$ silicotungstic acid. The precipitates are centrifuged two minutes after precipitation and are then washed three times with a cooled solution of 10 ml $3M$ HCl mixed with 5 ml silicotungstic acid.

The results of the Ba analyses of the cesium silicotungstate precipitates indicate that a substantial portion of the Ba activity is washed out of the cesium silicotungstate precipitates in preparing them for Ba analysis. As discussed in a later section of this paper, the extent of Ba removal from the precipitates depends on the number of washes, the wash solution used, and the extent of the washing process. Although no effort was made to time the washes exactly, the same number was used on each precipitate, and because of the rather mechanical nature of the process it is estimated that the timing of the entire wash procedure is reproduced to the order of 5 min. In any event, any effects of this kind on the final result are of a random type and are accounted for in the precision of the experiment.

The analysis for Ba in the cesium silicotungstate precipitate is begun 70 min. after precipitation. At this time most of the Cs^{139} has decayed to 85-min. Ba^{139}. To the cesium silicotungstate precipitate is added 2 ml standardized Ba carrier, 1 ml Sr carrier, 8 ml H_2O, and the mixture is then stirred and heated. The precipitate is then dissolved by adding 3 ml $6M$ NaOH. The mixed

* Now at the Department of Chemistry, Massachusetts Institute of Technology, Cambridge, Massachusetts.

[1] N. Sugarman, J. Chem. Phys. **17**, 11 (1949).

[2] O. Hahn and F. Strassmann, Naturwiss. **28**, 54 (1940).

[3] "Nuclei formed in fission," issued by The Plutonium Project, J. Am. Chem. Soc. **68**, 2411 (1946); Rev. Mod. Phys. **18**, 513 (1946).

[4] Heyn, Aten, and Bakker, Nature **143**, 516 (1939).

carbonates of the Ba and Sr are precipitated with 2 ml 1*M* Na_2CO_3. The precipitate is washed once with 10 ml H_2O and 1 ml 1*M* Na_2CO_3 and is dissolved in 2 ml 6*M* HCl. The subsequent analysis for Ba differs only slightly from the standard procedure[5] involving three precipitations of $BaCl_2$ with conc. HCl-ether reagent, a scavenging with $Fe(OH)_3$, and finally a precipitation of $BaCrO_4$ for radioactivity measurement. The chemical yield of the Ba is determined from the weight of $BaCrO_4$.

The levels of activity of the Ba samples, when corrected for chemical yield, which was of the order of 30 mg, and aliquot of original irradiated uranyl nitrate solution used, vary exponentially with the time of precipitation of Cs for a given irradiated solution. The many irradiated solutions used were normalized to the same activity level by analyzing an aliquot of the irradiated solution for Ba^{139} and correcting all activities to an arbitrarily chosen value. The data of the various experiments are given in Table I.

The Ba^{139} activity of each Cs precipitate is given in the last column of Table I. The results are corrected for aliquot of solution, chemical yield, normalization factor of a given irradiation to allow for intercomparison of irradiations, and for Ba adsorbed on the Cs precipitate. The latter correction amounting to about 3 counts per minute (c/min.) was important only for samples of late precipitations. A plot of these values *versus* time of precipitation of cesium silicotungstate appears in Fig. 1. A least squares analysis of the data yields a half-life for Cs^{139} of 9.5±0.2 min.

The half-life of Cs^{139} was previously determined from

TABLE I. Activities of 85-min. Ba^{139} extracted from cesium silicotungstate precipitates.

Experiment	Sample	Time of precipitation of Cs (τ) (minutes after end of irradiation)	Aliquot of irradiated solution (ml)	Ba^{139} activity at arbitrary time $+\tau$ (c/min.)	Ba^{139} activity per ml of solution corrected to 30 mg of $BaCrO_4$ precipitate (c/min.)	Normalization factor (correcting to 50,000 c/min.)	Normalized Ba^{139} activity corrected for adsorption (c/min.)
1	precipitate	20	4	3310	762	—	3092
	precipitate	40	10	2000	189	—	762
	total	—	1	15000	12430 } 12320		
	total	—	1	15300	12210 }	4.06	—
2	precipitate	15	4	3820	928	—	3577
	precipitate	25	15	8550	494	—	1907
	total	—	1	14800	13100 } 12950		
	total	—	1	14300	12800 }	3.86	—
3	precipitate	10	2	795	376	—	6538
	precipitate	30	10	925	87.8	—	1527
	total	—	1	3350	2950 } 2875		
	total	—	1	3400	2800 }	17.4	—
4	precipitate	15	1	3870	3610	—	5697
	precipitate	35*	2	920	427	—	672*
	precipitate	60	15	1600	130	—	202
	total	—	1	37400	31600 } 31600		
	total	—	1	37600	31600 }	1.58	—
5	precipitate	35	5	970	181	—	1112
	precipitate	55	10	480	48.2	—	293
	total	—	1	8900	8340 } 8130		
	total	—	1	8500	7920 }	6.15	—
6	precipitate	6.5	1	2130	2115	—	8185
	precipitate	50	5	500	94.4	—	362
	precipitate	65	5	163	27.5	—	104
	precipitate	80	5	50.1	9.5	—	33.5
	total	—	1	14200	13030 } 12920		
	total	—	1	14300	12810 }	3.87	—
7	precipitate	45*	2	200	93.5	—	318*
	precipitate	70	4	87.8	26.9	—	89.5
	precipitate	75	4	63.5	16.1	—	52.5
	precipitate	90	10	600	6.50	—	20.0
	total	—	1	17200	14450 } 14550		
	total	—	1	16900	14650 }	3.44	—
8	precipitate	85	10	57.0	6.53	—	24.8
	precipitate	95	10	38.0	3.96	—	14.1
	total	—	1	13800	11970 } 11960		
	total	—	1	13900	11950 }	4.18	—

* Points omitted from least squares analysis because of large deviations from curve.

[5] L. E. Glendenin, *National Nuclear Energy Series* (McGraw- Hill Book Company, Inc., New York, 1950), Div. IV, Vol. 9, Paper 288.

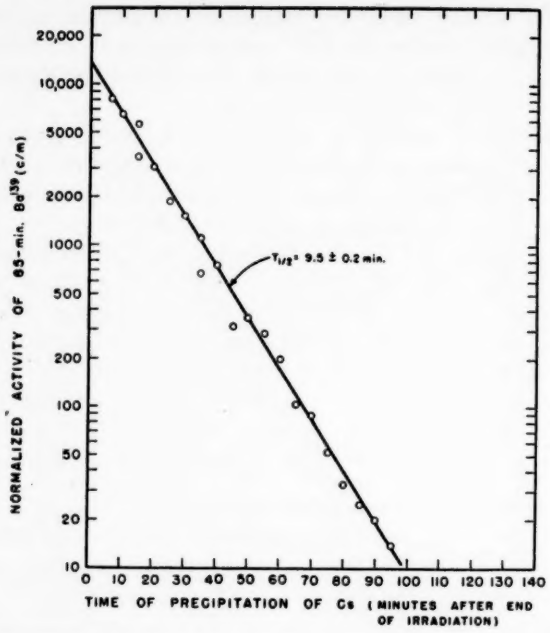

FIG. 1. Decay curve of Cs^{139} from 85-min. Ba^{139} activities extracted from cesium silicotungstate precipitates. Activities of 85-min. Ba^{139} in precipitates multiplied by normalization factors obtained by correcting total Ba activities to 50,000 c/min. (data of Table I).

the decay activities of gaseous fission products. Hahn and Strassmann[2] found a half-life of 7 min. for Cs^{139} and Heyn, Aten, and Bakker,[4] 10 min. Because of the discrepancy in these values and the disagreement of the Hahn and Strassmann value with that of 9.5 min. obtained by extraction of Ba^{139} (see above), the half-life of

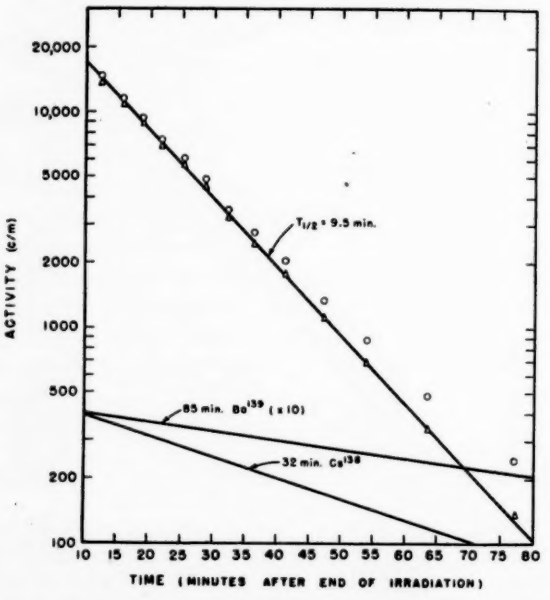

FIG. 2. Typical decay curve of Cs^{139} separated from irradiated uranyl nitrate. Counted through 1050 mg/cm² Al absorber. ○ Original points. △ Activities of 85-min. Ba^{139} and 32-min. Cs^{138} determined from later part of decay curve subtracted from original data.

Cs^{139} was also determined from the decay of a Cs sample isolated directly from irradiated uranyl nitrate.

Samples of uranyl nitrate were irradiated for 1 min. in the pneumatic tube of the Argonne Heavy Water Pile. The irradiated material was dissolved in 10 ml H_2O containing 2 ml Cs carrier (~10 mg/ml) and 1 ml Rb carrier (~10 mg/ml). A precipitation of the mixed Cs–Rb cobaltinitrites was performed about $1\frac{1}{2}$ min. after the end of irradiation. The centrifugation of the precipitation was finished by $2\frac{1}{2}$ min. after the end of irradiation. The purpose of these rapid operations was to minimize the activity of 32-min. Cs^{138} growing from 17-min. Xe^{138}. The cobaltinitrite precipitate was dissolved in dilute HCl and Cs was separated from Rb by a precipitation of Cs with BiI_3–HI reagent.[1] This precipitate was dissolved and a $Fe(OH)_3$ scavenging precipitation was made. The Cs was finally precipitated as the silicotungstate and counted. Radioactivity measurements usually began about 12 min. after the end of irradiation except in those cases where the first precipitation of Cs as the cobaltinitrite was purposely delayed about 10 to 15 min. to allow for more growth of 32-min. Cs^{138}. This was done in order to determine if the activity level of the Cs^{138} in any way affected the half-life of Cs^{139} obtained by graphical analysis. No effect was found. Decay curves were taken with interposed Al absorbers varying from 0–1430 mg/cm². Nineteen such curves yielded half-lives of Cs^{139} ranging from 9 to 10 min. A typical decay curve is given in Fig. 2. The average half-life found was 9.5±0.2 min. where the error is the average deviation of the 19 values from the mean. This result agrees with the value obtained by Ba^{139} isolation, indicating that the indirect method of obtaining the half-life of Cs has no inherent difficulties.

Two explanations may be advanced for the discrepancy between the half-life of Cs^{139} reported here and that determined by Hahn and Strassmann. First, they assumed that the contribution of 32-min. Cs^{138} to the total decay curve was negligible; and secondly, they calculated the contribution of the 85-min. Ba^{139} to the total decay curve assuming equal losses from absorption of the β-rays of Cs^{139} and Ba^{139} in the ~30 mg/cm² wall of their counter. Although both of these assumptions appear plausible, the half-life thus determined is less secure than that obtained from an analysis of complete decay curves where the Cs^{138} and Ba^{139} appear and their contributions can be determined.

HALF-LIFE OF Cs^{140}

The half-life of Cs^{140} was determined by the technique of Ba extraction from Cs precipitates. The procedure was the same as that used in the determination of the half-life of Cs^{139} except that here the 12.8-day Ba^{140} activity was measured. For precipitations performed at times less than 2 min. after the end of irradiation it was not feasible to remove an aliquot of the irradiated solution for precipitation as was done at later times. Instead, the entire irradiated solution was used for precipitation

TABLE II. Activities of 12.8-day Ba^{140} extracted from cesium silicotungstate precipitates.

Experiment	Sample	Time of precipitation of Cs (τ) (minutes after end of irradiation)	Aliquot of irradiated solution (ml)	Ba^{140} activity at arbitrary time $+\tau$ (c/min.)	Ba^{140} activity per 5 ml of solution corrected to 30 mg of $BaCrO_4$ precipitate (c/min.)	Normalization factor (correcting to 5000 c/min.)	Normalized activity of Ba^{140} (c/min.)
1	precipitate	4.00	15	81	25.2	—	32.8
	total	—	5	4300	3860	1.30	—
2	precipitate	3.50	15	218	71.3	—	49.1
	total	—	5	8200	7255	0.689	—
3	precipitate	4.00	15	138	44.0	—	40.8
	total	—	5	6000	5390	0.928	—
4	precipitate	2.50	15	290	98.0	—	91.4
	total	—	5	6200	5360	0.933	—
5	precipitate	2.00	15	630	205	—	129
	total	—	5	8900	7970	0.627	—
6	precipitate	3.00	15	272	89.3	—	71.8
	total	—	5	6800	6220	0.804	—
7	precipitate	4.50	15	80	32.9	—	28.5
	total	—	5	6400	5785	0.865	—
8	precipitate	3.25	15	171	55.7	—	61.8
	total	—	5	5000	4520	1.11	—
9	precipitate	2.25	15	238	76.7	—	110
	total	—	5	1500	3490	1.43	—
10	precipitate	3.75	15	200	64.1	—	42.6
	total	—	5	8000	7520	0.665	—
11	precipitate	2.75	15	220	73.0	—	80.1
	total	—	5	5000	4560	1.10	—
12	precipitate	5.00	15	80	28.8	—	18.1
	total	—	5	8500	7940	0.630	—
13	precipitate	4.25	15	265	87.2	—	43.4
	total	—	5	9000	10040	0.498	—
14	precipitate	4.75	15	100	34.5	—	22.6
	total	—	5	6800	7640	0.654	—
15	precipitate	4.25	15	86	35.2	—	28.4
	total	—	5	3800	6195	0.807	—

Experiment*	Sample	τ (min.)	Aliquot of irradiated solution (ml)	Ba^{140} activity (c/min.)	Ba^{140} activity per ml of solution corrected to 30 mg of $BaCrO_4$ precipitate (c/min.)	Total activity (precipitate +supernate) (c/min.)	Normalization factor (correcting to 5000 c/min.)	Normalized activity of Ba^{140} (c/min.)
16	precipitate	1.75	1.0	250	231	—	—	143
	supernate	—	0.1	320	7820**	8050	0.621	—
17	precipitate	1.25	1.0	2250	1985	—	—	232
	supernate	—	0.1	2500	40850**	42835	0.117	—
18	precipitate	1.00	1.0	620	571	—	—	241
	supernate	—	0.1	580	11250**	11820	0.423	—
19	precipitate	1.50	1.0	600	584	—	—	195
	supernate	—	0.1	580	14400**	14985	0.334	—

* Experiments 16–19 were made by precipitating Cs from total irradiated solution. Total Ba^{140} activity obtained from analysis of supernatant liquid correcting for Ba^{140} activity in precipitate.
** Activities multiplied by a factor 1.1 to correct for Ba carrier initially in supernate.

of cesium silicotungstate and the total activity to which the 12.8-day Ba^{140} activities in the precipitates were compared, was found by analyzing the supernatant solution after the centrifugation of the Cs precipitate and correcting for the Ba activity in the precipitate. The results of these experiments appear in Table II. No correction was made for adsorption of Ba on the Cs precipitates because of the negligibly small value. A plot

of the normalized 12.8-day Ba^{140} activity *versus* time of Cs precipitation is given in Fig. 3. A least squares analysis of the data yielded 66±2 sec. for the half-life of Cs^{140}.

Hahn and Strassmann[2] found a 40-sec. Cs activity of unassigned mass number in their study of short-lived

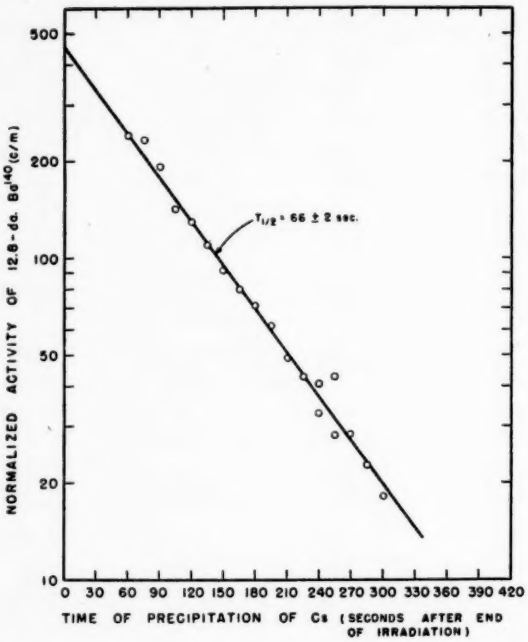
NORMALIZED ACTIVITY OF 12.8-da. Ba140 (c/m)
500
200
100
50
20
10
T1/2 = 66 ± 2 sec.
0 30 60 90 120 150 180 210 240 270 300 330 360 390 420
TIME OF PRECIPITATION OF Cs (SECONDS AFTER END OF IRRADIATION)

FIG. 3. Decay curve of Cs^{140} from 12.8-day Ba^{140} activities extracted from cesium silicotungstate precipitates. Activities of 12.8-day Ba^{140} in precipitates multiplied by normalization factors obtained by correcting total Ba activities to 5000 c/min. (data of Table II).

alkali activities. The large apparent discrepancy between this value and that of 66 sec. found for Cs^{140} may originate in their decay curve analysis in which the half-life of Cs^{139} was taken to be 7 min. rather than 9.5-min. as discussed earlier. Another possible explanation may be the presence of another short-lived Cs activity, such that its admixture with the 66-sec. Cs^{140} yields an apparent 40-sec. period.

LOSS OF DESCENDENT Ba ACTIVITY FROM CESIUM SILICOTUNGSTATE PRECIPITATES

An inspection of Figs. 1 and 3 shows that the activities of Ba^{139} and Ba^{140} in the cesium silicotungstate precipitates when extrapolated to zero time of precipitation in each case lead to values considerably less than the total Ba activity present. These two values of total Ba activity are determined by analysis of an aliquot not subjected to Cs precipitation and corrected by the normalization factors to the normalizing activities. For example, the extrapolated value of Ba^{139}, as seen from Fig. 1, is 13,500 c/m, whereas the normalizing activity is 50,000 c/m. Similarly, the extrapolated value of Ba^{140} (Fig. 3) is 468 c/m compared to a normalizing activity of 5000 c/m. If all of the Ba^{139} and Ba^{140} activities originated in Cs ancestors and were retained by the Cs precipitates, then the extrapolated values should equal the normalizing activities.

A quasi-theoretical treatment of the independent yields of fission products predicts that most of the Ba^{139} and Ba^{140} activities in the solution should result from β-decay of the Cs^{139} and Cs^{140} ancestors rather than directly from fission.[6] We have, in fact, confirmed this point for Ba^{139} in a separate investigation. The low extrapolated values of the Ba activities must then be caused by loss of Ba activity from Cs precipitates. Although some Ba activity is probably lost during the "setting" time of the Cs precipitates, analogous to the observed loss of descendent activities from silver halide precipitates in previous work,[1] there is in the present case, however, no single value of the "setting" time which is consistent with the data. Instead, it appears that the Ba activity is leached out of the precipitates in the washing process. Direct evidence supporting this view is the fact that different wash solutions, e.g., alcoholic silicotungstic acid, 6*M* HCl, and others yield extrapolated values of Ba which are quite different, although all give exponential curves for Cs^{139} with essentially the same half-life. Further, in comparing results from various wash solutions we observed a correlation between a higher extrapolated value of Ba and a poorer coseparation factor of Ba in the Cs precipitates, indicating that a wash solution which removes Ba coseparated on the Cs precipitate also leaches out Ba grown into the Cs precipitate from the decay of Cs. It was also noted that Cs precipitates washed more times with the same wash solution yielded lower Ba activities.

An interesting feature of all these results is the apparent reproducibility of the Ba activity after the standard wash process. The agreement in the half-life of Ba^{139} obtained with different wash solutions, the accurately exponential curves obtained for the Cs decay using a given wash solution (see Figs. 1 and 3), and the agreement in half-life of Cs^{139} obtained by the two different methods, all support this contention.

This document is based on work performed at the Argonne National Laboratory operated by the University of Chicago for the AEC.

SUMMARY

The experiments reported here establish the half-lives of two Cs fission products. The chain relations as modified in this work are given below.

Mass 139: 2.7-sec. I→41-sec. Xe→**9.5-min. Cs**→**85-min. Ba**→*Stable La*

Mass 140: 16-sec. Xe→**66-sec. Cs**→**12.8-day Ba**→40.0-hr. La→*Stable Ce*

Bold face denotes activities studied in this paper.

[6] Glendenin, Coryell, and Edwards, *National Nuclear Energy Series* (McGraw-Hill Book Company, Inc., New York, 1950) Vol. 9, Div. IV, Paper 52. See also Phys. Rev. **75**, 337 (1949).

An Experimental Determination of the Distribution of the Radon Decay Products in a Gas-Filled Spherical Vessel*

CHARLES R. MAXWELL, VICTOR P. HENRI,† AND DOROTHY C. PETERSON
Laboratory of Physical Biology, Experimental Biology and Medicine Institute, National Institutes of Health, Bethesda, Maryland

(Received June 13, 1949)

The distributions of RaC and of (RaA+RaB) between the walls and the gaseous phase of a spherical vessel filled with a gas-radon mixture were determined by the analyses of decay curves of the gamma-activity of the radon decay products left on the walls of the vessel when it was rapidly evacuated. The distributions of RaA and RaB were determined from these data. The effects of the size of the flask, the pressure of the gas, and the type of gas upon these distributions were investigated. It is suggested that the distributions of RaA and RaB when expressed as a function of the distribution of RaC are independent of these variables. The distributions in benzene and in carbon dioxide are reported.

I. INTRODUCTION

A KNOWLEDGE of the distribution of the radon decay products in a sphere filled with a gas-radon mixture is necessary for the calculation of the energy absorbed in the gas. This distribution cannot be calculated by the simple laws of diffusion because the decay products form aggregates of variable size in the gas phase. Harrington[1] and his co-workers[2,3] have shown that many of the aggregates are large enough to settle out under the influence of gravity and also that the distribution of particle size varies with the gas mixed with the radon.

The several experimental determinations[4–6] which have been made of the distribution of RaC and RaC′ indicate that the distribution of these elements is a function of the particular gas mixed with the radon as well as the pressure of the gas and the size of the container.

Because of experimental difficulties few results have been reported on the distribution of RaA and RaB. The distributions of these products have usually been obtained from theoretical considerations and the distribution of RaC.

In connection with studies of radon-gas mixtures being conducted in this laboratory it has been necessary to determine experimentally the distribution of the radon decay products. In addition to studying the particular systems being used here, a cursory investigation was made to determine some of the variables which influenced this distribution. The distribution in benzene, which is very susceptible to ionizing radiations, and in carbon dioxide which is inert[7] to ionizing radiations have been determined.

II. THEORETICAL CONSIDERATIONS

The gamma-activity of a flask containing radon is a measure of the RaB and RaC present, but because of the large differences in the energies of the two gamma-rays it should be possible by a suitable experimental set-up to reduce to a negligible amount the contribution of the RaB to the measured gamma-activity and thus to measure directly the amount of RaC present at any time. When RaA, RaB, and RaC are in equilibrium with radon, the gamma-activity of the flask is essentially constant for short periods of time, but if the radon is removed, the gamma-activity decreases steadily. The distributions of the decay products reported in this paper were obtained by the analysis of gamma-activity decay curves of the material left on the wall when the radon was removed.

Theoretically it should be possible to calculate from these decay curves and the classical equations of radioactive decay the relative amounts of RaA, RaB, and RaC left in the flask at t_0, when the radon was removed. However, the similarity of the curves for the formation of RaC from RaA and for the formation of RaC from RaB and the errors in the experimental values of the gamma-activity made it impossible to determine directly the small amounts of RaA present at t_0 in the presence of the much larger amounts of RaB and RaC. Instead, the amount of (RaA+RaB) in the flask was determined by treating the data as if the RaA were RaB. The error introduced by this assumption is negligible because the values of gamma-activity calculated for equilibrium mixtures of RaA, RaB, and RaC for the actual and for the assumed conditions differed by less

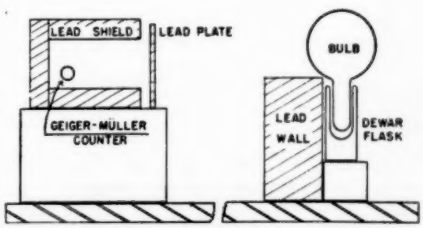

FIG. 1. Sketch of the apparatus.

* This work was done while the author was a National Institutes of Health Junior Research Fellow.

† Present address: Massachusetts Institute of Technology, Cambridge, Massachusetts.

[1] E. L. Harrington, Phil. Mag. **6** (7), 685–95 (1928).

[2] E. L. Harrington and O. A. Gratias, Phil. Mag. **11**, 285–96 (1931).

[3] E. L. Harrington and E. O. Braaten, Trans. Roy. Soc. Can. III **26**, 177–86 (1932).

[4] A. Luyckx, Bull. Soc. Chim. Belgium **43**, 179–88 (1934).

[5] S. C. Lind, J. Am. Chem. Soc. **41**, 541 (1919).

[6] P. Colmant, Bull. Soc. Chim. Belgium **41**, 431–63 (1932).

[7] S. C. Lind and D. C. Bardwell, J. Am. Chem. Soc. **47**, 2690 (1925).

than the probable counting error of the individual experimental values.

III. EXPERIMENTAL PROCEDURE

The effect upon the distribution of the decay products of (1) the radius of the spherical container, (2) the pressure and nature of the gas mixed with the radon, and (3) the concentration of the radon has been investigated.

Figure 1 is a sketch of the experimental apparatus.

The spherical bulbs used were made from 250-, 500-, 1000-, and 3000-ml distilling flasks. After the bulbs had been filled with the desired mixture of gas and radon in a high vacuum system, they were sealed and mounted so that the G-M counter saw the complete flask with the exception of the neck and a small portion (≈ 6 percent) of the spherical surface which was shielded from the Geiger-Müller counter by a 6-in. wall of lead. This small section of spherical surface was excluded to avoid the counting of any active material which might have been deposited there during the removal of the gas-radon mixture.

The bulb was allowed to stand for at least 5 hr. before the t_0 value of the gamma-activity was measured. This is more than enough time to establish radioactive equilibrium and, since the values for the distribution obtained with samples which had been allowed to stand for as long as 10 hr. showed no systematic trend from those obtained with a 5-hr. delay, it was assumed that distributional equilibrium was also established in this time. The condensable gas-radon mixtures were rapidly removed from the spherical volume seen by the counter by quickly filling the Dewar flask with liquid air. Starting $1\frac{1}{2}$ min. after the application of liquid air (time t_0), 1-min. counts of gamma-activity remaining in the flasks were made at $1\frac{1}{2}$-min. intervals for 41 min. The liquid air was removed, the flask brought to room temperature, and the experiment repeated after a lapse of 5 to 10 hr.

No particular precautions were taken to prevent convection currents in the flask during the equilibration period because the distributions under ordinary laboratory conditions were desired. The counting rate at t_0 was adjusted to between 6000 and 25,000 counts per minute by varying the thickness of the lead plate. Any error

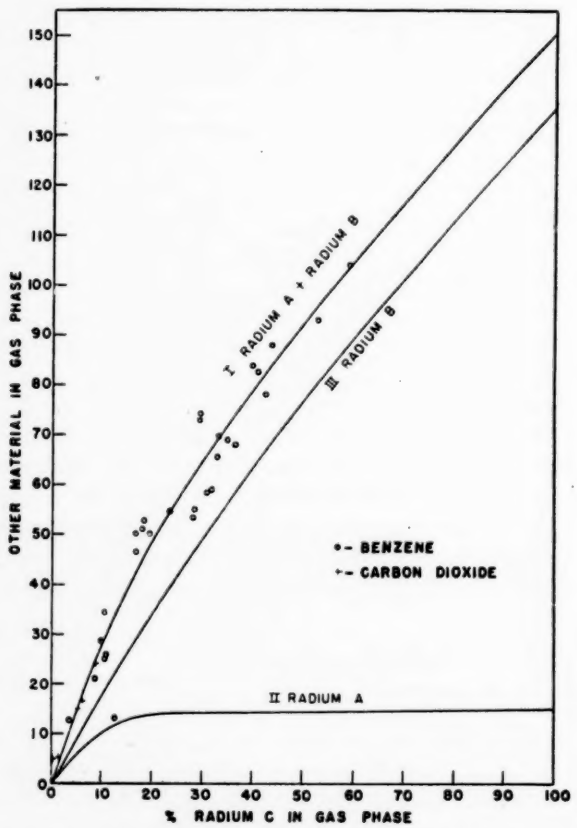

FIG. 2. The number of RaA, RaB, and (RaA+RaB) atoms in the gas phase for each 100 atoms of RaC in the sphere as a function of the percent of RaC in the gas phase.

TABLE I. Number of RaC and of (RaA+RaB) atoms found on the wall and in the gas phase of a gas-filled spherical flask for each 100 atoms of RaC in the equilibrium mixture.

Radius flask mm	Pressure of gas mm of Hg C_6H_6	CO_2	Radon mc	RaC on wall	(RaA+RaB) on wall	RaC in gas	(RaA+RaB) in gas
90	3		15.2	96.4	138.8	3.6	12.8
				87.5	138.3	12.5	13.2
90	10		15.3	89.5	126.7	10.5	24.9
				89.3	125.7	10.7	25.8
				90.2	123.0	9.8	28.7
90	80		14.5	56.0	63.7	44.0	87.8
				60.0	68.0	40.0	83.7
				40.7	47.9	59.3	103.8
90	30		15.7	68.9	93.0	31.1	58.5
				71.6	96.6	28.4	54.9
				68.0	92.7	32.0	59.0
90	80		310	83.3	101.5	16.7	50.0
				70.5	77.2	29.5	74.4
				59.0	69.0	41.0	82.5
				80.4	101.5	19.6	50.0
				66.8	81.8	33.2	69.7
				70.6	78.7	29.4	72.9
90	80		6	65.0	82.1	35.0	69.4
				47.2	58.5	52.8	93.0
				57.5	73.5	42.5	78.0
90	80		50	81.6	98.7	18.4	52.8
				81.9	100.6	18.1	50.9
				83.6	105.2	16.4	46.3
64	80		6	63.3	83.7	36.7	67.9
				67.0	86.1	33.0	65.4
49	80		5	71.8	98.0	28.2	53.5
				73.7	108.3	26.3	43.2
37	80		3	76.5	96.8	23.5	54.8
				89.4	117.2	10.6	34.4
64		17	20	98.6	146.3	1.4	5.2
				99.5	146.6	0.5	5.0
64		640	24	91.1	127.5	8.9	24.0
				93.7	135.2	6.3	16.4
				94.5	136.5	5.5	15.0

caused by a change in the scattering when the radon was frozen out was reduced by the lead shielding which restricted the vision of the G-M counter to little other than the bulb of radioactive mixture. The exact geometry is unimportant since only relative counting rates are needed.

IV. ANALYSIS OF EXPERIMENTAL DATA

The relative amounts of (RaA+RaB)—considered as RaB—and of RaC on the walls of the sphere at time t_0 were determined analytically by a least squares method

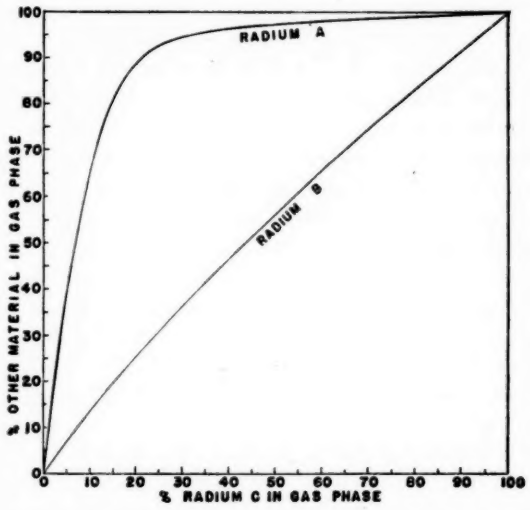

FIG. 3. Percent RaA and RaB in the gas phase as a function of the percent RaC in the gas phase.

which used all the observed points on each of the decay curves. Values for theoretical decay curves were calculated for these amounts of RaB and RaC and compared with the observed values. The agreement in every case was satisfactory; the deviations showed no trend and had on the average a value approximately equal to that of the probable counting error. It is therefore concluded that the effect of the RaB gamma-activity was negligible in our experimental set-up.

The analyses of the decay curves for the 310 mc–80 mm benzene mixture were made in a slightly different manner. These curves showed a greater decrease in gamma-activity during the first 20 min. than did the other curves. Since only the last portion of these curves could be accounted for by the simple decay of a mixture of RaB and RaC, the amounts of these materials reported on the walls were calculated with the data taken between 20 and 41 min. after t_0. The value for RaC calculated from these points was about four percent less than the value obtained by extrapolating the observed decay curves to zero time. With other mixtures this error was always less than one percent.

The data for the individual runs are recorded in Table I. Corrections, based on the assumption that the distribution on the wall is uniform, have been made for the fraction of the flask shielded from the counter and

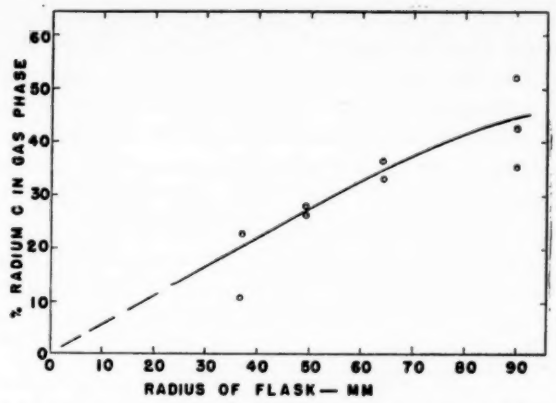

FIG. 4. Percent RaC in the gas phase as a function of the radius of a spherical vessel containing 6 mc of radon and 80 mm pressure of benzene vapor.

the data have been adjusted so that columns IV and V show the number of RaC and of (RaA+RaB) atoms on the wall of the sphere for each 100 atoms of RaC present at t_0. Columns VI and VII give the corresponding number of atoms in the gas phase. It was possible to calculate column VII from column V because the decay products were in equilibrium with radon at t_0. These are, of course, relative figures calculated from the corrected t_0 count and are independent of the geometry of the counting system and the actual amount of radon present. However, the amount of radon introduced into each gas mixture was determined before its introduction by comparing the shielded radon needle with a shielded standard radium source.

Curve I in Fig. 2 shows the number of (RaA+RaB) atoms in the gas phase for each 100 atoms of RaC in the sphere as a function of the percent RaC in the gas phase. The plotted values were taken from columns VI and VII in Table I. It has been possible, by considering the limiting conditions and the physical aspects of the diffusion and equilibria, roughly to divide this curve into two curves which show the approximate distributions of RaA and RaB. Curves II and III which represent these distributions were obtained in the following manner.

Since the radon decay products are in equilibrium with the relatively long-lived radon, RaA and RaB must approach, respectively, the values 15.1 and 136 for RaC = 100. Because the factors influencing the diffusion of these particles to the wall are the same for all the particles, it may be assumed that the fraction of any particular product reaching the wall will be roughly inversely proportional to the average time between the decay of the radon and the decay of the particular product. For RaA and RaB these times are 4.4 and (4.4+38.7). It follows that RaA approaches its limiting value much more rapidly than does RaB and that the increase in the values of (RaA+RaB) for values of RaC greater than approximately 30 are essentially increases in the amount of RaB in the gas phase. A first approxi-

mation of the distribution of RaB was obtained by extending a curve parallel to the observed (RaA+RaB) curve in the region between RaC=30 and RaC=100 and passing through the limiting value of RaB=136 and RaC=100 to the other limiting value of 0.0. A first approximation for the RaA distribution was then obtained by subtracting this curve from the observed curve. Curves II and III have been adjusted so that the RaA curve approaches its limiting value of 15.1 at RaC =100 instead of RaC=30. Although this division has been quite arbitrary it seems plausible and should be of considerable use in calculating the total energy absorbed by the gas phase from the alpha-particles.

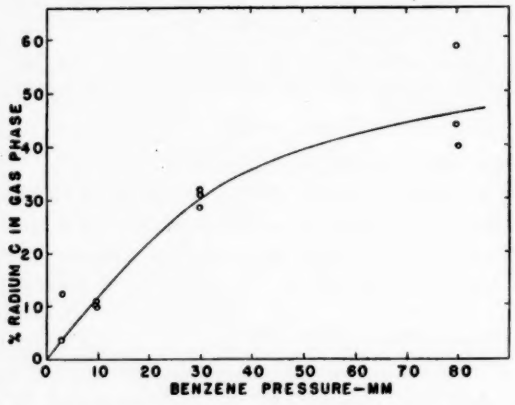

FIG. 5. Percent of RaC in the gas phase of a 3000-ml flask containing 16 mc of radon and various amounts of benzene vapor.

V. RESULTS

Figure 3 shows the fraction of the RaA and RaB in the gas phase as a function of the fraction of the RaC in the gas phase. These values were calculated from curves III and IV in Fig. 2.

Since the half-life of RaC is 1.6×10^{-4} sec., it seems reasonable to assume that the distribution of RaC′ is the same as the distribution of RaC.

Figure 4 shows the fraction of RaC in the gas phase as a function of the radius of the sphere for mixtures of 80 mm of benzene and 6 mc of radon. Figure 5 shows the fraction of RaC in the gas phase as a function of the pressure of benzene in 3000-ml spheres containing 16 mc of radon.

No conclusions can be drawn from the data in Table I as to the effect of the concentration of radon upon the distribution of RaC.

VI. DISCUSSION

The methods described here for determining the distribution of the radon decay products is applicable to any condensable system. However, certain precautions must be observed.

(1) As large a portion of the sphere as possible must be counted, because the distribution of the active deposit on the walls (and probably also in the gas phase) is often not uniform. This non-uniformity was observed in the 310 mc–80 mm benzene mixture by the erection of a special shielding system which allowed sections of the sphere to be counted. The relative activities in the lower one-third, middle one-third, and upper one-third of the sphere were respectively 60, 25, and 15. The solid material which deposits from the gas phase of the benzene mixture as a result of the effect of the ionizing radiations appeared to have roughly this same distribution.

(2) If any of the reaction products from the gas-radon mixture are non-condensable, the distribution determination should be made as soon as possible and particular care should be taken in the analysis of the decay curves. This non-condensable gas may markedly retard the freezing out of the smaller aggregates of active material and thus change the initial slope of the observed decay curve. The formation of H_2 and CH_4 from benzene[8] is believed to be the cause for the discrepancy between the theoretical and observed decay curves for the 310 mc–80 mm benzene mixture.

The few experiments with carbon dioxide show that the distribution of the decay products does, as is to be expected from Harrington's work, vary widely with the particular gas being studied. However, since the chemical effect of ionizing radiation on benzene is large and the effect on carbon dioxide is negligible, Fig. 2 indicates that the relative distributions may be independent of the particular gas-radon mixture. If so, the distribution of RaA and RaB in any mixture can be determined from Fig. 3 by the experimental determination of RaC.

ACKNOWLEDGMENT

The radon for these measurements was supplied by the U. S. Marine Hospital, Baltimore, Maryland, through the courtesy of Dr. John E. Wirth and Mr. Robert W. Swain.

[8] To be published.

Size Effect in Low Temperature Heat Capacities

ELLIOTT W. MONTROLL*
University of Pittsburgh, Pittsburgh, Pennsylvania
(Received August 17, 1949)

It has been shown by Bolt and Maa that the distribution of normal modes of vibration of an elastic continuum is given by $A\nu^2+B(S/V)\nu+0(1)$ where A and B are numerical constants and S/V is the ratio of the surface area to the volume of the continuum. When this result is applied to the theory of the vibrational heat capacity of a solid at low temperatures, the $A\nu^2$-term yields the well-known T^3 law and the $B(S/V)\nu$-term leads to a contribution proportional to T^2. About 0.5 to 10 percent of the heat capacity of non-metallic powders and materials with a domain structure can be attributed to the T^2 term at 1°K. The importance of the surface term increases with decreasing temperature.

It is well known that at low temperatures the electronic contribution to the heat capacity of a metal is proportional to the temperature. In a system of very small metallic particles, the proportionality constant is increased by a quantity proportional to $(S/V^{\frac{1}{3}})n^{-\frac{1}{3}}$ where n is the number of conduction electrons in the metal.

SIZE EFFECT IN LOW TEMPERATURE HEAT CAPACITIES

IN view of the current interest in the anomalous behavior of solids at very low temperatures, it seems worth while to re-examine the expected thermodynamic behavior of normal solids at temperatures of the order of 1°K and lower. Although our discussion will be limited to heat capacities, it applies to other thermodynamic quantities as well.

We will show that by including surface effects in the calculation of the distribution of normal modes of vibration of a crystalline solid, we obtain low temperature heat capacity functions of the form $aT^3+bT^2n^{-\frac{1}{3}}$ where the aT^3 term corresponds to the Debye T^3 law. It seems that the $bT^2/n^{\frac{1}{3}}$ term (in which n is the number of molecules in the crystal) might become noticeable at 1°K in powders and in non-isotropic crystals with domain structures. At temperatures below 0.1°K the T^2 term can be expected to contribute a considerable fraction to the total heat capacity. We shall also show that in metals the linear law $c_v=\gamma T$ for the electron heat capacity is still valid at very low temperatures, but that the constant γ increases as the particle size decreases.

The starting point of the theory of the vibration contribution to the heat capacity is the Einstein equation

$$c_v=k\int_0^{\nu_L}\frac{g(\nu)(h\nu/kT)^2d\nu}{\sinh^2(h\nu/2kT)}, \tag{1}$$

where $g(\nu)d\nu$=number of normal modes in frequency range $d\nu$ at ν and ν_L=largest frequency. According to the Debye continuum theory of lattice vibrations, the frequencies of normal modes of vibration in a rectangular solid of dimensions L_x, L_y, and L_z are

$$\nu=\begin{cases}\frac{1}{2}c_l[(n_x/L_x)^2+(n_y/L_y)^2+(n_z/L_z)^2]^{\frac{1}{2}}\\ \frac{1}{2}c_t[(n_x/L_x)^2+(n_y/L_y)^2+(n_z/L_z)^2]^{\frac{1}{2}}\end{cases}$$

$$n_x, n_y, n_z=0, 1, 2, \cdots, \tag{2}$$

where c_l and c_t are, respectively, the velocities of propagation of longitudinal and transverse elastic waves in the crystal.

The number of normal modes of the form (2) which are less than ν has been found by Bolt and Maa[1] to be

$$n(\nu)=(4\pi V\nu^3/3c_3)+(\pi S\nu^2/4c_2)+(L\nu/8c_1)+\cdots, \tag{3a}$$

$$c_j^{-1}=c_l^{-j}+2c_t^{-j} \tag{3b}$$

where V=volume of crystal$=L_xL_yL_z$, S=surface area $=2(L_xL_y+L_xL_z+L_yL_z)$, and L=length of edges $=4(L_x+L_y+L_z)$.

The first term in (3a) is correct for any shape of solid. The second has been proven so far to be correct for the distribution of normal modes in rectangular, cylindrical, and triangular continua. Only the first term in (3) has been considered in theories of the heat capacity of solids.

The frequency distribution $g(\nu)$ is $dn(\nu)/d\nu$, or

$$g(\nu)=4\pi V\nu^2/c_3+\tfrac{1}{2}\pi S\nu/c_2+L/8c_1+\cdots, \tag{4a}$$

and the total number of normal modes, $3n$, is given by

$$3n=\frac{4}{3}\frac{\pi V}{c_3}\nu_L^3+\frac{\pi S}{4c_2}\nu_L^2+\frac{L\nu_L}{8c_1}, \tag{4b}$$

where ν_L=largest possible frequency. Hence ν_L is related to n and the c's by

$$\nu_L=\left(\frac{9nc_3}{4\pi V}\right)^{\frac{1}{3}}\left[1-\frac{\pi S}{36c_2n^{\frac{1}{3}}}\left(\frac{9c_3}{4\pi V}\right)^{\frac{1}{3}}+0(n^{-\frac{1}{3}})\right]. \tag{5}$$

The symbol $0(n^{-\frac{1}{3}})$ means that the omitted terms are of the order of $n^{-\frac{1}{3}}$.

As $T\to 0$, the heat capacity is given by (we let $u=h\nu/kT$ and introduce the Debye temperature

* Present address: Physics Branch, ONR, Washington, D. C.

[1] R. H. Bolt, J. Acous. Soc. Am. **10**, 228 (1939); D. Y. Maa, J. Acous. Soc. Am. **10**, 235 (1939); G. M. Roe, J. Acous. Soc. Am. **13**, 1 (1941).

$\theta=h\nu_L/k$)

$$c_v/k=(2kT/h)\int_0^\infty g(2kTu/h)(u^2/\sinh^2 u)du$$

$$=(4\pi V\nu_L{}^3/c_3)\left(\frac{2kT}{h\nu_L}\right)^3 I_4$$

$$+\left(\frac{\pi S\nu_L{}^2}{2c_2}\right)\left(\frac{2kT}{h\nu_L}\right)^2 I_3+\frac{L\nu_L}{8c_1}\left(\frac{2kT}{h\nu_L}\right)I_2, \quad (6a)$$

where

$$I_m=\int_0^\infty (u^m/\sinh^2 u)du=4m!\zeta(m)/2^{m+1}$$

and

$$\zeta(m)=\sum_{n=1}^{\infty} n^{-m}.$$

By introducing the first approximation of ν_L, Eq. (5), and the result $\zeta(4)=\pi^4/90$ into Eq. (6a), we obtain

$$c_v/nk=\frac{12}{5}\pi^4(T/\theta)^3+\frac{9}{4}\zeta(3)(12\pi)^{\frac{1}{3}}$$

$$\times\left(\frac{c_3{}^{\frac{1}{3}}}{c_2}\right)\left(\frac{S}{V^{\frac{1}{3}}}\right)\frac{(T/\theta)^2}{n^{\frac{1}{3}}}+0\left(\frac{1}{n^{\frac{1}{3}}}\right). \quad (6b)$$

Now the ratio $c_3{}^{\frac{1}{3}}/c_2$ is given by

$$\left(\frac{1}{c_l{}^3}+\frac{2}{c_t{}^3}\right)^{\frac{1}{3}}\Big/\left(\frac{1}{c_l{}^2}+\frac{2}{c_t{}^2}\right)$$

$$=\left[1+2\left(\frac{c_l}{c_t}\right)^3\right]^{\frac{1}{3}}\Big/\left[1+2\left(\frac{c_l}{c_t}\right)^2\right];$$

but,[2]

$$(c_l/c_t)^2=2(1-\sigma)/(1-2\sigma)$$

where $\sigma=$ Poisson's ratio. Numerically σ is usually between 0.3 and 0.45. It can be shown that $3^{-\frac{1}{3}}\leq c_3{}^{\frac{1}{3}}/c_2\leq 1$. Hence in a crystal in the shape of a cube ($V=L^3$ and $S=6L^2$), the coefficient of $(T/\theta)^3$ is 234 and that of $n^{-\frac{1}{3}}(T/\theta)^2$ is $\simeq 50$.

If we let R be the ratio of the T^3 to the T^2 term in (6b) we obtain

$$R\simeq 26(T/\theta)(V/S)(\rho/M)^{\frac{1}{3}}N^{\frac{1}{3}}, \quad (7)$$

where N is Avogadro's number, ρ the density of the solid, and M the gram molecular weight. This equation can be specialized in several interesting cases:

(a) Cube with sides of length l. $R\simeq 3.6\times 10^{8}l(T/\theta)(\rho/M)^{\frac{1}{3}}$.
(b) Thin films $l\times l\times ql$ with $q\ll 1$. $R\simeq 11\times 10^{8}ql(T/\theta)(\rho/M)^{\frac{1}{3}}$.
(c) Wires of length l and radius ql with $q\ll 1$. Same as (b).

[2] See, for example, R. H. Fowler, *Statistical Mechanics* (Cambridge University Press, London, 1936), p. 127.

In many metals (for example, Al, Fe, Cu, Zn, Mo, Ag, and Pt) one finds that $0.44/\text{cm}\leq(\rho/M)^{\frac{1}{3}}\leq 0.52/\text{cm}$, and $200°\text{K}\leq\theta\leq 450°\text{K}$. Hence in cubes of length 10^{-4} cm of these metals, $R\simeq 100$ at $T=1°\text{K}$. The Debye θ for diamond is about 1800°K, and $(\rho/n)^{\frac{1}{3}}\simeq 0.61/\text{cm}$. Hence $R\simeq 12$. In A, Ne, Kr, and Xe, $55°\text{K}\leq\theta\leq 80°\text{K}$, and $0.31/\text{cm}\leq(\rho/M)^{\frac{1}{3}}\leq 0.41/\text{cm}$. Hence in these cases $R\simeq 200$. These rough computations, which are based on the continuum theory of specific heats, imply that the deviations from the T^3 law should become measurable at 1°K in powders or in crystals which have a domain structure. Similar results can be obtained for films of thickness 10^{-4} cm and wires of diameter 10^{-4} cm.

We shall now show qualitatively that a calculation based on the theory of vibrations of lattices of discrete particles should yield values of R somewhat smaller than those given above. Some remarks on the origin of the ν^2-term in (3a) must precede our justification of this statement.

Let the differential equations which describe lattice vibrations be solved by using reflecting boundary conditions at each surface. Then each integral point in the octant $n_x, n_y, n_z\geq 0$ of (n_x, n_y, n_z) space corresponds to a normal mode of vibration of the lattice. In a cubically shaped crystal of volume $V=l^3$, the number of longitudinal waves of frequency $\geq\nu$ is the number of integral points which are included inside and on the surface bounded by the coordinate planes and a spherical surface of radius $2\nu l/c_l$. This number is approximately one-eighth the volume of a sphere of this radius or

$$\tfrac{1}{8}[(4/3)\pi](2\nu l/c_l)^3=(4/3)\pi\nu^3 V/c_l{}^3$$

which is the first term in (3a). Notice[1] that each integral point on the (n_x, n_y), (n_y, n_z), and (n_z, n_x) planes is, by this counting procedure, shared by two octants. However, each of these points corresponds to a normal mode. Therefore, they are given only half the weight they should have. The second approximation to $n(\nu)$ is one-half the area of the quadrants of circles of radius $(2\nu l/c_l)$ in the coordinate planes, or $3(\frac{1}{2})(\frac{1}{4})\pi(2\nu l/c_l)^2=\frac{1}{4}\pi\nu^2 S/c_l{}^2$ where $S=6l^2=$ surface area of cube. This is the second term in (3a).

The distribution of normal modes of a lattice of discrete particles can be found in a similar way.[3] The main difference is that the surfaces of constant frequency in n_x, n_y, n_z space are not spherical. Instead, they sometimes have one branch with a highly concave surface. When the ratio of force constants of nearest to next-nearest neighbors is $\simeq 0.05$, the distance from the origin to the point at which $n_x=n_y=n_z$ on a surface of constant frequency is about one-tenth the distance from the origin to the points of intersection of the same surface with the coordinate axes. Hence, the ratio of the volume bounded by the coordinate planes and a highly concave constant frequency surface to the areas of the region of the coordinate planes included between the

[3] M. Blackman, Proc. Roy. Soc. **A148**, 384 (1935); **A159**, 416 (1937). E. Montroll, J. Chem. Phys. **15**, 575 (1947).

coordinate axes and the curve of constant frequency is smaller than that of the corresponding ratio for a spherical surface of constant frequency. This means that the ratio R should be somewhat smaller than (6a) in lattices composed of discrete particles.

The size effect in the electronic contribution to the heat capacity of a metal at low temperatures does not change the functional dependence of C_v on temperature, but merely changes the proportionality constant in the T law.

The number of Fermi-Dirac particles in the energy range $(\epsilon, \epsilon+d\epsilon)$ in a system at temperature T is given by[4]

$$N(\epsilon)d\epsilon=\frac{C(\epsilon)\epsilon^{\frac{1}{2}}d\epsilon}{e^{(\epsilon-\mu)/kT}+1} \tag{7}$$

where $C(\epsilon)d\epsilon$ is the number of quantum states of the system in the energy range $(\epsilon, \epsilon+d\epsilon)$; μ is the chemical potential and is chosen so that the total number of particles, N, of the system is $N=\int N(\epsilon)d\epsilon$. In a container with perfectly reflecting walls this number is twice (allowing for two spin states for each particle) the number of sets of non-negative integers n_x, n_y, n_z which satisfy the inequality

$$\epsilon\leq\frac{h^2}{8mV^{\frac{2}{3}}}(n_x^2+n_y^2+n_z^2)<\epsilon+d\epsilon, \quad n_x, n_y, n_z\geq 0.$$

By repeating the arguments employed by Bolt and Maa we find that the number of sets of n's which correspond to an energy $\leq\epsilon$ is

$$\frac{8\pi}{3}\frac{V(2m)^{\frac{3}{2}}}{h^3}\epsilon^{\frac{3}{2}}+\frac{\pi mS\epsilon}{h^2},$$

where S is the total surface area of the container. Hence

$$C(\epsilon)=\frac{4\pi V}{h^3}(2m)^{\frac{3}{2}}\epsilon^{\frac{1}{2}}+\frac{\pi mS}{h^2}+\cdots.$$

The chemical potential μ_0 at $T=0$ represents the state of largest possible energy for a particle in our system when all lower energy states are filled. Hence

$$N=\int_0^{\mu_0}C(\epsilon)d\epsilon=\frac{8\pi V}{3}\frac{(2m)^{\frac{3}{2}}}{h^3}\mu_0^{\frac{3}{2}}+\frac{\pi mS\mu_0}{h^2}.$$

The solution, μ_0, of this equation can be expressed as a power series in $N^{-\frac{1}{3}}$

$$\mu_0=\left(\frac{3N}{8\pi V}\right)^{\frac{2}{3}}\frac{h^2}{2m}\left\{1-\frac{S}{12V^{\frac{1}{3}}}\left(\frac{9\pi}{N}\right)^{\frac{1}{3}}+0(N^{-\frac{2}{3}})\right\}.$$

The following low temperature expansion has long been in use in quantum statistics

$$I=\int_0^{\infty}\frac{f(\epsilon)d\epsilon}{e^{(\epsilon-\mu)/kT}+1}$$
$$=\int_0^{\mu}f(\epsilon)d\epsilon+\pi^2/6(kT)^2(df/d\epsilon)_{\epsilon=\mu}+0(kT)^4.$$

Hence, the power series in (kT) for μ can be obtained from

$$N=\int_0^{\infty}N(\epsilon)d\epsilon=\int_0^{\infty}[4\pi V(2m)^{\frac{3}{2}}\epsilon^{\frac{1}{2}}+\pi mSh]\times\frac{d\epsilon/h^3}{(e^{(\epsilon-\mu)/kT}+1)}$$
$$=8\pi V(2m)^{\frac{3}{2}}\mu^{\frac{3}{2}}/3h^3+\pi mS\mu/h^2+\pi^3V(2m)^{\frac{3}{2}}(kT)^2/3h^3\mu^{\frac{1}{2}}+\cdots. \tag{8}$$

If we assume that $\mu=\mu_0[1+a(kT)^2+\cdots]$, substitute this equation into (8), and solve for a, we obtain

$$\mu=\mu_0\left\{1-\frac{\pi^2}{12\mu_0^2}\left[1-\frac{S}{12V^{\frac{1}{3}}}\left(\frac{9\pi}{N}\right)^{\frac{1}{3}}\right](kT)^2+0(kT)^4\right\}.$$

The internal energy of a perfect Fermi-Dirac gas is given by

$$E=\int_0^{\infty}\frac{\epsilon N(\epsilon)d\epsilon}{e^{(\epsilon-\mu)/kT}+1}$$
$$=\frac{8}{5}\pi Vh^{-3}\mu^{5/3}(2m)^{\frac{3}{2}}+\tfrac{1}{2}\pi mS\mu^2/h^2+\frac{\pi^3(kT)^2}{6h^3}[6V\mu^{\frac{1}{2}}(2m)^{\frac{3}{2}}+mSh]+\cdots$$
$$=\frac{3N}{40}\left(\frac{3N}{\pi V}\right)^{\frac{2}{3}}\frac{h^2}{m}\left\{1-\frac{5}{48}\frac{S}{V^{\frac{1}{3}}}\left(\frac{9\pi}{N}\right)^{\frac{1}{3}}\right\}+\tfrac{2}{3}\pi^3Vmh^{-2}(3N/\pi V)^{\frac{1}{2}}(kT)^2\left[1+\frac{1}{24}\frac{S}{V^{\frac{1}{3}}}\left(\frac{9\pi}{N}\right)^{\frac{1}{3}}\right]+\cdots$$

Also as $T\to 0$,

$$C_v/Nk=4kT\frac{\pi^2m}{h^2}\left(\frac{\pi V}{3N}\right)^{\frac{2}{3}}\left[1+\frac{1}{24}\frac{S}{V^{\frac{1}{3}}}\left(\frac{9\pi}{N}\right)^{\frac{1}{3}}\right].$$

The first term is the well-known "T law" for the specific heat of a Fermi-Dirac gas. The complete equation shows that the analytic form of the low temperature heat capacity does not change in going from a large to a small particle; only the slope changes.

An additional effect of particle size on heat capacity at low temperature has been discussed by Frölich.[5] He takes into account the fact that in a system of a finite number of particles the energy distribution function is discrete and not continuous. As the particle size decreases, this effect becomes increasingly important.

[4] See, for example, J. E. Mayer and M. G. Mayer, *Statistical Mechanics* (John Wiley and Sons, Inc., New York, 1941), p. 378.

[5] H. Frölich, Physica 4, 406 (1937).

Line Intensities and Absorption for the 15-Micron Carbon Dioxide Band*

LEWIS D. KAPLAN
*U. S. Weather Bureau, Albuquerque, New Mexico***

(Received August 19, 1949)

Thorndike's value of 560×10^{10} cycles per centimeter-atmosphere for the total intensity of the 15-micron carbon dioxide band is used to calculate the line intensities at one atmosphere and 300°K. Calculation of absorption results in good agreement with published absorption curves by Martin and Barker. Absorption for 203 millibars and 218°K is recalculated, correcting previous errors and using better approximations.

INTRODUCTION

As pointed out in a previous paper,[1] it is possible to calculate the absorption of many gases on the basis of available experimental data and the complete theoretical treatment of absorption intensities given in the literature, provided only that the matrix element of the dipole moment or some quantity proportional to it is known. The total intensity of a vibration-rotational band is such a quantity, and has been determined by A. M. Thorndike[2] for the 15μ-band of carbon dioxide. Thorndike obtained a mean value of 560×10^{10} cycles per cm-atmosphere, but expressed some doubt as to its accuracy. It was thought advisable, therefore, to calculate the absorption on the basis of this value for path lengths for which laboratory measurements have been made, in order to see whether or not an experimental verification would result. The wave band chosen was from 14 to 16μ, and the measurements used for comparison were those of Martin and Barker[3] and Rubens and Ladenburg.[4] It was assumed that Thorndike's value was valid for 300°K and that the half-width of the carbon dioxide lines was 0.17 cm^{-1}.

The total intensity of a vibration-rotational band is given by[5]

$$\sum S=\frac{8\pi^3\sum d_{v''}\exp(-h\sum_i v_{i'}\nu_i/kT)\nu[1-\exp(h\nu/kT)](V_{v'|K|'}^{v''|K|''})^2}{3h\sum d_v\exp(-h\sum_j v_j\nu_j/kT)}, \tag{1}$$

where the summation in the numerator is over all transitions involved in the band; that in the denominator, over all vibrational states of the molecule. The primed and double-primed quantities represent the lower and upper state, respectively; v and K are the vibrational and angular momentum quantum numbers, ν the transition frequency, ν_i and ν_j the frequencies corresponding to the energy level, d_v the degeneracy of the level v, and $V_{v'|K|'}^{v''|K|''}$ the matrix element of the dipole moment corresponding to the transition $v'|K|'\rightarrow v''|K|''$. The quantities ν, $d_{v''}$ and $(V_{v'|K|'}^{v''|K|''}/V_{0^10^1}^{0^00^0})^2$ are given in Table I for the transitions $v_1'v_2'^{|K|'}v_3'\rightarrow v_1''v_2''^{|K|''}v_3''$ involved in the 15μ band.[6] It was assumed that the $01^10\rightarrow10^00$ transition shared the $01^10\rightarrow02^00$ intensity in the ratio 3:7.[1]

CALCULATION OF LINE INTENSITIES

Solving Eq. (1) for $8\pi^3(V_{0^10^1}^{0^00^0})^2/3h$, a value of 0.14092 per cm-atmosphere is obtained. This may now be used for calculation of the line intensities. The intensity of a vibration-rotational line is given by[5]

$$S=\frac{F_vF_r\exp[-h\sum_i(v_i\nu_i+J'^2Bc+J'Bc)/kT][1-\exp(-h\nu/kT)]}{T\sum d_v\exp(-h\sum_j v_j\nu_j/kT)}, \tag{2}$$

where

$$F_v=8\pi^3Bcd_{v''}(V_{v'v''})^2/3k \tag{3}$$

and

$$F_r=2(A_{J'|K|'}^{J''|K|''})^2(2J''+1)\nu/c. \tag{4}$$

* This work was carried on at the Department of Physics, University of New Mexico, Albuquerque, New Mexico, under the sponsorship of the U. S. Weather Bureau, Department of Commerce, and is published with permission of the Chief, U. S. Weather Bureau.

** Present address: Department of Meteorology, University of Chicago, Chicago 37, Illinois.

[1] L. D. Kaplan, J. Chem. Phys. **15**, 809 (1947).

[2] A. M. Thorndike, J. Chem. Phys. **15**, 868 (1947).

[3] P. E. Martin and E. F. Barker, Phys. Rev. **41**, 291 (1932).

[4] H. Rubens and E. Ladenburg, Verh. d. D. Phys. Ges. **7**, 170 (1905).

[5] D. M. Dennison, Rev. Mod. Phys. **3**, 280 (1931).

[6] G. Herzberg, *Infrared and Raman Spectra of Polyatomic Molecules* (D. Van Nostrand Company, New York, 1945), pp. 80–81, 272–276. The first few polynomials $F_{v_i}|K|_i(\xi)$, where $\xi=\alpha_i^{\frac{1}{2}}\rho_i$, are, in normalized form for Eq. (II, 58), p. 81: $F_{00}=\pi^{-\frac{1}{4}}$, $F_{11}=-\pi^{-\frac{1}{4}}\xi$, $F_{20}=\pi^{-\frac{1}{4}}(1-\xi^2)$, $F_{22}=(2\pi)^{-\frac{1}{4}}\xi^2$, $F_{31}=(4\pi)^{-\frac{1}{4}}\xi(2-\xi^2)$, $F_{33}=(6\pi)^{-\frac{1}{4}}\xi^3$.

B is the rotational constant, equal to 0.390 cm^{-1} for carbon dioxide, J is the rotational quantum number, and $(A^{J''|K|''}_{J'|K|'})^2$ is the sum of the squares of the direction cosine matrix elements taken with respect to two axes fixed in space and perpendicular to the axis of the molecule and to each other.[7] It is assumed in these equations that the moment of inertia around the principal axis of the molecule is negligible in comparison with that around an axis perpendicular to it.

The line intensities for the P and R branches of the $00^00 \rightarrow 01^10$ transition, the R branch of the $01^10 \rightarrow 02^00$ transition and P branch of the $01^10 \rightarrow 10^00$ transition were calculated and are given in Table II as a function of J'. Most of the frequencies are taken from Martin and Barker,[3] and the rest determined by an extrapolation made in such a way that the line centers would coincide. In such a case, the line shape remains unchanged and the total line intensity is the sum of the two individual intensities. The fourth and fifth significant figures were of course not considered to be accurate, but they were retained for the calculations to be described in the following sections.

CALCULATION OF ABSORPTION AND COMPARISON WITH EXPERIMENTAL RESULTS

For all practical purposes the black body radiation distribution for the hot source used in spectroscopic measurements may be considered as linear from 14 to 16 microns. Thus, if $I_{0\nu}$ is the emitted radiation at ν and $I_0(\nu_Q)$ that at ν_Q, which is used here to represent the frequency corresponding to 15μ (the center of the Q branch),

$$I_{0\nu}=I_0(\nu_Q)+b(\nu-\nu_Q), \tag{5}$$

where $I_0(\nu_Q)$ and b are constants. The fractional absorption of the radiation incident in the band $\Delta\nu$ from 14 to 16μ is then

$$\bar{A}=\int_{\nu_Q-\Delta\nu/2}^{\nu_Q+\Delta\nu/2} I_{0\nu}A(\nu)d\nu \Big/ \int_{\nu_Q-\Delta\nu/2}^{\nu_Q+\Delta\nu/2} I_{0\nu}d\nu$$

$$=\frac{1}{\Delta\nu}\int_{\text{band}} A(\nu)d\nu+\frac{b}{2I_0(\nu_Q)\Delta\nu}$$

$$\times\int_{-\Delta\nu/2}^{+\Delta\nu/2} A(\nu-\nu_Q)d(\nu-\nu_Q)^2, \tag{6}$$

TABLE I. Values for numerator of Eq. (1).

Transition	$\bar{\nu}=\nu/c$	$d_{J''}$	$(V^{v''}_{v'}\|^{K}_{K}\|^{J''}_{J'}/V_{0^10^0})^2$
$00^00 \rightarrow 01^10$	667.3	2	1
$01^10 \rightarrow 02^20$	668.1	2	2
$01^10 \rightarrow 02^00$	618.5	1	1
$01^10 \rightarrow 10^00$	720.8		
$02^00 \rightarrow 03^10$	646.1	2	2
$02^20 \rightarrow 03^30$	Not Obs.	2	3

[7] The equations for $(A^{J''|K|''}_{J'|K|'})^2$ are given by D. M. Dennison, reference 5, pp. 313–314. The factor 2 in Eq. (4) is due to the non-appearance of alternate rotational levels.

where $A(\nu)$ is the fractional absorption at ν. If the absorption spectrum is symmetrical with respect to ν_Q, A is an even function of $\nu-\nu_Q$ and the second integral on the right-hand side disappears. Actually, this is so nearly the case that the second integral can reasonably be considered negligible in comparison with the first. The total absorption is then obtained by averaging the absorption over the band, as in the case for incident radiation independent of frequency.

TABLE II. Line intensities for the 15μ CO_2 band.*

	$00^00 \rightarrow 01^10$		$01^10 \rightarrow 02^00$			$00^00 \rightarrow 01^10$		$01^10 \rightarrow 10^00$	
$\bar{\nu}$ (cm^{-1})	J'	$S_P(J')$	J'	$S_R(J')$	$\bar{\nu}$ (cm^{-1})	J'	$S_R(J')$	J'	$S_P(J')$
666.0	3	0.6028			668.1	0	0.6175		
664.4	5	1.1625			669.6	2	1.2267		
662.9	7	1.6569			671.3	4	1.8033		
661.3	9	2.0674			672.8	6	2.3062		
659.7	11	3.3824			674.5	8	2.7332		
658.2	13	2.5970			676.0	10	3.0627		
656.7	15	2.7113			677.6	12	3.2874		
655.1	17	2.7313	49	0.0031	679.2	14	3.4051		
653.6	19	2.6684	47	0.0043	680.8	16	3.4206	50	0.0028
652.1	21	2.5370	45	0.0058	682.5	18	3.3438	48	0.0039
650.5	23	2.3518	43	0.0076	684.1	20	3.1872	46	0.0053
649.0	25	2.1302	41	0.0100	685.7	22	2.9677	44	0.0072
647.5	27	1.8880	39	0.0128	687.3	24	2.7045	42	0.0096
646.0	29	1.6384	37	0.0162	689.0	26	2.4135	40	0.0125
644.4	31	1.3933	35	0.0201	690.6	28	2.1103	38	0.0160
643.1	33	1.1630	33	0.0245	692.1	30	1.8104	36	0.0201
641.5	35	0.9520	31	0.0292	693.7	32	1.5229	34	0.0249
639.9	37	0.7649	29	0.0342	695.3	34	1.2591	32	0.0302
638.5	39	0.6038	27	0.0393	697.0	36	1.0215	30	0.0360
637.0	41	0.4683	25	0.0443	698.6	38	0.8147	28	0.0421
635.5	43	0.3567	23	0.0488	700.1	40	0.6378	26	0.0483
634.0	45	0.2671	21	0.0526	701.8	42	0.4914	24	0.0543
632.5	47	0.1966	19	0.0553	703.3	44	0.3718	22	0.0597
631.0	49	0.1423	17	0.0567	705.2	46	0.2769	20	0.0642
629.6	51	0.1014	15	0.0564	706.7	48	0.2027	18	0.0674
628.1	53	0.0710	13	0.0544	708.4	50	0.1460	16	0.0689
626.7	55	0.0489	11	0.0504	710.0	52	0.1034	14	0.0684
625.3	57	0.0332	9	0.0445	711.7	54	0.0761	12	0.0658
623.9	59	0.0221	7	0.0368	713.5	56	0.0494	10	0.0608
622.8	61	0.0145	5	0.0275	715.0	58	0.0333	8	0.0536
620.9	63	0.0094	3	0.0170	716.6	60	0.0221	6	0.0442

* In wave numbers per cm-atmosphere, for $T=300°K$.

Elsasser[8] has derived an expression for the absorption coefficient of a series of overlapping equidistant lines of equal intensity:

$$k(\nu)=S\sinh\beta/D[\cosh\beta-\cos(2\pi\nu/D)], \tag{7}$$

where $\beta=2\pi\gamma/D$; γ is the half-width of the line and D the line spacing; and has shown that this results in the absorption

$$A=\sinh\beta\int_0^y \exp(-y\cosh\beta)J_0(iy)dy, \tag{8}$$

where

$$y=Su/D\sinh\beta, \tag{9}$$

u is the path length reduced to S.T.P., and $J_0(iy)$ is the zero-order Bessel Function of imaginary argument. These equations are applicable to the R and P branches of the 15μ carbon dioxide spectrum, since the intensity envelope is a smooth curve with little change in slope and the line spacing changes slowly and regularly.

[8] W. M. Elsasser, Phys. Rev. **54**, 126 (1938).

Mean line spacings were assigned as follows:

P branch:	$3 \leq J' \leq 27$	$D = 1.55$ cm^{-1}
	$29 \leq J' \leq 49$	$D = 1.50$ cm^{-1}
	$51 \leq J' \leq 57$	$D = 1.45$ cm^{-1}
R branch:	$0 \leq J' \leq 38$	$D = 1.60$ cm^{-1}
	$40 \leq J' \leq 56$	$D = 1.65$ cm^{-1}.

The sum of the line intervals is 89.3 cm^{-1}, i.e., the width of the band. Equation (8) was solved numerically for each of these five values of D, using intervals of $\Delta y = 0.01$ for $y \leq 2.45$, $\Delta y = 0.1$ for $y \leq 9.5$, and $\Delta y = 1$ for $y \geq 10$. The absorption due to each line was interpolated from this table for each path length.

For very small values of y (<0.045), $J_0(iy)$ was taken as unity, so that Eq. (8) reduces to

$$A = \tanh\beta[1 - \exp(-y\cosh\beta)]. \qquad (10)$$

The absorption by the Q branch was taken directly from the curves of Martin and Barker, interpolating for $u = 1$ cm. Complete absorption by the Q branch was assumed for $u = 4$ and $u = 20$ cm. Transitions other than those included in Table II were not considered in the absorption calculations, as they would be submerged by the lines of the $00^00 \rightarrow 01^10$ transition.

Before averaging the absorption by means of Eq. (6), the effect of the wings of the Q branches of the $00^00 \rightarrow 01^10$, $01^10 \rightarrow 02^20$, $01^10 \rightarrow 02^00$ and $01^10 \rightarrow 10^00$ transitions, upon which the P and R branch lines were superimposed, had to be taken into account. Elsasser's expression for the fractional transmission, due to the wings of many lines whose distance from the frequency considered is large compared to the half-width, was used:[9]

$$\tau_{\text{cont}} = \exp[-\gamma u \sum S_i/\pi(\nu - \nu_i)^2], \qquad (11)$$

where S_i is the intensity of the line at frequency ν_i. If τ_{cont} is considered linear within one line interval, it can be shown, by an argument very similar to that used in discussing Eq. (6), that the resultant fractional transmission is given by the simple relationship

$$\tau = \tau_{\text{cont}}\tau_{\text{line}}, \qquad (12)$$

where τ_{line} is one minus the absorption as determined from Eq. (8).

[9] W. M. Elsasser, Phys. Rev. **53**, 768 (1938).

TABLE III. Percent absorption, calculated and observed.

Path-length (cm-atmospheres)	Calculated 290°K	Calculated 300°K	Observed
0.004	0.93	0.93	1*
0.05	6.4	6.5	8.0*
0.23	20.0	20.3	20.0*
0.68	39.5	40.0	38.7*
1	47.8	48.5	48.0**
1.58	57.9	58.7	57.7*
4	75.7	76.8	73.3**
20	93.5	94.3	91.2**

* Martin and Barker. ** Rubens and Ladenburg.

The results of the absorption calculations are given in Table III for the temperatures 290°K and 300°K. The observed values were taken from a table compiled by G. S. Callendar.[10] Good agreement has been obtained in the intermediate range of path lengths. It should be noted that it is the transmission that is measured directly rather than the absorption, so that the discrepancies at small path length can be explained by small fractional errors in measured radiation or gas amounts, or by small inaccuracies in the representation in the published curves. The discrepancy with the measured absorption at 4 and 20 cm by Rubens and Ladenburg is more serious. Even this, however, can be explained on the basis of the poor resolution necessary in 1905 due to the inadequacies of the thermopiles then available. The widths of both the slit and the thermopile were 0.8 mm, which would result in a spectral transmittance distribution approximately triangular in shape and with base about 39 cm^{-1} at 14μ and 25 cm^{-1} at 16μ.[4] Thus the spectral regions of very high transmission beyond the band interval considered here are weighted into the absorption at the extremities of the band. Since the greater part of the transmission occurs at the band edges for large path lengths, this would result in much too high values of transmission for this particular interval as given by the curves of Rubens and Ladenburg. On the basis of these considerations, it is the opinion of this author that the results of Table III justify the use of Thorndike's value of 560×10^{10} cycles per cm-atmosphere for the total intensity of the band, and the value of 0.17 cm^{-1} for the half-width of the lines.

RECALCULATION OF ABSORPTION FOR 203 MILLIBARS AND 218°K

In a previous paper on this subject,[1] the author made several serious errors which require correction. These are:

(1) The line intensities for 218°K were improperly normalized. Equation (10) is incorrect and should be replaced by Eqs. (2), (3), and (4) of the present paper. The ordinates of Figs. 4 and 5 and the line intensities of Table I should be multiplied by a factor of about 1.296.

(2) The values given for the absorption as calculated from Callendar's empirical formula were erroneous.[11] The correct values are smaller (see Table V of this paper).

(3) The superimposed absorption spectrum, due to the wings of the Q branches, was not taken into account.

(4) The approximations used in calculating the absorption values given in Table II were too crude.

A discussion of the last point is in order, as it required a complete recalculation of the absorption. The equation of Ladenburg and Reiche used for small absorption

$$A\Delta\nu = Su\exp(-x)[J_0(ix) - iJ_1(ix)], \qquad (13)$$

where $x = Su/2\pi\gamma$, does not take into account the over-

[10] G. S. Callendar, Quart. J. Roy. Met. Soc. **67**, 263 (1941).

[11] The author is grateful to Dr. Callendar for bringing this to his attention.

lapping of neighboring lines. The approximate equation due to Elsasser, on the other hand,[12]

$$A_i=\varphi[(\pi\gamma u S_i)^{\frac{1}{2}}/D_i], \tag{14}$$

where φ represents the probability function, which was used for moderate and large values of absorption, is derived by assuming that $\sinh\beta=\beta$ and $\cosh\beta=1$ in Eq. (7) of the present paper.[8] An examination of Eq. (7) will show that this results in an infinite value for the absorption coefficient at the line center, and too high values at all frequencies. A comparison of absorption calculated from Eq. (14) with that calculated from Eq. (8) showed values considerably too large for all except very large values of absorption.

For the small half-width of 0.04 cm^{-1} at 203 millibars and 218°K,[1,13] Eq. (8) can be simplified by a reasonable approximation. If $\cosh\beta=1+b$, the exponential can be expanded and all terms of degree higher than the first neglected for y not large. Equation (8) then becomes

$$A_i=\sinh\beta\int_0^y(1-by)\exp(-y)J_0(iy)dy$$
$$=\sinh\beta\exp(-y)[(y-by^2/3)J_0(iy)$$
$$-(y-by^2/3-by/3)iJ_1(iy)] \tag{15}$$

as may be verified by differentiating the right-hand site with respect to y. A comparison of Eq. (13) with this expression shows that the equation of Ladenburg and Reiche also leads to too large values of the absorption. Equation (15) was used to calculate absorption for $y<10$. For $y>10$, a modified form of Eq. (14) was used, multiplying the absorption coefficient with a factor that would give the correct value midway between two adjacent lines. The modified equation is

$$A=\varphi\{\sinh\beta[y/(1+\cosh\beta)]^{\frac{1}{2}}\}. \tag{16}$$

The values obtained from Eqs. (15) and (16) for $y=10$ are tabulated in Table IV for the various line spacings. It should be noted that the values obtained by Eq. (15) are too small; those by Eq. (16), too large; the latter discrepancy being the larger for $y=10$. This inaccuracy decreases rapidly for larger values of y. It is believed that the errors in the final tabulated results due to these approximations are too small to affect the last of the significant figures given.

The absorption in the vicinity of the Q branch was calculated with the use of Fig. 5 of the previous paper[1] after applying the corrective factor 1.296. The overlapping of the wings of the Q branches was taken into account in the manner described in the previous section.

The results of the absorption calculations are given in the second column of Table V. The third column contains the absorption as determined from the absorption curve of the previous paper with the corrective factor of 1.296 applied. The good agreement with the recalculated values for small path lengths is the result of the fact that the error due to the neglecting of the wings of the Q branches has a sign opposite to that due to the use of the approximations represented by Eqs. (13) and (14). The fourth column gives the absorption as calculated from Callendar's formula[10]

$$A=1-[1+n(u)^x(P/P_0)^{x/2}]^{-1}, \tag{17}$$

where $n=0.9$ and $x=0.84$ are empirical constants and P is the pressure. No better results are obtained either by taking the temperature effect upon the line-width into account with[2]

$$A=1-[1+n(u)^x(P/P_0)^{x/2}(T_0/T)^{x/4}]^{-1} \tag{18}$$

or by changing the constants (say to $n=0.923$ and $x=0.89$) to give better conformity with the calculated absorption given in Table III.

The discrepancy for large path lengths might perhaps be explained by the decrease of the Boltzmann factor for the ends of the band at the lower temperature. There does not, however, seem to be any explanation for the discrepancy for small path lengths other than that Callendar's formula is not applicable to conditions different from those prevailing during the observations to which it was fitted. It appears from Table V that calculations of flux divergence from Callendar's formula for path lengths greater than 20 cm-atmospheres and pressures and temperatures similar to that discussed here will lead to much too low results.[14]

The author is greatly indebted to Dr. Edward Teller for his continued interest in this work and for his valuable discussions and criticisms. He also wishes to express his gratitude to Dr. George Peterson, Head of the Department of Psychology, University of New Mexico, for the use of the Monromatic calculator, without the use of which the numerous calculations could not have been performed.

TABLE IV. Absorption for $y=10$.

D (cm^{-1})	Eq. (15)	Eq. (16)
1.45	0.4103	0.4169
1.50	0.3979	0.4042
1.55	0.3862	0.3923
1.60	0.3752	0.3810
1.65	0.3647	0.3703

TABLE V. Percent absorption for 203 millibars and 218°K.

Path-length (cm-atmospheres)	Calculated absorption	From previous paper with factor 1.296	Absorption from Callendar's formula Eq. (17)	Eq. (18)	Eq. (17) with $n=0.923$, $x=0.89$
0.004	0.62	0.71	0.44	0.47	0.33
0.05	5.2	5.2	3.6	3.8	3.0
1	29.5	30.3	31.4	32.9	31.1
4	51.1	54	59.5	61.1	60.8
20	75.1	84	85.0	85.9	86.7

[12] Note that this is erroneously written in the previous paper.

[13] L. D. Kaplan, J. Chem. Phys. **16**, 426 (1948).

[14] It is the author's opinion that laboratory measurements of absorption, or calculations as described in this paper, are not applicable directly to calculation of radiative flux divergence in the atmosphere. This will be discussed in a forthcoming paper.

The Absorption Spectra of Methane, Carbon Dioxide, Water Vapor, and Ethylene in the Vacuum Ultraviolet

PHILIP G. WILKINSON* AND HERRICK L. JOHNSTON
Department of Chemistry, The Ohio State University, Columbus, Ohio

(Received June 13, 1949)

Quantitative absorption measurements were made of methane, carbon dioxide, water vapor, and ethylene at 30°C in a Cario and Schmidt-Ott vacuum fluorite spectrograph from 1400 to 2000A. Values of the atmospheric absorption coefficient, α, in the equation, $I=I_0\exp(-\alpha x)$, ranging from two for carbon dioxide to 800 for ethylene were found. Resonance wave-lengths and oscillator strengths were calculated from absorption curves and found to be consistent with refractive index data.

I. INTRODUCTION

A NUMBER of investigations have been made in the past of the quantitative absorption spectra of gases below 1800A,[1] and more recently, a paper on ethylene appeared in the literature while this one was being written.[2]

This paper reports the absorption coefficients of methane, carbon dioxide, water vapor, and ethylene in the vacuum ultraviolet. Particular care was exercised in removing traces of oxygen which can cause erroneous results since oxygen absorbs strongly in this region.

Oscillator strengths were computed from the quantitative absorption data for the well-defined electronic transitions; these were then compared with those calculated from data on the dispersion of the refractive index.

II. EXPERIMENTAL APPARATUS

A Cario and Schmidt-Ott vacuum fluorite spectrograph[3] fitted with a Hanovia hydrogen discharge tube and a Pyrex absorption cell were employed in the investigation. Both the hydrogen discharge, which gives a "many-lined" spectrum and a continuum extending from 1000 to 5000A,[4] and a discharge through carbon dioxide, which gives an intense emission band spectrum of carbon monoxide extending from 1605A into the ultraviolet, were employed as light sources.† Lithium fluoride windows limited most observations to wavelengths above 1400A. The blackening of the Eastman III–O type ultraviolet-sensitized photographic plates was calibrated by timed exposures and calibrated screens giving a Schwarzschild factor of 0.96. Otherwise, the calculation of the absorption coefficient, including corrections for weak background scattering, followed closely the method of Ladenburg and Van Voorhis.[1]

In order to insure high purity, all gases employed were vacuum-distilled and analyzed for oxygen. The methane was prepared by vacuum distillation of Ohio natural gas by the method of Storch and Golden.[5] In order to remove traces of oxygen, a small amount of hydrogen was added to the methane and the mixture passed over platinized asbestos at 200°C. A gas analysis showed less than 0.00001 percent oxygen which permitted pressures up to 40 cm of methane to be employed in the absorption cell.

Carbon dioxide, which showed about 0.001 percent oxygen was prepared by the thermal decomposition of sodium bicarbonate followed by drying and careful resublimation. Water free from oxygen (less than 0.00001 percent) was easily prepared by vacuum distillation. Tank ethylene was passed over metallic sodium

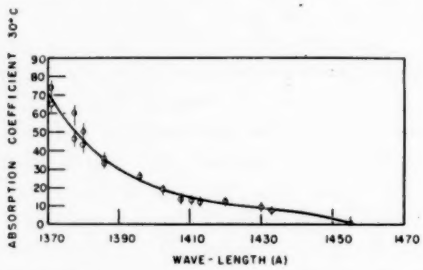

FIG. 1. The atmospheric absorption coefficient, α, of methane at 30°C.

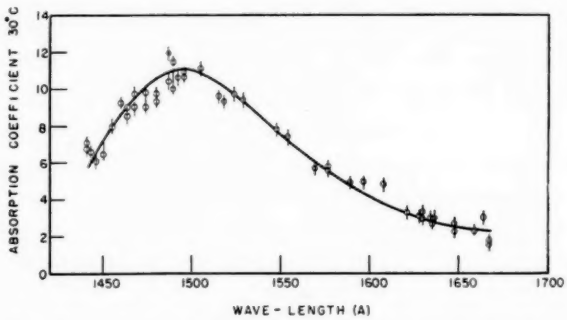

FIG. 2. The atmospheric absorption coefficient, α, of carbon dioxide at 30°C.

* Now at the Naval Research Laboratory, Washington, D. C.

[1] Ladenburg, Van Voorhis, and Boyce, Phys. Rev. **40**, 1018 (1932). R. Ladenburg and C. C. Van Voorhis, Phys. Rev. **43**, 315 (1933). Scheibe, Povenz, and Lindström, Zeits. f. physik. Chemie **20B**, 283 (1933). L. W. Pickett, J. Chem. Phys. **8**, 293 (1940). J. Romand and B. Vodar, Comptes Rendus **226**, 238, 890 (1948).

[2] Platt, Klevens, and Price, J. Chem. Phys. **17**, 466 (1949).

[3] G. Cario and H. D. Schmidt-Ott, Zeits. f. Physik **69**, 719 (1931).

[4] T. Lyman, Astrophys. J. **23**, 181 (1906).

† Although the dispersion and resolution of the spectrograph are 15A/mm at 1600A and about 1A, respectively, the actual resolution obtained may be as low as 10A due to the use of emission lines for many measurements.

[5] H. H. Storch and P. L. Golden, J. Am. Chem. Soc. **54**, 4662 (1932).

and fractionally distilled. No analysis was made since up to one percent oxygen could be tolerated because of the high absorption of ethylene.

III. SPECTRA

The absorption coefficient for one atmosphere, α, was calculated according to the equation:

$$I = I_0 \exp(-\alpha x), \quad (1)$$

in which I_0 is the light intensity recorded on the photographic plate at a given wave-length with the absorption chamber evacuated, and I is the light intensity under the same conditions after passing through a column of gas x cm in length at atmospheric pressure and 30°C.

Methane

Twenty photographs of the absorption of methane were made at 0.02 to 40 cm pressure in a path length of 38 cm. No bands were found from 1350 to 1800A. Only continuous absorption was observed and this occurs only below 1455A as shown in Fig. 1.

Carbon Dioxide

Since carbon dioxide decomposes photo-chemically in the vacuum ultraviolet, a complication might be expected from the oxygen arising in the light path during the photographic exposure. In order to ascertain experimentally whether the photo-chemically formed oxygen diffused out of the light path fast enough to eliminate this complication, photographs of the carbon dioxide absorption were made at 1458, 1463.5, and 1474A at the same pressure in both a static and in a fast flowing system. In the latter the oxygen should be swept out as fast as it is formed. The photographic densities agreed closely for the two conditions, which indicates that photo-chemically formed oxygen caused only small errors.

Thirty photographs of the absorption of carbon dioxide were made in a flowing system at pressures from 0.2 to 2.4 mm from 1440 to 1700A and the spectrum is recorded in Fig. 2. The maximum value of α for the continuum is 11.0 and lies at 1495A, which is 45A higher than the maximum of the oxygen absorption. Three weak absorption bands were found at 1690, 1673, and 1662A.

Water Vapor

The absorption spectrum of water vapor was photographed in a flowing system with 10 plates at pressures from 0.4 to 13 mm from 1430 to 1859A and is recorded in Fig. 3. Three diffuse bands superimposed on a continuum appear with a maximum value of α of about 100 at 1608, 1648, and 1718A.

Ethylene

Ethylene was photographed in absorption on six plates from 1430 to 2000A at pressures from 0.02 to 0.4 mm. The absorption coefficients are plotted in Fig. 4 and show a continuous spectrum with a maximum value of α of about 800 at 1614A adjacent to six strong absorption bands at 1652, 1665, 1689, 1729, and 1744A. Other weak bands are observed above 1770A.

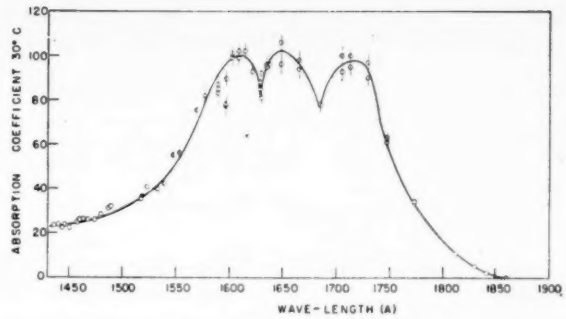

FIG. 3. The atmospheric absorption coefficient, α, of water vapor at 30°C.

IV. DISCUSSION AND CONCLUSIONS

The summary of the absorption data on methane, carbon dioxide, water vapor, and ethylene is given in Table I. The first column gives the molecule, the second the investigator, the third gives a brief description of the method of preparation, the fourth gives the maximum product of pressure and path length (both in cm) used in each case, and the fifth gives the qualitative results.

Rose[6] reported continuous absorption in methane below 1869A. Since under his experimental conditions the oxygen impurity would have to be less than 0.00014 percent, and since he mentioned no gas analysis, it is presumed that he was actually photographing the absorption of oxygen which extends to 1950A. The same comments apply to the data of Leifson.[7] As recorded in Table I our path length-pressure product was greater than Leifson's but still showed no absorption above 1455A. This result agrees with the qualitative data of Duncan and Howe[8] who worked at low pressures.

Group theory predicts that for molecules of tetrahedral symmetry, the upper electronic state which combines with the ground state on absorption is completely

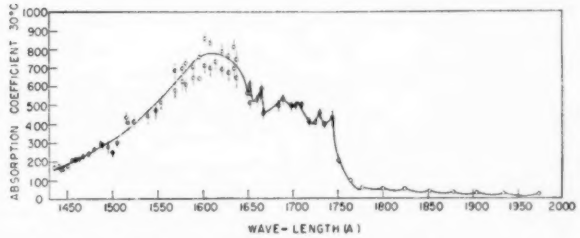

FIG. 4. The atmospheric absorption coefficient, α, of ethylene at 30°C.

[6] A. Rose, Zeits. f. Physik **81**, 745 (1933).
[7] S. W. Leifson, Astrophys. J. **63**, 73 (1926).
[8] A. B. F. Duncan and J. P. Howe, J. Chem. Phys. **2**, 851 (1934).

TABLE I. Summary of absorption data on methane, carbon dioxide, water vapor, and ethylene.

Gas	Investigator	Gas preparation and analysis	Pressure path length product (cm²)	Observations
Methane	Leifson[a]	Heating sodium acetate and soda lime. Dried over P_2O_5.	114	Continuous absorption below 1800A. Six bands below 1558A.
	Rose[b]	Not mentioned.	1140	Complete continuous absorption up to 1869A.
	Duncan and Howe[c]	Grignard reaction using pure CH_3I. Fractionated in vacuum.	10	Continuous absorption from 950–1450A. Max. between 1200 and 1300A.
	This research.	Distilled from natural gas. See text. Gas analysed less than 0.00001 percent oxygen.	1520	Continuous absorption below 1455A. No discrete absorption.
Carbon dioxide	Leifson[a]	Hydrogen chloride and calcium carbonate. Dried over phosphorus pentoxide.	114	Absorption bands at 1692, 1675, 1660, and 1647A. General absorption commencing at 1610A and extending to lower wave-lengths.
	Rathenau[d]	Thermal decomposition of magnesium carbonate. Distilled in vacuum.	About 5	No absorption bands above 1147A. Bands below. Continuum not observed.
Carbon dioxide	Price and Simpson[e]	Not mentioned.	24	Diffuse bands below 1700A. Continuous absorption between 1620 and 1250A. Maximum about 1460A.
	This research.	Thermal decomposition of sodium bicarbonate. Sublimed in vacuum. See text. Gas analyzed 0.001 percent oxygen.	9.5 for continuous absorption. 352 for observation of discrete bands.	Continuous absorption from 1667 to 1441A. (Limit of spectrograph.) Bands at 1690, 1673, 1662A. Maximum of continuum at 1495A.
Water vapor	Leifson[a]	Not mentioned.	Not mentioned.	Strong absorption bands between 1780 and 1610A. Maximum at 1700A.
	Rathenau[d]	Not mentioned.	Not mentioned.	Continuous absorption from 1784A to below 1400A, superimposed by broad and weak bands.
	This research.	Pumped on with high vacuum. Percent oxygen less than 0.00001.	11	Continuous absorption from 1859A to 1436A superimposed by three absorption bands at 1608 1648, and 1718A.
Ethylene	Scheibe and Grieneisen[f] W. C. Price[f] Snow and Allsopp[f]	Not mentioned.	Not mentioned.	Absorption bands between 1650 and 2000A. Continuous absorption below 1650A.
	Price and Tutte[f]	Not mentioned.	Not mentioned.	Measured positions of bands accurately. Followed continuous absorption down to 1000A. Maximum of continuum at 1630A.
	Platt, Klevens and Price[g]	Tank ethylene.	0.07	Bands above 1580A. Continuous absorption with maximum at 1625A and absorption coefficient of 1600.
	This research.	Tank ethylene passed over sodium. Condensed and distilled in vacuum. Percent oxygen less than 0.1 percent.		Bands above 1650A. Continuous absorption from 1777 to 1436A (limit of apparatus). Maximum of continuum at 1614A and absorption coefficient 800.

[a] See reference 7.
[b] See reference 6.
[c] See reference 8.
[d] See reference 10.
[e] See reference 11.
[f] See reference 12.
[g] See reference 2.

repulsive.[9] Thus, the absorption of methane in this spectral region can only be continuous.

[9] H. A. Jahn and E. Teller, Proc. Roy. Soc. (L) **A161**, 220 (1937); H. A. Jahn, Proc. Roy. Soc. (L) **A164**, 117 (1938); H. Sponer and E. Teller, Rev. Mod. Phys. **13**, 91 (1941).

Carbon dioxide, as has been shown, possesses a real continuum between 1441 and 1659A which is so weak that it is probably a forbidden transition. Rathenau[10]

[10] G. Rathenau, Zeits. f. Physik **87**, 32 (1933).

did not observe the continuum; however, Leifson[7] and Price and Simpson[11] did.

Although the pressure path length product employed in this research was three times that of Leifson,[7] the reported absorption band at 1647A was not observed; three others at 1690, 1672, and 1660A were observed.

The diffuse absorption reported by Price and Simpson[11] was not observed. Their reported maximum of absorption at 1460A might indicate the presence of some oxygen as an impurity.

The water vapor absorption data of Fig. 3 agree with the qualitative data of previous investigators.[7,10] The temperature of the absorption cell was maintained high enough so that there was no possibility of water vapor condensation on the windows.

The absorption spectrum of ethylene reported in this research is in good agreement with the qualitative data of previous investigators.[12] According to Price,[12] the six strong lines adjacent to the continuous absorption belong to an overlapping electronic transition. There is some indication (Fig. 4) that the four other bands found by Price at shorter wave-lengths are present although the many lined spectrum of hydrogen limits the resolution. Very recent data by Platt *et al.*[2] gives general agreement but yields quantitative values about twice ours at some points. No plausible explanation of this is possible at this time.

V. THE OSCILLATOR STRENGTH

By plotting the absorption coefficient as a function of the frequency and integrating graphically under the curve corresponding to one electronic transition, it is possible to compute the oscillator strength for the transition.[1,13,14] The results have been tabulated in Table II. Oscillator strengths for these same transitions may also be computed from measurements of the dispersion of the refractive index. The resonance wave-length, which should correspond closely with the wave-length for the maximum of the absorption, and the oscillator strengths from dispersion data are given also in Table II. The comparison of oscillator strengths and wave-lengths by the two methods is fair for methane and ethylene but poor for carbon dioxide. R. S. Mulliken has stated in a private communication that this transition in carbon dioxide may well be a forbidden one particularly since a strong allowed transition exists at lower wave-lengths. The absorption of carbon dioxide is then analogous to carbon disulfide in which the longest wave-length absorption (with a maximum near 3200A) is due to a forbidden transition.[15]

If the carbon dioxide transition involved is a forbidden one, then the usual dispersion equation, which in theory yields true oscillator strengths only for allowed electronic transitions,‡ may be incorrect. On the other hand, if the transition is a permitted one, perhaps the number of terms in Fuch's dispersion equation should be increased.

TABLE II. Comparison between the results of absorption spectra and dispersion data for methane, carbon dioxide, water vapor, and ethylene.

Molecule	Wave-length at max. abs. (A)	Oscillator strength (abs.)	Resonance wave-length (disp.) (A)	Oscillator strength (disp.)	Investigator
Methane	1250*	0.4*	1255.5	0.42	Friberg[a]
Carbon dioxide	1495	0.004	1480	0.75	Fuchs[b]
Water vapor	1608	0.03	—	—	—
Ethylene	1614	0.30	1604	0.528	Friberg[c]
	1625	0.34 ±0.15			Platt *et al.*[d]

* The absorption peak was estimated from the data of Duncan and Howe (see reference 8). By consideration of the theoretical shape of a purely continuous absorption, it was possible to estimate the oscillator strength from the data in Fig. 1.

[a] S. Friberg, Zeits. f. Physik **41**, 378 (1927).
[b] O. Fuchs, Zeits. f. Physik **46**, 519 (1927).
[c] S. Friberg, Zeits. f. physik. Chemie **B26**, 195 (1934).
[d] See reference 2.

[11] W. C. Price and D. M. Simpson, Proc. Roy. Soc. (L) **A169**, 501 (1938).
[12] G. Scheibe and H. Grieneisen, Zeits. f. physik. Chemie **25B**, 52 (1934); W. C. Price, Phys. Rev. **47**, 451 (1935); C. P. Snow and C. B. Allsopp, Trans. Faraday Soc. **30**, 93 (1934); W. C. Price and W. T. Tutte, Proc. Roy. Soc. (L) **A174**, 207 (1940).
[13] R. S. Mulliken, J. Chem. Phys. **7**, 14 (1939).
[14] R. Ladenburg, Verh. d. D. Phys. Ges. **16**, 769 (1914); R. Ladenburg, Zeits. f. Physik **4**, 451 (1921).
[15] R. S. Mulliken, Rev. Mod. Phys. **14**, 204 (1942).
‡ Reference 13, p. 17.

The Photolysis of Methyl Iodide*,†

ROBERT D. SCHULTZ‡ AND H. AUSTIN TAYLOR
Department of Chemistry, New York University, New York, New York and Department of Chemistry, Brookhaven National Laboratory, Upton, New York

(Received August 15, 1949)

The photolysis of methyl iodide by 2537A radiation has been investigated under varying conditions of light intensity, temperature, iodine removal by rotating silver vanes and added carbon dioxide. Methane production is independent of temperature in the range 40°–100°C, directly dependent on the light, nearly independent of efficiency of iodine removal and is inhibited by carbon dioxide. Ethane production increases rapidly as the efficiency of iodine removal is increased. It is argued that methane results from the reaction, with iodide, of "hot" methyl radicals produced in the primary reaction. Ethane is formed from the association of cold methyl radicals. A possible decrease in ethane production with increase in temperature can be accounted for by the reaction of CH_3+I_2 having an activation energy of ~1 kcal.

THE continuous absorption band with a maximum at 2500A exhibited by methyl iodide, first observed by Herzberg and Scheibe[1] has been interpreted by Goodeve and Porret.[2] On the basis of calculated and observed extinction coefficients, the band is shown to be complex involving transitions to two separate upper states. One band leads to dissociation giving an excited iodine atom ($^2P_{\frac{1}{2}}$) and an unexcited methyl; the other band gives products neither of which is excited. From the data given by Goodeve and Porret it appears that at 2537A, absorption in the band resulting in an unexcited iodine atom is extremely small compared to the absorption resulting in the excited iodine. Taking the energy of the C—I bond as 54 kcal. and the excitation energy of the iodine as 22 kcal., conservation of momentum requires that the absorption of 112 kcal./mole by CH_3I will result in methyl radicals with 32 kcal. excess energy. It is not at all obvious in the previous studies of methyl iodide photolysis that sufficient attention has been paid to the fact that these methyl radicals are "hot," nor has its bearing on their ultimate fate as methane and ethane been investigated. To this end a careful study of these products under varying conditions of temperature, light intensity, iodine removal and added carbon dioxide has been made.

EXPERIMENTAL

The purification of methyl iodide as usually recommended in the literature includes drying with P_2O_5. If any alcohol is present such a treatment could give ether and acetal which would remain in the final product. Merck methyl iodide was therefore freed from iodine and oxygen compounds by passage through a column, 30 cm long and 9 mm diameter, packed with 200 mesh silica gel. The effluent was fractionally distilled through a vacuum-jacketed column, 75 cm long and 15 mm in diameter, packed with 3 mm diameter glass spirals, using a 20 to 1 reflux ratio. The entire distillate came over at 42.3°C but only the middle third fraction was used. This was stored at room temperature in the absence of air in a Pyrex bulb closed with a stopcock greased with a fluorocarbon oil.[3] Two pieces of copper wire served to pick up traces of iodine which might be formed on standing. After six months' storage the liquid remained colorless and the wire showed no evidence of corrosion.

The purification procedure was checked with the aid of a Baird Associates infra-red recording spectrophotometer. By comparing spectrograms of the purified CH_3I with those of CH_3I containing known added amounts of impurities, the product was shown to contain less than 0.2 percent oxygen containing impurities. It may be stated here that the bands reported by Courtoy[4] at 1182 and 1167 cm^{-1} do not belong to methyl iodide but probably to dimethyl ether as an impurity in his sample.

The reaction vessel was 500 cc spherical flask of fused silica. It was attached to the system through a ball joint. A Pyrex enclosed magnetic stirrer to which vanes of silver foil were fastened was operated by a rotating horseshoe magnet. The stirrer was introduced through a ground joint in the neck of the reaction vessel, the vanes being coiled on the stirrer axis. During rotation the vanes spread out and served not only to effect iodine removal and thus alter the stationary methyl radical concentration but also to maintain good mixing of the contents of the reaction flask.

The light source was a low pressure mercury arc, Hanovia SC 2537. To remove 1849A radiation a 2 mm filter of Corning 791 glass was interposed between the lamp and reaction vessel. The lamp was in the shape of a rectangular grid covering an area approximately 10 by

* Abstract from a thesis presented in partial fulfillment of the requirements for the degree of Doctor of Philosophy at New York University, June, 1949, based on work completed at the Brookhaven National Laboratory where the first author was employed as Research Fellow during 1948–49.

† Research carried out, in part, under the auspices of the AEC.

‡ Present address: Applied Physics Laboratory, The Johns Hopkins University, Silver Spring, Maryland.

[1] G. Herzberg and G. Scheibe, Zeits. f. physik Chemie. **B7**, 390 (1930).

[2] D. Goodeve and C. F. Porret, Proc. Roy. Soc. **A165**, 31 (1938).

[3] Because of the solubility in methyl iodide other greases were not found satisfactory. Perfluorolube oil FC-334, with a boiling point 190–210°C at 10 mm was supplied through the courtesy of the Jackson Laboratories, E. I. du Pont de Nemours, Inc.

[4] C. Courtoy, Ann. Soc. Sci. Bruxelles, Ser I, **60**, 122 (1946).

15 cm. The diameter of the quartz tubing was 8 mm. A Sola constant voltage transformer maintained an input voltage of 110 volts to a Variac supplying 38 volts at 1.0 amp. to a 5000 volt, 1.32 kva transformer which operated the lamp. An aluminum reflector was placed behind the lamp and the whole was housed in a large box which prevented drafts affecting the lamp performance while permitting sufficient ventilation to prevent overheating. The relative position of the lamp and reaction vessel was carefully reproduced for all runs.

The filling manifold was a Pyrex tube one end of which led to the reaction flask while the other end led to a U-trap in series with a conventional high vacuum pump system. The U-trap immersed in liquid nitrogen prevented mercury vapor from diffusing into the reaction vessel. The filling manifold carried a number of freeze-out bulbs. Prior to each run, a portion of the methyl iodide, purified as described above, was frozen on the walls of one of these bulbs immersed in CO_2-methanol mush and thoroughly degassed by evacuation after repeated thawing and refreezing. The residual pressure above the methyl iodide after freezing in liquid nitrogen was less than 1 micron as read on a Pirani gauge connected to the filling manifold and less than 10^{-5} mm as read on a McLeod gauge on the vacuum manifold side of the U-trap.

The bulb containing the degassed methyl iodide was now immersed in water at 20°C and opened to the previously evacuated reaction vessel thermostated at 40°C. After attainment of the 331 mm equilibrium pressure of methyl iodide (as measured on a nickel diaphragm gauge attached to the reaction vessel through a Kovar metal to Pyrex seal) the reaction vessel was closed and the oven temperature raised to the desired value. The gauge now served to indicate the average temperature as well as the pressure in the reaction vessel provided room temperature was high enough to prevent condensation in the tubing external to the oven.

After irradiation, the reaction vessel was opened to a bulb immersed in secondary-butyl chloride mush at −131°C. Products volatile at this temperature could diffuse through a U-tube safety trap also at −131°C and were frozen out in a trap immersed in solid nitrogen obtained by pumping on liquid nitrogen until the pressure was reduced to 15 mm or less. The residual CH_3I was thawed and refrozen at least four times and a total of at least one half hour was allowed for the diffusion of products.

In the runs with added CO_2, the CH_3I-CO_2 mixture was frozen out at −145 to −150°C. This temperature was obtained by passing dry tank nitrogen at an appropriate rate into the low temperature bath immersed in liquid nitrogen. Blank runs with synthetic mixtures of methane, ethane, ethylene, carbon dioxide, and methyl iodide served to check the efficiency of the method of product recovery.

The products frozen out in the solid nitrogen trap were vaporized and transferred by means of a Toepler pump to a 60 cc gas cell fitted with rock salt windows. The infra-red absorption by the contents was then measured in the range 2–16μ using the Baird instrument already mentioned. CH_4 absorption at 7.7μ, C_2H_6 at 6.8μ, C_2H_4 at 10.6μ and C_2H_2 at 7.3μ were used for the analysis. The spectrogram obtained for the products from a given run was matched against those given by known amounts of pure gases under the same optical conditions of the spectrophotometer. In this way variations in the resolution of the instrument due to adjustments of the optical system during the course of the research were not of significance. The values obtained in this way for methane are good to ±1 mm. The values for ethane are good to ±5 mm since the band at 6.8μ is not strong but has the advantage that it does not appreciably overlap the methane bands.

RESULTS

The results obtained are tabulated in Table I. A direct comparison with the six runs reported by West and Schlessinger[5] is difficult because of the considerable differences in the quantity and composition of the product gas obtained by them in different experiments under nearly identical conditions. The relative ratios of methane and ethane found in presence and absence of silver are in approximate agreement. The ethylene yields reported by West and Schlessinger are surprisingly high especially since Jungers and Yeddanapalli[6] have shown that methyl radicals from the photolysis of methyl iodide induce polymerization in ethylene. The error probably arises from the use of fuming sulfuric acid as the quantitative absorbent for ethylene.

The present results are much more self-consistent. Complete reproducibility of results is, however, hardly to be expected in view of several uncontrollable variables including stirring speed, aerodynamic shape of the silver vanes and extent of reaction of iodine on the silver surface. The rate of iodine fixation probably decreases as the silver surface becomes progressively covered with silver iodide during a run. Such variables affecting the iodine concentration and hence also the methyl radical concentration might be expected to affect both the methane and ethane yields. That methane formation is nearly constant when corrected to 100 percent area of illumination is significant suggesting that methane is formed from methyl radicals whose concentration depends only on the amount of light absorbed and is independent of other variables. Such would be the "hot" radicals produced in the primary act of light absorption. The variability in ethane yield, on the other hand, and especially its obvious dependence on stirring speed suggests that it must result from "cold" methyl radicals.

This conclusion is amply verified by the results in Table I which may be summarized as follows: (1) The

[5] W. West and L. Schlessinger, J. Am. Chem. Soc. **60**, 961 (1938).

[6] V. C. Jungers and L. M. Yeddanapalli, Trans. Faraday Soc. **36**, 483 (1940).

TABLE I. Results of photolysis of methyl iodide by 2537A light, (initial pressure CH_3I, 331 mm measured at 40°C inside reaction vessel).

Run No.	Conditions and remarks	Percent area of illumination[a]	Temp. °C	Time hr.	mm pressure in infra-red analytical cell[b] @25°C C_2H_6	CH_4	C_2H_4	C_2H_2	Av. rates corrected to 100 percent area of illumination $\frac{\Delta(C_2H_6)}{\Delta t}$[b]	$\frac{\Delta(CH_4)}{\Delta t}$[b]
1	Ag present (2 leaves), moderate stirring	100	40	16	135	50	trace	trace	8.4 mm/hr.	3.1 mm/hr.
2	Ag present (2 leaves), moderate stirring	100	100	8	60	24	trace	—	7.5	3.0
3	Ag present (1 leaf), stirrer jammed part way through run	50	40	16	31	24	trace	—	3.9	3.0
4	Ag present (2 leaves), stirrer also jammed	50	40	16	31	25	trace	—	3.9	3.1
[c]5	No Ag, no stirring, reaction vessel gradually fogged with decomposition products during run	50	40	(*ca.* 2 weeks)	~30	~300	trace	trace		
6	Ag present (2 leaves), rapid stirring	50	40	16	130	24	trace	trace	16.3	3.0
7	Ag present (2 leaves), no stirring	50	40	16	20	24	trace	—	2.5	3.0
8	No Ag, no stirring	50	40	16	trace	20	—	—	—	2.5
9	No Ag, no stirring	50	100	16	trace	19	—	—	—	2.4
10	No Ag, CO_2 (331 mm @ 40°C), added	100	40	16	trace	25	—	—	—	1.6
11	No Ag, no stirring	100	40	16	trace	38	—	—	—	2.4
12	No Ag, CO_2 (331 mm @ 40°) added	100	40	16	trace	21	—	—	—	1.3
13	No Ag, CO_2 (662 mm @ 40°C) added	100	40	16	trace	16	—	—	—	1.0
14	Ag present (2 leaves), stirring, 700–900 rpm	100	40	16	135	47	trace	trace	8.4	2.9
15	Ag present (2 leaves) stirring, 700–1000 rpm	100	100	16	82	50	trace	—	5.1	3.1

[a] In the experiments indicated, 50 percent of the Corning 791 Filter was made opaque by coating with a thin layer of Aquadag and scraping away alternate $\frac{1}{16}$-inch strips.
[b] Pressures of products refer to pressures inside the analytical cell which has approximately 0.1 the volume of the reaction vessel.
[c] With the exception of run No. 5, fogging of the reaction vessel with decomposition product (i.e. CH_2I_2, I_2, C_2H_4 polymer?) was negligible, in that only a very slight film was noticeable on the walls after the run. Prior to the next run, this was burned off at red heat in air. In the runs without silver small quantities of a brown liquid (i.e. CH_2I_2, I_2) deposited in the tubing external to the oven. In the runs with silver much smaller amounts of this liquid product were deposited.

apparent activation energy for methane formation in the presence and absence of silver is zero in the temperature range 40°–100°C; (2) In the absence of silver, ethane yield is negligible, while in presence of silver ethane is formed in amounts up to five times that of methane, dependent on stirring conditions. In the apparatus used, rapid stirring with silver foil increased ethane formation by as much as four times that with the foil stationary; (3) The presence of silver increases methane formation by about 25 percent of the methane yield in the absence of silver, and stirring with the silver is without effect; (4) The presence of CO_2 cuts down the rate of methane formation. Quantitatively the effect is represented by the equation:

$$\left[\frac{\Delta[CH_4]}{\Delta t}\right]_{CO_2\ \text{present}} = \frac{[CH_3I]}{[CH_3I]+\alpha[CO_2]}\left[\frac{\Delta[CH_4]}{\Delta t}\right]_{CO_2\ \text{absent}}$$

relating the rates of methane production in presence and absence of CO_2 to the partial pressures of CH_3I and of CO_2. The value of the constant α may be calculated from runs 10, 11, 12 and 13 and gives an average value of 0.67; (5) The effect of temperature on ethane production is not large in the range studied. The effect, if any, as judged from runs 14 and 15 may be to decrease the ethane yield as the temperature increases.

DISCUSSION

Accepting the primary reaction to be:

$$CH_3I \rightarrow CH_3^* + I(^2P_{\frac{1}{2}}) \quad (1)$$

in which for 2537A radiation, CH_3^* represents a methyl radical with excess energy amounting to 32 kcal. per mole, the above results necessitate the following reactions to account for the products.

$$CH_3^* + CH_3I \rightarrow CH_4 + CH_2I \quad (2)$$

$$CH_3^* + M \rightarrow CH_3 + M \quad (3)$$

$$CH_3 + CH_3 = C_2H_6 \quad (4)$$

$$I + I = I_2 \quad (5)$$

$$CH_3 + I_2 \rightarrow CH_3I + I. \quad (6)$$

Reaction (2) as the sole source of methane seems necessary on the basis of (a) zero activation energy for its

production (b) independence of iodine fixation by silver and (c) inhibition by CO_2. If normal methyl radicals reacting with methyl iodide produced methane one would expect by analogy with other similar reactions an energy of activation of up to 8 kcal. The temperature range covered should have been ample to show any such effect. Furthermore, since the stationary concentration of normal methyl radicals must be highly dependent on the efficiency of iodine fixation by silver, the independence of the latter in the methane production rules out any reaction of the normal radicals. Finally the value of 0.67 for α previously found now has an obvious interpretation meaning that CO_2 is 67 percent as effective as methyl iodide in cooling a "hot" methyl radical by collision.

As additional support of the above argument there may be cited the work of Ogg, reported by Williams and Ogg,[7] on the effect of an inert gas in the photolysis of a mixture of methyl iodide, iodine, and hydrogen chloride. The inert gas inhibited the reaction of methyl radicals with hydrogen chloride to form methane in favor of the iodine reaction. Williams and Ogg conclude that the methane is produced from hydrogen chloride almost entirely by reaction with hot methyl radicals. Phibbs and Darwent[8] have also presented evidence for the presence of hot methyls in mercury dimethyl photolysis.

That the quantum yield of methane production in methyl iodide photolysis is as low as 0.003 requires that reaction (2) has a low probability factor of this order. This however, is not unreasonable even for a "hot" reaction since, in the case considered, it is necessary for three translational and three rotational degrees of freedom to disappear and be replaced by at least five vibrations in the collision complex. Unless the reactants at the instant of collision are so orientated that the necessary transfer can be easily accomplished, reaction (2) will not occur and the "hot" radical will merely lose kinetic energy in the collision, that is, reaction (3) occurs. It is obvious in this connection that the most probable collision site on the methyl iodide molecule will be the comparatively large iodine atom rather than the small hydrogen atoms; reaction (3) preferred over (2).

The stationary concentration of "hot" methyl radicals is thus given essentially by reactions (1) and (3) and is seen to be constant at fixed illumination, independent of iodine concentration. The rate of methane production should therefore be independent of iodine concentration and should be the same in the presence and absence of silver. The small increase in methane yield in the presence of silver can be ascribed to the reaction:

$$CH_3^* + C_2H_6 \rightarrow CH_4 + C_2H_5$$

since appreciable amounts of ethane are then present. Alternatively, there is the possibility of a disproportionation reaction:

$$2CH_3 \rightarrow CH_4 + CH_2,$$

it being true that small amounts of ethylene are found when silver is present.

A methyl radical having lost its excess energy by reaction (3) will, in the absence of silver, most probably react with iodine to reform methyl iodide. If iodine can be removed sufficiently rapidly by fixation as silver iodide, the methyl radical concentration will be able to build up to the point where reaction (4) becomes appreciable. The tremendous dependence of ethane yield on iodine pick-up thus has a ready explanation. It may be remarked here that ethane production by a Walden inversion type reaction:

$$CH_3 + CH_3I \rightarrow C_2H_6 + I$$

seems unlikely since it obviously does not occur to any noticeable extent as a "hot" reaction and should not therefore be expected as a "cold" reaction.

The effect of temperature on the ethane yield is not too reliable in view of the great dependence of ethane on stirring conditions. This dependence was not too well realized in the earliest experiments. In runs 14 and 15 great care was exercised to reproduce so far as possible the iodine fixation. Stirring speeds were measured with a stroboscopic tachometer at the start and finish of each run, with the results indicated in Table I. It may be significant therefore that the ethane yield is less at the higher temperature as runs 1 and 2 would also indicate. If it is true that the steady state concentration of iodine was the same in runs 14 and 15, calculation by the usual steady state method shows that an energy of activation of about 1 kcal for reaction (6) would be sufficient to account for the observed decrease in ethane. Despite the inconclusiveness of this value it is of interest to compare it with the value estimated by Andersen and Kistiakowsky[9] namely 0.5 ± 0.5 kcal.

The first author wishes to express his gratitude to Dr. A. O. Allen of the Chemistry Department of Brookhaven for valuable advice, criticism and suggestions.

[7] R. Williams and R. A. Ogg, J. Chem. Phys. **15**, 696 (1947).
[8] M. K. Phibbs and B. de B. Darwent, Trans. Faraday Soc. **45**, 541 (1949).
[9] H. G. Andersen and G. B. Kistiakowsky, J. Chem. Phys. **11**, 6 (1943).

Kinetics of Heterogeneous Nucleation

D. TURNBULL
Research Laboratories, General Electric Company, Schenectady, New York
(Received July 18, 1949)

Consider a phase transition $\alpha \rightleftarrows \beta$. Stable β-embryos can be retained in the temperature range of α-stability in cavities of suitable extraneous solids present in the system. Retained β-embryos may nucleate the $\alpha \rightarrow \beta$-transformation in the range of β-stability.

Using these concepts a theory for the effect of thermal history upon the kinetics of phase transformations is proposed. The kinetics of heterogeneous nucleation in the absence of retained embryos is discussed.

INTRODUCTION

MOST of the theories for the kinetics of nucleation that have been advanced apply to "homogeneous nucleation" which is initiated in the interior of a single phase. The nucleation theory of Becker and Doring[1] was successful semiquantitatively in accounting for the experimental results of Volmer and Flood[2] on the rate of nucleation of liquids in supersaturated vapors.

Although theories of homogeneous nucleation have had some qualitative success in explaining certain features of the kinetics of nucleation in condensed systems, many investigations have indicated that nucleation in these systems is "heterogeneous," that is nuclei form preferentially at some interface in the system. Particularly for liquid-solid transformations in relatively large volumes of liquid the evidence seems decisive that at least the first few nuclei that appear originate by a heterogeneous mechanism at the surfaces of the containing vessel or of colloidal inclusions in the system. If the growth rate is rapid these few nuclei may transform the entire sample without the formation of homogeneous nuclei.

An important characteristic of liquid-solid transformations in relatively large samples is the very marked effect of thermal history upon the rate of the process first observed by Othmer.[3] Richards and co-workers[4,5] have made comprehensive studies of the phenomenon and obtained convincing evidence that it must be explained in terms of extraneous structures present in the system. Webster[6] has shown that the effect also is important in the solidification of certain bulk metals. Similarly, the author has observed that the solidification of gallium is very thermal history dependent. Gallium is advantageous for study because of the very rapid growth rate (at least 1 cm/sec. at 0°C) of the crystal so that the kinetics of the transformation are generally controlled by the nucleation rate alone.

The effect of thermal history upon the kinetics of many liquid-solid bulk transformations is illustrated schematically in Fig. 1. ΔT_+ is the number of degrees above the melting point, T_m, to which the liquid is heated after melting. ΔT_- is the number of degrees that the liquid must be subsequently sub-cooled in order for nucleation to occur during some specified holding time at the lower temperature. In the region of the curve *ab* which usually extends only a few degrees above the melting temperature, ΔT_- is strongly dependent upon ΔT_+ while in the region *bc* ΔT_- is virtually independent of ΔT_+. For example, in gallium samples the region *ab* extended to about 20° above the melting point but for a given sample ΔT_- was found to be independent of ΔT_+, within experimental error, for values of the latter ranging between 50 and 1050°.

The following are a number of other important features of the thermal history effect.

1. The length of time in the sub-cooled range does not alter the relation between ΔT_- and ΔT_+ significantly. In experiments with gallium the whole curve was shifted only 1–2° toward higher temperatures when the holding time was shifted from the order of a few minutes to one day.

2. Increasing the time at temperature above the melting point, after a certain minimal period—usually of the order of a few minutes, does not significantly affect the value of ΔT_- subsequently observed.

3. ΔT_- is generally characteristic of the highest temperature attained in the ΔT_+ region.

4. When a sample is solidified after having been heated in the *bc*-region the ΔT_- *vs.* ΔT_+ relation originally obtained is usually not changed significantly. Certainly this is true for gallium. However, there are exceptions to this behavior. Hinshelwood and Hartley[7] observed that after sulfur samples are heated into the *bc*-region and then solidified the ΔT_- *vs.* ΔT_+ relation is altered so that the ΔT_+ coordinate of *b* is only an insignificant fraction of its former value.

5. Richards demonstrated that the phenomenon was highly sensitive to added inclusions such as activated charcoal or powdered quartz. These inclusions greatly increased the temperature (by as much as 100–150° in some cases) in the ΔT_+ region that it was necessary to reach before ΔT_- became independent of ΔT_+.

6. According to Richards the maximum sub-cooling

[1] R. Becker and W. Doring, Ann. d. Physik (5) **24**, 719 (1935).
[2] M. Volmer and H. Flood, Zeits. f. physik. Chemie **170A**, 273 (1934).
[3] P. Othmer, Zeits. f. anorg. allgem. Chemie **91**, 235 (1915).
[4] W. T. Richards, J. Am. Chem. Soc. **54**, 479 (1932).
[5] Richards, Kirkpatrick, and Hutz, J. Am. Chem. Soc. **58**, 2243 (1936).
[6] W. L. Webster, Proc. Roy. Soc. **140A**, 653 (1933).
[7] C. N. Hinshelwood and H. Hartley, Phil. Mag. **43**, 78 (1922).

obtainable for bulk specimens is independent of added inclusions. However, the author observed that this value was specific for particular gallium specimens and ranged from 35 to 55°. The specificity was not significantly changed by heating to ΔT_+ values of 1050°.

Richards proposed a qualitative theory for the effect of thermal history upon the transformation kinetics based on the concept that extraneous structures retain a "crystalline adsorbate" above the melting temperature. This adsorbate is stabilized in the region of liquid stability by a negative heat of adsorption on the extraneous structures. As the temperature of the liquid is increased the crystalline adsorbate becomes less stable and finally disappears altogether at some elevated temperature. He supposes that its rate of reformation is very slow so that the process of heating into the *bc*-region is essentially irreversible, as observed.

Other investigations that demonstrated the role of extraneous surfaces in promoting the nucleation of solid phases in liquids are those of Goetz,[8] Hammer[9] and Meyer and Pfaff.[10]

Although it has been recognized (see Johnson and Mehl[11]) that a large number of solid-solid transformations are nucleated preferentially at grain boundaries, there seems to be little systematic information regarding the role of extraneous particles of other phases located either at the grain boundary or within the grain in promoting nucleation in solid-solid transformations. In view of the evidence on liquid-solid transformations it is expected that such influences may prove to be very important in many reactions involving only solid phases. Avrami[12] has developed a theory for the kinetics of such transformations in which it is supposed that all nuclei originate from pre-existing embryos, some of which presumably might be stabilized by extraneous particles of other phases.

It is the purpose of this paper to develop further the theory of the kinetics of heterogeneous nucleation. An explanation for the effect of thermal history upon transformation kinetics will be offered along the lines of the basic concepts suggested by Richards, but in more explicit terms containing the interfacial energies involved rather than heats of adsorption. A more mechanistic explanation will be offered for the irreversibility of the phenomena with respect to temperature.

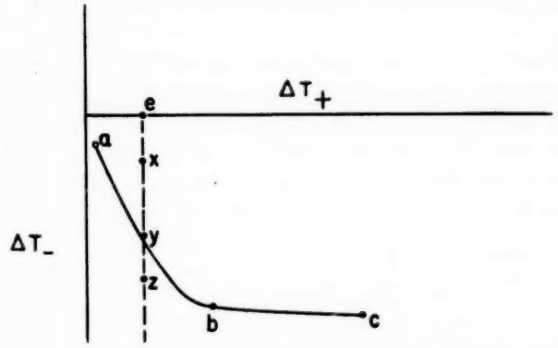

FIG. 1. Effect of thermal history on temperature of rapid nucleation in liquid-solid transformations.

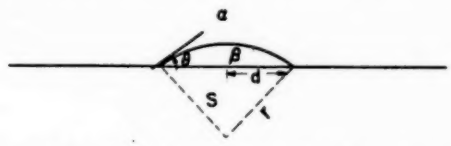

FIG. 2. β=embryo on a flat surface. θ=equilibrium contact angle.

THEORY

Volmer[13] has calculated the work of nucleating a phase β in the transformation $\alpha \rightarrow \beta$, where β is considered to be the low temperature modification, on a flat solid substrate denoted by S. Let the contact angle between the β-embryo and S be θ as shown in Fig. 2. Then for $180° > \theta > 0$

$$\sigma_{\alpha-S} = \sigma_{\beta-S} + \sigma_{\beta-\alpha} \cos\theta, \quad (1)$$

where σ denotes interfacial energy. If it is assumed that the σ's are isotropic the free energy ΔF required to form an embryo having the shape of a spherical sector is,[13]

$$\Delta F = [\pi r^3 (f_\beta - f_\alpha)/3v_\beta + \pi r^2 \sigma_{\beta-\alpha}] \times [2 - 3\cos\theta + \cos^3\theta], \quad (2)$$

where f is the free energy per atom, v=volume per atom, and r is the radius of the sphere. In the region of α-stability there is no possibility of retaining β-embryos on flat surfaces for which the condition $\theta > 0$ holds since the term involving surface energy in (2) is always positive for this condition. Volmer[13] shows that the work of forming a nucleus of critical size is,

$$[16\pi\sigma_{\beta-\alpha}{}^3 v_\beta{}^2/3(f_\beta - f_\alpha)^2][(2+\cos\theta)(1-\cos\theta)^2/4] \quad (3)$$

which differs from the work of forming a nucleus in the interior of α by the factor $[(2+\cos\theta)(1-\cos\theta)^2/4]$.

When $\sigma_{\alpha-S} > \sigma_{\beta-S} + \sigma_{\beta-\alpha}$ some β-adsorbate can be retained on S at temperatures not greatly exceeding the equilibrium temperature, T_0. If this β-adsorbate is removed by heating to a temperature greatly exceeding T_0 the only positive work of subsequently nucleating β on S at $T < T_0$ is that of forming the periphery of the β-embryo.

Volmer[14] has pointed out that stable embryos of phase β can be retained in cavities of various types in the substrate S at temperatures in excess of T_0 under the proper conditions which may include values of θ considerably greater than zero such that no β-adsorbate

[8] A. Goetz, Phys. Rev. **35**, 193 (1930).
[9] C. Hammer, Ann. d. Physik **33**, 445 (1938).
[10] J. Meyer and W. Pfaff, Zeits. f. anorg. allgem. Chemie **217**, 257 (1934).
[11] W. A. Johnson and R. F. Mehl, Trans. A.I.M.E. **135**, 416 (1939).
[12] M. Avrami, J. Chem. Phys. **7**, 1103 (1939).
[13] M. Volmer, Zeits. f. Elektrochemie **35**, 555 (1929).
[14] M. Volmer, *Kinetik der Phasenbildung* (Steinkopf, Leipzig, 1939), p. 103.

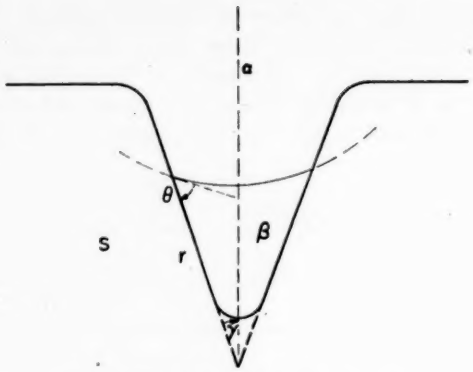

FIG. 3. Nucleation in a conical cavity.

is stable on a perfectly flat surface. This concept will form the basis of our theory for the effect of thermal history upon the kinetics of the $\alpha \rightarrow \beta$-transition. In our treatment the retention of embryos in conical and cylindrical cavities will be considered.

Consider a conical cavity in surface S as shown in Fig. 3. It is assumed that the bottom and edges of the cavity are rounded. Neglecting the volume change due to the rounding of the bottom of the cavity the work of forming the embryo in the cavity is:

$$\Delta F = \pi r^3 (f_\beta - f_\alpha)\varphi / v_\beta + \pi r^2 \sigma_{\beta-\alpha}[2\mu - \sin\gamma \cos\theta], \quad (4)$$

where φ and μ are trigonometric functions given by:

$$\varphi = [\sin^2\gamma \cos\gamma/3 - 2\sin^3\gamma/3 \cos^3(\gamma+\theta) + \sin^3\gamma \tan(\gamma+\theta)/\cos^2(\gamma+\theta) - \sin^3\gamma \tan^3(\gamma+\theta)/3]$$

$$\mu = [\sin^2\gamma/\cos^2(\gamma+\theta) - \sin^2\gamma \tan(\gamma+\theta)/\cos(\gamma+\theta)].$$

In Eq. (4) the surface energy term can be negative for values of γ and θ such that $\cos\theta > [2\sin\gamma/\cos^2(\gamma+\theta)] \times [1-\sin(\gamma+\theta)]$. Figure 4 shows the free energy relations involved in forming β-embryos in cavities for $T > T_0$ for this situation.

At each temperature above T_0 there is a stable position of the $\alpha-\beta$-interface specified by r_0. As the temperature increases r_0 becomes less and the embryos will disappear altogether when r_0 becomes of the order of the dimensions of the bottom of the cavity. After the embryos have been destroyed by the high temperature treatment a positive free energy at a lower temperature must be expended (see Fig. 4b) to reform them because this process must begin on surfaces which are approximately flat (i.e., on the rounded bottom of the cavity).

In cylindrical cavities (see Fig. 5) the work of embryo formation is given by:

$$\Delta F = \pi r^2 h (f_\beta - f_\alpha)/v_\beta + 2\pi r \sigma_{\alpha-\beta} \times [r(1-\cos\theta)/\sin^2\theta - h\cos\theta]. \quad (5)$$

For values of h sufficiently large the surface energy term in Eq. (5) will be negative. However, the factor that determines whether or not β-embryos will be retained in the pores above the transformation temperature is the coefficient p, of h in (5)

$$p = \pi r^2 (f_\beta - f_\alpha)/v_\beta - 2\pi r \sigma_{\alpha-\beta} \cos\theta.$$

If p is negative β-embryos are retained. This condition is fulfilled when

$$m = 2\sigma_{\alpha-\beta} \cos\theta (v_\beta)/(f_\beta - f_\alpha) > r. \quad (6)$$

The work of embryo formation as a function of h and r is shown schematically in Fig. 6. Again it is noted that after retained β-embryos are destroyed by heating to high temperatures their reformation at a lower temperature involves an increase in free energy. For each temperature there is a critical value of $r = m$ such that no β-embryos are retained in pores exceeding this size. m decreases sharply as the temperature increases.

The existence of retained embryos in cavities on the container wall or in extraneous particles explains satisfactorily the effect of thermal history on the rate of nucleation. Suppose that the β-phase is heated above T_0 by varying amounts $= \Delta T_+$. The maximum values of γ and r for conical and cylindrical cavities in which embryos are retained are shown as functions of ΔT_+ in Fig. 7.

When α is now sub-cooled into the β-region, the embryos retained in the conical or cylindrical cavities will immediately grow to the mouth of the cavity. However, they are not nuclei for the $\alpha-\beta$-transformation unless the radius at the cavity opening equals or exceeds the critical radius for nucleation of a spherical

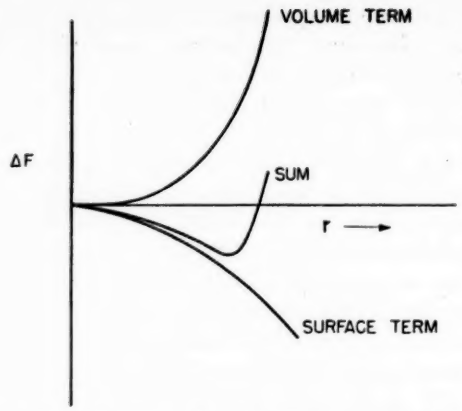

FIG. 4a. Free energy of embryo formation in conical cavity above transformation temperature.

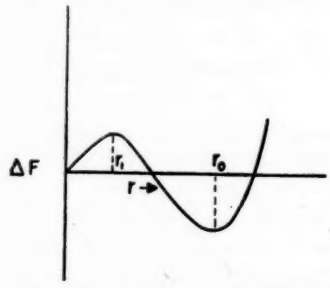

FIG. 4b. Free energy of embryo formation in conical cavity with a rounded bottom.

sector of β on the flat surface

$$d^*=-2\sigma_{\alpha-\beta}v_\beta \sin\theta/(f_\beta-f_\alpha). \quad (7)$$

For simplicity it is assumed that the edges of the cavity openings are curved but that the radii of curvature are negligible in comparison with the radii of the openings. Thus, for cylindrical cavities m decreases with ΔT_+ and since d^* decreases with increasing ΔT_- it is evident that the degree of sub-cooling required to cause a β-embryo retained in a cylindrical cavity to become a nucleus will increase as ΔT_+ increases. Similar arguments hold for the promotion of β-embryos in conical cavities to nuclei since the dimensions of the mouths of the cavities will be proportional roughly to γ.

Reformation of β-embryos in cavities at low temperatures after they have been destroyed by a high temperature treatment will be a sluggish process because of the free energy barrier (Figs. 4b and 6) to be surmounted. In some instances the extraneous particles that carry the cavities catalyzing nucleation may dissolve in the α-phase at high temperature. When this occurs, the $\alpha-\beta$-transition may be no longer thermal history sensitive for the particular sample.

It is interesting to inquire how the observed nucleation rate of the $\alpha-\beta$-transformation changes with time and temperature when embryos are retained. Suppose (see Fig. 1) that samples are heated into the α-range to a ΔT_+ value indicated by e and then quenched to the various values shown. Specimens quenched to z will have retained β-embryos which are supercritical, and these will nucleate immediately. If the growth rate is very slow, some embryos which were only slightly sub-critical may nucleate and grow. In any event, the nucleation rate will be a maximum at zero time and will fall off sharply thereafter.

When the sample is quenched to a ΔT_- value of x, all retained β-embryos are sub-critical with respect to nucleation at this temperature. The additional free energy necessary to nucleate them may be so large that no nuclei will form in a reasonable period of time.

At a ΔT_- indicated by y there are a number of retained embryos which are very close to the critical size for nucleation. These retained embryos may nucleate in time, but still later the nucleation rate will decrease as the retained embryos are used up. In general, the rate of nucleation, I, for this case will go through a maximum with time as shown in Fig. 8. If y is very close to the curve ΔT_- *vs.* ΔT_+ or if the rate of transport across the interface is very rapid, the initial increase, $0x$, may not be observed at all.

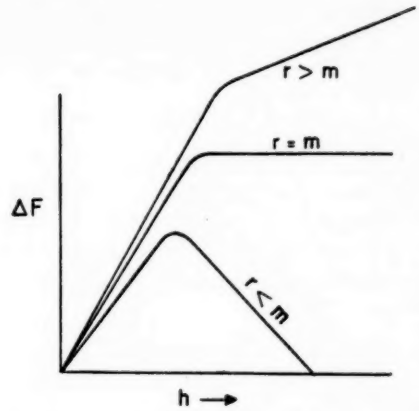

FIG. 6. Free energy of embryo formation in a cylindrical cavity as a function of h.

For example, Hammer[9] has published curves showing the variation in I with time for some liquid-solid transitions which resemble the curve in Fig. 8 excepting that the initial increase is absent. The way in which the total number of nuclei appearing isothermally in the range yz changes with temperature will be governed by the size distribution curve for cavities in which embryos are retained. Since the number of cavities generally will increase with decreasing cavity size, the nucleation number will increase as the temperature is lowered.

From Eqs. (6) and (7) and setting

$$f_\beta-f_\alpha\approx\lambda(T_0-T)/T_0,$$

where λ = heat of transformation per atom, a simple equation relating ΔT_- and ΔT_+ can be derived for cylindrical cavities,

$$\Delta T_-/\Delta T_+=\tan\theta. \quad (8)$$

This equation holds only for one type of catalyst and

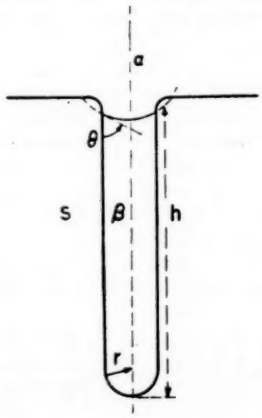

FIG. 5. Nucleation in cylindrical cavity.

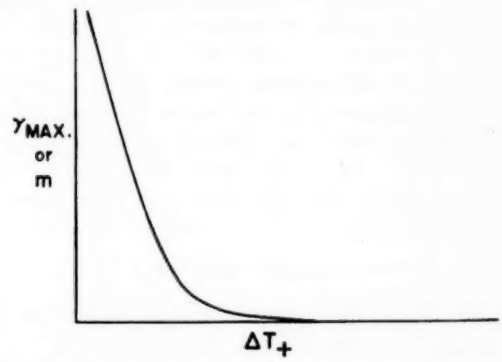

FIG. 7. Effect of thermal history on dimensions of cavities in which embryos can be retained.

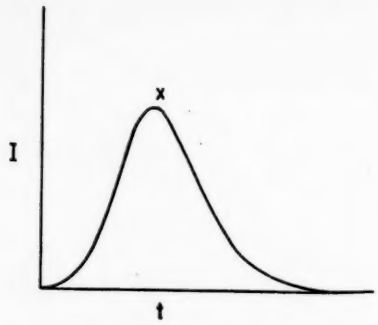

FIG. 8. Nucleation rate as function of time for a limited number of nucleation sites.

where the rate of production of nuclei on flat surfaces or in the interior of α by thermal fluctuations is practically nil. This will be so for relatively small values of ΔT_-. For larger values of ΔT_- the number of nuclei produced by thermal fluctuations becomes very large in comparison with the number originating from embryos retained in cavities; under these conditions, ΔT_- is constant with respect to ΔT_+ as shown by the *bc* portion of Fig. 1.

In order to find the order of magnitude of cavity sizes necessary to explain the observed effects in terms of the theory developed, some calculations were made for the gallium liquid-solid transformation catalyzed by a substrate such that θ between the solid gallium (in equilibrium with the liquid) and the substrate was 60°; thus, $\Delta T_- \approx 1.7 \Delta T_+$. It was assumed that the interfacial energy between liquid and solid gallium[18] is 55 ergs/cm^2. For $\Delta T_+ = 5$ embryos of solid gallium are retained in cylindrical cavities having diameters $\lesssim$140A. These embryos are capable of growing at $\Delta T_- \gtrsim 8.5$, and the number of gallium atoms contained in the spherical sector at the mouth of the cavity is of the order of 6000. It is evident that nucleation by thermal fluctuations at this value of ΔT_- in the absence of retained embryos is impossible. For $\Delta T_+ = 20°$ the maximum diameter of cavities in which embryos are retained is $\approx$35A and $\Delta T_- \approx 34°$. However, the number of atoms contained in the spherical sector at the cavity mouth is only about 100, so that nucleation by thermal fluctuations must become predominant at this temperature or slightly below it for the conditions assumed in the calculation.

When a specimen is cooled into the β-region from a temperature in the α-range where retained embryos have been destroyed the nucleation problem becomes one of forming nuclei on catalytic surfaces which are essentially flat. At steady state the number, n, of embryos of critical size per unit area of a given surface is

$$n \approx n_S \exp(-\Delta F^*/kT), \qquad (9)$$

where n_S is the number of α-surface atoms per unit area and ΔF^* is given by Eq. (4).

The steady state rate of nucleation per unit surface, I_S, is $I_S = K \exp[-(\Delta F^* + q)/kT]$, where q is the activation energy required to move an atom across the $\alpha-\beta$-interface. ΔF^* differs from the free energy required for interior nucleation, ΔF_i^*, only by a factor involving the contact angle. Therefore, ΔF^* will vary with temperature in approximately the same way as ΔF_i^* while q remains essentially constant. Consequently I_S will generally pass through a maximum as the temperature is lowered from T_0 just as does I for interior nucleation. Also before the establishment of a steady state of surface nucleation a transient in which I_S accelerates with time should be observed as pointed out earlier.[15] These features of heterogeneous nucleation in the absence of retained embryos are very similar qualitatively to those predicted by the theories of homogeneous nucleation. However, since ΔF^* is much smaller, the rate of heterogeneous nucleation will generally be much greater at a given temperature than the rate of homogeneous nucleation.

In some reactions there may be only a limited number of sites that promote nucleation. In this case the observed rate of nucleation may fall off with time after the rising transient in a way similar to that shown in Fig. 8. In the absence of a transient the rate of nucleation will change with time according to the equation given by Avrami[12] providing that all of the preferred nucleation sites are equivalent.

In order to test the theories of homogeneous nucleation rigorously it is important to devise experiments in which nucleation catalysts are eliminated or localized. Experiments are usually performed on bulk samples where one or more nuclei originating from catalytic sites are able to transform the entire sample under observation. In order to prevent this from occurring, it is desirable that the sample be broken into a large number of small isolated parts. This is accomplished in the well-known experiments of V. Schaefer[16] on the nucleation of snow crystals in a fog of water droplets. B. Vonnegut[17] has used a somewhat similar technique in his study of the liquid-solid transition in tin particles. Also, the author[18] has applied this procedure to mercury and gallium. In these investigations a much larger degree of sub-cooling was obtained than can generally be obtained when bulk samples are sub-cooled.

Observations of the kinetics of transformations on fine dispersions have the following advantages to the study of nucleation:

1. Since the linear growth rate in transformations is approximately constant and the rate of nucleation is proportional to the volume, it is highly probable that in very small droplets one nucleus transforms the whole mass of the droplet. Therefore, observations on the rate of transformation constitute a direct measure of the nucleation rate.

2. Only a negligible number of droplets contact the container walls at any point, so that any points on these walls which promote nucleation are no longer effective.

---

[15] D. Turnbull, Metals Tech. **15**, T.P. 2365 (1948).
[16] V. J. Schaefer, Bull. Am. Meteorolog. Soc. **29**, 175 (1948).
[17] B. Vonnegut, J. Colloid Science **3**, 563 (1948).
[18] D. Turnbull, J. App. Phys. **20**, 817 (1949).

3. Extraneous particles promoting nucleation, if their number is not large, may be localized on a negligible proportion of the droplets.

4. If the interfaces are properly chosen, nucleation takes place at the interior of the droplet rather than at the surface. This requires that the material at the interface "wet" the parent phase better than the phase which is forming.

Thus, the technique of observing transformation kinetics on finely dispersed droplets of the mother phase covered by a good wetting agent appears to offer the most promise in measuring rates of homogeneous nucleation in condensed systems. For this purpose it is highly desirable to have dispersions in which the droplet size is very uniform, and accurately known. Under these conditions a simple kinetic expression may be written for the rate at which volume is transformed per unit time as follows:

$$dV/dt = Iv(V_0 - V), \tag{10}$$

where V = total volume transformed in time, t, V_0 = total volume at $t=0$, I = rate of nucleation per unit volume, and v = volume of the droplet. This expression assumes that the transient in the nucleation rate is over and a steady state obtains. Equation (10) may be integrated to give:

$$V = V_0[1 - \exp(-Ivt)]$$

for the volume transformed in time t.

THE JOURNAL OF CHEMICAL PHYSICS VOLUME 18, NUMBER 2 FEBRUARY, 1950

Free Radical Formation in the Photolysis of Some Aliphatic Aldehydes, Acetone, Azomethane, and Diazoethane*

D. H. Volman, P. A. Leighton, F. E. Blacet, and R. K. Brinton
Department of Chemistry, Stanford University, Stanford University, California,
and
Division of Chemistry, University of California, Davis, California

(Received June 29, 1949)

The formation of free radicals from some aldehydes, acetone, azomethane, and diazoethane was studied by use of the metallic mirror technique of Paneth. Various wave-length regions were used. Implications of the results for the mechanism of the primary process in the photolysis of the compounds are discussed.

INTRODUCTION

THE Paneth metallic mirror technique was used in the experiments described in this report to study free radical formation from several compounds when irradiated. Previous to this investigation Pearson[1] had shown that acetone yields free radicals, and Glasebrook and Pearson[2] have demonstrated that there is an equivalence between the number of acetyl and methyl radicals formed in the photolysis of this compound. Likewise it has been shown that methyl radicals are produced in the photolysis of acetaldehyde[3] and that propionaldehyde[4] yields ethyl radicals. These earlier experiments were carried out with the full light of mercury arcs and comparative data in different spectral regions were lacking. Experiments which were designed to obtain such comparative information for acetaldehyde and acetone are reported herein.

There has been considerable speculation concerning the primary processes in the photolysis of acrolein, crotonaldehyde, and formaldehyde.[5] Since the mirror removal technique provides a method of demonstrating the formation of free radicals, investigations of these aldehydes also have been made. In addition, experiments with glyoxal and azomethane are reported. These two compounds were studied primarily as an aid in explaining data obtained for the photolysis of mixtures of acetaldehyde and glyoxal[6] and acetaldehyde and azomethane.[7]

Experiments with diazoethane were carried out in order to clarify conflicting data on photo and thermal production of free radicals from the compound[8,9] and

* The major portion of the experimental work reported herein was carried out at Stanford University in 1938. Some additional work on acetaldehyde and the experiments on diazoethane were carried out at the University of California in 1949.

A considerable portion of this paper was presented at the twenty-third annual meeting of the Pacific Division, A.A.A.S., Stanford University, June 28, 1939, under the title "The effect of wave-length on free radical production in the photolysis of acetone and acetaldehyde." Some of the results were presented in a symposium discussion, J. Chem. Phys. **7**, 781 (1939).

[1] T. G. Pearson, J. Chem. Soc. 1718 (1934).

[2] A. L. Glasebrook and T. G. Pearson, J. Chem. Soc. 567 (1937).

[3] T. G. Pearson and R. H. Purcell, J. Chem. Soc. 1151 (1935).

[4] May, Taylor, and Burton, J. Am. Chem. Soc. **63**, 249 (1941).

[5] Compare W. A. Noyes and P. A. Leighton, *The Photochemistry of Gases* (Reinhold Publishing Corporation, New York, 1941), pp. 339–351.

[6] F. E. Blacet and R. W. Moulton, J. Am. Chem. Soc. **63**, 868 (1941).

[7] F. E. Blacet and A. Taurog, J. Am. Chem. Soc. **61**, 3024 (1939).

[8] F. O. Rice and A. L. Glasebrook, J. Am. Chem. Soc. **56**, 2472 (1934).

[9] Barrow, Pearson, and Purcell, Trans. Faraday Soc. **35**, 880 (1939).

as a prelude to future kinetics work with this substance.[10]

EXPERIMENTAL

Apparatus

The technique employed was similar to that used by Pearson and Purcell.[3] The reaction tube was of clear quartz. The metallic mirrors were of tellurium and were formed in a stream of oxygen-free-hydrogen. The density and width of successive mirrors were made closely the same by matching them with a standard mirror deposited in front of the illumination zone. Estimation of the size of the mirrors and the time of complete removal was carried out by visual means. This method of producing similar mirrors and the method of observation were justified by the fact that results on the time of removal of successive mirrors acted on by free radicals produced from the same compound under identical conditions were reproducible within 15 percent.

In experiments to determine the rate of production of free radicals, the system was first completely evacuated by use of a mercury diffusion pump. A mirror was produced and the supply of hydrogen then stopped. When the residual hydrogen had been removed, vapors of the compound being investigated were allowed to pass down the tube at a pressure of approximately 2 mm of mercury in the illumination zone. The mirrors were steam-heated to 100° during all experiments to prevent possible polymer condensation on the surface.[3] The distance between irradiation zone and mirror was 9 cm.

Light Sources

Comparative data for three different spectral regions were obtained. For the shortest wave-lengths, a cold mercury-argon arc which emits approximately 95 percent of its light between 2000 and 4000A as the 2537A resonance line was used. For somewhat longer wave-lengths, a magnesium spark was used. Since the strong magnesium spark lines lie in the region between 2770 and 2830A, the radiation may be considered to be effectively within these limits. For still longer wave-lengths, a calcium spark in conjunction with a glass filter was employed. With this light source, the effective radiation was in the region 3160–3180A. For the experiments with azomethane, a Westinghouse 3*H* mercury arc with a soft glass filter, giving wave-lengths longer than 3340A, was used. Glyoxal was irradiated in the full intensity of a relatively strong Hanovia medium pressure mercury arc. Diazoethane was irradiated with an extremely strong Hanovia mercury-rare gas discharge yielding largely mercury resonance radiation, and by a bank of four 1000-watt projection lamps.

TABLE I. Results of mirror removal experiments.

Light source	Compound	Average removal time, seconds
Mercury Resonance lamp	Acetone	185
	Crotonaldehyde	260
	Acrolein	225
2537A	Acetaldehyde	No removal
	Formaldehyde	No removal
Magnesium spark 2770–2850A	Acetone	31
	Acrolein	40
	Acetaldehyde	45
	Formaldehyde	105
Calcium spark 3160–3180A	Acetone	62
	Acetaldehyde	47
	Formaldehyde	207
Hanovia mercury arc *Ca.* 2300–3700A	Glyoxal	No removal
3*H* mercury arc 3340A	Azomethane	Removal

Materials

Acetaldehyde was prepared by the acid depolymerization of paraldehyde. Formaldehyde was prepared as needed by decomposing polyoxymethylene at 140°. Crotonaldehyde was obtained by fractionation of a crude commercial product. The acetone and acrolein were C.P. Eastman products which were further purified by drying over anhydrous calcium sulfate and fractionating. Glyoxal was prepared by oxidizing ethylene with selenium dioxide.[6] Azomethane was made by preparing dimethyl-hydrazine dihydrochloride and oxidizing this with cupric chloride.[7] Diazoethane was prepared by the action of sodium cyclohexoxide on *N*-nitroso-β-ethylaminoisobutyl methyl ketone, similar to the method described by Adamson and Kenner.[11]

Results

The results obtained with several aldehydes, acetone, and azomethane are given in Table I. The times of removal are the average of three to ten trials.

By determining the photolysis rate for a known rate of free radical production, it is possible to gain further insight into the primary mechanism. Some experiments were performed on acetone and acetaldehyde in which non-condensable gases formed in the system due to photo-decomposition were not pumped out but were measured by means of a McLeod gauge. The rate of pressure increase in the system thus measured may be taken as a relative photolysis rate. The values in the last column of Table I, the average removal time, are inversely proportional to the number of free radicals striking the mirror. The reciprocals of these times are then the relative rates of free radical production. Combining both sets of data, the results of Table II were obtained. The values are referred to that for acetaldehyde in the region 3160–3180A taken as a unity.

[10] D. H. Volman and R. K. Brinton gratefully acknowledge the assistance of a Frederick Gardner Cottrell grant from the Research Corporation for work with diazoethane.

[11] D. W. Adamson and J. Kenner, J. Chem. Soc. 1551 (1937).

Table I indicates that light of wave-length 2537A is not effective in producing mirror removing fragments from acetaldehyde and formaldehyde. Since these results were somewhat surprising, the experiments were repeated using very fine mirrors and decreasing the distance between lamp and mirror with similar negative results. When acetone and acetaldehyde were passed through together in equal quantities, the same result as for acetone was obtained.

It was found that mixtures of acetaldehyde and mercury produced free radicals when illuminated by resonance radiation. Mercury vapor was introduced by placing a porcelain boat filled with liquid mercury at the entrance to the reaction tube. Under these conditions which were otherwise the same as described for the results in Table I, mirrors were readily removed.

TABLE II. Comparison between the number of free radicals and the rate of photolysis.

Wave-length, A	Relative number of free radicals for the same rate of gaseous product formation: Acetone	Acetaldehyde
3160–3180	1.06	1.0
2800	3.5	1.3
2537	10.6	—

Recently, about 10 years after these results with acetaldehyde were obtained, we have reinvestigated the irradiation with resonance radiation. Using a helical high intensity mercury-rare gas discharge we found that mirrors were removed quite easily. Since it is reported that there is considerable 1849A light from such lamps, the experiments were repeated with a coating of mineral oil, an efficient filter for radiations shorter than 2000A, about the reaction tube. The results were similar to those with unfiltered light. The most obvious explanation for the difference in these results and our earlier ones is that of insufficient intensity in the original experiments.

Experiments with Diazoethane

Diazoethane was irradiated with the resonance lamp described both in unfiltered and oil filtered light. In each case mirrors were readily removed. When irradiated with light from a bank of four 1000-watt tungsten filament projection lamps, no removal of mirrors was observed.

The production of free radicals from diazoethane by thermal means was also attempted. When diazoethane alone was heated to various temperatures in the range 450° to 750°C, each experiment resulted in an explosion generally within a few seconds of allowing the compound to enter the reaction tube. The time was insufficient to determine whether any of the mirror had been removed. A single experiment in which a mixture of diazoethane and hydrogen flowed in the tube at 750°C resulted in very rapid mirror removal without explosion. Substitution of nitrogen for hydrogen in a single experiment again resulted in an explosion. The explosions were all of moderate intensity and in some of the cases appear definitely to have been confined to the low pressure gas at room temperature and not to have occurred within the liquid stored at about −25°. These results with their attendant effects on the apparatus have temporarily discouraged further experiments along the same line.

DISCUSSION

From studies of the ratio C_2H_6/CO obtained in acetone photolysis at different wave-lengths, Spence and Wild[12] proposed that the decrease in this ratio toward unity indicated that at 3130A the predominate primary process is the formation of stable molecules,

$$CH_3COCH_3^* \rightarrow C_2H_6 + CO.$$

At shorter wave-lengths, the increase in the ratio C_2H_6/CO was interpreted as indicating an increase in the proportion of photo-activated molecules decomposing into free radicals,

$$CH_3COCH_3^* \rightarrow CH_3 + COCH_3.$$

Gorin,[13] on the basis of experiments on the photolysis of acetone at 60–80° in the presence of iodine, differs with Spence and Wild. His conclusion was that even at 3130A, the primary process is predominately a decomposition into free radicals.

The results obtained in this research support the contention of Spence and Wild. From Table II it is found that for the same rate of formation of products, there are 3.2 times as many radicals formed at 2810A as at 3170A and 10 times as many at 2537 as at 3170. If it is assumed that at 2537A all of the photolysis occurs by a free radical mechanism, then at 2810 only $3.2/10.6 \times 100$ or 33 percent of the photo-activated molecules decomposing do so by giving free radicals; at 3170 a similar calculation gives 10 percent.

The results given in Table II for acetaldehyde are inconclusive due to the failure to obtain mirror removal at 2537A. The differences observed for the wave-lengths studied are not significant in view of the complexity of the mechanism of decomposition of acetaldehyde and its dependence on light intensity. The more recent work of Blacet and Loeffler[14] on the photolysis of acetaldehyde in the presence of iodine shows convincingly that both reactions,

$$CH_3CHO^* \rightarrow CH_3 + HCO$$
$$CH_3CHO^* \rightarrow CH_4 + CO$$

occur and that there is a greater fraction of decomposition by a free radical mechanism at longer wave-lengths compared to shorter wave-lengths.

The photolysis of crotonaldehyde at room temperature has been studied by Blacet and Roof.[15] In the

[12] R. Spence and W. Wild, J. Chem. Soc. 352 (1937).
[13] E. Gorin, J. Chem. Phys. 1, 256 (1939).
[14] F. E. Blacet and D. E. Loeffler, J. Am. Chem. Soc. 64, 893 (1942).
[15] F. E. Blacet and J. G. Roof, J. Am. Chem. Soc. 56, 73 (1936).

region 2400–3660A no decomposition was found to occur. Blacet and Volman[16] have made a study of the photo-chemical oxidation of crotonaldehyde. The addition of nitrogen to the reaction mixture causes a decrease in oxidation quantum yield. This has led to the postulation that the primary process in photolysis must include a deactivation,

$$CH_3C_2H_2CHO^*+M\rightarrow CH_3C_2H_2CHO+M^*.$$

In the mirror experiments, it was demonstrated that free radicals were definitely produced at 2537A. Therefore a rupture such as

$$CH_3C_2H_2CHO^*\rightarrow CH_3C_2H_2+CHO$$

must also occur.

Blacet, Fielding, and Roof[17] from studies of the photolysis of acrolein have postulated that the primary process is to some extent

$$CH_2CHCHO^*\rightarrow CH_2CH+HCO.$$

The fact that mirrors were removed at wave-lengths 2537A and 2810A tends to confirm this view.

The work of several investigators[5] on formaldehyde has led to the conclusion that free radicals are not formed at wave-lengths greater than 2750A. Gorin,[13] however, obtained evidence of free radicals formation at longer wave-lengths. It has been demonstrated here that free radicals are formed, and the indications are that wave-lengths somewhat longer than 2750A can produce them. It may be observed that formaldehyde gave the same anomolous result at 2537A as acetaldehyde, perhaps for the same reason of low intensity combined with low free radical yield.

With azomethane it was found that light of wave-length greater than 3340A produced free radicals. This tends to confirm results obtained on the photolysis of mixtures of azomethane and acetaldehyde[7] at long wave-lengths which have been explained by assuming methyl radicals formed from azomethane. Thus it was possible to study the action of methyl radicals on acetaldehyde.

The negative mirror results obtained with glyoxal are not conclusive evidence that free radicals are not formed since the action of formyl radicals on tellurium is not known. However, the results on the photolysis of mixtures of glyoxal and acetaldehyde[6] are in keeping with an hypothesis of no free radical production from irradiation of glyoxal.

There has been some mirror work with diazoethane in an attempt to confirm the existence of the ethylidene radical. Rice and Glasebrook[8] decomposed diazoethane at 650° and found no evidence of free radical formation. Barrow, Pearson, and Purcell[9] report mirror removal at lower temperatures, 400–450°. They also report mirror removal when diazoethane is irradiated with mercury arcs. We have attempted to clarify these somewhat conflicting thermal data, however, the explosions already referred to have prevented any positive conclusions being drawn. The evidence now suggests that thermally diazoethane alone yields free radicals and removes mirror at temperatures in the neighborhood of 400–500° but not at 650° or higher. Also that in the presence of hydrogen at 750° free radicals are formed. As the other workers have already suggested, these results are perhaps to be explained on the basis of the formation of ethylidene and its rapid isomerization to ethylene. The results with hydrogen present may possibly be due to a rapid reaction

$$CH_3CH:+H_2\rightarrow CH_3CH_2+H.$$

Although we were unable to show mirror removal in our thermal experiments with diazoethane alone, it is difficult to explain the explosion results unless free radicals are formed.

The irradiation results appear to be somewhat clearer. Our results confirm the formation of free radicals at short wave-lengths. However, we have also shown that free radicals are not formed at wave-lengths above 3100A. Although these results suggest the possible formation of ethylidene radicals at the shorter wave-lengths, other explanations based on other radicals are not ruled out. It may be observed that the photochemical data are not consistent with the hypothesis of a primary rupture to ethylidene radical followed by isomerization requiring some activation energy to ethylene.[9] If this were the case, it might be expected that longer wave-lengths, less energy, would result in free radicals of appreciable life, while shorter wave-lengths could yield an energy rich radical which would rapidly isomerize to ethylene.

[16] F. E. Blacet and D. H. Volman, J. Am. Chem. Soc. **61**, 582 (1939).

[17] Blacet, Fielding, and Roof, J. Am. Chem. Soc. **59**, 2375 (1937).

A Calculation of the Energy Absorbed in a Spherical Volume Containing a Gas-Radon Mixture

CHARLES R. MAXWELL AND VICTOR P. HENRI*
Laboratory of Physical Biology, Experimental Biology and Medicine Institute, National Institutes of Health, Bethesda, Maryland
(Received June 13, 1949)

A graphical method for the calculation of the energy absorbed from the alpha-particles emitted by radon and its decay products is described. Factors, calculated by this method, are presented for use in calculating the energy absorbed in any spherical volume. These factors are compared with similar factors calculated with analytical expressions presented by other investigators. The orders of magnitude of the energy absorbed from recoil atoms, beta-particles and gamma-rays are given.

I. INTRODUCTION

A KNOWLEDGE of the energy absorbed by the gas in a gas-radon mixture is necessary for the interpretation of the chemical effects of the ionizing radiations on the gas. A calculation of this energy requires (1) a knowledge of the rate of energy loss of an alpha-particle along its path in the gas and (2) a knowledge of the distribution of the decay products between the gas phase and the walls of the container.

Several analytical methods have been presented for calculating the ionizations produced by alpha-particles in a spherical volume. These methods differ in the mathematical approximations taken for the Bragg curves of the α-particles and in the values used for the distribution of the radon decay products.

In all these methods, and in the method to be presented here, the number of variables was reduced by expressing the size of the spherical vessel as a ratio of the radius (r) of the sphere and the path length (p) of the radon alpha-particle in the gas which fills the sphere. $R=r/p$ and $\rho=p/r$ have both been used.

Lind and Lunn[1,2] assumed that the rate of ion production is constant along the alpha-particle track and developed the average path method for use with spheres of diameter less than $R=1$.

Mund[3] assumed the validity of the Geiger law when used with the extrapolated ranges of the alpha-particles and derived expressions for the number of ionizations produced in the gas phase as a function of ρ. Equations were derived for Rn, RaA, and RaC′ uniformly distributed in the gas phase and for RaA and RaC′ on the walls of the sphere.

Glockler and Heisig[4] and Colmant[5] have modified Mund's equations by using "concordant" ranges instead of the extrapolated ranges in the Geiger approximation of the Bragg curve. Capron[6] has derived a set of equations similar to those of Mund by using two empirical functions to approximate the observed Bragg curves of Curie and Henderson.

Because of a limited knowledge of the distribution of the radon decay products and because of the labor involved in the use of their equations, each of the above authors assumed a probable distribution of the decay products and calculated the ionization produced in a series of spheres. These data were presented as tables of factors as a function of ρ. The ionizations produced in any sphere (for the particular distribution) could then be easily calculated by interpolation on a plot of these factors.

The present paper describes a graphical method for the calculation of the energy absorbed from the alpha-particles emitted by radon and its decay products. This method, which utilizes the latest experimental range-energy relationship, was adopted because no simple mathematical expression could be found to describe this relationship so that an analytical solution could be made with comparable accuracy.

The energies absorbed from Rn, RaA, and RaC′ in the gas phase and from RaA and RaC′ on the walls of the sphere have been calculated for a series of spheres with radii from $R=0.1$ to $R=10$. The data from these calculations are recorded as a table of efficiency factors, F, defined as:

$$F=\frac{\text{energy absorbed from alpha-particle } X}{\text{total energy of alpha-particle } X}.$$

With these factors, the energy absorbed from α-particles in any sphere may be readily calculated for any distribution of RaA and RaC′.

The distribution of the decay products is a property of the particular system being studied. A method for determining this distribution and some of the variables which influence it will be reported in a subsequent paper.

II. ENERGY ABSORBED FROM α-PARTICLES

Method of Calculation

Curves of energy loss as a function of path traversed were prepared for the α-particles emitted by Rn, RaA,

* Present address: Massachusetts Institute of Technology, Cambridge, Massachusetts. This work was done while the author was a National Institutes of Health Senior Research Fellow.

[1] S. C. Lind, J. Phys. Chem. **16**, 567–72 (1912).

[2] S. C. Lind, *The Chemical Effects of Alpha-Particles and Electrons* (Chemical Catalog Company, Inc., New York, 1928), pp. 93.

[3] W. Mund, J. Phys. Chem. **30**, 890–94 (1926).

[4] G. Glockler and G. B. Heisig, J. Phys. Chem. **36**, 769–79 (1932).

[5] P. Colmant, Bull. Soc. Chim. Belg. **41**, 464–74 (1932).

[6] P. C. Capron, Bull. Soc. Chim. Belg. **43**, 25–34 (1934).

TABLE I. Efficiency factors for the absorption of energy from alpha-particles in a gas-filled spherical volume. R=(radius of sphere)/(range of Rn α-particle in gas mixture).

	In gas phase			On wall	
R	Rn	RaA	RaC′	RaA	RaC′
0.1	0.0502	0.0427	0.0269	0.0285	0.0181
0.2	0.1032	0.0875	0.0553	0.0592	0.0353
0.3	0.1595	0.1369	0.0850	0.0918	0.0522
0.4	0.2230	0.1853	0.1154	0.1286	0.0785
0.5	0.2999	0.2483	0.1501	0.1715	0.1011
0.6	0.3739	0.3061	0.1819	0.2212	0.1263
0.7	0.4414	0.3733	0.2176	0.2610	0.1518
0.8	0.5013	0.4405	0.2559	0.2913	0.1824
1.0	0.5888	0.5257	0.3441	0.3331	0.2450
1.2	0.6484	0.5972	0.4213	0.3595	0.2879
1.4	0.7022	0.6543	0.4942	0.3809	0.3180
1.6	0.7338	0.6956	0.5508	0.3966	0.3407
1.8	0.7652	0.7279	0.5946	0.4075	0.3583
2.0	0.7870	0.7542	0.6325	0.4172	0.3739
2.5	0.8303	0.8036	0.7032	0.4336	0.4001
3.0	0.8589	0.8361	0.7505	0.4465	0.4156
4.0	0.8945	0.8763	0.8131	0.4594	0.4364
5.0	0.9217	0.9029	0.8570	0.4684	0.4538
7.0	0.9371	0.9314	0.8979	0.4839	0.4642
10.0	0.9615	0.9531	0.9258	0.4869	0.4834

and RaC′ using data taken from Fig. 11 of the work of Holloway and Livingston[7] on the range-energy relationship of α-particles. The energies and mean ranges in dry air at 15°C and 76 cm pressure used were:

	Mean range	Energies
Radon	4.051 cm	5.486 Mev
Radium A	4.657 cm	5.998 Mev
Radium C'	6.907 cm	7.680 Mev

The active material in the gas phase was assumed to be uniformly distributed and the volume was divided into 13 concentric spherical shells. The radii of the shells were selected so that $\frac{(R\,\text{max}-R\,\text{av})}{(R\,\text{sphere})}\times\frac{(\text{volume of shell})}{(\text{volume of sphere})}$ was less than 0.005 for each shell. In this manner the errors associated with the geometrical approximation were distributed uniformly through the sphere. All of the α-particles emitted in each of these shells were considered to have been emitted from one point located at the average radius of that shell. These points were plotted on a scale drawing of a great circle section through the spherical volume. From each of these points radial lines were drawn at 10° intervals to the circumference of the great circle. These lines represent the average path lengths of the α-particles emitted in each of 19 zones defined on the sphere by polar angles differing by 10°. The lengths of these lines were measured and the corresponding energy absorbed in the gas phase was read from the curves of energy loss previously prepared. Each of these energies was multiplied by the probability of emission in the corresponding zone and by the fraction of the total volume represented by the particular point. The sum of these energies was taken as the energy absorbed in the gas phase.

For the energy absorbed from RaA and RaC′ on the walls only one point on the spherical surface was required. The same method was used but with radial lines drawn at 5° intervals.

Results

The data from the calculations of the energy absorbed in a series of spheres are listed in Table I. R in Column I is defined as the ratio of the radius of the sphere to the range of the radon alpha-particle in the gas which fills the sphere. The factors recorded in the other columns are defined as the ratio of the energy absorbed in the gas phase from the indicated alpha-particle to the total energy of that alpha-particle.

As an example of the use of these factors to calculate the energy absorbed in any sphere consider the case of hexane when mixed with Rn in a spherical vessel under the following conditions:

(a) radius of sphere 8.0 cm; (b) temperature 25°C; (c) pressure 80 mm; (d) 90 percent RaC′ on wall, 40 percent RaA on wall. Solution:

(1) The molecular stopping power of hexane relative to air may be calculated from the atomic stopping powers. For a radon alpha-particle it is according to the data of Bethe.[8]

$$\frac{6(0.9260)+14(0.2224)}{2}=4.335.$$

(2) The range of the radon alpha in the gas which fills the sphere is then

$$4.051\times\frac{1}{4.335}\times\frac{760}{80}\times\frac{298}{288}=9.186\text{ cm where}$$

4.051 is the range of the Rn α-particle in dry air at 760 mm pressure and 15°C.

(3) R is then 8.0/9.4=0.871.

(4) The efficiency factors for R=0.871 are read from a plot of Table I and the average energy absorbed in the gas phase for each radon disintegration is as follows:

From Rn (gas) (5.486) (1.00) (0.535)=2.94 Mev.
RaA (gas) (5.998) (0.60) (0.472)=1.70
RaA (wall) (5.998) (0.40) (0.308)=0.74
RaC′ (gas) (7.680) (0.10) (0.290)=0.22
RaC′ (wall) (7.680) (0.90) (0.205)=1.42

Total 7.02 Mev.

III. ENERGY ABSORBED FROM OTHER PARTICLES

Beta-Particles

The energy absorbed from the beta-particles from RaB and RaC can be calculated with sufficient accuracy

[7] M. G. Holloway and M. S. Livingston, Phys. Rev. 54, 18–37 (1938).

[8] M. S. Livingston and H. A. Bethe, Rev. Mod. Phys. 9, 273–5 (1937).

for spheres with radii of $R<25$ by Lind's[1,2] average path method. Lind has shown that the average path lengths for particles emitted at random in a spherical volume and for particles emitted from the wall of the sphere are respectively 0.75 and 0.50 of the radius of the sphere.

The range-energy relationship for beta-particles in terms of Mev and grams of absorber (aluminum) is expressed by the following equations:[9]

$$E=1.85X+0.245, \quad X>0.3 \text{ gram/cm}^2, \tag{1}$$

$$E=1.92X^{0.725}, \quad X<0.3 \text{ gram/cm}^2. \tag{2}$$

In the region from 0.20 to 0.65 Mev, Eq. (2) is approximated by

$$E=2.4X+0.1. \tag{3}$$

It follows that the energies absorbed from beta-particles in spheres with $R<25$ are given by:

$$\text{RaB in gas } E=0.009R, \tag{4}$$

$$\text{RaB on wall } E=0.006R, \tag{5}$$

$$\text{RaC in gas } E=0.0069R, \tag{6}$$

$$\text{RaC on wall } E=0.0046R. \tag{7}$$

Recoil Atoms

Since the ranges of the recoil atoms from alpha-decays are approximately 1/350[10] of the range of the alpha-particles, the energy absorbed from these atoms is nearly independent of the size of the spheres for $R>0.05$. Depending upon the distribution of the decay products the energy absorbed in the gas phase from the recoil atoms will be between 0.22 Mev and 0.35 Mev for $R>0.05$. Thorough discussions of the effects of recoil atoms in small spheres are given by Lind[11] and Colmant.[5]

The energies of the recoil atoms from the beta-decays are less than 50 e.v. and may be neglected.

Gamma-Rays

The energy absorbed from the gamma-rays is very small and may be neglected.

Backscattering

A calculation of the energy contribution of backscattered α-particles and β-particles has not been made because the amount of backscattering[12] will depend upon the surface of the bombardment vessel and upon the residual energy of the particle when it strikes the surface. Each experimental set-up will have an individual solution. However, the energy contribution of these particles will usually be a very small fraction of the total energy absorbed.

IV. DISCUSSION

The advantages of the efficiency factors presented here over the analytical equations previously presented are twofold. (1) They were calculated from the latest experimental range-energy curves and not from mathematical approximations to earlier determinations of this relationship. (2) They give directly the energy absorbed and not the ionizations produced. They have the advantage that they can be used for any distribution of the radon-decay products and not just for one particular distribution.

TABLE II. A comparison of calculated efficiency factors for the energy absorbed in a gas from α-particles.

	Radon in gas			RaA on wall			RaC′ on wall		
ρ[a]	M. and H.[b]	G. and H.[c]	Capron[d]	M. and H.	G. and H.	Capron	M. and H.	G. and H.	Capron
0	1.000	1.000	1.000	0.500	0.500	0.500	0.500	0.500	0.500
0.1	0.961	0.9550	0.9584	0.485	0.4777	0.4860	0.475	0.4568	0.4856
0.2	0.916	0.9102	0.9169	0.470	0.4607	0.4720	0.450	0.4310	0.4713
0.4	0.830	0.8215	0.8348	0.434	0.4260	0.4440	0.403	0.3794	0.4425
0.5	0.789	0.7779	0.7944	0.418	0.4087	0.4300	0.375	0.3536	0.4281
0.8	0.665	0.6518	0.6767	0.372	0.3568	0.3879	0.303	0.2761	0.3850
1.0	0.590	0.5730	0.6026	0.333	0.3222	0.3599	0.243	0.2245	0.3563
1.1	0.552	0.5356	0.5670	0.316	0.3049	0.3458	0.218	0.1987	0.3419
1.3	0.484	0.4656	0.4998	0.282	0.2703	0.3178	0.173	0.1593	0.3131
1.5	0.418	0.4027	0.4382	0.248	0.2356	0.2898	0.145	0.1344	0.2844
1.7	0.365	0.3481	0.3833	0.214	0.2010	0.2617	0.124	0.1165	0.2556
2.0	0.300	0.2841	0.3153	0.171	0.1624	0.2197	0.101	0.0973	0.2125
2.4	0.235	0.2295	0.2530	0.136	0.1310	0.1730	0.082	0.0799	0.1658
3.0	0.180	0.1792	0.1963	0.104	0.1021	0.1324	0.063	0.0631	0.1275
4.0	0.131	0.1314	0.1434	0.074	0.0748	0.0959	0.046	0.0467	0.0923
5.0	0.104	0.1042	0.1131	0.058	0.0592	0.0753	0.035	0.0371	0.0725
7.0	0.075	0.0743	0.0795	0.040	0.0416	0.0528	0.025	0.0263	0.0508
10.0	0.050	0.0488	0.0550	0.028	0.0289	0.0364	0.018	0.0182	0.0351

[a] ρ = (range of Rn α-particle in gas)/(radius of spherical container).
[b] M. and H.—this paper.
[c] G. and H.—Glockler and Heisig, reference 4.
[d] Capron—reference 6.

[9] Lapp and Andrews, *Nuclear Radiation Physics* (Prentice-Hall, Inc., New York, 1948), pp. 180.
[10] L. Wertenstein, Ann. de physique **1**, 347 (1914).
[11] S. C. Lind, J. Am. Chem. Soc. **41**, 551–59 (1919).
[12] W. Riezler, Proc. Roy. Soc. London **A134**, 154–170 (1931).

The error associated with the geometrical approximations necessary for the graphical calculation may be reduced to any desired value by the use of a larger number of concentric spherical shells and of radial lines. However, calculations indicate that the use of increments smaller than those reported here would not have appreciably changed the reported values of energy absorbed. The difference between the two values calculated for one point with radial lines at 10° intervals and again with radial lines at 5° intervals was −0.15 percent. The difference between the two values calculated in the same manner for another point was +0.21 percent.

The error which has been introduced by treating the RaC→RaC″→RaD disintegrations as RaC→RaC′→RaD disintegrations is less than 0.02 percent of the energy absorbed from the RaC′ alpha-particle.

If it is assumed that the average energy loss per ionization is constant along the track of an alpha-particle, a comparison can be made of these graphical factors and the previously reported analytical equations. Table II offers such a comparison. Columns 2, 5, and 8 are taken from a plot of Table I. Columns 3, 6, and 9 were calculated by the equations of Mund[3] using the Geiger two-thirds power law and the concordant ranges proposed by Glockler and Heisig.[4] Columns 4, 7, and 10 were calculated by Capron[6] by the use of two empirical equations to represent experimental Bragg curves. The graphical factors and the factors calculated with Mund's equations differ systematically and have a maximum difference of 10 percent. Capron's factors for radon in the gas phase agree fairly well with the other two sets of factors but his factors for RaA and RaC′ on the wall are in marked disagreement with the other two, particularly for spheres of small radii. It might be pointed out that these factors are themselves inconsistent since they indicate that the rate of ionization along the first part of the RaC′ alpha-particle track is greater than the rate of ionization along the first portion of the RaA alpha-particle track.

THE JOURNAL OF CHEMICAL PHYSICS VOLUME 18, NUMBER 2 FEBRUARY, 1950

Primary Step in the Mercury Photo-Sensitized Decomposition of Propane and of Hydrogen

C. R. MASSON AND E. W. R. STEACIE
Division of Chemistry, National Research Council, Ottawa, Canada
(Received August 15, 1949)

An attempt has been made to obtain resonance emission of HgH bands in propane-mercury mixtures illuminated with λ2537. It is concluded that if HgH is formed in the primary step in the photo-sensitized decomposition of paraffins, it must possess excess energy and largely dissociate immediately.

Further experiments with mercury-hydrogen mixtures illuminated with λ2537 have also been made, and the mechanism of the production of excited HgH molecules is discussed.

AN attempt has been made to elucidate the primary step in the mercury-photo-sensitized decomposition of propane. There are two possible mechanisms:

$$Hg(^3P_1)+C_3H_8=HgH+C_3H_7 \quad (1)$$

followed by

$$HgH=Hg(^1S_0)+H \quad (2)$$

or

$$Hg(^3P_1)+C_3H_8=Hg(^1S_0)+C_3H_7+H. \quad (3)$$

If the reaction proceeds via formation of HgH in its normal state, it should be possible to secure excitation and emission of HgH bands in the system.

HgH bands may be observed in fluorescence on irradiating mixtures of mercury vapor, hydrogen, and nitrogen with 2537A radiation. Gaviola and Wood[1] have determined the best conditions for observing the bands. Beutler and Rabinowitsch[2] have given the following mechanism for the formation of excited HgH:

$$Hg(^3P_0)+H_2=HgH+H+0.62\text{ v}, \quad (4)$$

$$HgH+Hg(^3P_0)=Hg(^1S_0)+HgH^*. \quad (5)$$

This mechanism is supported by the experiments of Rieke.[3] Olsen,[4] however, has unsuccessfully attempted to secure resonance excitation of HgH in mixtures of mercury vapor, hydrogen, and nitrogen, and has concluded that HgH molecules are not present in the normal state, but are formed in excited states which dissociate after emission. The suggested mechanism of Olsen, which is similar to the original interpretation of Gaviola and Wood, is

$$Hg(^3P_0)+H_2=Hg(^1S_0)+2H, \quad (6)$$

$$Hg(^3P_1)+H=HgH^*. \quad (7)$$

Evidence that free atomic hydrogen is necessary for

[1] E. Gaviola and R. W. Wood, Phil. Mag. **6**, 1191 (1928).
[2] H. Beutler and E. Rabinowitsch, Zeits. f. physik. Chemie **B8**, 403 (1930).
[3] F. F. Rieke, J. Chem. Phys. **4**, 513 (1936).
[4] L. O. Olsen, J. Chem. Phys. **6**, 307 (1938).

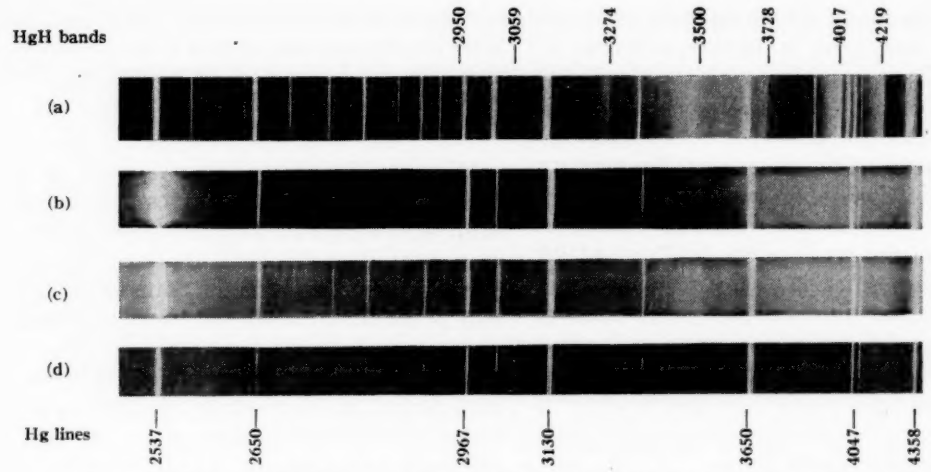

FIG. 1. (a) Source of HgH. (b) Excitation with Hg—H_2 and Hg—A discharge. (c) Excitation with Hg—A discharge. (d) Excitation with Hg—H_2 discharge.

securing the bands is afforded by Gaviola and Wood's observation that the HgH radiation is extinguished if a little oxygen is admitted to the system, the OH band at 3065A appearing instead.

There is, however, the following practical objection to Olsen's work. In attempting to secure resonance, Olsen employed only one discharge lamp to irradiate his resonance cell. The radiation consisted of either the HgH band radiation with the mercury resonance line 2537A considerably quenched, or, alternatively, the mercury spectrum with intense 2537A emission. Olsen's experiments using either of these sources singly do not conclusively prove that HgH cannot be excited by resonance, since the low concentration of excited mercury atoms may mean the practical absence of HgH molecules from the system when the hydrogen-filled discharge is used alone. In either of the above mechanisms for the formation of excited HgH, the presence of metastable Hg($^3P_0$) atoms is a necessary condition for securing the bands.

HYDROGEN

Experiments similar to Olsen's which we have made have shown (Fig. 1) that on irradiating a mixture of mercury vapor (20°C), hydrogen (0.01 mm) and nitrogen (5 mm) with a mercury-hydrogen discharge, very little excitation of the mercury to higher states occurs as a result of the weakness of the resonance line 2537A in the source. A more conclusive test for resonance would be to irradiate the mixture with both a mercury and a mercury-hydrogen discharge simultaneously. Any resonance excitation of HgH would then be observed as an increase in the intensity of the HgH bands when both lamps are used together as compared with the intensity of the bands when the mercury lamp is used alone.

Figure 1(a) shows a spectrogram of the mercury-hydrogen discharge used in the present work. The lamp was operated at about 2.5 kva. It was constructed entirely of quartz, the discharge portion being spiral-shaped to surround the resonance cell. The spectrogram shows the main HgH bands clearly defined.

An argon-filled mercury lamp with oxide-coated electrodes and quartz spiral discharge tube served as source of 2537A radiation. It was operated at about 0.5 kva. A Hilger intermediate quartz spectrograph having a dispersion of about 45A per mm at 3500A was used.

The resonance cell was similar to that described by Bender.[5] The gases were saturated with mercury vapor at room temperature before entering the cell near the front window. In experiments with both lamps, the hydrogen-filled lamp was placed nearer the front window to reduce scattered light from this source to a minimum.

Experiments using a static mixture of mercury vapor (20°C), hydrogen (0.01 mm), and nitrogen (5 mm) in the cell showed that the intensity of the 3500A HgH band observed in fluorescence was considerably reduced when both lamps were employed as source, as compared with the intensity of the band when the argon-filled lamp was used alone. Further, on irradiating with the hydrogen-filled discharge alone, there was practically no emission of HgH radiation from the system. The spectrograms are reproduced in Figs. 1(b), 1(c), and 1(d), respectively. Exposure times were the same in each (5 min.). (In Fig. 1(c) there is observed, in addition to the main HgH band emission, a faint OH band at 3064A arising from a trace of water vapor present in the nitrogen.)

This almost complete disappearance of the HgH band emission which occurs when the hydrogen-filled discharge is used is due to the rise in temperature of the cell gases when the hot hydrogen lamp is running. The same effect was produced by heating the resonance cell to about 100°C, using the mercury lamp alone as source; under these conditions no emission of HgH radiation occurred. This observation shows that it was impossible for Olsen to obtain resonance excitation of HgH under his experimental conditions.

[5] P. Bender, Phys. Rev. **36**, 1535 (1930).

A water-cooled resonance cell fitted with an outer quartz jacket was employed in further attempts to secure resonance. Exposures taken with the same mixture of gases in this cell, however, showed no increase in intensity of the 3500A HgH band when both lamps were used as compared with the intensity when the mercury lamp was used alone. The intensity of the OH 3064A band was, however, reduced and there was a faint increase in intensity of the heads of the 4017 and 4219A HgH bands. The exposures in these experiments (4 min.) were such that no scattered HgH light could be detected on the plate. Longer exposures (up to 45 min.) showed no increase in the band intensities apart from that due to scattered light, and it is concluded that it is not possible to secure resonance excitation of the HgH molecules present in this system.

The fact that a relatively small rise in temperature completely eliminates HgH radiation suggests that the lack in resonance emission is due to the low stability of HgH. In the first place, the heat of dissociation of HgH is only 8.5 kcal. as compared with 15.5 for CdH. If the activation energies of the reverse reactions are zero, as seems probable, these values are also the activation energies of the decompositions of the two hydrides. On this basis, the relative lifetimes at room temperature of normal HgH and CdH molecules will be in the ratio $\exp[-7000/(2\times300)]$ or 10^{-5}. It will thus be relatively much easier to detect CdH, and the lack of resonance emission by HgH may be merely due to its relatively low stationary concentration. In fact, it is possible that the normal HgH molecules present largely arise by the ordinary thermal equilibrium

$$Hg(^1S_0)+H\rightleftarrows HgH+8.5 \text{ kcal.}$$

A further factor may contribute to this cause. In the case of CdH formation, the reaction

$$Cd(^3P_1)+H_2\rightarrow CdH+H$$

is almostly exactly thermoneutral. It is therefore impossible for the CdH molecules to be formed in this way with excess vibrational energy. In the case of HgH, however, the reaction

$$Hg(^3P_1)+H_2\rightarrow HgH+H$$

is exothermic to the extent of 17.8 kcal. It is thus possible for HgH to be formed with excess energy, and largely to dissociate before its next collision. From a photo-chemical standpoint, the fact that C—H bonds are always broken in mercury-photo-sensitized reactions of organic compounds rather than C—C suggests that HgH has a transitory existence, even if its life is so short that it cannot be detected by resonance emission.

PROPANE

Mixtures of mercury vapor (approx. 10°C) and propane (10^{-2} mm to 16 mm) were irradiated with each lamp separately and with both lamps. No HgH bands were emitted, so that HgH, if present, cannot be excited by resonance. This behavior is distinctly different from that of cadmium vapor and propane[6] illuminated by a cadmium resonance lamp.

Attempts to detect the presence of HgH by collision excitation with metastable $Hg(^3P_0)$ atoms were not successful. Mixtures of mercury vapor (10°C), nitrogen (15 mm), and propane (2×10^{-2} mm to 2 mm) were irradiated with the mercury lamp alone. HgH bands were emitted, but these were of the same intensity as those obtained on irradiating nitrogen alone, thus originating from a trace of moisture present. Shorter exposures using nitrogen at 4 mm pressure and propane at pressures varying from 10^{-1} mm to 2 mm showed HgH bands decreasing in intensity with increasing propane pressure, this being accompanied by a decrease in the intensity of the resonance line 2537A. Evidence is thus obtained that the quenching of mercury resonance radiation by propane is not accomplished by the formation of HgH.

A few experiments were carried out using spectroscopically pure argon in place of nitrogen in the resonance cell. This gas is also efficient in quenching excited mercury to the metastable state. On irradiating a mixture of 0.5-mm propane, 15-mm argon, and mercury vapor (10°C) with the mercury lamp, no HgH emission occurred.

From these experiments it is concluded that HgH is not formed in detectable amounts in the mercury-photo-sensitized decomposition of propane. However, as discussed, it may have a transitory existence. The primary process cannot, therefore, be settled unambiguously.

One of the authors (C.R.M.) wishes to thank the National Research Council of Canada for the award of a Post-Doctorate Fellowship.

The authors are indebted to Dr. G. Herzberg for discussions and advice.

[6] E. W. R. Steacie and D. J. LeRoy, J. Chem. Phys. **12**, 34 (1944).

The Infra-Red CO Bands as Wave-Number Standards in the Infra-Red Region

K. NARAHARI RAO
Yerkes Observatory, University of Chicago, Williams Bay, Wisconsin
(Received June 10, 1949)

The predicted positions of the lines in the (1,0), (2,0) and (3,0) rotation-vibration bands of carbon monoxide are given and the possibility of using them as secondary standards in the infra-red region of the spectrum is discussed.

WITH the aid of results obtained in two previous investigations[1,2] it has been possible to compute the positions of the lines in the fundamental and the overtone bands of the carbon monoxide molecule. It is considered that these are suitable for use as wave number standards in the infra-red region of the spectrum. The present paper gives the computed positions of the (1,0), (2,0) and (3,0) rotation-vibration bands of CO along with a discussion of the limitations of their accuracy.

The wave numbers of the lines in the R and P branches of the rotation-vibration bands of a diatomic molecule are given by the following formulas:

$$R(J)=\nu_0+F'(J+1)-F''(J), \quad (1)$$

$$P(J)=\nu_0+F'(J-1)-F''(J), \quad (2)$$

where

$$F(J)=B_vJ(J+1)-D_vJ^2(J+1)^2. \quad (3)$$

Here the standard nomenclature is used. In the case of the CO molecule the quantities given on the right-hand side of (1) and (2) are known with a high degree of accuracy.[1,2] It was found that the rotational constants B_v and D_v for the electronic ground state of the CO molecule can be represented by the relations

$$B_v=1.93139-0.017485(v+\tfrac{1}{2}), \quad (4)$$

$$D_v=6.43\times10^{-6}+0.04\times10^{-6}(v+\tfrac{1}{2}). \quad (5)$$

The separations of the vibrational levels from $v=0$ to 4 of the same state were found to have the following values:

$$\begin{aligned}\Delta G_{1/2}&=2143.38\ \text{cm}^{-1},\\ \Delta G_{3/2}&=2116.74\ \text{cm}^{-1},\\ \Delta G_{5/2}&=2090.27\ \text{cm}^{-1},\\ \Delta G_{7/2}&=2064.01\ \text{cm}^{-1}.\end{aligned} \quad (6)$$

Using these data the positions of lines in the (1,0), (2,0) and (3,0) rotation-vibration bands of the CO molecule were calculated according to relations (1) (2). The results are given in Table I.

A check on the correctness of these wave numbers can be obtained with the help of the Cameron bands of carbon monoxide which are due to a transition from a $^3\Pi$ state to the ground state $^1\Sigma$ of the CO molecule. A discussion of the structure of these bands was given in a previous paper.[2] The data used in the following discussion have been taken from that investigation.

TABLE I. Wave numbers of the lines in the (1,0), (2,0) and (3,0) rotation-vibration bands of the CO molecule.

	(1,0) band $\nu_0=2143.38$ cm^{-1}		(2,0) band $\nu_0=4260.12$ cm^{-1}		(3,0) band $\nu_0=6350.39$ cm^{-1}	
J	$R(J)$	$P(J)$	$R(J)$	$P(J)$	$R(J)$	$P(J)$
0	2147.19		4263.90		6354.13	
1	50.97	2139.53	67.60	4256.27	57.77	6346.54
2	54.71	35.65	71.24	52.36	61.30	42.59
3	58.41	31.74	74.80	48.37	64.72	38.54
4	62.08	27.79	78.29	44.32	68.04	34.38
5	65.71	23.81	81.72	40.20	71.25	30.12
6	69.31	19.79	85.07	36.00	74.36	25.75
7	72.87	15.74	88.35	31.74	77.36	21.28
8	76.39	11.65	91.56	27.41	80.26	16.70
9	79.88	07.53	94.70	23.01	83.05	12.02
10	83.33	03.38	97.77	18.54	85.73	07.24
11	86.75	2099.19	4300.76	14.01	88.30	02.35
12	90.13	94.97	03.69	09.40	90.77	6297.36
13	93.47	90.72	06.54	04.73	93.13	92.27
14	96.77	86.43	09.32	4199.99	95.39	87.08
15	2200.04	82.11	12.02	95.18	97.53	81.78
16	03.27	77.76	14.66	90.30	99.57	76.37
17	06.46	73.38	17.22	85.36	6401.50	70.87
18	09.61	68.96	19.70	80.35	03.32	65.26
19	12.73	64.51	22.12	75.27	05.04	59.55
20	15.80	60.03	24.46	70.12	06.64	53.74

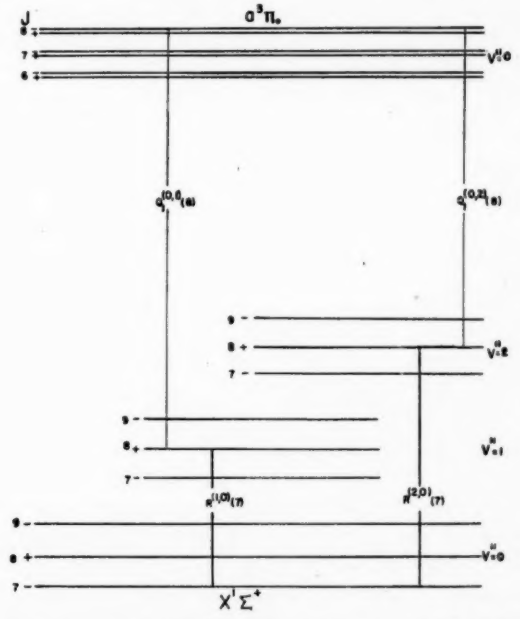

FIG. 1. Energy level diagram illustrating the relations given in (7), (8), and (9). Only one triplet component ($^3\Pi_0$) of the upper state is drawn here. The relations hold for the other two components as well.

[1] G. Herzberg and K. N. Rao, J. Chem. Phys. **17**, 1099 (1949).
[2] K. N. Rao, Ap. J. **110**, 304 (1949).

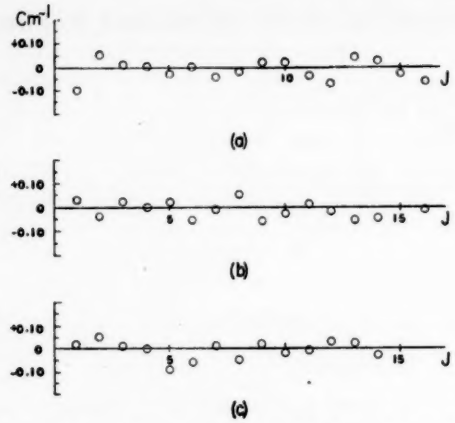

FIG. 2. Observed minus computed values of lines for different J values.

The validity of the following relation is easily understood from the energy level diagram (Fig. 1):

$$[P^{(0,1)}(K)-P^{(0,2)}(K)] \text{ or } [Q^{(0,1)}(K)-Q^{(0,2)}(K)] \text{ or } [R^{(0,1)}(K)-R^{(0,2)}(K)] = [R^{(2,0)}(J-1)-R^{(1,0)}(J-1)]. \quad (7)$$

The differences of wave numbers of the lines given on the left-hand side of (7) are obtained from the measurements of the Cameron bands. These are, therefore, purely observed quantities. On the other hand, those on the right side are from the data in Table I and they, therefore, are purely computed quantities. The differences of the observed and computed values are plotted against J in Fig. 2a. In these plots, average values of the differences of corresponding unblended lines in all the different branches of the (0, 1) and (0, 2) Cameron bands have been used. It can be noticed that the observed values differ from the computed ones by less than ± 0.05 cm^{-1} in most places. The same accuracy was obtained from the other bands studied, as can be seen from Figs. 2b and 2c which represent the observed *minus* computed values of the following relations:

$$[P^{(0,2)}(K)-P^{(0,3)}(K)] \text{ or } [Q^{(0,2)}(K)-Q^{(0,3)}(K)] \text{ or } [R^{(0,2)}(K)-R^{(0,3)}(K)] = [R^{(3,0)}(J-1)-R^{(2,0)}(J-1)], \quad (8)$$

$$[P^{(1,3)}(K)-P^{(1,4)}(K)] \text{ or } [Q^{(1,3)}(K)-Q^{(1,4)}(K)] \text{ or } [R^{(1,3)}(K)-R^{(1,4)}(K)] = [R^{(4,0)}(J-1)-R^{(3,0)}(J-1)]. \quad (9)$$

In representing relation (9), for the (4,0) infra-red band the computed positions given in a previous paper[1] have been used.

Lagemann, Nielsen, and Dickey[3] measured the positions of the lines in the (1,0) and (2,0) bands with an infra-red spectrometer. In order to see how their measured values compare with the present predicted positions, the deviations of their measurements from the data given in Table I are plotted against m (m is $J+1$ for the R branch and $-J$ for the P branch) in the next diagram (Fig. 3). It is seen that their data have a systematic shift amounting to 0.2 to 0.3 cm^{-1}. In the

[3] Lagemann, Nielsen and Dickey, Phys. Rev. **72**, 284 (1947).

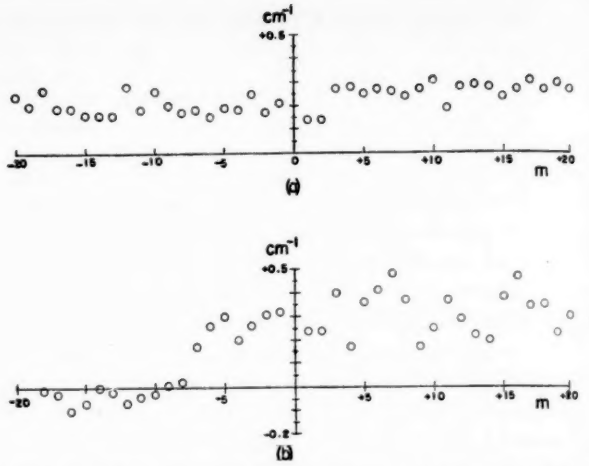

FIG. 3. Values observed by Lagemann, Nielsen, and Dickey minus computed values for (1,0) and (2,0) bands for different m values.

case of the (2,0) band besides this constant shift the scatter of points is rather large. These discrepancies are attributed to the lack of standards in the infra-red region of the spectrum, which makes it necessary to rely on the accuracy of the circle on which the grating is mounted. Whereas in the visible and the ultraviolet there is the great advantage in having a large number of comparison lines within any interval one is interested in, this is not so in the infra-red.

The CO infra-red bands have been frequently used in the past as secondary standards in the infra-red since they are easy to produce. Only 2- and 20-cm paths at atmospheric pressure are required for the (1,0) and (2,0) bands respectively, but 1000 cm for the (3,0) band. It is obvious from the above discussion that a remeasurement of the infra-red bands would be highly desirable, but as long as such a remeasurement is not available, it is felt that the wave numbers derived here are more reliable than those existing at present in the literature. It is, therefore, suggested that the computed positions given in Table I be used as secondary standards rather than the observed positions. It is, however, very important to bear in mind the limitations of these data. The relative accuracy of the predicted positions of the lines in each of the rotation-vibration bands considered is high on account of the precision with which the rotational constants of the electronic ground state of the CO molecule were obtained. But the uncertainty in determining the absolute $\Delta G_{v+\frac{1}{2}}$ values restricts the absolute accuracy of these predicted positions, it is believed, to within ± 0.1 cm^{-1}.

The computational work in this investigation was carried out at the National Research Council, Ottawa, Canada. I wish to express my gratefulness to the officials of that institution for providing me with all the required facilities. Finally, it is a pleasure to acknowledge my sincere thanks to Dr. G. Herzberg under whose supervision this work was carried out and to the Government of India for the award of a fellowship.

An Upper Limit to the Metastability of Supersaturated Vapors*

SIDNEY W. BENSON AND EDWARD GERJUOY
Division of Physical Sciences, University of Southern California, Los Angeles, California
(Received August 17, 1949)

A thermodynamic criterion for (mechanical) instability is applied to the condensation of supersaturated vapors. Values of the maximum thermodynamic compressibility of a vapor as a function of temperature are calculated from the Van der Waals' and Berthelot Equations of State and from a newly developed, modified equation. In all cases, the upper limits predicted lie above the reported experimental values. With the exception of the Van der Waals' equation the predicted values appear much too high. The bearing of these results on the utility of the same thermodynamic criterion for estimating maximum tensile strength of liquids is discussed.

IN a previous paper[1] a purely thermodynamic criterion has been used to determine the limits of metastability of liquids under tension. This criterion is $(\partial P/\partial V)_T=0$. When applied to liquids, making use of the Van der Waals' and Berthelot Equations of State in reduced form, quite acceptable values are obtained for the maximum tensile strengths. It was also demonstrated that these equations give good qualitative representations of such properties of liquids and vapors as reduced volume, coefficient of thermal expansion, bulk compressibility and energy of vaporization. Consequently it was thought worthwhile to extend the method to systems of supersaturated vapors.

For each equation of state, the equations obtained by setting the partial derivative $(\partial\pi/\partial\phi)_\theta=0$ was solved for ϕ (the reduced volume) and π (the reduced pressure) as a function of the reduced temperature, θ. The value of π so obtained is the value of the reduced pressure at the maximum in the reduced isotherm of the equation of state. For each equation of state, the vapor pressure curves as a function of θ were calculated from the equation (actually used in reduced form):

$$P_v(V_v-V_l)=-\int_{V_l}^{V_v}PdV$$

which is equivalent to equating the free energies of liquid and vapor.

From the curves for the maximum reduced pressures and the reduced vapor pressures it was then possible to calculate for any reduced temperature the values of $\pi_{\text{max.}}/\pi_{\text{vap.}}=R_s$, the ratio of the maximum supersaturation pressure to the vapor pressure.

In addition to the previously mentioned equations, a third equation developed recently by one of the authors (S. W. Benson) was tried. It is a modified Van der Waals' type equation which can be put into reduced form:

$$\pi=Z\left[\frac{\theta}{\phi-b\phi^{-\frac{1}{2}}}-\frac{a}{\theta^{\frac{1}{2}}\phi^{5/3}}\right].$$

It gives an excellent fit to most of the properties of liquids and vapors, far better than either the Van der Waals' or Berthelot equations and will be reported on soon in a forthcoming paper. The quantities Z, a, and b are universal constants in the above equation.

Values for the maximum supersaturation ratios R_s for different reduced temperatures are shown in Table I.

For purposes of comparison we quote the values obtained by Volmer and Flood[2] for polar vapors in the presence of air: methyl alcohol $(\theta=0.526)R_s=3.20$; ethyl alcohol $(\theta=0.527)R_s=2.34$; *n*-propyl alcohol $(\theta=0.502)R_s=3.05$; *i*-propyl alcohol $(\theta=0.520)R_s=2.80$; *n*-butyl alcohol $(\theta=0.484)R_s=4.60$; nitromethane $(\theta\cong0.45)R_s=6.05$; ethyl acetate $(\theta=0.465)R_s=9$ to 12; water $(\theta=0.425)R_s=4.2$.

Measurements of supersaturation ratios have also been reported by other investigators.[3–5] Scharrer's results[3] agree fairly well with those of Volmer and Flood for water and alcohols. He includes in addition ratios for non-polar substances, i.e., benzene $(\theta=0.45)R_s=5.4$; chlorobenzene $(\theta=0.41)R_s=9.5$. Scharrer reports much the same values as these when the condensation took place in the presence of ions with or without de-ionizing fields. (For chlorobenzene he finds, surprisingly, that R_s is increased in the presence of positive ions, going from 9.5 to 10.2.)

TABLE I. Maximum supersaturation ratios R_s.

Reduced temp. θ	Van der Waals' equation R_s	Berthelot equation R_s	Modified equation R_s
0.450	11	—	350
0.500	6.4	900	88
0.550	4.4	170	30
0.600	3.2	40	13
0.650	2.7	15	7.5
0.700	2.2	6.9	4.9
0.750	2.0	4.2	3.4

* This investigation was partially supported by the ONR under Task Order Contract No. N6-ori-77/2 at the University of Southern California.

[1] S. W. Benson and E. Gerjuoy, "Tensile strength of liquids I," J. Chem. Phys. **17**, 914 (1949).

[2] M. Volmer and H. Flood, Zeits. f. Physik. Chemie **A170**, 273 (1934).

[3] L. Scharrer, Ann. d. Physik **35**, 619 (1939).

[4] Loeb, Kip, and Einarrson, J. Chem. Phys. **6**, 264 (1938).

[5] Richard Head, "Investigations of spontaneous condensation phenomena," Ph.D. thesis, California Institute of Technology (1949).

Loeb's results[4] seem to indicate higher values for R_s* than the previously quoted authors but he also adopted a more severe requirement for condensation, namely cloud formation rather than the 1–4 droplets/cc used by the others.** He also finds that small amounts of impurities have a considerable effect on the values observed. Thus in the case of benzene amounts of moisture in the neighborhood of 0.02 percent decrease the values of R_s by more than 30 percent.

Head[5] using a variety of experimental techniques involving pressure changes produced in fast moving, moist air streams has observed values of R_s as high as 80 for water vapor ($\theta \sim 0.36$).

It would seem on comparing these data with the values in Table I that the Van der Waals' equation gives rather good agreement whereas the other two equations predict much too high values. However, this conclusion is tempered by the observation that this is due to the fact that the Van der Waals' equation gives a very poor representation of vapor pressures, the computed values being much too high. Similarly, the Berthelot equation predicts the highest supersaturation ratios because it gives vapor pressures which are far too low. The modified equation gives a fairly good fit to vapor pressures and so its predicted supersaturation ratios should probably be given the most credence. In all cases it is encouraging to note that the temperature dependence reported is in agreement with the equations with respect to sign.

DISCUSSION

These results lend some support to the author's previous work on the tensile strength of liquids.[1] The basic assumption involved in using $(\partial P/\partial V)_T = 0$ as a criterion for the maximum tensile strength of a liquid is that the liquid has an equation of state even at negative pressures, and that this equation gives *all* metastable states of the liquid. If the Van der Waals or Berthelot equations approximate the true equations of state at negative pressures, then the criterion $(\partial P/\partial V)_T = 0$, yields the maximum tension which the liquid can possibly support at any temperature. Whether or not this tension can be attained, depends of course on the experimental conditions and on the available mechanisms for taking the metastable one-phase system over into the stable, two-phase, liquid-vapor system.

Similar considerations apply to the maximum supersaturation pressure attainable by a vapor. Thus it is significant that the values in Table I do lie above the observed values. (The one or two exceptions are with the Van der Waals' equation, where, as has already been pointed out, the values of R_s are probably too low.) If observed supersaturation ratios exceed the predicted maximum ratios it would be necessary either to abandon the criterion $(\partial P/\partial V)_T = 0$ as an estimate of the limits of metastability, or else to infer that the Van der Waals' and Berthelot equations do not yield even approximately accurate representations of the metastable regions of the vapor isotherms. In either event the authors' previous calculations on tensile strength would not be credible.

That the observed values of R_s are so much lower than the predicted ratios for what is believed to be the best of the three equations of state, the modified equation, is no cause for alarm. For liquids, tensile strengths varying all the way from zero to hundreds of atmospheres have been reported. Presumably, the higher values result because of greater experimental care and because the experimental conditions are less favorable to the formation of critical sized bubbles. Although fewer experimental data are available for vapor condensation than for liquid tensile strength measurements† the experimental results quoted above indicate the existence of a greater variability in supersaturation ratios than has previously been supposed.

It must be mentioned finally that for condensation processes, there is the theory of Becker and Doring[6] which predicts values, fairly close to most of the experimental results of Volmer and Flood. This theory uses a model which involved only the statistical production of molecular clusters at the saturation limits. It is thus quite possible that such cluster formation provides a molecular mechanism for taking the metastable, supersaturated vapor system over into the stable two-phase system so that the thermodynamic ratios of Table I can never be attained. However, a considerable amount of experimental work would be required to justify such a conclusion at present. The experiments done so far leave room for considerable criticism. In particular it has been reported that condensation is often accompanied by considerable turbulence,[3] indicating that the process may not occur homogeneously and may be initiated at selected sites in the apparatus. The Becker-Doring model makes no provision for such possible heterogeneity. It may be of some value in this regard to study the effects of both dust particles and container surface on condensation phenomena. Loeb's findings on the effects of exceedingly small amounts of impurities seem also very significant with respect to the possible heterogeneous nature of the phenomenon.

ACKNOWLEDGMENT

The authors wish to express their appreciation to Mr. Charles Foy for his assistance in performing the numerical computations.

* From Loeb's data for "pure" benzene one can calculate a value of $R_s \sim 75$ at $\theta \sim 0.41$, considerably higher than any of the other values reported.

** There seems to be considerable dispute as to the actual criteria to be employed for the condensation onset.

† In particular it is to be noted that there is a lack of diversity in the experimental techniques employed in measuring condensation in vapors. A similar paucity in the case of liquids would have led to much narrower limits of variability in the observed tensile strengths.

[6] R. Becker and W. Doring, Ann. d. Physik **24**, 719 (1935).

Rotation-Vibration Spectra of Diatomic and Simple Polyatomic Molecules with Long Absorbing Paths

III. The Spectrum of Cyclopropane (C_3H_6) from 2.3 to 0.6μ

S. P. SINHA*
Yerkes Observatory of the University of Chicago, Williams Bay, Wisconsin
(Received March 30, 1949)

The absorption spectrum of cyclopropane has been investigated under high resolution (21-ft. grating) in the photographic infra-red and under low resolution (with a photoelectric infra-red spectrometer) in the region 1.2 to 2.3μ with absorbing paths up to 1760 meters. A large number of overtone and combination bands, about 150, have been found. Provisional vibrational assignments of nearly all the strong bands from 2.3 to 1.3μ are given. For the weaker bands no unique assignments are possible.

The parallel band at 10970A has been resolved and its rotational structure has been analyzed. The moment of inertia in the lower state is found to have the value $I_B = 42.1_5 \times 10^{-40}$ g cm².

A. INTRODUCTION

THE need for studying the absorption spectra of diatomic and simple polyatomic molecules in the region of overtone and combination bands, using long absorbing paths, has been indicated in the first paper of this series.[1] Cyclopropane on which an extensive study does not appear to have been made in this region was selected for the present work.

B. EXPERIMENTAL

Both absorption tubes described previously were employed.[1] In the smaller tube up to 20 traversals were used, giving a path length of 20×1.5=30 meters, while in the larger tube up to 80 traversals were used corresponding to a path length of 80×22=1760 meters.

Spectra in the region 0.6 to 1.2μ were taken with a 21-ft. concave grating spectrograph using Eastman F, N, M, and Z plates. The lowest pressure and path used in the photographic region were 80 mm and 24 m, respectively. For the weakest bands the maximum path length (1760 m) and a pressure of 250 mm were used. The time of exposure varied from less than a minute for F and N plates to about 40 hours for Z plates in the region of about 1.2μ.

In the region 1 to 2.4μ the spectra were obtained with the infra-red spectrometer built by Dr. G. P. Kuiper[2] (using a photo-conductive PbS cell as the receiving element), and only the shorter tube was used. The pressure varied from about 1 mm to 250 mm and 20 traversals were used. The cyclopropane was obtained from the Ohio Chemical and Manufacturing Company. It is considered to have a purity of 99.5 percent. No further purification was attempted.

TABLE I. Wave numbers of the lines of the 1.097 μ-band of C_3H_6.

J	R(J)	P(J)
1	9117.64	
2	18.97	
3	20.28	
4	21.54	
5	22.92	
6	24.11	9107.23
7	25.58	9105.57
8	26.82	04.12
9	28.15	02.78
10	29.42	01.39
11	30.71	00.06
12	32.01	9098.82
13	33.07	97.47
14	34.22	96.11
15	35.58	94.79
16	36.58	93.38
17	37.94	92.00
18	39.16	90.65
19		89.13
20		87.65
21		86.08

Q branch from 9116.3 to 9108.3 cm^{-1}

C. ROTATIONAL ANALYSIS

A large number of photographic infra-red bands were obtained, but the rotational structure was resolved only for the band at 1.097μ. The structure appeared best at a path length of about 1000 m when the pressure of the gas was about 80 mm. The band has a strong unresolved Q branch, about 12 cm^{-1} wide, and a P and an R branch on either side. It is therefore clearly a parallel band. Even under the most favorable conditions the lines of the P and R branches are quite wide and diffuse, presumably due to the fact that the individual sub-bands forming the band do not coincide very closely. Even with this in mind the Q branch seems rather too

TABLE II. Fundamentals of cyclopropane.

ν_1 (a_1')	3029 cm^{-1}	(liqu.)	ν_8 (e')	3024.4 cm^{-1}	
ν_2 (a_1')	1504	(liqu.)	ν_9 (e')	1432	
ν_3 (a_1')	1189	(liqu.)	ν_{10} (e')	1027.6	
ν_4 (a_1'')	(1000)		ν_{11} (e')	868	
ν_5 (a_2')	(1070)		ν_{12} (e'')	3080	(liqu.)
ν_6 (a_2'')	3103.0		ν_{13} (e'')	(1120)	
ν_7 (a_2'')	872		ν_{14} (e'')	740	(liqu.)

* Present address: Science College, Patna University, Patna, India.

[1] H. J. Bernstein and G. Herzberg, J. Chem. Phys. **16**, 30 (1948).

[2] Kuiper, Wilson, and Cashman, Astrophys. J. **106**, 243 (1947).

TABLE III. Combination and overtone bands of cyclopropane.

νvac (obs.) cm^{-1}	Type[a]	Intensity	Assignment[b]	νvac (calc.)[c]
4100	b	200	$\nu_4+\nu_{12}$ (E') $\nu_5+\nu_8$ (E') $\nu_{10}+\nu_{12}$ (A_2'')	4080 4094 4108
4189	b	750	$\nu_3+\nu_8$ (E')	4213
4219	b	800	$\nu_6+\nu_{13}$ (E')	(4223)
4271 4294	b b	860 830	$\nu_3+\nu_6$ (A_2'')	4292
4350	v.b.	70		
4378	v.b.	40	?$\nu_1+\nu_9$ (E')	4461
4479 4504 4528	b P s Q || b R	880	$\nu_9+\nu_{12}$ (A_2'') $\nu_2+\nu_8$ (E')	4512 4528
4572 4602 4625	h P v.s. Q || b R	360	$\nu_2+\nu_6$ (A_2'')	4607
4689	b	50	$\nu_6+\nu_{11}+\nu_{14}$ (E') $\nu_6+\nu_7+\nu_{11}$ (E')	4711 4743
4813	u	60		
4835	s	60		
4848	s	90		
4871		60		
4885	s	70		
4904	s	20		
4930	b	50		
4954		50		
5009	s	50		
5060 5072 5090	s P? s Q? ||? h R?	80		
5125 5134 5145	h P? Q? ||? h R?	50		
5167	v.s. Q||	70	$\nu_3+\nu_{10}+\nu_{12}$ (A_2'')	5297
5235	o.v.	60		
5457	s	19		
5547	s	8		
5633	s.h.	20		
5669	b.h. P?	22		
5696	s Q?	19		
5718	s.h. R?	18		
5767	b	9		
5793	b	8		
5891 5919 5947	b.h. P v.s. Q || h R	850	$2\nu_8$ (E') $\nu_1+\nu_8$ (E')	6049 6054
5964 5983 5997	b.h. P v.s. Q || h R	1000	$\nu_8+\nu_{12}$ (A_2'')	6104
6018	v.s.h. Q||?	890	$\nu_1+\nu_6$ (A_2'')	6132
6139	s.h. Q?	860	$2\nu_{12}$ (E')	6160
6159	s R?	770	$\nu_6+\nu_{12}$ (E')	6183
6313	v.b.	0.8		
6480	v.b.	0.2		
6649	b	8		
6719	v.s.	23		
6729	s.h.	23		
6838 6857	(h) b.h. $Q\perp$?	11 13		
6984	v s.h. Q	15		
7005	b R?	15		
7106	s.h.	22		
7119	s	20		
7169	s.h.	29		
7202	s	23		
7312	o.v.	20		
7398	v.s.h. Q?	28		
7436	v.s.h. Q?	30		

[a] Abbreviations: s = sharp, v.s. = very sharp, b = broad, v.b. = very broad, h = hump (i.e., no distinct minimum), p.h. = peak with side humps, s.h. = sharp peak with side humps, b.h. = broad peak with side humps, u = unsymmetrical, o.v. = overlapped by H_2O, P.I. = photographic infra-red.

[b] Only the active species are given.

[c] Based on the harmonic oscillator approximation.

TABLE III.—*Continued.*

νvac (obs.) cm^{-1}	Type[a]	Intensity	Assignment[b]	νvac (calc.)[c]
7479	s	12		
7544	s.h. Q?	18		
7738	b.h.	0.9		
8014	v.b.	3		
8147	v.b.	4		
8460	(P.I.) b	1.2		
8484	(P.I.) b	1.5		
8583	(P.I.) h	3		
8686	(P.I.) v.s.h. Q	28	$3\nu_8$ (E') $\nu_1+2\nu_8$ (E') $2\nu_1+\nu_8$ (E') $2\nu_8+\nu_{12}$ (A_2'')	9073 9078 9082 9128
8771[d] 8799[d] 8938 9006[e] 9054	(P.I.) s.h. Q (P.I.) h P.I. s P.I. p.h. P.I. s	100 90 19 22 (11)	$\nu_6+2\nu_8$ (A_2'') $2\nu_1+\nu_6$ (A_2'') $\nu_8+2\nu_{12}$ (E') $\nu_1+2\nu_{12}$ (E') $2\nu_6+\nu_8$ (E')	9152 9161 9184 9189 9230
9112	P.I. s PQR||	18	$3\nu_{12}$ (A_2'') $\nu_6+2\nu_{12}$ (A_2'') $3\nu_6$ (A_2'')	9240 9263 9309
9235	P.I.	0.3		
9409 9418	P.I. b P.I. b	0.4		
9494 9505	P.I. b P.I. b	2.4		
9535 9547	P.I. b P.I. b	1.5		
9630	P.I. v.b.	1.3		
9779 9797 9806	P.I. b P.I. b P.I. b	0.9		
9814 9828 9833 9844 9856 9872 9881 9889	P.I. b P.I. b P.I. b P.I. b P.I. b P.I. b P.I. b P.I. b	1.3		
9913 9922	P.I. b P.I. b	(0.5)		
9938 9951	P.I. b P.I. b	1.9		
9967	P.I. v.b.	(0.5)		
9985 9988	P.I. P.I.	(1.0)		
10033	P.I.	0.5		
10055 10059	P.I. P.I.	(1.0)		
10079	P.I. doublet	(0.1)		
10126	P.I. b	(0.1)		
10131	P.I. doublet	(0.1)		
10153	P.I. doublet	1.3		
10166	P.I.	(0.3)		
10192	P.I. b.u.	1.4		
10215	P.I. v.b.	(0.3)		
10238	P.I. b	(0.3)		
10254	P.I. b	(0.3)		
10279 10297 10316	P.I. b P.I. b P.I. b	0.9		
10499	P.I. b	0.3		
10813	P.I. v.b.	0.3		
11090	P.I. v.b.	0.1		
11220	P.I. (b)	(0.8)		
11309	P.I. (b)	(0.3)		
11318	P.I. (b)	(0.7)		
11330	P.I. b	(0.3)		
11333	P.I. b	(0.1)		
11350	P.I. b	(0.7)		

[d] At higher pressure complete absorption from 8720 to 8840 cm^{-1}.

[e] At higher pressure extending from 8960 to 9050 cm^{-1}.

TABLE III.—*Continued.*

νvac (obs.) cm^{-1}	Type[a]	Intensity	Assignment[b]	νvac (calc.)[c]
11355	P.I. b	(0.6)		
11370	P.I. u.b.	(0.7)		
11387	P.I. v.b.	(0.6)		
11403	P.I. b	(0.8)		
11408	P.I. (b)	(2)		
11424	P.I. u.b.	(2)		
11449	P.I. v.b.	(6)		
11462	P.I. b	(9)		
11477	P.I. b	18		
11494	P.I. v.b.	(5)		
11532	P.I. b	(1)		
11539	P.I. b	(0.7)	$4\nu_{C-H}$	
11548	P.I. b	(0.3)		
11559	P.I. b	(0.3)		
11574	P.I. b	(1)		
11594	P.I. v.b.	(0.3)		
11619	P.I. b	(0.2)		
11644	P.I. b	(0.2)		
11679	P.I. b	(0.1)		
11686	P.I. (b)	(0.3)		
11753	P.I. v.b.	(0.2)		
11774	P.I. (b)	(0.2)		
11795	P.I. v.b.	(0.3)		
11818	P.I. (b)	(0.2)		
11849	P.I. s	1.2		
11880	P.I. v.b.	(0.2)		
11913	P.I. (s) *Q?*	0.4		
11937	P.I. v.b. *R?*			
12184	P.I. v.b.	0.4		
12335	P.I. v.b.	(0.2)		
12575	P.I. v.b.	(0.1)		
12655	P.I. v.b.	(0.2)		
13205	P.I. (s)	(0.05)		
13982	P.I. b	(0.5)		
14002	P.I. b	(0.5)		
14033	P.I. v.b.	(1)	$5\nu_{C-H}$	
14055	P.I. v.b.	(1)		
14081	P.I. v.b.	(1)		
14104	P.I. v.b.	(0.2)		
14201	P.I. (b)	(0.05)		
14514	P.I. (b)	(0.05)		
14585	P.I. (b)	(0.03)		
16497	P.I. v.b.	(0.1)	$6\nu_{C-H}$	

wide, but calculations made with probable values of the molecular constants indicate that the width is not altogether beyond the range of what can be accounted for.

Table I gives the wave numbers of the band lines with the most probable numbering. Because of the diffuse nature of the lines, the scatter of the combination differences Δ_2F' and Δ_2F'' is appreciable. The rotational constants obtained from them are therefore not as accurate as one might wish. The following values were obtained:

$$B''=0.664_0 \text{ cm}^{-1}, \quad I_B''=42.1_5\times10^{-40} \text{ g cm}^2$$

and

$$B'=0.660_3 \text{ cm}^{-1}, \quad I_B''=42.3_8\times10^{-40} \text{ g cm}^2.$$

From a plot of $R(J-1)+P(J)$ against J^2 one obtains[3]

$$B'-B''=0.0026 \text{ cm}^{-1}, \quad \nu_0=9115.1_0 \text{ cm}^{-1}.$$

[3] See G. Herzberg, *Infrared and Raman Spectra of Polyatomic Molecules* (D. Van Nostrand Company, Inc., New York, 1945), in future referred to as I.R.S.

Smith[4] has made a high resolution study of the infra-red bands of cyclopropane and has analyzed the fine structure of the 3103 cm^{-1} band. The most recent value of B'' proposed by Smith is 0.6680 cm^{-1}.[5] The slight difference between this value and the one from the photographic infra-red band is probably within the uncertainty of the two determinations.

D. VIBRATIONAL ANALYSIS

The Raman spectrum of cyclopropane has been studied, among others, by Ananthakrishnan[6] and by Harris, Ashdown, and Armstrong.[7] The infra-red spectrum has been studied by Bonner,[8] Linnett,[9] and Smith[4]. The fourteen fundamental frequencies obtained in this way have been summarized by Herzberg.[10] They are given in Table II. Species designations are added assuming the molecule to belong to point group D_{3h}. Uncertain frequencies are in parentheses. Of the six species that occur only two, A_2'' and E', are infra-red active leading to six infra-red active fundamentals.

A few overtone and combination bands have been found by the above-mentioned investigators. In addition, Eyster[11] has obtained a few photographic infra-red bands with an absorbing path of 6 m. With the much longer path used in the present investigation a very large number of bands have been found both in the photographic infra-red and in the region beyond it. These bands are listed in Table III. Figure 1 shows parts of this spectrum as obtained with the prism spectrometer. The intensities given in Table III are based on the values $(I_0-I)/I_0$ for the peaks (where I_0 is the incident intensity and I the transmitted intensity) taking the intensity of the strongest band equal to 1000 and assuming that Beer's law holds. Since the latter assumption is certainly not accurately fulfilled and since, moreover, the bands have very different widths, the intensities given must be considered as quite rough. Particularly for weaker bands near stronger ones the height of the continuous background is uncertain and therefore for them the intensities are even more uncertain than for single bands. Some of the bands in the photographic region were obtained also on the prism spectrometer and their intensities were obtained from the recording in the way outlined above. The intensities of the other photographic bands were estimated. Such values are put in parentheses.

A satisfactory assignment of the observed bands presents considerable difficulties. As one would expect, the series of overtones of the C—H stretching vibration stands out in the infra-red spectrum. In the present

[4] L. G. Smith, Phys. Rev. **59**, 924 (1941).
[5] G. Herzberg, I.R.S., p. 437.
[6] R. Ananthakrishnan, Proc. Ind. Acad. Sci. **4A**, 82 (1936).
[7] Harris, Ashdown, and Armstrong, J. Am. Chem. Soc. **58**, 852 (1936).
[8] L. G. Bonner, J. Chem. Phys. **5**, 704 (1937).
[9] J. W. Linnett, J. Chem. Phys. **6**, 692 (1938).
[10] I. R. S., p. 352 ff.
[11] E. H. Eyster, J. Chem. Phys. **6**, 576 (1938).

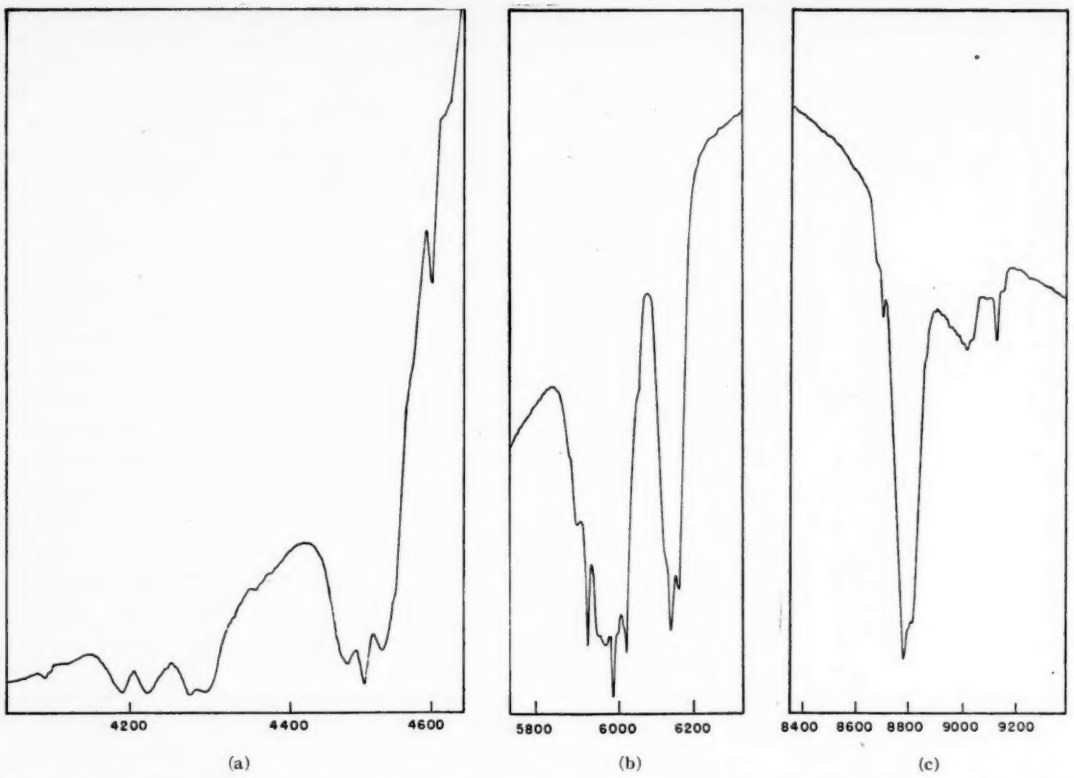

FIG. 1. Parts of the infra-red absorption spectrum of cyclopropane as recorded with Dr. Kuiper's infra-red spectrometer. The path length was 30 m for all three parts. The pressure was 3 mm in (a) and (b), and 27 mm in (c).

work they have been observed up to $6\nu_{CH}$. But in the region of each overtone there are a number of bands since there are four C—H stretching fundamentals. To be sure, only two of these, ν_6 and ν_8, are infra-red active; but, for the overtones, combinations with the inactive fundamentals may arise. Thus, in the case of $2\nu_{CH}$ (near 6000 cm^{-1}) the following bands may be expected:

$$\begin{array}{lll} \nu_1+\nu_6\,(A_2'') & \nu_1+\nu_8\,(E') & \nu_6+\nu_{12}\,(E') \\ 2\nu_8\,(E') & \nu_8+\nu_{12}\,(A_2'') & 2\nu_{12}\,(E'). \end{array}$$

Additional bands in the same region arise on account of the close resonance between $2\nu_2$ and ν_1. The number of expected bands increases rapidly for $3\nu_{CH}$ and higher overtones. Five of the above components of $2\nu_{CH}$ can be reasonably well assigned, as indicated in Table III, on the basis of the frequencies of the fundamentals and the assumption that the anharmonicities are not too large and too different for different vibrations.

Similarly, the binary combinations of a C—H stretching and a C—H bending vibration in the region 4000–4650 cm^{-1} can be fairly readily assigned. However, the bands observed between 4650 and 5800 cm^{-1}, which must be ternary combinations, cannot be uniquely assigned. About 120 ternary combinations may be expected in this region and, since neither the anharmonicity constants nor the relative intensities for these predicted bands are known, each observed band can be assigned within the accuracy of the harmonic oscillator approximation to several (sometimes up to 10) different combinations.

Unfortunately, in the case of cyclopropane the band envelopes are not of much help in assigning the bands to particular vibrational transitions. The moment of inertia about the axis of symmetry is only 1.63 times that about an axis perpendicular to it. Therefore, the separations of the Q branches of the sub-bands of a band are only 0.39 times those of the lines in the P and R branches if the Coriolis interaction constant ζ is zero. For negative values of ζ the separations of the Q branches are even smaller. In such cases the $\perp$ bands under low resolution look very much like $\parallel$ bands (compare the similar situation for CHF_3).[1] A number of bands with a strong and sharp central maximum and a broader maximum on each side of it have been found (for example, at 4504, 4602, 9112 cm^{-1} see Fig. 1). While it is likely that these are all $\parallel$ bands, only in the case of the band 9112 cm^{-1} whose fine structure has been resolved (see Section C) is this conclusion unambiguous. On the other hand, broad maxima are most likely $\perp$ bands.

A number of bands with two maxima have been found. It is likely that these are $\parallel$ bands in which because of a larger difference of B' and B'' the R and the Q branch coalesce.

With the exception of the band at 9112 cm^{-1}, even in

the photographic region a clear distinction between || and ⊥ bands is impossible. The reason for the diffuse nature of most of the || bands in this region is apparently the fact that the sub-bands no longer coincide even approximately. For this reason the assignments given in Table III for the bands in the region $3\nu_{CH}$ must be considered as decidedly tentative. No specific assignments are given for the bands in the regions $4\nu_{CH}$, $5\nu_{CH}$, and $6\nu_{CH}$.

The author is deeply indebted to Dr. G. Herzberg for his kind help and valuable suggestions and to Dr. G. P. Kuiper for the use of his infra-red spectrometer. He is also thankful to Patna University, India, for the award of a Birla Scholarship.

THE JOURNAL OF CHEMICAL PHYSICS VOLUME 18, NUMBER 2 FEBRUARY, 1950

Quantitative Determination of Extinction Coefficients in the Vacuum Ultraviolet: Divinyl Ether*

ANNA J. HARRISON, CHARLOTTE L. GADDIS,** AND ESTHER M. COFFIN**
Department of Chemistry, Mount Holyoke College, South Hadley, Massachusetts

(Received August 15, 1949)

A method of determining the molar extinction coefficients of organic compounds in the vapor phase in the vacuum ultraviolet has been developed. Measurements made with a fluorite spectrograph on flowing vapor samples of divinyl ether show a precision of 3 to 8 percent and satisfactory agreement with measurements made from 2360 to 2100A with a Beckman DU spectrophotometer. The absorption spectrum of divinyl ether is completely free from fine structure. The extinction coefficient increases rapidly from a value of 10 at 42,400 cm^{-1} to a maximum of 15,900 at 49,200 cm^{-1} and decreases to a minimum value of 4000 before beginning to rise again at 56,700 cm^{-1}. The oscillator strength of the band is 0.45.

THE vacuum ultraviolet absorption studies in this laboratory have been extended to include measurements of molar extinction coefficients of organic compounds in the vapor phase. Such quantitative data are particularly useful for comparison with theoretical predictions concerning electronic transitions of organic molecules. The method of measurement which has been developed is somewhat similar but different in essential details from that used by Platt[1] and co-workers.

Standard spectrographic practices have been used. The reciprocity law behavior of the spectrographic plates has been studied and the results have justified the use of a simple empirical time calibration of the plates. The long-wave region of the vacuum spectrograph corresponds to the short-wave region of the Beckman DU spectrophotometer. Measurements of several compounds have been made with both instruments and the results in all cases have shown satisfactory agreement. The final measurements of divinyl ether, the compound used during the development of the method, are reported here. The measurements of other compounds will be reported in papers dealing with series of related compounds.

EXPERIMENTAL

Spectrographic measurements.—The equipment consists of three separate systems: the spectrograph, the vapor handling system and the light source. Fluorite windows are used throughout and the narrow spaces between the windows of the separate systems are filled with flowing nitrogen. The spectrograph and the light source have been described.[2] The spectrograph is a fluorite prism instrument which has a dispersion that varies from about 10A per millimeter at 2000A to about 2.5A per millimeter at 1400A. Ilford QI plates are used. The light source is a water cooled hydrogen lamp which is operated with flowing hydrogen. Even though this lamp is only operated during the time of the plate exposures, its reproducibility has been repeatedly demonstrated.

A flowing vapor system in a separate absorption tube is used in preference to the introduction of vapor into the spectrograph. This reduces the probability of measuring the absorption of photochemical products and protects the spectrograph from the deposition of products which might reduce the transmission of the instrument. The system for handling the vapor, Fig. 1, is of all Pyrex glass construction with the exception of the windows which are cemented to the absorption tube, *B*. The method depends upon establishing a steady rate of flow which is determined by the vapor pressure of the compound, the dimensions of two constrictions and the capacity of the pumps. The pressure in the absorption tube *B* is controlled by controlling the vapor pressure of the compound with a temperature bath around the sample tube, *A*.

* This work was supported in part by the ONR under Contract NR-055-160.

** Abstracted from theses presented as partial fulfillment of the requirements for the degree of Master of Arts.

[1] L. E. Jacobs and J. R. Platt, J. Chem. Phys. **16**, 1137 (1948).

[2] E. P. Carr and H. Stücklen, Zeits. f. physik. Chemie **B25**, 57 (1934); J. Chem. Phys. **4**, 760 (1936).

After the system is flushed with nitrogen and evacuated with stopcocks 1, 2, and 3 closed, two calibration exposures of t_1 and t_2 minutes are made. The nitrogen is flushed from the sample tube by alternately opening stopcocks 1 and 2 for a few seconds at a time. Stopcock 1 is then left open and an exposure of t_c minutes is made of the compound after the pressure becomes constant. The system is again flushed with nitrogen and evacuated and two more calibration exposures of t_3 and t_4 minutes are taken. The particular times used depend upon the part of the spectrum being studied and the width of the slit in the spectrograph. For this work calibration exposures of 0.50, 1.00, 1.50, and 2.00 minutes and a compound exposure of 3.00 minutes have been used.

The condensation of vapors in the McLeod gauge has been avoided by constructing a gauge with a series of gradated bulbs and nine calibration marks. With this, readings are made over a wide range of pressures without using large differences in mercury levels. A study has been made of the validity of using the pressure just beyond the absorption tube as the pressure in the absorption tube. To do this the gauge was connected through a three-way stopcock to both the entrance and exit tubes of the absorption tube and the pressure of a flowing vapor was read alternately on the two sides of the absorption tube. The variations in the readings were random and of the usual order found in setting and reading the gauge.

The study of a compound can usually be made with six to eight plates. No real difficulties have been encountered with leaks and the spectra have been free from evidences of contamination by either stopcock grease or sealing compound. Since the transmission of the absorption tube gradually decreases with use the windows are occasionally removed and cleaned.

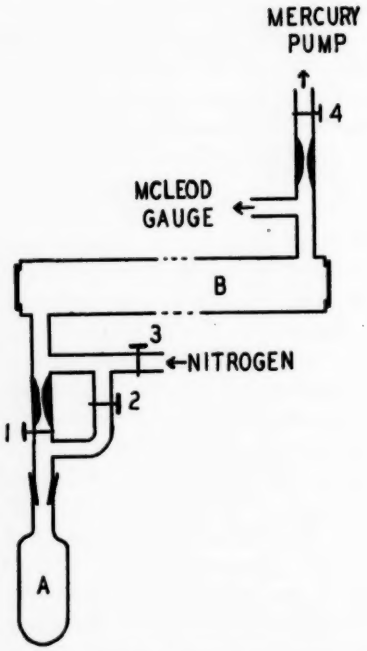

FIG. 1. Vapor system used with the vacuum spectrograph. *A* is a 10 ml sample tube. *B* is a 32.5 cm absorption tube with fluorite windows. A steady state of flow is established which depends upon the vapor pressure of the sample, the dimensions of the constrictions and the capacity of the pumps. The vapor pressure is controlled by controlling the temperature of the sample tube *A*.

Microphotometer measurements.—A microphotometer record is made with a recording instrument. Each recording has six curves: the base line (zero response of the galvanometer); traces of the time exposures t_1, t_2, t_3 and t_4; and a trace of the t_c exposure of the compound. At a particular wave-length, the distance from the base line to each of the traces is measured and the logarithm of the distance to the calibration trace is plotted against the logarithm of t_c/t where t is t_1, t_2, etc. These points give a smooth curve which approaches a straight line. From this and the logarithm of the distance to the compound trace is read a value of $\log t_c/t$ for the compound. Within the limits of the reciprocity law, this value is the optical density, and assuming that the vapor is an ideal gas at the pressures used the molar extinction coefficient is easily calculated.

The reciprocity law for the Ilford QI plates has been checked by using vibrating copper screens. The percent transmission of these screens was determined with the Beckman DU spectrophotometer and checked with a photometer which had been calibrated by a step tablet. This step tablet had been calibrated by the Research Laboratories of the Eastman Kodak Company. Measurements with the spectrophotometer showed the percent transmission of the screen to be independent of the wave-length over the region 8000 to 2100A and it has been assumed that this percent transmission could be used for the shorter wave-lengths. Some of the screens gave a much more severe test than demanded by the actual spectrographic measurements: for example a 25-second exposure of the full light source as compared to a 305-second exposure of the light source through a screen having a 8.18 percent transmission. Comparisons which were made with the microphotometer showed the same darkening of the photographic plate. A difference of less than one percent in the photometer response would have been detectable. Jacobs and Platt[1] have reported the Schwarzschild factor of Ilford Q plates to be 0.95.

Beckman measurements.—The vapor handling system used with the Beckman DU spectrophotometer consists of a small sample tube, a one centimeter fused quartz absorption cell, a vapor chamber, an inclined mercury manometer, a McLeod gauge and a mercury vapor pump. The cell is connected to the Pyrex system through a graded seal and is carried by a wooden holder in the regular cell carriage of the spectrophotometer. A glass coil in the connecting tube allows for the movement of the absorption cell in and out of the light path.

Divinyl ether.—The divinyl ether was obtained as Vinethene from Merck and Company. It was placed over flake potassium hydroxide for several days and

distilled through a modified Fenske column. Measurements were made on fractions having not more than 0.02°C variation in boiling point.

RESULTS

Typical values of the logarithm of the extinction coefficient, logϵ, obtained with the vacuum spectrograph are given in Table I. In general the mean deviation in this function is of the order of 0.01 to 0.03. This corresponds to a mean deviation of three to eight per-

TABLE I. Logϵ, vacuum spectrograph measurements.

Wave number	Plate 73 (0.089 mm)	Plate 74 (0.047 mm)	Plate 75[a] (0.043 mm)	Plate 77 (0.025 mm)	Plate 78[b] (0.029 mm)	Plate 79 (0.032 mm)
46,260	3.68	3.71	3.74	3.71	—	3.64
49,180	—	—	—	4.22	4.19	4.18
52,360	—	—	—	4.02	3.98	3.96
55,300	3.70	3.70	3.71	3.70	—	3.63
58,440	3.71	3.70	3.69	3.73	—	3.62

[a] Pressure too high for measurement at the top of the band.
[b] Two-minute calibration curve was not reliable and values were not calculated in the regions that depended upon this calibration.

cent in the value of the extinction coefficient. The average values of logϵ obtained by the spectrographic measurements and the average value of logϵ obtained by the Beckman measurements are plotted in Fig. 2 as a function of wave number. The agreement over the region covered by the two instruments is well within the mean deviations of the separate methods and it is tentatively concluded that the accuracy of the spectrographic measurements is of the same order as their precision. No attempt has been made to carry the measurements of this compound into the discontinuous region of the hydrogen spectrum.

During the development of this method measurements were made with a 60 cm absorption tube and with longer time exposures but with fewer calibration exposures. The average values of the extinction coefficient obtained were essentially the same as those reported here but the precision of the measurements was decreased by the greater uncertainty in the calibration curves. Another series of measurements was made with nonflowing vapor. The presence of bands which increased with continued radiation gave evidence of photo-chemical reaction.

The absorption spectrum of divinyl ether is completely free of fine structure. The extinction coefficient increases from a value of 10 at 42,400 cm^{-1} to a maxi-

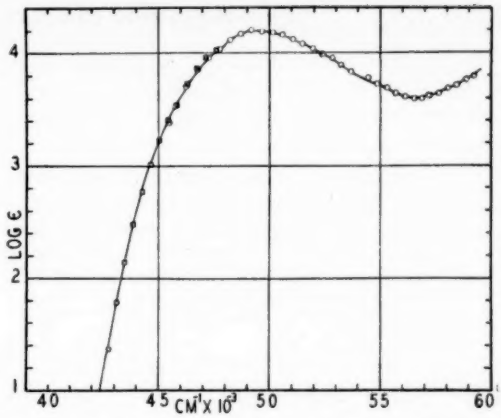

FIG. 2. Logarithm of the molar extinction coefficient *vs.* wave number for divinyl ether in the vapor phase. Average vacuum spectrograph measurements are shown as circles; average Beckman spectrophotometer measurements as squares.

mum of 15,900 at 49,200[3] cm^{-1} and decreases to a minimum value of 4000 at 56,700 cm^{-1} before beginning to increase again. There is a very slight step-out at 48,000 cm^{-1} which seems to be real although hardly detectable. The oscillator strength[1] of the band is 0.45.

Divinyl ether is, of course, both an oxygen containing compound and an unsaturated compound and at this time not enough compounds have been studied to permit a detailed analysis of the spectrum. A few comparisons can, however, be made. Fine structure, which is so characteristic of related compounds such as diethyl ether,[4] furan,[5] and low molecular weight unsaturated hydrocarbons,[2] does not appear. The position of the band of divinyl ether is at smaller wave numbers than the first band of either diethyl ether or non-conjugated hydrocarbons and is at larger wave numbers than the position of the first broad band of the conjugated hydrocarbons. These positions indicate some conjugation in divinyl ether. Limited conjugation has also been proposed to explain heats of hydrogenation.[6] The position of the broad band underlying the fine structure of furan is similar to that of divinyl ether but the intensity of absorption of the furan as shown by both the extinction coefficients and the oscillator strength is much less than that of the divinyl ether.

[3] The maximum in the microphotometer tracing is at 50,600 cm^{-1}. The difference between this apparent maximum and the true maximum arises from the continually decreasing intensity of the hydrogen continuum at shorter wave-lengths.
[4] G. Scheibe and Grieneisen, Zeits. f. physik. Chemie **B25**, 52 (1934).
[5] L. W. Pickett, J. Chem. Phys. **8**, 293 (1940).
[6] G. B. Kistiakowsky and co-workers, J. Am. Chem. Soc. **60**, 440 (1938).

The Behavior of Glass Electrodes in Acid Solutions*

EDWARD E. SINCLAIR† AND ARTHUR E. MARTELL
Department of Chemistry, Clark University, Worcester, Massachusetts
(Received August 15, 1949)

Negative glass electrode errors were measured for solutions of hydrochloric acid and sulfuric acid with soft, intermediate, and hard glasses. While all the glasses measured showed negative errors, in general, the greatest deviations occurred with the soft glasses and intermediate glasses. The errors were very much greater in hydrochloric acid than in sulfuric acid solutions. The deviations observed were too great to be accounted for by the reduced activity of water alone, and were probably due in part to participation of the anion in the electrode process.

INTRODUCTION

THE negative errors of the glass electrode were discovered by MacInnes and Belcher[1] in 1931 and were considered by them to be due to the participation of anions in the glass electrode reaction. On the other hand, Dole later investigated the negative errors of Corning 015 glass electrodes[2] and found that they are apparently independent of the nature and amount of both cations and anions present in the test solution, including the hydrogen ion. In order, therefore, to account for the negative errors, he postulated that the proton migrates through the glass membrane carrying a molecule of water with it. In dilute solutions of both the test solution and the electrolyte within the glass electrode, the water so carried is transferred between two solutions in which the water activity differs but slightly. Under such circumstances, the net transfer taking place during the reversible operation of a cell such as:

calomel, saturated KCl, 0.1N HCl, glass,
xN HCl, saturated KCl, calomel (I)

is presumably not measurably different from the net reaction occurring under identical conditions in the equivalent hydrogen gas electrode cell:

calomel, saturated KCl, 0.1N HCl, $H_{2(g)}$, Pt, $H_{2(g)}$,
xN HCl, saturated KCl, calomel. (II)

When, however, the test solution is concentrated, the activity of the water in the test solution is low, with the result that the net transfer occurring in Cell (I) is then measurably different from that occurring in Cell (II), since there is no water transferred during the reversible operation of Cell (II).

On the basis of this hypothesis, Dole derived the following (approximate) equation for the negative errors of the glass electrode:

$$\Delta E = (RT/F) \ln a_{H_2O}, \quad \text{(a)}$$

where R, T, and F have their usual significance, ΔE refers to the glass electrode error, and a_{H_2O} refers to the activity of the water in the test solution.

Although the errors found by Dole for the Corning 015 glass electrode in both HCl and H_2SO_4 solutions were in fair agreement with the errors predicted by Eq. (a),[2] it cannot be rightfully said that the hypothesis of Dole has been adequately confirmed experimentally in view of contradictory measurements reported by Hubbard and co-workers in 1939.[6] Hubbard reported that Corning 015 glass electrodes had been repeatedly prepared which showed no definite voltage departures in strong H_2SO_4 solutions while doing so in strong HCl solutions.

In view of the contradictory data thus far presented in the literature, it was decided to re-examine the behavior of soft glass electrodes in strongly acid solutions. In addition, it was felt that the behavior of intermediate and hard glasses of the type studied by Lengyel and Blum[4] should be examined in the strongly acid region, since no information of this type is as yet available for comparison.

Accordingly, glasses of the composition employed by Lengyel and Blum were purchased from the Corning Glass Works. These glasses were prepared in the research laboratories of the latter company from pure components and with a stated accuracy of composition of about one-tenth of one percent. The following sections of this paper describe the experimental technique employed and the results obtained in the examination of the behavior of electrodes prepared from these glasses in strongly acid solutions.

EXPERIMENTAL

Cell Assembly

Cells (III) and (IV), which are the same as those employed by MacInnes and Belcher[1] and by Dole and

* Abstracted from a dissertation presented by Edward E. Sinclair to the faculty of Clark University in partial fulfillment of the requirements for the degree of Doctor of Philosophy.

† Present address: Department of Chemistry, Amherst College, Amherst, Massachusetts.

[1] D. A. MacInnes and D. Belcher, J. Am. Chem. Soc. **53**, 3315 (1931).

[2] M. Dole, J. Am. Chem. Soc. **54**, 3095 (1932).

[3] Hubbard, Hamilton, and Finn, J. Research Nat. Bur. Stand. **22**, 339 (1939).

[4] B. Lengyel and E. Blum, Trans. Faraday Soc. **30**, 461 (1934).

co-workers,[2,5] were used in this research.

Ag, AgCl, 0.1N HCl, glass, test solution, saturated KCl, calomel, (III)

Pt, $H_{2(g)}$, test solution, saturated KCl, calomel. (IV)

Use of these cells permits both the calculation and direct measurement of Cell (V) in which the glass and hydrogen gas electrodes are compared directly:

Ag, AgCl, 0.1N HCl, glass, test solution, $H_{2(g)}$, Pt. (V)

The advantage of using Cells (III) and (IV) instead of Cell (V) alone lies chiefly in the ability to follow trends in the potentials of the glass and hydrogen gas electrodes independently.

Figure 1 shows the general cell assembly. The experimental cell (about 200 ml in volume) was equipped with ten mercury seal cups to accommodate six glass electrodes, two hydrogen gas electrodes, and a hydrogen gas inlet and outlet. Equipment inserted in the cell was provided with a glass sleeve which fitted into the mercury cups. This effectively sealed the cell from the atmosphere and yet permitted rapid interchange of electrodes.

The liquid junction stopcock was constructed according to the recommendations of Ferguson, Hitchens, and Van Lente.[6] The junction was established with the aid of a partially evacuated pipette by drawing first saturated KCl, then the test solution, into the bore of the stopcock through the drainage tube.

The calomel cell was filled with triple-distilled mercury and calomel prepared electrolytically from pure mercury and HCl by the method of Ellis.[7] The electrolyte was saturated KCl solution prepared from KCl which had been twice recrystallized from water.

All glass electrodes used in this investigation were made by the method of MacInnes and Dole[8] on mounting tubes of about 5-mm o.d. and 3.5-mm i.d. Freshly prepared electrodes were leached overnight in 0.1N HCl before use, and were prepared for service by partially filling with 0.102N HCl and inserting a silver-silver chloride electrode. The latter was then sealed to the supporting tube with paraffin wax.

The hydrogen gas electrodes were prepared by the conventional method described by Weissberger.[9] The hydrogen gas used was commercial electrolytic hydrogen, which was purified by passing through copper turnings at 500°C and then run through a presaturating vessel in accordance with standard practice.

No attempt was made to ascertain the precise concentration of the test solutions used in view of the fact that the glass electrode potentials were being compared with the hydrogen electrode potentials in the same solution. The 0.102N HCl used as a reference electrolyte within the glass electrodes, however, was prepared from the maximum boiling azeotrope in accordance with the method of Foulk and Hollingsworth.[10]

Temperature control was effected by means of a constant temperature oil bath maintained at 25.00 ±0.01°C.

Measurement of Potentials

In view of the extremely high resistance of glass, special apparatus is needed for precise determination of the glass electrode potentials. In this investigation, a Leeds & Northrup thermionic amplifier designed by R. H. Cherry[11] was employed in connection with a Leeds & Northrup 2420-C galvanometer and a Type K potentiometer. The amplifier tube was operated at the maximum plate voltage of nine volts, so that the galvanometer easily showed an unbalance of 0.0001 volt on the experimental cell.

A special check resistor of 1.2×10^{11} ohms was used to "zero in" the amplifier. The check resistor was provided with a metal shield by the manufacturer, but no provision was made for keeping it or the grid input sleeve dry during use. Accordingly, special drying chambers which fitted snugly over the grid input stud were made to accommodate the check resistor and grid input lead. The drying chambers were made with

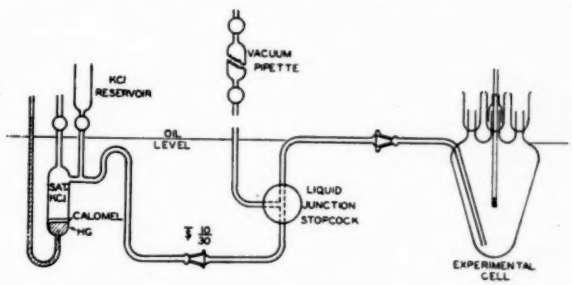

FIG. 1. General cell assembly.

Pyrex 774 tubing and steel tubing of the proper diameter, the latter being sealed into the Pyrex tube with low melting DeKothinsky cement. The shielded cable leads were sealed into the drying chambers through amphenol plastic and the latter was bonded to both the glass and cable by means of a cement made by dissolving the plastic in chloroform. Anhydrone was used as the drying agent in both the drying chambers and in the amplifier tube compartment.

RESULTS

The compositions of the glasses used in this investigation are indicated in Table I. Inasmuch as all of the

[5] M. Dole and B. Z. Wiener, Trans. Am. Electrochem. Soc. **72**, 107 (1937).
[6] Ferguson, Hitchens, and Van Lente, J. Am. Chem. Soc. **54**, 1285 (1932).
[7] J. H. Ellis, J. Am. Chem. Soc. **38**, 740 (1916).
[8] D. A. MacInnes and M. Dole, Ind. Eng. Chem. Anal. Ed. **1**, 57 (1929).
[9] A. Weissberger, *Physical Methods of Organic Chemistry* (Interscience Publishers, Inc., New York, 1946), Vol. II, p. 1056.
[10] C. W. Foulk and M. Hollingsworth, J. Am. Chem. Soc. **45**, 1220 (1923).
[11] R. H. Cherry, Trans. Am. Electrochem. Soc. **72**, 33 (1937).

glasses employed, with the exception of Corning 015, were specifically made to duplicate the composition of the glasses used by Lengyel and Blum,[4] the Lengyel and Blum designations for these glasses are retained. Glass D_1 and Corning 015 are samples of the so-called soft type of glass. Glasses D_p and D_s are the Lengyel and Blum intermediate glasses, while D_u and D_a are samples of hard, Pyrex-like glasses. Thus, it will be seen that the range of composition of glasses covered in the work of Lengyel and Blum has been reasonably well covered in this investigation.

Table II is presented to indicate the type of results obtained in the calculation of Cell (V) from measurements with Cells (III) and (IV). Direct measurements of Cell (V) have invariably agreed with the calculated potentials to within 0.1 mv. Hydrogen gas electrode potentials were corrected to a partial pressure of hydrogen gas of 760 mm Hg at 25°C in accordance with standard practice. Attention is directed to the fact that in the preparation of the data of Table II, a correction was made for the asymmetry potential of each glass electrode in the purely arbitrary manner described herewith, but that this expedient was merely for convenience in the presentation of the data.

On the basis of measurements involving several samples of Glass D_s and Corning 015, to which correction had been made for the experimentally determined asymmetry potential, it was determined that the correct value for Cell (V) with the particular reference electrolyte employed was 0.3518 ± 0.0002 volt. It was decided that for the purposes of this investigation, no particular advantage would be gained by measuring the asymmetry potential of each subsequent glass electrode employed. Accordingly, the arbitrary assumption was made that in any given series of measurements, the difference between the observed e.m.f. of Cell (V) in $0.01N$ test solution and the value of 0.3518 volt was due to the asymmetry potential of the particular glass electrode concerned. This difference was then applied as a constant correction to the e.m.f. values of Cell (V) for that particular glass electrode.

The negative errors calculated from the e.m.f. values of Cell (V) for the various glasses measured are summarized in Table III for concentrations ranging from $0.001N$ to $10N$ of sulfuric and hydrochloric acid solutions. As explained above, these errors are relative to the e.m.f. value of Cell (V) in $0.01N$ test solution. It should be stressed at this point that the values given for solutions more concentrated than $1N$ are not necessarily constant values, but are the values recorded after about three hours of observation in each case. This will be discussed in greater detail in the following paragraphs.

TABLE I. Composition of glasses.

Glass	SiO_2	% CaO	% Na_2O	% B_2O_3	% Al_2O_3
015	72.0	6.0	22.0	—	—
D_1	71.4	7.5	21.1	—	—
D_s	69.5	—	23.5	7.0	—
D_p	67.0	7.0	22.0	4.0	—
D_u	56.8	2.6	23.4	—	17.2
D_a	72.0	—	11.0	12.1	4.9

Discussion of Results

Several generalizations can be drawn on the basis of the measurements on the whole.

1. It has been confirmed that all of the glasses examined behave as virtually perfect hydrogen gas electrodes in pure HCl and H_2SO_4 solutions of concentration less than about $1N$. In most cases, the change in e.m.f. shown by the glass electrodes under any given set of circumstances agreed with the change in e.m.f. shown by the hydrogen gas electrode under the same circumstances to within 0.2 mv, or well within experimental uncertainties. Glass D_a, however, had such a large electrical resistance that the potentials of electrodes prepared from it could only be determined to within 2 mv.

2. All the glasses examined show deviations from hydrogen electrode behavior in HCl solutions of concentrations of $1N$ and/or greater, and to a lesser extent in H_2SO_4 solutions of the same concentrations. These deviations are such that the e.m.f. of Cell (V) becomes less than the constant value observed in dilute acid solutions, and they may, therefore, be identified with the negative errors of the glass electrode.

3. The e.m.f. behavior of all the glasses examined is distinctly different in strongly acid solutions than the e.m.f. behavior in dilute acid solutions. This difference in behavior has apparently not been previously reported. Thus, it has been observed that the e.m.f. of Cell (V) rapidly attains a steady and reproducible value in both HCl and H_2SO_4 solutions of concentrations of about $1N$ and less, but that the attainment of a steady e.m.f. value in solutions more concentrated than $1N$ is a much slower process by comparison. This is particularly true in the case of the soft glasses in strong HCl solutions, but it is also true of all the other glasses examined.

TABLE II. Glass D_s in sulfuric and hydrochloric acid solutions. Cell (V) at 25°C.

Electrode	$0.001N$ (volt)	$0.01N$* (volt)	$0.1N$ (volt)	$1N$ (volt)	$5N$ (volt)
A. Sulfuric acid solutions. *Versus* hydrogen electrode					
D_s-1	0.3523	0.3518	0.3517	0.3514	0.3477
D_s-2	0.3522	0.3518	0.3515	0.3514	0.3506
D_s-3	0.3519	0.3518	0.3518	0.3516	0.3482
D_s-4	—	0.3518	0.3519	0.3517	—
D_s-5	—	0.3518	0.3525	0.3524	—
Average value	0.3521	0.3518	0.3519	0.3517	0.3488
Average error	0.0003	0.0000	0.0001	−0.0001	−0.0030
B. Hydrochloric acid solutions. *Versus* hydrogen electrode					
D_s-1	0.3519	0.3518	0.3505	0.3494	0.3406
D_s-2	0.3518	0.3518	0.3523	0.3521	0.3464
D_s-3	0.3519	0.3518	0.3521	0.3513	0.3419
D_s-6	0.3519	0.3518	0.3512	0.3505	0.3453
Average value	0.3519	0.3518	0.3515	0.3508	0.3436
Average error	0.0001	0.0000	−0.0003	−0.0010	−0.0082

* Reference values.

TABLE III.

Glass	No. of electrodes	Average errors, volt 0.001N	0.01N	0.1N	1N	5N	10N
				Sulfuric acid solutions			
015	6	−0.0004	0.0000	0.0000	−0.0005	−0.0014	−0.0076
D_1	1	—	0.0000	−0.0003	−0.0011	—	−0.0075
D_4	5	0.0003	−0.0000	0.0001	−0.0001	−0.0030	—
D_p	4	−0.0009	−0.0000	0.0002	−0.0005	−0.0001	—
D_u	3	0.001	−0.000	0.001	−0.001	−0.009	—
D_a	1	0.002	0.000	0.002	0.000	0.000	—
				Hydrochloric acid solutions			
015	10	0.0000	−0.0000	−0.0001	−0.0022	−0.0600	—
D_4	4	0.0001	0.0000	−0.0003	−0.0010	−0.0082	—
D_p	3	0.0001	0.0000	—	−0.0009	−0.0051	—
D_u	2	0.000	0.000	0.000	−0.002	−0.012	—
D_a	1	0.001	0.000	−0.001	−0.001	−0.008	—

Table IV shows this sort of behavior with a Corning 015 electrode and an electrode prepared from Glass D_u in a typical series of measurements in HCl solutions. The constancy of the e.m.f. values in all but 5N solution is striking. In 5N acid solution, however, the e.m.f. is not constant and is still decreasing somewhat after 16 hr. The error observed after 16 hr. is, in both cases, greater than the error predicted by Eq. (a) of Dole.[2] As shown in Table IV, the 015 electrode was later immersed in a buffer solution of pH 4 but had not completely regained its original (dilute solution) potential 4 hr. after its long immersion in 5N HCl.

Data given in Tables I–IV for solutions stronger than 1N are, therefore, not to be taken as constant e.m.f. values. They are merely the values observed usually about three hours after immersion of the electrodes in the strong acid solution.

Observations of the e.m.f. values in strongly acid solutions were, in most cases, not carried out over sufficiently long periods of time to ascertain what the final stable e.m.f. values might have been. In spite of this, it is clear that the final stable values in HCl solutions would not agree with the values predicted by Eq. (a) of Dole.[2] In all cases, the errors demonstrated by the various 015 electrodes used in this investigation were greater after about 3 hr. immersion in 5N HCl than the errors predicted by Eq. (a).

TABLE IV. Showing the slow attainment of steady e.m.f. values of Cell (V) in strongly acid solutions.

Time	015-14 (volt)	D_u-2 (volt)	Time	015-14 (volt)	D_u-2 (volt)
	0.01N HCl			5N HCl	
12:00 M	0.3517	0.352 ±0.001	7:55 P.M.	0.3187	0.343 ±0.001
1:15 P.M.	0.3517	0.352 ±0.001	8:45 P.M.	0.3014	0.340 ±0.001
2:00 P.M.	0.3518	0.352 ±0.001	9:30 P.M.	0.2933	0.338 ±0.001
			10:15 P.M.	0.2880	0.337 ±0.001
	0.1N HCl		10:05 A.M.	0.2512	0.334 ±0.001
3:15 P.M.	0.3516	0.352 ±0.001	10:30 A.M.	0.2506	0.335 ±0.001
3:50 P.M.	0.3515	0.352 ±0.001	11:00 A.M.	0.2500	0.335 ±0.001
			———	Buffer solution pH 4	
	1N HCl		1:25 P.M.	0.3494	———
			2:25 P.M.	0.3501	———
5:45 P.M.	0.3498	0.350 +0.001	3:00 P.M.	0.3504	———
6:25 P.M.	0.3497	0.349 ±0.001	3:30 P.M.	0.3505	———
6:55 P.M.	0.3497	0.349 ±0.001			
7:25 P.M.	0.3497	0.349 ±0.001			

	1N HCl		5N HCl	
	015-14	D_u-2	015-14	D_u-2
Error observed	−2.1 mv	−3 mv	−118 mv	−17 mv
$(RT/F)\ln a_{H_2O}$	−1.5 mv		−10.4 mv	

In strong H_2SO_4 solutions, the negative errors were not observed to exceed the values predicted by Eq. (a), at least not within 20 hr. immersion in the concentrated acid solution, but in some cases, virtually no errors were observed in the strong H_2SO_4 solutions.

CONCLUSIONS

In view of the experimental results presented in this paper in comparison with the results predicted by Dole's theory of the negative errors, it is to be concluded that the assumption of water transport through the glass membrane does not satisfactorily account for the negative errors of the glass electrode. It would seem, therefore, that the only remaining possibility of accounting for these deviations would be to attribute them to the anions. This was the original suggestion of MacInnes and Belcher[1] concerning the negative deviations. Thus, the results of this research favor the concept of MacInnes and Belcher over that of Dole[2] concerning the behavior of glass electrodes in acid solutions.

Letters to the Editor

THIS section will accept reports of new work, provided these are terse and contain few figures, and especially few half-tone cuts. The Editorial Board will not hold itself responsible for opinions expressed by the correspondents. Contributions to this section should not exceed 600 words in length and must reach the office of the Managing Editor not later than the first of the month preceding that of the issue in which the letter is to appear. No proof will be sent to the authors. The usual publication charge ($8.00 per page) will not be made and no reprints will be furnished free.

Some Calculated Properties of Tritium*

E. F. HAMMEL
Los Alamos Scientific Laboratory, University of California, Los Alamos, New Mexico
December 16, 1949

APPLICATION of quantum theory to the condensed permanent gases by J. De Boer[1] resulted in a modified law of corresponding states in terms of reduced P, V, and T variables, plus a parameter Λ^*. On the basis of this theory, De Boer and Lunbeck[2] predicted a number of properties of the helium isotope of mass three. Several of these properties, including the vapor pressure, were subsequently determined,[3] and the experimental results agree quite closely with those predicted by De Boer and Lunbeck.[2] In the present paper, De Boer's theory is applied to tritium. Since the prediction of the He^3 properties involved a graphical extrapolation, whereas the prediction of the tritium properties involves an interpolation, it is hoped that an even closer agreement between theoretical and experimental results will be observed when data on tritium become available.

In Table I, the constants pertinent to the calculation are collected. Corresponding values for H_2 and D_2 are included for comparison where $\Lambda^*=h/\sigma(m\epsilon)^{\frac{1}{2}}$, k is Boltzmann's constant, N is Avogadro's number, and σ and ϵ are characteristic quantities of the intermolecular field defined by the potential function representing the interaction between two molecules of the gas, *viz:*

$$\varphi(r)=\epsilon\left(\frac{4}{(r/\sigma)^{12}}-\frac{4}{(r/\sigma)^{6}}\right).$$

TABLE I.

	Λ^*	ϵ/k (°K)	N/σ^3 (cm³/mol)	ϵ/σ^3 (atmos.)	ϵ (10^{-16} ergs)	σ (AU)
H_2	1.73	37.0	15.12	203	50.75	2.92
D_2	1.22	37.0	15.12	203	50.75	2.92
T_2	1.00	37.0	15.12	203	50.75	2.92

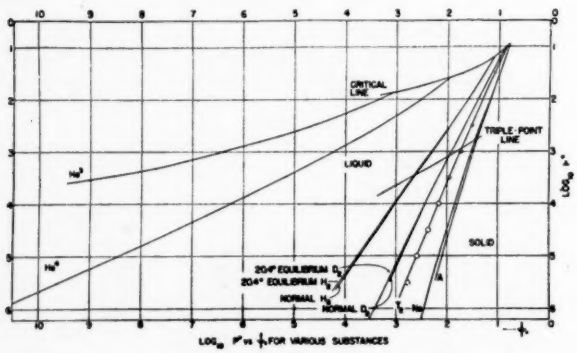

FIG. 1. $\text{Log}_{10}P^*$ *vs.* I/T^* for various substances.

Thus for $r=\sigma$, $\varphi(r)=0$; and $\epsilon=\varphi(r)$
for the value of r satisfying the equation $\partial\varphi/\partial r=0$.

The variables of the reduced equation of state are defined in terms of "molecular" units as follows:

$$P^*=P\sigma^3/\epsilon,$$
$$V^*=V/N\sigma^3,$$
$$T^*=kT/\epsilon.$$

The vapor pressures of tritium may be obtained from the theory by plotting experimental $\log P^*$ *vs.* $1/T^*$ curves for the light elements as in Fig. 1; from this, a series of reduced isobars is constructed, *viz.*, Fig. 2. From the latter graph, the vapor pressure *vs.* temperature curve (Fig. 1 or Fig. 3) for tritium is immediately

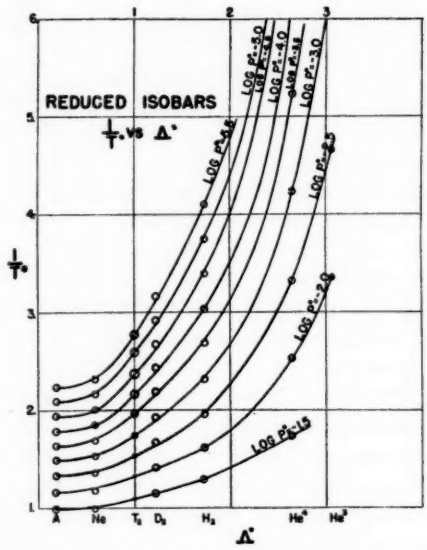

FIG. 2. Reduced isobars I/T^* *vs.* Λ^*.

obtainable. The results are tabulated in Table II, which also includes calculated data for deuterium above the boiling point.

Using the modified law of corresponding states, a plot of a given reduced property *vs.* Λ^* permits a prediction of that property for other substances with different Λ^*'s. In Table III, the critical

TABLE II.*

Tritium	
T (°K)	P (mm Hg)
12.2	0.154
13.3	0.488
14.3	1.54
15.6	4.88
17.1	15.4
18.9	48.8
20.2	95.1
21.3	154.4
21.58	181.2
22.2	233.8
23.0	322.6
24.2	488.0
25.0	643.5
26.0	867.3
27.0	1162.0
27.9	1544.0
33.9	4880.0

Deuterium (Above boiling point)	
T (°K)	P (mm Hg)
24.2	919.5
24.5	1007.5
25.0	1143.0
25.5	1304.0
26.0	1462.0

* Estimated uncertainty in the various temperatures associated with each vapor pressure: ±0.3°K.

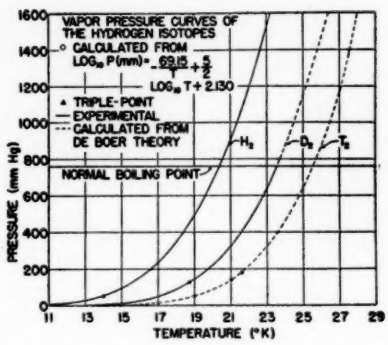

FIG. 3. Vapor-pressure curves of the hydrogen isotopes.

TABLE III.

Critical constants.

	T_c (°K)	V_c (cm³/mole)	P_c (atmos.)
H_2	33.19†	66.95†	12.98†
D_2	41.1*	56.7*	18.9*
T_2	43.7*	53.7*	20.8*

Triple-point constants

	T_{tr} (°K)	V_{tr} (liq.) (cm³/mole)	V_{tr} (solid) (cm³/mole)	P_{tr} (atmos.)	P_{tr} (mm Hg)
H_2	13.96†	26.10†	23.25†	0.071†	53.7†
D_2	18.72†	23.14†	20.48†	0.168†	128.0†
T_2	21.65*	21.90*	19.24*	0.248*	188.0*

Molecular constants

	θ (°K)	V_0 (cm³/mole)	U_0 (cal./mole)
H_2	105†	22.57†	183‡
D_2	97†	19.49†	276‡
T_2	87*	18.6*	316*

* Calculated by De Boer's Theory (see reference 1 of text).
† From "Compilation of thermal properties of hydrogen in its various isotopic and other para modifications," Woolley, Scott, and Brickwedde, J. Research Nat. Bur. of Stand. **41**, 379 (1948).
‡ Scott, Brickwedde, Urey, and Wahl, J. Chem. Phys. **2**, 454 (1934).

constants, triple-point constants, and several molecular constants for D_2 and T_2 so calculated are presented for comparison with corresponding experimental data for H_2.

The value of U_0 can be inserted into the theoretical equation for the vapor pressure, *viz:*

$$\log_{10}P = U_0/(2.303RT) + 5/2\,\log_{10}T + \text{const.},$$

where the contribution of the thermal motion is neglected. This equation should be fairly accurate over a limited temperature range, especially at low temperatures. By choosing the constant equal to 2.130, an analytical representation of the calculated vapor pressures in mm Hg, of solid tritium previously presented in Table II is obtained.

* This document is based on work performed at Los Alamos Scientific Laboratory of the University of California under AEC Contract W-7405-Eng-36.

[1] J. De Boer, Physica **XIV**, 139 (1948).
[2] J. De Boer and Lunbeck, Physica **XIV**, 1101 (1948).
[3] Sydoriak, Grilly, and Hammel, Phys. Rev. **75**, 303 (1949).

The Diffusion of $AgNO_3$ and Ag^+ Ion in Aqueous Solution

S. G. WHITEWAY, D. F. MACLENNAN, AND C. C. COFFIN
Department of Chemistry, Dalhousie University, Halifax, Nova Scotia
December 10, 1949

ADAMSON and co-workers have recently published[1,2] curves showing that at low concentrations the observed self-diffusion coefficients of Na^+ ion in aqueous solution are appreciably greater than the theoretical. In their experiments the diffusion volume was defined by a porous diaphragm of sintered glass and a radioactive isotope was used as a tracer for sodium. They suggest that this increased diffusion is due to the enhanced mobility of Na^+ ion on the glass walls of the microscopic channels in the porous disk and point out that a similar effect has been observed in the conductance of alkali metal salt solutions.[3] The object of this note is to present some data obtained in this laboratory on the diffusion of $AgNO_3$ and Ag^+ ion which do not exhibit the effect observed by Adamson.

These measurements were made at 25° in McBain-Northrup diffusion cells[4] calibrated with 0.1N KCl as outlined by Gordon.[5] The amount of $AgNO_3$ diffusing from solutions of various concentrations into water (bulk-diffusion) was determined by titration with standard KSCN solutions. At the lowest concentrations radioactive silver (Ag^{110}, half-life 225 days) was used as an indicator. The diffusion of Ag^+ ions between $AgNO_3$ solutions of identical concentration (self-diffusion) was followed with the same radioactive isotope. All counting was done on aliquots with an end window G-M tube. Except for several self-diffusion experiments referred to later, the only stirring was that due to difference in density.

The results of these measurements are shown in Figs. 1 and 2. The former refers to bulk-diffusion and the latter to self-diffusion. The points represent experimental data. The curve in Fig. 1 is drawn through values calculated from the Onsagar-Fuoss Equation[6] for a 1:1 electrolyte at 25°, *viz.*,

$$D(\text{cm}^2/\text{sec.}) = 2RT\left(\frac{\bar{M}}{c}\right)\left(1+\frac{c\partial\ln\gamma}{\partial c}\right)10^3, \qquad (1)$$

where

$$\frac{\bar{M}}{c} = \left(1.0748\times10^{-20}\frac{\lambda_1^0\lambda_2^0}{\Lambda^0}\right) - \left(\frac{[\lambda_1^0-\lambda_2^0]^2}{2[\Lambda^0]^2}\,\frac{3.1322\times10^{-19}}{\eta_0(DT)^{\frac{1}{2}}} \times\frac{(\Gamma)^{\frac{1}{2}}}{(1+\kappa a)}\right) + \left(\frac{9.304\times10^{-13}}{\eta_0(DT)^2}c\phi(\kappa a)\right).$$

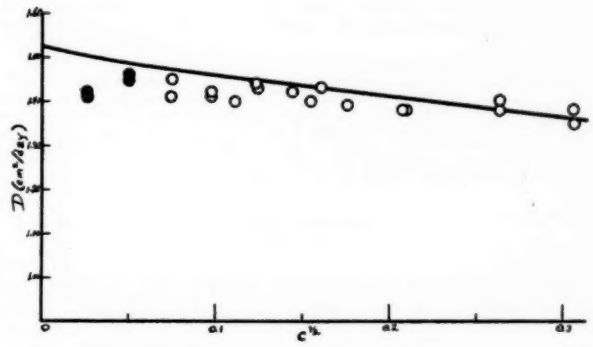

FIG. 1. Diffusion constants of $AgNO_3$ at 25°. The points represent experimental results. Filled circles are runs with radioactive silver. The curve is that of Eq. (1).

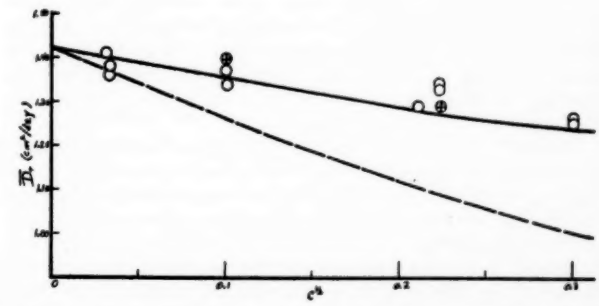

FIG. 2. Diffusion constants of Ag^+ at 25°. The points represent the experimental results. Circles with crosses are runs with mechanical stirring. The lower curve is that of Eq. (2). The upper curve is that of Eq. (3).

The variation of the activity coefficient of $AgNO_3$ solutions at 25° was taken from the data of Robinson and Tait[7] while the data of Harned[8] was used to evaluate $\phi(\kappa a)$ for various values of c.

The lower curve of Fig. 2 is that of the equation as given by Adamson,[1] *viz.*,

$$\bar{D}_+(\text{cm}^2/\text{sec.}) = RT1.074\times10^{-17}\lambda_+\left(1+\frac{c\partial \ln\gamma_+}{\partial c}\right), \quad (2)$$

where

$$\lambda_+ = \lambda_+^0 - (0.221\lambda_+^0 + 29.9)(c)^{\frac{1}{2}}.$$

The upper curve is that of the equation

$$\bar{D}_+ = \bar{D}_+^0\left(1+\frac{c\partial \ln\gamma_+}{\partial c}\right), \quad (3)$$

where

$$\bar{D}_+^0 = RT1.074\times10^{-17}\lambda_+^0.$$

In Eq. (2) λ_+ varies with concentration while in Eq. (3) it is assumed that the thermodynamic factor adequately describes all concentration effects. Since the ionic activity coefficient cannot be measured directly the activity coefficient of $AgNO_3$ determined by Robinson and Tait[7] was used. The general applicability of Eq. (3) to the self-diffusion of ions is being investigated.

It is evident from the figures that at low concentrations Ag^+ does not behave in the same way as Na^+. In the case of silver, theory and experiment agree reasonably well at infinite dilution and Eq. (3) fits the self-diffusion data satisfactorily in this concentration range.

The data of these figures are in a sense "preliminary." It is intended to repeat the tracer experiments with Ag^{110} of a higher specific activity and with a counter of more favorable geometry, *viz.*, a dipping counter. Two of the points in Fig. 2 were obtained with cells in which the contents were stirred by intermittent rotation of the diaphragm (half-minute on—half-minute off). It will be observed that these points are not out of line with the results of the unstirred runs. More stirred self-diffusion runs at low concentration are planned.

A studentship, a bursary, and a grant for apparatus from the National Research Council of Canada are gratefully acknowledged.

[1] A. W. Adamson, J. Chem. Phys. **15**, 762 (1947).
[2] Adamson, Cobble, and Nielsen, J. Chem. Phys. **17**, 740 (1949).
[3] K. J. Mysels and J. W. McBain, J. Coll. Sci. **3**, 45 (1948).
[4] J. W. McBain and T. H. Liu, J. Am. Chem. Soc. **53**, 59 (1931).
[5] A. R. Gordon, J. Chem. Phys. **5**, 522 (1937).
[6] H. S. Harned and A. L. Levy, J. Am. Chem. Soc. **71**, 2781 (1949).
[7] R. A. Robinson and D. A. Tait, Trans. Faraday Soc. **37**, 569 (1941).
[8] H. S. Harned, Chem. Rev. **40**, 461 (1947).

The Structure of Polymer-Plasticizer Gels As Shown by the Electron Microscope

W. R. Richard and P. A. S. Smith
University of Michigan, Ann Arbor, Michigan
December 16, 1949

We wish to report the use of high density organo-mercury compounds as plasticizing agents for high polymers in the study of the structure of gel systems. The opacity to electrons imparted to the plasticizers by their high mercury content makes possible the use of the electron microscope to examine visually the scale of dispersion of the components of a polymer-plasticizer gel.

Compatible organo-mercury compounds have been obtained by the addition of mercuric acetate to various unsaturated esters, such as acrylates, methacrylates, and allyl esters. The data described in this preliminary communication were obtained using methyl α-acetoxymercuri-β-methoxypropionate (A), and methyl α-acetoxymercuri-β-methoxyisobutyrate (B). Compound (A) is a viscous oil, $\rho=2.29$ at 25°C, which could be distilled at 165°/0.5 mm with partial decomposition; compound (B) is a colorless, crystalline solid; m.p. 71.5–72.5°; $\rho=2.2$ at 25° (supercooled liquid).

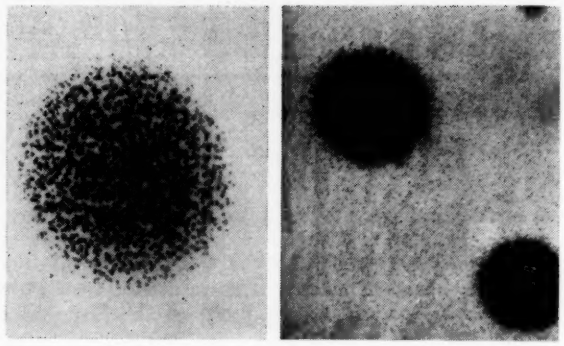

A B

FIG. 1. Electron micrographs ×10,000 of polyvinyl butyral plasticized with compounds (A) and (B) at volume fraction of plasticizer $\phi_1=0.45$.

Micrographs of polyvinyl butyral films plasticized with compounds (A) and (B) at volume fraction $\phi_1=0.45$ are shown in Fig. 1. Ovals, made up of a cluster of discrete small spheres of diameters between approximately 1300A and 180A as shown in Fig. 1A, appear at $\phi_1=0.27$ and become larger in size and number with increasing concentration of compound (A). Films plasticized with (B) at $\phi_1=0.33$ and above have small spheres of diameters between approximately 160A and 115A distributed at random, together with a few large dense ovals at $\phi_1=0.45$, as shown in Fig. 1B. Micrographs of gels at $\phi_1=0.2$, 0.12, and 0.032 appear the same as unplasticized film showing no structure.

These pictures appear to indicate submicroscopic phase-separation commencing at plasticizer-polymer ratios above a reproducible threshold value. In order to correlate this observation with independent data, measurements of the stiffness of polyvinyl butyral plasticized with both compound (A) and compound (B) were made and plotted on a logarithmic scale against temperature.[1,2] The temperature of maximum slope (Tm) in the series of curves obtained is plotted against volume-fraction of plasticizer (ϕ_1) in Fig. 2[3].

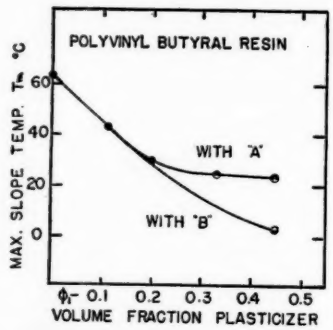

FIG. 2. Temperature of maximum slope, (Tm), of log stiffness-temperature curves of polyvinyl butyral plasticized with compounds (A) and (B), plotted against volume fraction of plasticizer (ϕ_1).

The threshold of incompatibility occurs in the region of departure of the curves from a straight line as judged by the apparent phase separation shown by the electron micrographs. In addition bulk exudation was observed to occur after 1 week in the samples plasticized with compound (A) at $\phi_1=0.33$ or higher (Fig. 2, curve A).

The use of high density organo-mercury plasticizers also allows a choice to be made of the correct parameter, weight-fraction or volume-fraction, for correlating the behavior of plasticizers in high polymer gels. The initial slopes of the curves in Fig. 2 correspond closely to that given by dibutyl phthalate in polyvinyl butyral.* However, when the same data are plotted against weight fraction the slope of the curves obtained with the high density

mercurated plasticizers differ considerably from those obtained with plasticizers with densities near unity, such as dibutyl phthalate.

The authors wish to express their appreciation to N. N. T. Samaras, H. W. Mohrman, and C. K. Bump of Monsanto Chemical Company for resin and the use of the laboratory in determining stiffness curves, and to R. C. Williams and R. M. Fisher of the University of Michigan for aid in the techniques used in electron microscopy.

[1] R. F. Clash, Jr. and R. M. Berg, Modern Plastics **21**, 119 (1944).
[2] G. J. Dienes and F. D. Dexter, Ind. Eng. Chem. **40**, 2319 (1948).
[3] L. Nielsen and R. Levreault, Nature **164**, 317 (1949).
* Obtained by E. McIntyre and shown by R. Buchdahl at the High Polymer Forum of the American Chemical Society Meeting (September 19, 1949).

Parabolic Oxidation Rates of Metals

WALTER J. MOORE
Department of Chemistry, The Catholic University of America, Washington, D. C.
December 2, 1949

THE rate of growth of the thickness, y, of an adherent oxide film on a metal often follows the "parabolic law," $dy/dt=K/y$. The growth of the film proceeds by a diffusion of reactants through the oxide barrier. In most cases, it appears likely that the metal ions diffuse outward to the oxide-oxygen interface. Electrons also move outward to combine with adsorbed oxygen atoms, forming oxide ions. Thus successive layers of metal oxide are built up. Owing to the formation of new oxide ions at the oxide-oxygen interface, there is a continuous solution of vacancies in the layer of oxide being formed. The resultant departure from stoichiometric composition makes the oxide a p-type semiconductor and also provides a mechanism for cation diffusion.

On the basis of this picture Mott and Gurney[1] derived the expression $K=2D_i(f_1-f_2)$. Here D_i is the cation diffusion coefficient; f_1 and f_2 are the fractions of defects at the phase interfaces. Gulbransen[2] combined this equation with the Eyring[3] equation for D_i to obtain $K=2\lambda^2(kT/h)\exp(\Delta S^{\ddagger}/R)\exp(-\Delta H^{\ddagger}/RT)$. The closest cation to cation distance in the oxide is usually taken for λ. The derivation of the Gulbransen equation assumes that either f_1 or f_2 is negligible compared with the other.

The $\Delta S^{\ddagger}$ and $\Delta H^{\ddagger}$ are composite quantities that include the entropy or enthalpy of formation of the vacancies (or other defects) and the entropy and enthalpy of activation for diffusion. In Table I are collected the available data on the parabolic rate constants for metal oxidation, in terms of the parameters of the transition state theory. Except for beryllium, there is relatively little variation in the $\Delta F^{\ddagger}$ values, so that reactions with high $\Delta H^{\ddagger}$ also have high $\Delta S^{\ddagger}$.

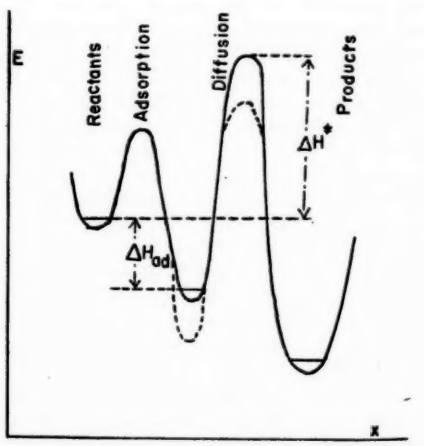

FIG. 1. Potential energy profile for oxide film formation.

TABLE I. Constants of the transition state theory for oxidation of metals.

	Ref.	Oxide	$\lambda-A$	$\Delta H^{\ddagger}$ kcal.	$\Delta S^{\ddagger}$ cals./deg.	$\Delta F^{\ddagger}$ at 800°K kcal.
Aluminum	(1)	Al_2O_3	2.72	21.4	−28.6	44.3
Iron	(1)	FeO	3.03	21.2	−27.2	43.0
Zirconium	(2)	ZrO_2	3.42	16.8	−27.3	38.7
Titanium	(3)	TiO_2	2.95	24.3	−22.8	42.6
Nickel	(4)	NiO	2.95	34.3	−11.0	42.3
Copper	(5)	Cu_2O	3.01	35.5	− 0.3	35.3
Cobalt	(6)	CoO	3.01	38.9	+ 8.1	32.4
Zinc	(7)	ZnO	3.20	33.7	−13.9	44.8
Beryllium	(8)	BeO	2.69	59.5	− 3.4	62.2

[1] E. A. Gulbransen and W. S. Wysong, J. Phys. Colloid Chem. **51**, 1087 (1947).
[2] E. A. Gulbransen and K. F. Andrew, Metals Trans. **185**, 515 (1949).
[3] E. A. Gulbransen and K. F. Andrew, Metals Trans. **185**, 741 (1949).
[4] W. J. Moore and C. F. Downey, unpublished data.
[5] N. B. Pilling and R. E. Bedworth, J. Inst. Metals **29**, 529 (1923).
[6] J. S. Dunn and F. J. Wilkins, *Review of Oxidation and Scaling of Metals* (H. M. Stationery Office, London, 1935), p. 67.
[7] W. J. Moore and J. K. Lee, unpublished data.
[8] D. Cubicciotti, personal communication.

In Fig. 1 is a schematic diagram of the potential energy barriers for vacancy formation (adsorption of oxide ions) and vacancy diffusion. The processes at the oxide-metal interface are omitted, but they may be of importance in certain instances. It will be noted that for equal diffusion barriers, the higher the heat of adsorption, the lower the effective $\Delta H^{\ddagger}$. Since a high heat of adsorption implies an immobile adsorbed film, it may also be associated with a large negative ΔS of adsorption. This correlation may help explain the approximate constancy of $\Delta F^{\ddagger}$. In a case like that of beryllium, however, one must assume that $\Delta S^{\ddagger}$ for the diffusion process itself is exceptionally high, suggesting an extended region of disorder around the diffusing vacancy or interstitial ion.

These studies are part of a program initiated through a Frederick Gardner Cottrell grant from the Research Corporation.

[1] N. F. Mott and R. W. Gurney, *Electronic Processes in Ionic Crystals* (Oxford University Press, Oxford, 1940), p. 255.
[2] E. A. Gulbransen, Trans. Electrochem. Soc. **83**, 301 (1943). We have removed an erroneous factor of 2 from the equations of Mott and Gurney and of Gulbransen.
[3] H. Eyring, J. Chem. Phys. **4**, 283 (1936).

On the Interpretation of the "Vapor Snake" in Freezing Cyclohexane

F. C. FRANK
H. H. Wills Physical Laboratory, Royal Fort, Bristol, England
December 13, 1949

PHIBBS and Schiff[1] describe an interesting phenomenon occurring when a sealed tube containing outgassed cyclohexane is plunged into solid CO_2-acetone mixture: the development of a snake-like tubular cavity, sheathed with solid, growing at the rate of 3 cm/sec. in the interior of the liquid. They attribute this to the very high pressure vapor of cyclohexane at its melting point (35 mm at 6.4°C) "along with the observed fact that crystallization tends to take place only at a liquid-vapor interface in the absence of dissolved gas." I will suggest that the latter is not a contributory cause of the phenomenon, but a parallel effect of the same cause. It is indeed theoretically conceivable that an oriented layer of molecules at the free surface of a liquid should nucleate the solid phase more readily than does the different kind of order reigning in the interior, or at the surface of contact with some solid, and experimental evidence of this would be most interesting: but it seems certain in this case that freezing occurs most readily at the free surface because the temperature is lowest there. The whole of the "vapor snake" phenomenon can be explained on the grounds that transfer of vapor into and through the cavity provides a mechanism of heat transfer additional to that of conduction through the solid sheath on the walls, which alone applies when the tube is not cooled above the liquid surface.

If the liquid (or solid) surface, of area A, is at an absolute temperature T, at which it has a pressure p dynes/cm² and the space above it is in contact with a large condensing surface at much lower temperature so that the vapor pressure there is relatively negligible, and if no incondensable gas is present to present a diffusion barrier, the liquid will evaporate at a rate of $GAp(mkT)^{-\frac{1}{2}}$ molecules per second, where m is the mass of a molecule, k Boltzmann's constant, and G a numerical factor of order 1 which we must estimate. If the mean free path were large compared with the tube diameter, G would be $(2\pi)^{-\frac{1}{2}}\sim 0.4$; it would be $\gamma^{\frac{1}{2}}[2/(\gamma+1)]^{(\gamma+1)/2(\gamma-1)}\sim 0.66$, say, if A were the throat area of a convergent-divergent nozzle, in which the gas reaches the speed of sound after expanding by a factor $[\frac{1}{2}(\gamma+1)]^{1/(\gamma-1)}$, where γ is the specific heat ratio. In our case G will be less, but we ought not to be seriously overestimating it if we suppose the vapor reaches half the speed of sound after a similar expansion, and take G to be $\frac{1}{4}$. In that case, multiplying the rate of evaporation by the latent heat to obtain the rate of abstraction of heat, and inserting data for cyclohexane in the neighborhood of its melting point, the resulting heat flux is $10p$ watts/cm², where p is now measured in mm of mercury, i.e., 350 watts/cm² at the melting point. This is large when compared with the latent heat of fusion, 32 joules/g, or the conduction flux through a glass wall 1 mm thick, with a temperature drop of 80°, which is 6 watts/cm². Since the cooled wall above the liquid surface itself, has several times the area of the liquid surface itself, conduction through these upper walls, and transport of heat with vapor from the free surface to them, will be more effective in cooling the liquid than direct conduction through the walls, even after the vapor pressure has been considerably reduced by fall of temperature. Near the melting point, a vapor space behaves as a very good conductor of heat, as compared with glass, or solid cyclohexane.

The sequence of phenomena observed by Phibbs and Schiff may be interpreted as follows:

(a) Vapor condenses on the cooled upper walls, and evaporates from the free surface, refrigerating it rapidly to a temperature well below the melting point, so that it freezes to a solid crust. At the same time freezing occurs in a thin sheath on the walls below, but this sheath grows in thickness less rapidly than the upper crust, since the heat of solidification of the latter escapes through a much larger area of glass wall.

(b) Once the liquid is sealed beneath a solid crust, the contraction accompanying further freezing develops a negative pressure, which presently becomes sufficient to nucleate a vapor bubble: a normal contraction cavity to begin with. The pressure then reverts to equality with the vapor pressure. The evaporation of vapor to fill this cavity already effects a significant degree of cooling, enough to freeze a skin of liquid of about a thousandth of its radius in thickness (since the density of the vapor at the melting point is 2×10^{-4} times that of the liquid, while the latent heat of vaporization is 12 times the latent heat of fusion). In addition, vapor transfer in the cavity effects a transfer of heat from warmer to colder points on its surface. The tubule behaves like a wire of good thermal conductor, with one end embedded in the upper crust which is still being cooled, well below the melting point, by evaporation from solid at the free surface.

(c) As freezing progresses, the cavity extends. Its rate of increase in volume is determined simply by the rate of removal of heat through the glass walls, divided by the latent heat of fusion and multiplied by the contraction on freezing. The cavity would be expected to expand spherically, but for the fact that it becomes sheathed with solid, which prevents it from expanding anywhere except at the tip. The rate of advance of the tip will simply be the maximum linear crystallization velocity (since, unless severely supercooled, a liquid needs contact with the solid, as well as cooling, in order to freeze). The highest such velocity recorded by Tammann[2,3] for an organic substance is about 2 cm/sec. for butylphenol, though for water[3] it is at least 10 cm/sec., so that 3 cm/sec. for cyclohexane would not appear unreasonable. On this view, an ampoule of different size and shape would give a "snake" of different diameter but the same rate of increase in length.

The requirements for a well-developed "snake" phenomenon would appear to be a fairly high vapor pressure at the melting point, a high crystallization velocity, a high ratio of latent heat of evaporation to latent heat of fusion, and an initial temperature not far above the melting point.

The further observations of Phibbs and Schiff are all intelligible from this point of view. If the liquid is cooled from below only, or confined over mercury, no sealing crust develops, so there can be no contraction cavity. If dissolved gas is present, it will be expelled on freezing, nucleating bubbles at many places instead of one, and under a sealing crust each will develop as a fine thread with surrounding solidification. With more than a very little incondensable gas, the efficiency of heat transfer in vapor spaces would be less: but it could be very much reduced and still remain large compared with thermal conduction through the solid. Phibbs and Schiff have demonstrated very neatly an important effect which might easily be overlooked, but may well play a significant part in a variety of crystallization processes in which it is less plainly evident. Incidentally, they seem to have established a "record" of 3 cm/sec. in measured crystallization velocities for organic liquids.

[1] M. K. Phibbs and H. I. Schiff, J. Chem. Phys. **17**, 843 (1949).
[2] G. Tammann, *The States of Aggregation*, translated by R. F. Mehl (D. Van Nostrand Company, Inc., New York, 1925), p. 266.
[3] G. Tammann and A. Büchner, Zeits. f. anorg. u. angew. Chemie **222**, 12 (1935).

Vector Model for Spin-Orbit Interaction in Polyatomic Molecules

S. I. WEISSMAN
Department of Chemistry, Washington University, Saint Louis, Missouri
December 23, 1949

IN a recent communication McClure[1] has given the "selection rules" for perturbations between singlet and triplet levels under some of the point groups. His method is based on an analysis of the behavior of one of the terms which appear in the spin-orbit perturbation operator in a many-electron system. It is the purpose of this note to point out that McClure's results are complete and independent of the explicit form of the spin-orbit coupling term used by him.

The symmetry classification of the complete electronic wave functions of a polyatomic molecule may be determined by a procedure similar to the one used for atoms.[2] Direct products are taken between the matrices of the irreducible representations of the spin functions and the corresponding matrices of the irreducible representations of the orbital functions. The resulting representations are reduced to yield the symmetry classifications of the resulting electronic states. Spin-orbit perturbations may mix only states of the same symmetry.

All singlet wave functions have the symmetry of the orbital part of the wave function since the singlet spin function belongs to the identity representation. Triplet spin functions, in spherical symmetry, belong to the three-dimensional representation of even parity, $D_+^{(1)}$, of the sphere group. This representation describes the way in which an axial vector transforms. Under lower symmetry the three components of the triplet spin function transform among themselves according to the representations into which $D_+^{(1)}$, reduces. The classifications of triplet wave functions as obtained from the product representations of the spin functions are orbital functions. This procedure is formally identical with the one used by McClure.

The classifications of states of any multiplicity are easily obtained by the vector model procedure. For systems of even numbers of electrons, singlet, triplet, quintuplet, etc., spin functions transform according to the representations into which

$D_+^{(0)}$, $D_+^{(1)}$, $D_+^{(2)}$, etc., respectively reduce under the symmetry in question.

For odd numbers of electrons the same procedure is used; the functions are however classified according to the appropriate two-valued group.[3]

This procedure will be illustrated in a paper now being prepared on the polarization of singlet-triplet transitions.

[1] D. S. McClure, J. Chem. Phys. **17**, 665 (1949).
[2] E. Wigner, Gruppentheorie. p. 198.
[3] H. Bethe, Ann. d. Physik **3**, 133 (1929); H. A. Jahn, Proc. Roy. Soc. **164**, 117 (1938); W. Opechowskie, Physica **7**, 552 (1940).

Raman Spectrum of Fluorine

D. ANDRYCHUK
Division of Physics, National Research Council of Canada, Ottawa, Ontario
December 23, 1949

THE Raman spectrum of fluorine has not been observed up to the present time. Garner and Yost[1] made an attempt to obtain the Raman spectrum of the liquid but no Raman lines were found. Considerable improvements in the light sources and the speed of photographic plates have been made since that time. It was therefore decided to make an attempt at obtaining the Raman effect of fluorine gas at atmospheric pressure.

A water-cooled mercury arc lamp of 1.4 kw capacity, the type developed at the University of Toronto, with magnesium oxide-coated reflectors, was used. The irradiated portion of the quartz Raman tube was 14 in. long. The spectrum was recorded in $8\frac{3}{4}$ hr. in a spectrograph with an $f/2.3$ camera lens on 103-a-F photographic plates.

Two weak Raman lines were found corresponding to the two mercury lines 4047A and 4358A. The observed Raman shifts were 891.4 cm^{-1} and 892.8 cm^{-1}, respectively. The mean, 892.1 ± 2 cm^{-1}, is the first vibrational quantum $\Delta G_{\frac{1}{2}}$ of the F_2 molecule.

Murphy and Vance[2] in calculating the thermodynamic properties of fluorine estimated $\Delta G_{\frac{1}{2}}$ to be 856 ± 17 cm^{-1} by applying Badger's rule to the electron diffraction value of r_0 (=1.48A). Adoption of the new experimental value of $\Delta G_{\frac{1}{2}}$ here obtained will introduce changes in the thermodynamic functions calculated by them.

The author is grateful to Dr. G. Herzberg for suggesting the problem.

[1] C. S. Garner and D. M. Yost, J. Am. Chem. Soc. **59**, 2738 (1938).
[2] G. M. Murphy and J. E. Vance, J. Chem. Phys. **7**, 208 (1939).

Metallic Valences*

A. I. SNOW
Institute for Atomic Research, Iowa State College, Ames, Iowa
December 2, 1949

TWO different sets of valences are now being applied to metals in alloys, that of Hume-Rothery,[1] Mott and Jones,[2] and Pauling.[3,4] In the former, metallic valences approach a minimum of or nearly zero for the transition metals, whereas in the latter a maximum of about 5.78 is reached for the same metals.

Hume-Rothery[5] has investigated the effect of manganese, iron, and nickel on the α/β brass equilibrium, assuming that the major factor influencing the ternary isothermal, solid-solubility boundaries is the electron-to-atom ratio. By comparison of predicted and experimental curves for isothermal solubility as a function of added transition element, he finds that if the metallic valences of copper, zinc, and aluminum are 1, 2, and 3, respectively, then the valences of manganese, iron and nickel are 2, 1, and 0.4–0.6, respectively.

Hume-Rothery[5] states that, ". . . whatever may be the validity of Pauling's views regarding the numbers of electrons responsible for cohesion in the crystals of the transition elements, these numbers are not the effective valences of the atoms as regards their influence on the α/β equilibrium," and, ". . . the directions of the curves are quite different from those to be expected for elements of valency 5 or 6."

Hume-Rothery's conclusions are valid only if copper and zinc have valences of 1 and 2, respectively. If one chooses a valence of 5.44 for copper, as suggested in Pauling's[3,4] papers, and 3 for aluminum, one obtains a valence of 4.22 for zinc from the 550°C $\alpha/\alpha+\beta$ boundary in the copper-aluminum-zinc system. Using these values for zinc and copper, on examination of the empirical ternary solubility curves given by Hume-Rothery,[5] the following valences are obtained: iron 5.44; manganese 4.22; and nickel 5.93–6.17. Pauling's[4] values are zinc 4.44; iron 5.78; manganese 4.16 and 5.78; and nickel 5.78. Not too much reliance is to be placed on the exactness of the valences obtained, but the calculation outlined above does show that Pauling's valences, if changed slightly, form a self-consistent set.

Using the valences quoted above, one obtains exactly the same theoretical solubility curves as does Hume-Rothery. Giving copper a valence of 5.44, nickel has the highest valence of the three transition elements considered, whereas manganese has the lowest valence, a result in opposite order to that obtained by assuming copper to be univalent.

The particular ternary alloys considered by Hume-Rothery in his paper do not offer a means of distinguishing between the two viewpoints on valence, since both yield identical isothermal solubility curves.

Methods of choosing between the two valence sets are not plentiful since, in general, the two valence sets give results which are very close to each other. For example, Pauling[6] has found that both valence ideas lead to the more-or-less complete filling of Brillouin zones for the gamma-alloys and other alloys with filled zone properties. One method of distinguishing between the two valence sets is to consider a ternary solid solution in which two of the components have valences for which Hume-Rothery and Pauling give identical values. If the third element is one on whose valence the two views disagree, different isothermal ternary solubility curves will be predicted on the basis of the two views. By comparison of calculated and empirical solubility curves, one may distinguish between the two points of view.

Even if constancy of electron-to-atom ratio, on which the above argument depends, is a valid concept one must, however, consider carefully the effects of electronegativity, relative atomic size, and the orbitals available for bond formation in all of the components of the solid solution.

These points will be discussed in a future paper.

The author wishes to acknowledge the aid given to him by helpful discussion and criticism of this paper by Dr. R. E. Rundle.

* This document is based on work performed in the Ames Laboratory of the AEC. Contribution No. 81 from the Iowa State College Institute for Atomic Research, Ames, Iowa.
[1] W. Hume-Rothery, *The Structure of Metals and Alloys* (The Institute of Metals, London, 1936).
[2] N. F. Mott and H. Jones, *The Theory of the Properties of Metals and Alloys* (Clarendon Press, London, 1936).
[3] L. Pauling, Phys. Rev. **54**, 899 (1938).
[4] L. Pauling, J. Am. Chem. Soc. **69**, 542 (1947).
[5] W. Hume-Rothery, Phil. Mag. **39**, 89–97 (1948).
[6] F. J. Ewing and L. Pauling, Rev. Mod. Phys. **20**, 112 (1948).

Macroscopic Space Charge in Electrolytes during Electrolysis

D. A. MACINNES, T. SHEDLOVSKY, AND L. G. LONGSWORTH
Laboratories of the Rockefeller Institute for Medical Research, New York, New York
December 19, 1949

IN a recent paper[1] Reed and Schriever claim to have observed non-linear potential gradients in a conducting electrolyte solution of *uniform* composition. Since this observation, if substantiated, would invalidate all work on the transference numbers of electrolytes by the moving boundary method, it appears essential to examine critically the conditions of their experiments. Poisson's relation requires the existence of a space charge ρ in

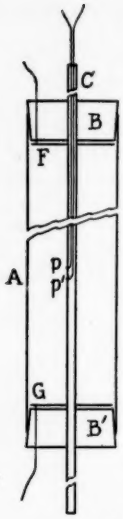

FIG. 1.

any region, such as a boundary layer, in which the composition, and hence the conductivity, κ, varies with the distance, x, i.e.,

$$\frac{d^2V}{dx^2}=\frac{i}{A}\frac{d}{dx}\left(\frac{1}{\kappa}\right)=-\frac{4\pi\rho}{\epsilon}.$$

Here i is the current and A the (uniform) cross-sectional area of the column. The magnitude of this space charge at a moving boundary was computed in 1897 by Kohlraush[2] for a typical case and he concluded that it is of no significance in transference experiments, a conclusion supported by all subsequent work. It is basic to the moving boundary method, however, that the potential gradient in the interior of a homogeneous conducting solution be given accurately by Ohm's law.

Reed and Schriever's work is subject to the criticism that, in the horizontal trough they used, the concentration gradients that tend to develop at the vertical electrodes are disturbed by gravity. Thus in the electrolysis of aqueous copper sulfate the concentrated solution of this salt formed at the anode falls to the bottom of their trough, while the dilute solution at the cathode rises. Erratically changing concentration differences must thus develop in an unstirred system and are by no means negligible.

The most serious error in Reed and Schriever's work probably arises, however, from their choice of electrodes. Every material used by these workers is incompletely reversible. The stresses and imperfections in practically all crystalline metals render them unsuitable for quantitative potentiometric measurements.

To avoid these errors we believe that the experiment should have been set up in a vertical tube for gravitational stability. Moreover, the potential gradient along the column of solution can best be explored by using as probes a pair of closely spaced reversible electrodes fixed relative to each other, and independent of the working electrodes.

Although we were quite certain of the outcome, an experiment was set up with the simple equipment shown in Fig. 1. The vertical glass tube A, about 30 cm long and $5\frac{1}{2}$ cm in diameter, was fitted with the stoppers B, B' through the centers of which ran a vertically movable glass tube C, carrying insulated silver wires. These wires were sealed through the wall of the tube with fused silver chloride to form the probe electrodes, p, p', about 6 mm apart. For the working electrodes F and G flat helices of heavy silver wire were used. The electrodes were given a coating of silver chloride electrochemically, thus making the probe electrodes reversible. After filling the apparatus with 0.003N KCl, three series of measurements were made with about 2, 4, and 6 volts across the terminals. The potential differences between the probes: 43, 89, and 131 mv, respectively, remained constant, within a few tenths of a millivolt, throughout the length of the tube A. However, after the current had been on for about a half hour the gradient near the bottom cathode dropped by nearly a millivolt in the case of the two higher currents and increased slightly near the anode, since solution tends to become more concentrated at the bottom and less concentrated at the top.

This experiment, admittedly relatively crude, gave no indication of any appreciable space-charge effects in the uniform solution. We believe that it indicates the type of experiment that Reed and Schriever might better have carried out to test the presence, or much more probable absence, of any significant deviations from Ohm's law in solutions of electrolytes.

[1] C. A. Reed and W. Schriever, J. Chem. Phys. **17**, 955 (1949).
[2] Kohlraush, Ann. der Physik **62**, 209 (1897).

Erratum: Raman Effect, Infra-Red Absorption, Dielectric Constant, and Electron Diffraction in Relation to Internal Rotation

[J. Chem. Phys. **17**, 591 (1949)]

S. MIZUSHIMA, Y. MORINO, I. WATANABE, T. SIMANOUTI, AND S. YAMAGUCHI

Chemical Laboratory, Faculty of Science, Tokyo University, Bunkyoku, Tokyo

ON page 594 of this paper the Raman frequency 859 cm^{-1} of asymmetrical tetrachloroethane should be 959 cm^{-1}. According to the private communication of Mr. A. Opler who kindly pointed out this misprint, the infra-red absorption frequencies observed by him are in excellent agreement with our Raman frequencies. The fact that no further normal frequency was observed by the infra-red absorption would be another experimental evidence for the only one configuration of asymmetrical tetrachloroethane molecule.

On the same page "the chlorine atoms or polysubstituted ethanes" should be "the chlorine atoms of polysubstituted ethanes."

The Photo-Decomposition of Acetaldehyde: Individual Rate Constants by the Sector Method

R. E. DODD

Chemistry Department, King's College, University of Durham, Newcastle-on-Tyne, England

December 15, 1949

HADEN AND RICE[1] have reported the use of intermittent illumination in the high temperature photolysis of acetaldehyde. Without absolute intensity measurements the independent results from such measurements are values of the ratio k_t/k_p, where k_p and k_t are, respectively, rate constants for chain propagation and chain termination. Combined with the best absolute value of $k_pk_i^{\frac{1}{2}}k_t^{-\frac{1}{2}}$ (obtained from absolute measurements of quantum yields of the reaction under steady illumination), this ratio gives k_ik_p and k_ik_t, k_i being the quantum yield of the primary process.

Haden and Rice used two temperatures only, and their light intensities were low enough to permit deviations from the kinetic $I_{\text{abs}}^{\frac{1}{2}}$ law, with consequent greater complexity, and uncertainty, in the interpretation of the sector results.[2] Figure 1 shows the $\log(k_t/k_p)-1/T$ plot of results now obtained by the sector method, at a variety of temperatures and at light intensities for which the square root law is valid. Haden and Rice's results are plotted as solid points and show good agreement. The straight line gives an activation energy -10.4 kcal./mole (± 1.0), corresponding to E_t-E_p.

The activation energy of the steady reaction, $E_p-\frac{1}{2}E_t$, has been variously reported as 8.6,[3] 9.6,[4] 10.0[5] kcal./mole, the light intensities used increasing in the same direction. Haden and Rice have used Leermakers' value of 10.0 kcal./mole on the ground that the others require correction for the monomolecular chain termination, which is responsible for the discrepancies in activa-

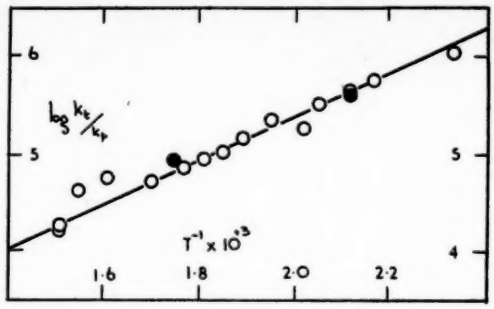

FIG. 1.

tion energy and also for deviations from the square root law at low light intensities. From their sector experiments, Haden and Rice obtain a value for the rate constant of such a chain termination, which, if used to correct the reported activation energies, not only raises the first two, but also Leermakers', to 10.4 kcal./

TABLE I.

	Frequency factors (mole^{-1} cc sec.$^{-1}$)	
	k_p	k_t
Present work	8.0×10^{12}	5.3×10^{13}
Haden and Rice	7.4×10^{12}	2.7×10^{14}
Collision numbers	8.3×10^{12}	9.0×10^{12}

mole (±0.2). Thus, combining activation energies from the steady and the intermittent reactions, we obtain

$E_p = 10.4 \pm 1.0$ kcal./mole and $E_t = 0 \pm 2.0$ kcal./mole.

Using Rollefson and Grahame's absolute values of quantum yield at 200°C, and putting $k_i = 0.2$, values for the frequency factors for k_p and k_t may be obtained and compared with the collision numbers. Table I also includes Haden and Rice's stated values, they having used Gorin's[6] $k_i = 0.7$, Rollefson and Grahame's quantum yield at 200°C, and Leermakers' activation energy.

Thus the termination reaction, which must be a bimolecular association, probably

$$\text{either} \quad CH_3 + CH_3 \rightarrow C_2H_6 \qquad (1a)$$
$$\text{or} \quad CH_3 + CHO \rightarrow CH_4 + CO, \qquad (1b)$$

has little or no activation energy. Furthermore, contrary to suggestions[7] by Steacie, Darwent, and Trost, and by Bamford and Dewar, that such radical reactions having low activation energies will usually also have low collision efficiencies of the order 10^{-5}–10^{-6}, it appears that whichever radical association is here involved has a normal frequency factor. This may well be an argument in favor of (1b), where two products are formed.

This work will be published in greater detail elsewhere when the parallel investigation of higher aldehydes is complete.

[1] W. L. Haden and O. K. Rice, J. Chem. Phys. **10**, 445 (1942).
[2] O. K. Rice, J. Chem. Phys. **10**, 440 (1942).
[3] G. K. Rollefson and D. C. Grahame, J. Chem. Phys. **8**, 98 (1940).
[4] J. W. Mitchell and C. N. Hinshelwood, Proc. Roy. Soc. (London) **159A**, 32 (1937).
[5] J. A. Leermakers, J. Am. Chem. Soc. **56**, 1537 (1934).
[6] E. Gorin, J. Chem. Phys. **7**, 256 (1939).
[7] Steacie, Darwent, and Trost, Faraday Soc. Discussions **2**, 80 (1947); C. H. Bamford and M. J. S. Dewar, Nature **163**, 256 (1949); see also M. G. Evans and M. Szwarc, Trans. Faraday Soc. **45**, 940 (1949).

The Infra-Red and Raman Spectra of Chlorine Monofluoride*

E. A. JONES, T. F. PARKINSON,** AND T. G. BURKE
K-25 Laboratories, Carbide and Carbon Chemicals Corporation, Oak Ridge, Tennessee
December 22, 1949

THE infra-red spectrum of gaseous chlorine monofluoride has been observed from 2–15μ and the Raman spectrum obtained in the liquid state. Studies were made on the material prepared by three methods: (a) fractional distillation from a cylinder of commercial ClF_3, in which appreciable quantities of ClF exist as an impurity; (b) combination of suitable quantities of ClF_3 and Cl_2 at elevated temperatures;[1] (c) direct combination of F_2 and Cl_2.[2,3]

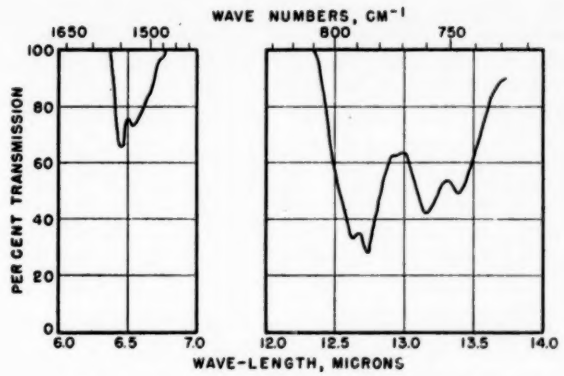

FIG. 1. Infra-red spectrum of chlorine monofluoride.

The infra-red spectrum was studied using a Perkin-Elmer Model 12B spectrometer equipped with rocksalt optics. The absorption cells were 10 cm in length and were machined from fluorothene[4] bar stock. The optical windows were sealed to the cell by means of a chemically resistant sealing wax (fluorothene-*W*) of the same chemical constitution as fluorothene, but of lower molecular weight. The rocksalt windows were attacked slowly by the gas at low pressures but at elevated pressures (e.g., ¾ atmos.) the reaction rate was considerably increased. This attack alters the infra-red transmission of the windows and results in several specific absorption bands associated with a corrosive film or other surface changes. No gaseous reaction products with detectable infra-red absorption were formed. Measurements on evacuated cells before and after corrosion by ClF have shown that these window bands do not fall in the region of the ClF absorption.

The Raman studies were made in a fluorothene tube which was connected to a copper transfer system. The liquid ClF was condensed into a Raman tube mounted vertically in an unsilvered Dewar and maintained at approximately −120°C by a stream of cooled nitrogen. The Raman spectrum was obtained with a Lane-Wells spectrograph and irradiation unit. The 5460 Hg line was used for excitation as ClF condenses to a yellow liquid which absorbs in the 4047 and 4358A regions. Exposure times were of the order of two hours. The filter used consisted of a combination of a solution of neodymium nitrate plus a Wratten filter 57A wrapped around the fluorothene tube.

The fundamental infra-red absorption band of ClF is shown in Fig. 1. The fundamental has its center at 772 cm^{-1}. Typical of diatomic molecules it displays *P* and *R* branches but no *Q* branch. In this case, both the *P* and *R* branches are doublets. This is attributed to the two isotopic forms, $Cl^{35}F$ and $Cl^{37}F$.

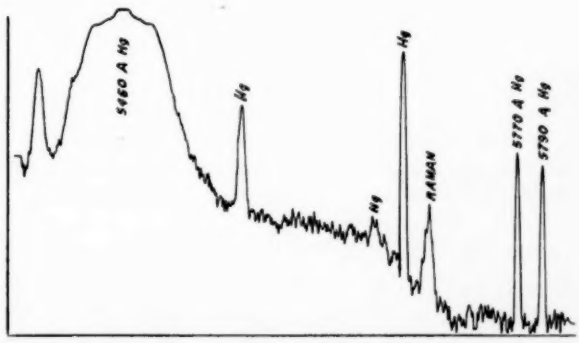

FIG. 2. Raman spectrum of chlorine monofluoride.

The electronic spectrum of chlorine monofluoride has been investigated by Wahrhaftig[5] and Schmitz and Schumacher.[6] From a value for ω_e and $X_e\omega_e$ given by these authors, the fundamental is predicted to fall at 773.4 cm^{-1} and at 772.4 cm^{-1}, respectively. Both are in good agreement with the observed position.

The first overtone falls in a region of strong water vapor absorption at 6.26μ, which has hampered the study of the band. Using a 10-cm cell filled to a pressure of $\frac{2}{3}$ atmos., a band centered at 1535 cm^{-1} has been observed. This is 8 cm^{-1} higher than the position predicted from the electronic spectrum, but is probably within the experimental error introduced by water vapor absorption.

Figure 2 shows a microphotometer tracing of the Raman spectrum of liquid ClF. A single line is observed at a shift of 758 cm^{-1}. This is to be compared to the value 772 cm^{-1} for the fundamental of the gas. Attempts to resolve the line to show the isotope effect have been unsuccessful.

* This document is based on work performed for the AEC by Carbide and Carbon Chemicals Corporation, at Oak Ridge, Tennessee.
** Present address: Physics Department, University of Virginia, Charlottesville, Virginia.
[1] H. Schmitz and J. Schumacher, Zeits. f. Naturforschung **2a**, 362 (1947).
[2] O. Rugg and H. Krug, Zeits. f. anorg. allgem. Chemie **190**, 270 (1930).
[3] L. Domange and J. Neudorffer, Comptes Rendus **226**, 920 (1948).
[4] For details in using fluorothene in infra-red and Raman spectroscopy, see J. S. Kirby-Smith and E. A. Jones, J. Opt. Soc. Am. **39**, 780 (1949).
[5] A. Wahrhaftig, J. Chem. Phys. **10**, 248 (1942).
[6] See reference 1, p. 359.

Note on the Derivation of the Frequency Spectrum of a Crystal from Specific Heat Measurements

H. GRAYSON-SMITH
Department of Physics, University of Alberta, Alberta, Canada
AND
J. P. STANLEY
Computation Centre, University of Toronto, Toronto, Canada
December 5, 1949

THE portion of the specific heat of a solid which is due to lattice vibrations is given by

$$C_v(T)=3R\int_0^\infty E(h\nu/kT)\rho(\nu)d\nu, \tag{1}$$

where $E(x)=x^2e^x/(e^x-1)^2$ and $\rho(\nu)d\nu$ is the number of modes of vibration in the frequency range ν to $\nu+d\nu$. Equation (1) has usually been used to calculate $C_v(T)$ on the basis of a more or less reasonable assumption concerning the frequency spectrum $\rho(\nu)$. It would be of great interest to calculate $\rho(\nu)$ from experimental values of $C_v(T)$. Montroll[1] has given a method by which this problem can be formally solved, but the solution involves gamma- and zeta-functions of a complex argument, which have not yet been tabulated, with laborious numerical integration.

One of us (J.P.S.) has devised a much less laborious method. Let $pkT/h=\tau$, $p\nu=l$, $C_v(T)=\gamma(\tau)$, $\rho(\nu)=g(l)$, where p is an arbitrary constant. Let also $E(x)$ be expanded in powers of e^x. Equation (1) becomes

$$\tau^2\gamma(\tau)=(3R/p)\sum_{n=1}^{\infty} n\int_0^\infty l^2g(l)e^{-nl/\tau}dl. \tag{2}$$

Let

$$l^2g(l)=(2p/\pi)\sum_{m=1}^{\infty} a_m(1-\cos ml)/m, \tag{3}$$

which is chosen because the Laplace transform has a convenient form. We then obtain

$$\gamma(\tau)=3R\sum_{m=1}^{\infty} a_m(\coth m\pi\tau-1/m\pi\tau). \tag{4}$$

In order that $\gamma(\tau)$ may represent the specific heat of a solid, it must satisfy the following asymptotic conditions. For large values of τ, $\gamma(\tau)\to 3R$, therefore $\Sigma a_m=1$. As $\tau\to 0$ the specific heat approaches zero as AT^3, where A is an experimental constant. Therefore $\Sigma ma_m=0$ and $\Sigma m^3a_m=(15A/R)(h/\pi pk)^3$. The arbitrary constant p is chosen so as to make the important values of τ lie within a tractable range. Then it is possible, using at most six terms of the series, to make the function (4) agree very well with any specific heat which is due only to lattice vibrations, and which therefore increases monotonously. Finally the frequency spectrum can be determined by means of Eq. (3).

An attempt has been made to apply this method to bismuth, which has no transitions below 300°K and has a negligible electronic specific heat,[2] but which evidently has a vibration spectrum very different from that of an elastic continuum. The experimental curve was constructed from measurements by Keesom and van den Ende[3] below 12°K, Armstrong and Grayson-Smith[2] from 14° to 22°K, and Anderson[4] above 60°K. These were combined by plotting a smooth curve of the apparent Debye Θ as a function of T.

There was no difficulty in fitting the smoothed curve of C_v with a function of the form (4), and hence of deriving a function $\rho(\nu)$. The derived frequency spectrum showed a steep double maximum at frequencies which dominate in determining the specific heat around 50°K, where two sets of data join. However, the result proved to be extremely sensitive to details of the specific heat curve in the region where dC_v/dT is large. A slight change in the manner of smoothing the data made the two maxima coalesce into a single, much less marked maximum. This disappointing result is clearly intrinsic to the problem, and is not due to using only a finite number of terms, because $\rho(\nu)$ is unique for a given fitted curve $\gamma(\tau)$. Montroll's method must therefore give the same result for the same smoothed curves, with the same sensitivity to a small change in the smoothing.

The conclusion is that the mathematical problem of inverting Eq. (1) can be solved with a reasonable amount of labor, but that no physical meaning can be attached to the result unless the original experimental data have a higher degree of internal consistency than any at present available. To obtain any information on crystal vibrations in this way it will be necessary to have accurate specific heat measurements, made on the same sample by the same method, throughout the range 2° to 300°K. We have been unable to find a single suitable example.

[1] E. W. Montroll, J. Chem. Phys. **10**, 218 (1942).
[2] L. D. Armstrong and H. Grayson-Smith, Can. J. Research **A27**, 9 (1949).
[3] W. H. Keesom and J. N. van den Ende, Proc. Acad. Sci. Amsterdam **33**, 243 (1930).
[4] C. T. Anderson, J. Am. Chem. Soc. **52**, 2720 (1930).

On the Assignment of the Triplet-Singlet Emission of Benzene

D. P. CRAIG
Sir William Ramsay and Ralph Forster Laboratories, University College, London, England
December 7, 1949

CALCULATIONS have been made upon the triplet states of benzene in a non-empirical approximation[1] taking account of configuration interaction[2] between configurations based on molecular orbital wave functions. The results agree with the valence-bond theory[3] and the single-configuration molecular orbital theory[1] in making the $^3B_{1u}$ state the lowest of the triplets, lower than the $^3B_{2u}$ state by 2.5 ev in this calculation. There is thus an unusual measure of agreement between the theoretical methods on the identity of this lowest triplet state, comparable only with the agreement there is between them that the lowest singlet state is $^1A_{1g}$.

However, Shull's observation[4] that active origins in the triplet-singlet emission of benzene are provided by b_{2g} as well as e_{2g} vibrations has been interpreted by Shull, and by McClure,[5] to mean that the triplet state concerned (presumably the lowest triplet state) has some $^1B_{1u}$ character; and further, using selection rules analogous to those for intercombinations in diatomic molecules, McClure[5] has deduced from this that the triplet state must

be $^3B_{2u}$ and not $^3B_{1u}$ as favored theoretically. The purpose of this note is to suggest that active b_{2g} vibrations may occur also in a $^3B_{1u}-{}^1A_{1g}$ transition and therefore that the experimental facts at present available are not against the identification of the lowest triplet state as $^3B_{1u}$.

It is a question of the mixing by combined magnetic (spin-orbit) and vibrational perturbations of the triplet state with either the well-known $^1E_{1u}$ state (for perpendicular bands) or with an A_{2u} state (parallel bands). Since the magnetic perturbations act on space wave functions as A_{2g} or E_{1g} operators[5] there are the following possibilities.

(i) If the triplet state is $^3B_{1u}$, the total space perturbation required is E_{2g} for perpendicular bands and B_{2g} for parallel bands. The relevant decompositions into spin-orbit and vibrational perturbations are:

$$E_{2g}=A_{2g}\times e_{2g};\quad E_{1g}\times b_{2g};\quad E_{1g}\times e_{1g}.$$
$$B_{2g}=A_{2g}\times b_{1g};\quad E_{1g}\times e_{2g}.$$

The first symbol applies to the magnetic and the second to the vibrational perturbation. There are of course no actual b_{1g} vibrations of benzene.

(ii) If the triplet state is $^3B_{2u}$, perpendicular bands demand a total space perturbation E_{2g}, and parallel bands B_{1g}. The decompositions for the first have already been given. For the second they are: $B_{1g}=A_{2g}\times b_{2g}$; $E_{1g}\times e_{2g}$.

These decompositions, which exhaust the possibilities, show that active b_{2g} vibrations may be accounted for in cases (i) and (ii), and in neither case is it necessary to assume borrowing from parallel-type transitions, whose existence in benzene is as yet uncertain. It is however necessary to invoke the in-plane component of the spin-orbit coupling which cannot cause mixing of pure π-type electronic wave functions but acts only in cooperation with vibrations. This latter fact might account for the weakness of the b_{2g} perturbations relative to e_{2g}, and the whole situation would then run parallel with a case studied by Garforth and Ingold[6] in the fluorescence of benzene, in which case both perturbations are vibrational: Garforth and Ingold showed that two out-of-plane vibrations, b_{2g} and e_{1g}, neither of which separately is capable of mixing π-type electronic wave functions, can together effect considerable mixing of the plane symmetric $^1B_{2u}$ and $^1E_{1u}$ states of benzene.

The writer concludes therefore that the designation $^3B_{1u}$ for the lowest triplet state of benzene remains tenable.

[1] M. Goeppert-Mayer and A. L. Sklar, J. Chem. Phys. **6**, 645 (1938).
[2] D. P. Craig, Proc. Roy. Soc. (in press).
[3] A. L. Sklar, J. Chem. Phys. **5**, 669 (1937).
[4] H. Shull, J. Chem. Phys. **17**, 295 (1949).
[5] D. S. McClure, J. Chem. Phys. **17**, 665 (1949).
[6] F. M. Garforth and C. K. Ingold, J. Chem. Soc. 427 (1948).

Magnetic Susceptibilities of $TlCl_2$ and Tl_2Cl_3

DALE J. MEIER AND CLIFFORD S. GARNER
Department of Chemistry, University of California, Los Angeles, California
December 19, 1949

THALLIUM chlorides corresponding to the empirical formulas $TlCl_2$ and Tl_2Cl_3 have been known for many years. Although the empirical formulas may appear to indicate valence states of thallium other than the well-known +1 and +3, the configuration, first proposed by Werner,[1] which represents these compounds as thallous chlorothallates is usually assumed.[2,3] In this manner, $TlCl_2$ has been considered to represent $Tl^{I}Tl^{III}Cl_4$, and Tl_2Cl_3 to represent $Tl^{I}{}_3Tl^{III}Cl_6$. The evidence[4] for this representation is that these chlorides resemble other chlorothallates of the types $CuTlCl_4$ and $(NH_4)_3TlCl_6$. Also, recently McConnell and Davidson[5] have shown by the use of radioactive thallium that the thallium atoms in Tl_2Cl_3 are not equivalent, which is the expected result if the compound is a thallous chlorothallate. Still, it has not been conclusively demonstrated that valence states other than +1 and +3 are not present in either $TlCl_2$ or Tl_2Cl_3. We have investigated this question by measurements of the magnetic susceptibilities of the two solid compounds.

The ground state electronic configuration of gaseous thallium atoms is $6s^26p$ beyond the gold core.[6] Both Tl (I) and Tl (III) would thus be expected to be diamagnetic, and this has been shown for Tl (I) by Klemm and Tilk.[7] A +2 state would be paramagnetic because of one unpaired electron, provided this state does not exist as a dimer, analogous to Hg_2^{++}, for which diamagnetism would be expected. This appears to be the situation for the dichlorides of gallium and indium, the congeners of thallium. The dichlorides of these two elements are diamagnetic.[7] Since neither element possesses a stable +1 oxidation state, it is unlikely that these compounds would be represented in the same manner as $TlCl_2$ above. It is more likely that these +2 ions are dimers.[8]

$TlCl_2$ and Tl_2Cl_3 were prepared according to directions given by Mellor.[4] $TlCl_2$ was prepared by passing a slow stream of anhydrous Cl_2 over anhydrous TlCl. The reaction tube was heated sufficiently to maintain the reaction mixture in a molten condition, and the Cl_2 was passed over the mixture until no further change in appearance of the molten mixture could be detected. A color change of dark brown to pale yellow was noted as the reaction progressed. After solidification the compound was very pale yellow in color. Since this compound is not stable in the presence of water, all subsequent transfer operations were carried out in a dry box. Tl_2Cl_3 was prepared by saturating a boiling solution of $TlCl_3$, slightly acidified with nitric acid, with freshly precipitated TlCl. Upon allowing the solution to cool, bright yellow crystals of Tl_2Cl_3 separated. These were washed repeatedly with small portions of hot water to dissolve any of the more soluble TlCl that might have coprecipitated. The product was dried in an oven at 105°C.

Weighed amounts of the compounds were analyzed by reducing the thallium to the +1 state with SO_2, precipitating and weighing the thallium as Tl_2CrO_4, and precipitating and weighing the chloride as AgCl. The analytical results are as follows: $TlCl_2$, 73.8 percent Tl, 26.6 percent Cl (calculated: 74.24 percent Tl, 25.76 percent Cl); Tl_2Cl_3, 79.2 percent Tl, 20.8 percent Cl (calculated: 79.35 percent Tl, 20.65 percent Cl).

The magnetic susceptibilities of the solids were measured at room temperature by the Gouy method.[9] For each determination the weight of sample taken was approximately 5 grams.

Both $TlCl_2$ and Tl_2Cl_3 were found to be diamagnetic. This indicates, as discussed above, that these compounds are either thallous chlorothallates, with only +1 and +3 thallium, or if +2 thallium is present it exists as a dimer.

[1] A. Werner, *New Ideas on Inorganic Chemistry* (Longmans, Green, and Company, London, 1911), p. 83.
[2] H. J. Emeléus and J. S. Anderson, *Modern Aspects of Inorganic Chemistry* (D. Van Nostrand Company, Inc., New York, 1938), p. 145.
[3] A. F. Wells, *Structural Inorganic Chemistry* (Oxford University Press, London, 1945), p. 516.
[4] J. W. Mellor, *A Comprehensive Treatise on Inorganic and Theoretical* Chemistry (Longmans, Green and Company, London, 1922), Vol. V, p. 448.
[5] H. McConnell and N. Davidson, J. Am. Chem. Soc. **71**, 3845 (1949).
[6] R. F. Bacher and S. Goudsmit, *Atomic Energy States* (McGraw-Hill Book Company Inc., New York, 1932), p. 479.
[7] W. Klemm and W. Tilk, Zeits. f. anorg. allgem. Chemie **207**, 175 (1932).
[8] W. M. Latimer, *Oxidation Potentials* (Prentice-Hall, Inc., New York, 1938), pp. 147, 149.
[9] L. G. Gouy, Comptes Rendus **109**, 935 (1889).

The Dissociation Energies of the C−H Bond in Propylene and the C−C Bond in Butene-1

M. SZWARC AND A. H. SHEON
Chemistry Department, Manchester University, Manchester, England
November 18, 1949

IT was expected that the recent investigation of the pyrolysis of propylene[1] would provide the necessary data for the estimation of the C−H bond dissociation energy in this compound; this then, in conjunction with relevant thermochemical data, would make it possible to compute the heat of formation of allyl radical. The experimental results—supplemented by a further study of

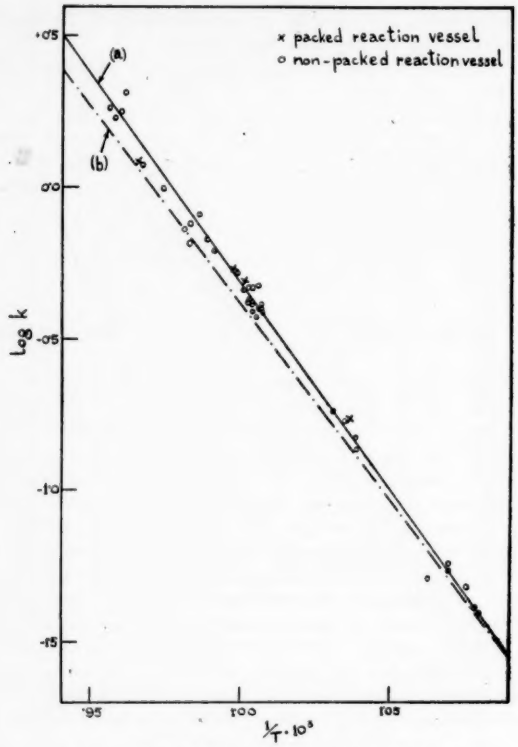

FIG. 1. (a) $E=63$ kcal./mole, $\nu=2.5\cdot10^{13}$ sec.$^{-1}$.
(b) $E=60$ kcal./mole, $\nu=5.0\cdot10^{13}$ sec.$^{-1}$.

the pyrolysis of isobutene[2]—indicated that this decomposition was a chain reaction, the initiation step being

$$CH_2{:}CH\cdot CH_3 \rightarrow CH_2{:}CH\cdot CH_2\cdot + H. \qquad (1)$$

On the basis of reasonable frequency factors for the individual steps and an assumed chain length it was deduced that $D(CH_2{:}CH\cdot CH_2{-}H)$ is ~78 kcal./mole. In view of the uncertainties inherent in this treatment we attempted to obtain new and independent evidence for the heat of formation of allyl radical from the pyrolysis of butene-1.

The existing thermochemical data lead to a relationship between the C—H bond dissociation energy in propylene and the C—C bond dissociation energy in butene-1, i.e. $D(CH_2{:}CH\cdot CH_2{-}H)-D(CH_2{:}CH\cdot CH_2{-}CH_3)=15.3$ kcal./mole. Therefore, the estimation of the latter bond dissociation energy enables us to calculate the D(C—H) in propylene.

Since the allyl radical is stabilized by its resonance energy, we have to expect that the weakest bond in butene-1 is $CH_2{:}CH\cdot CH_2{-}CH_3$, and, therefore, the decomposition of butene-1 should yield methyl and allyl radicals as the products of the initial dissociation process. The kinetics of the thermal decomposition of butene-1, as reported in the literature,[3] is difficult to interpret due to various side reactions. In order to eliminate these complicating factors, we applied in the present investigation the technique essentially similar to that used in these laboratories for the determination of bond energies,[4] i.e. pyrolyzing gaseous butene-1 in a stream of toluene. It was shown in the previous communications[4] that toluene removes readily and efficiently the various radicals produced in the pyrolysis according to Eq. (2)

$$C_6H_5\cdot CH_3 + R\cdot \rightarrow C_6H_5\cdot CH_2\cdot + RH. \qquad (2)$$

The stable benzyl radicals formed by reaction (2) eventually dimerize.

The pyrolysis of butene-1 was investigated by a flow method over the temperature range 935°K to 1046°K, the pressure of toluene—which was used as a carrier gas—varying from 4 to 16 mm Hg, and the molar ratio of butene-1 to toluene being 1:30. Under these conditions the rate of decomposition of butene-1 was measured by the rate of formation of methane. Analysis of the non-condensed gases* showed, however, that small amounts of hydrogen were formed in addition to methane. The hydrogen content varied from 10–25 percent increasing with temperature. We suspected that hydrogen was the result of a side reaction, i.e. the direct decomposition of butene-1 into H_2 and butadiene, and indeed the ultraviolet analysis of the products condensable in liquid air proved the presence of the latter.

Variation of the partial pressure of butene-1 by a factor of 6, of the time of contact by a factor of 3, of the surface to volume ratio by a factor of 4.5 proved that reaction

$$CH_2{:}CH\cdot CH_2\cdot CH_3 \rightarrow CH_2{:}CH\cdot CH_2\cdot + CH_3\cdot \qquad (3)$$

is a homogeneous gas reaction of the first order. The unimolecular rate constant seems to be almost unaffected by variation of toluene pressure.

In order to determine the activation energy of process (3) we adopted three methods:

(i) The plot of log$k$ against $1/T$ is shown in Fig. 1 by the full line (a), k denotes here the unimolecular rate constant for reaction (3) calculated on the assumption that the rate of decomposition is measured by the rate of formation of non-condensed gases. This line gives the activation energy as 63 kcal./mole and the frequency factor $2.5\ 10^{13}$ sec.$^{-1}$.

(ii) By making the appropriate correction for the presence of hydrogen, the dotted line (b) is obtained. The activation energy is then 60 kcal./mole only and the frequency factor 5.10^{12} sec.$^{-1}$.

(iii) Assuming the value of 10^{13} sec.$^{-1}$ for the frequency factor[5] of reaction (3) and using the Arrhenius equation $k=10^{13}e^{-E/RT}$ sec.$^{-1}$, where k, is the rate constant based on the formation of methane only, we arrived at the average value of 62.2 kcal./mole for the activation energy.

Making the usual assumption, that the recombination of radicals formed does not involve any activation energy, we conclude that the dissociation energy of the discussed C—C bond in butene-1 is 62±2 kcal./mole. This value leads to $D(CH_2{:}CH\cdot CH_2{-}H)=77.3\pm2$ kcal./mole, and to the heat of formation of allyl radical equal to 30.2±2 kcal./mole. Assuming that the decrease of the C—H bond dissociation energy in propylene as compared with the C—H bond dissociation energy in methane is attributed to the resonance energy of allyl radical, we obtain for the latter the value of 24±2 kcal./mole.

Finally it is necessary to mention that the ratio of dibenzyl to methane formed in this decomposition is definitely lower than the expected 1:1. This observation, which is analogous to that made in the case of allyl bromide decomposition,[4] is explained by the possible interaction of the stable allyl and benzyl radicals, which might produce either ω-phenyl-butene-1 (association) or allene and toluene (disproportionation). We consider that the decomposition of allyl radicals into allene and hydrogen atoms is energetically impossible under our experimental conditions, since on the basis of the derived value for $D(CH_2{:}CH\cdot CH_2{-}H)=77.3\pm2$. kcal./mole the C—H bond dissociation energy in allyl radical, i.e $D(CH_2{:}C\cdot CH_2)$, should be 67.7±2 kcal./mole.

$$\begin{matrix} & | \\ & H \end{matrix}$$

In conclusion we wish to thank Petrochemicals Ltd., Manchester, for the supply of butene-1 and the ultraviolet analysis of the products, and Monsanto Chemicals Ltd. for the research grant to one of us (A.H.S.). A full account of this work is in course of preparation.

* We understand by "non-condensed gases" the products which pass through the liquid air trap at a pressure of a few mm Hg.

[1] M. Szwarc, J. Chem. Phys. **17**, 284 (1949).
[2] M. Szwarc, J. Chem. Phys. **17**, 292 (1949).
[3] (a) G. Calingaert, J. Am. Chem. Soc. **45**, 130 (1923). (b) C. D. Hurd and A. R. Goldsby, J. Am. Chem. Soc. **56**, 1812 (1934). (c) F. O. Rice and O. K. Rice, *The aliphatic free radicals* (The Johns Hopkins Press, Balitmore, 1935) p. 125.
[4] (a) M. Szwarc, J. Chem. Phys. **16**, 128 (1948). (b) M. Szwarc, J. Chem. Phys. **17**, 431 (1949). (c) M. Szwarc, J. Chem. Phys. **17**, 505 (1949). (d) M. Szwarc, Proc. Roy. Soc. **198A**, 267 (1949). (e) M. Szwarc, Proc. Roy. Soc. **198A**, 285 (1949). (f) M. Szwarc and B. N. Ghosh, J. Chem. Phys. **17**, 744 (1949).
[5] M. Polanyi and E. Wigner, Zeits. f. physik. Chemie **A139**, 439 (1928).